SYSTEMIC APPROACH TO THE NONLINEAR BEHAVIOR OF SOME POWER CONVERTERS

Ph.D.Dissertation

Supervised by Prof. dr. ing. Nicolae Budişan

Writen by OCTAVIAN DRANGA

"POLITEHNICA"UNIVERSITY OF TIMISOARA

In all chaos there is a cosmos, in all disorder a secret order, in all caprice a fixed law.

C. G. Jung

CONTENTS

CHAPTER 1

INTRODUCTION – THE ACTUALITY OF THE STUDY

A new class of nonlinear phenomena has been detected widely in engineering and natural systems during more than two decades of intense studies (section 1-1). The main purpose of this introductory chapter is to summarize the state of the art in the application of nonlinear dynamics theory in power electronics. The continuing development of high-power semiconductor devices made possible the high-efficiency solid-state power conversion. Operation of these devices as switches implies that power converters are essentially nonlinear time-varying dynamical systems (section 1-2). Although hereby they become difficult to study, the effort is worthwhile because of their many practical applications and increasingly importance in the delivery and utilization of electrical energy. Traditional analysis approaches do not always provide reliable models since nonlinear effects are generally ignored and this sometimes misleads to a circuit supposed to perform acceptably while in practice it will not (section 1-3). Techniques and ideas of nonlinear dynamics offer another way of investigating these circuits, which is more accurate and able to reproduce nonlinear phenomena like chaos, quasiperiodicity and subharmonics (section 1-4).

1-1 CHAOS: A "NEW" CLASS OF NONLINEAR PHENOMENA

Three centuries after the publication of Newton's "Principia" (1687), the discovery of chaotic dynamics has doubted one of the basic doctrines of classical science, according to which a deterministic system is completely predictable, i.e., given the initial condition and the mathematical model, its behavior can be predicted for all time. Simply put, a chaotic system is a deterministic system exhibiting random behavior.

Although only relatively recently identified as a robust phenomenon, chaos has certainly been encountered by scientists many times in the last century but it was dismissed as physical noise. The history of chaotic dynamics can be traced back to the work of Henri

Poincaré on celestial mechanics around 1900 [1]. However, after discovering the extreme sensitivity to initial conditions in a simplified computer model of atmospheric convection Lorenz gave in 1963 the first suspicion that chaos might be important in a real physical system [2]. Lorenz's paper, which appeared in an obscure journal, was largely overlooked for some years. The term *chaos* was first time used by Li and Yorke in their 1975 paper "Period three implies chaos" [3]. In 1976, May published an influential article describing how simple nonlinear systems can exhibit complex, chaotic behavior [4]. In the late 1970s, the cascade of period-doublings, which form one of the commonest routes to chaos, was analyzed by Feigenbaum [5]. Over the past two decades there has been a great advancement in the theory of *nonlinear dynamics* and it has been found that various and interesting nonlinear phenomena are very common in a large number of physical systems. Chaos is such a widespread phenomenon that it has now been reported almost in every scientific discipline: astronomy, biology, biophysics, chemistry, engineering, geology, mathematics, medicine, meteorology, plasmas, physics and even the social sciences.

It is no coincidence that computers have permeated society during the same two decades in which chaos has grown into an independent field of research. Actually, the available computing power has spurred much of the research in chaotic dynamics. The reason is that computers can calculate solutions of nonlinear systems. This is extremely important, since unlike linear systems, where closed-form solutions can be written, few nonlinear systems and no chaotic systems possess closed-form solutions. Computers allow numerical "experiments" to be performed quickly and easily: parameters can be changed, system equations modified and solutions displayed. Therefore, *simulations* represents a powerful tool for gaining intuition about nonlinear systems and for exploring the exciting terrain of chaotic dynamics and they are used to this end during this thesis, too. However, simulations have their limitations. Computers have finite precision and inevitably generate errors when evaluating floating-point expressions. Furthermore, they are naturally discrete-time and there are unavoidable errors when they are used to simulate continuous-time systems. Finally, a simulation is of little or no help in proving theoretical results since even if the result of a simulation were completely accurate, it is just one solution of one system from one initial condition using one set of parameter values. The moral is that, although simulations are a useful tool, their results must be interpreted carefully, checked against intuition and theory, and used only for purposes for which they are suited.

1-2 SOURCES OF NONLINEARITY IN POWER CONVERTERS

The application area chosen in this thesis for the study of nonlinear phenomena, with an emphasis on chaotic behavior, is represented by *power converters*. Although they do not have an end of their own, power converters are always an intermediary between an energy producer and an energy consumer. The field is one of growing importance: it is estimated that during the twenty-first century, 90% of the electrical energy generated in developed countries will be processed by power converters before its final consumption. This "green" technology has three main aims:

- To convert electrical energy from one form to another and to facilitate its regulation and control
- To achieve high conversion efficiency and therefore low waste heat
- To minimize the mass of power converters and the equipment (such as motors) that they drive

There are four basic types of power converter, since electrical power supplies can be either DC or AC: AC-DC converters (also called rectifiers), DC-AC converters (also called inverters), DC-DC converters and AC-AC converters. Here AC typically denotes nominally sinusoidal voltage waveforms, while DC denotes nominally constant voltage waveforms. Small deviations from nominal are tolerable. A DC-DC converter and an inverter are subject of the study comprised in present thesis.

Power converters technology is increasingly found in the home and workplace [6,7,8,9]. Familiar examples are the domestic light dimmer, switched-mode power supplies in personal computers, heating and lighting controls, electronic ballasts for fluorescent lamps, drives for industrial motion control, induction heating, battery chargers, traction applications such as locomotives, solid-state relays and circuit breakers, off-line DC power supplies, spacecraft power systems, uninterruptible power supplies (UPSs), conditioning for alternative energy sources, automobile electronics, electric vehicles, etc.

In order to reduce energy costs, high efficiency is needed, but also because it reduces the amount of dissipated heat that must be removed from the power converter. In large, high-power systems, efficiencies of higher than 99% can be obtained, while small, low-power systems may have efficiencies closer to 80%. The goal of high efficiency conditionates that the power processing components of the circuit be close to lossless. Two basic groups that can be approximated by real components are available:

- Switching components, like transistors and diodes. They are operated cyclically and serve to vary the interconnections or the topological state of the circuit during a cycle. Switches turn on and off in response to an applied signal, which in feedback-controlled systems depends on the state variables. Passive switches (diodes) have a highly nonlinear v - i characteristic.
- Reactive (energy storing) components, like inductors and capacitors. They are characterized by differential equations: $v = L\ di/dt$ for an inductor, $i = C\ dv/dt$ for a capacitor. The capacitors and inductors perform filtering actions, regulating power flows by absorbing, storing and supplying energy.

Power converters use components from both groups. The switching components steer the energy around the circuit, while the reactive components act as intermediate energy stores and input/output reservoirs. Ideal switches, capacitors and inductors do not dissipate power and circuits containing only such elements do not dissipate power neither (provided that the switching operations do not result in impulsive currents or voltages, a constraint that is respected by power converters). In particular, an ideal switch has zero voltage across itself in its on (or closed, or conducting) state, zero current through itself in its off (or open, or blocking) state and requires zero time to make a transition between these two states. Therefore, its power dissipation is always zero. Of course, practical components diverge from ideal behavior, resulting in some power dissipation. However, for the types of dynamic behavior examined in this thesis, it suffices to assume *ideal* components.

The presence of both types of component detailed above implies that the circuits are *nonlinear, time-varying dynamical systems*, with two implications:

- Power converters are difficult to analyze
- Power converters are likely to show a wealth of unusual behavior.

There are also several unavoidable sources of unwanted nonlinearity in practical power converters:

- The semiconductor switching devices have intrinsically nonlinear DC characteristics. They also have nonlinear capacitances and most suffer from minority carrier charge storage.
- Nonlinear inductances abound: transformers, chokes, magnetic amplifiers and saturable inductors used in snubbers.
- The control circuits usually involve nonlinear components: comparators, PWMs, multipliers, phase-locked loops, monostables and digital controllers.

1-3 LIMITATIONS OF CONVENTIONAL APPROACHES

Power converters are tipically modeled by taking an average over a switching cycle, an approach first proposed by Wester [10]. Since a linear model is required by conventional control theory, the averaged circuit is generally linearized about a suitable operating point. State space averaging, developed by Čuk, operates on the state equations of the circuit [11,12]. "Injected and absorbed" currents are used by an alternative method [13]. Vorperian suggested a method of treating the switch-diode combination in isolation from the converter circuit [14,15]. Regardless of the details, these methods have the same purpose: to replace the nonlinear, time-varying dynamical system with an averaged, linearized one. The justification is that when designing the control circuit, one need no longer be concerned with the microscopic details of the power switching. Clearly, something is lost in the process.

The conventional averaging technique gives a useful representation of the system and allows simple design procedures for operation in certain regimes. However, it has some evident limitations. For example, the standard analysis by averaging predicts that the buck DC-DC converter will be stable over the whole operating range of input voltage and load resistance. But it was revealed by numerical simulations and experiments that this converter exhibits subharmonics and chaos over a significant range of parameter values [16,17,18]. No method that relies upon linearization can predict such effects, which are typical to nonlinear systems. In addition, the process of averaging can suppress behavior that a more detailed model might display.

Some cases of instability can be predicted by nonlinear averaged models, e.g., the Hopf bifurcation in the autonomous Čuk converter [19]. However, the nonlinear averaged model is also of little or no use in predicting and analyzing subharmonics and chaos such exhibited by the already mentioned buck converter. For the Čuk converter, where nonlinear averaging can successfully predict the first instability, it failed to throw any light on the subsequent bifurcation sequences. More detailed analyses based on the other models and techniques may therefore be warranted for safe and reliable operation of a power converter. Power electronics researchers have begun only relatively recently to use the methodology of nonlinear dynamics in the analysis of power converters.

1-4 HISTORY OF INVESTIGATION OF NONLINEAR DYNAMICS AND CHAOS IN POWER CONVERTERS

In 1927 Van der Pol had observed first time chaotic effects in an electronic circuit [20,21]: a relaxation oscillator, containing a battery, a neon bulb, a capacitor and a resistor, was driven by a sinusoidal signal and tuned to generate subharmonics, but "an irregular noise" was often heard. Van der Pol dismissed this "noise" as a "subsidiary" phenomenon and for over 50 years there was little interest in explaining such phantom oscillations. Baillieul, Brockett and Washburn suggested that chaos could occur in DC-DC converters incorporating a pulse-width modulator (PWM) control in 1980 [22]. The first modern experimental report of electronic chaos (in a driven resonant circuit using a varactor diode as a nonlinear circuit) was published in 1981 by Linsay [23]. The driven resistance-inductance-diode circuit has a close relative in power converters, since when a transformer feeds a rectifier diode, the leakage inductance resonates with the diode's nonlinear capacitance to give a chaotic transient when excited by the switches. The first autonomous chaotic electronic circuit was built in 1983 by Chua and Matsumoto [24]. The double scroll oscillator (usually known simply as *Chua's circuit*) has been widely investigated as the archetypal chaotic electronic circuit [25].

Brockett and Wood presented in 1984 a conference paper describing chaos in a controlled buck DC-DC converter [26]. The first detailed analysis of chaos in power converters was a letter by Hamill and Jefferies in 1988 [27]. Chaos in a switching converter was further described by Wood at a 1989 conference [28] and several other ways by which chaos can appear in power converters were identified by Deane and Hamill soon after [29]. These ideas were further developed in [30,31], mainly concerned with prediction and experimental confirmation of chaos in DC-DC converters under various control schemes.

Trajectories obtained by the integration of the exact mathematical models were used by these initial investigations [32], but it was difficult to go beyond the empirical phenomena observation with this kind of system approach. After it was definitely proved that all feedback-controlled switching circuits are inherently nonlinear and exhibit various nonlinear phenomena, the efforts aimed to develop system modeling that permits the theoretical investigation of such phenomena. Hamill and Deane proposed nonlinear map-based modeling, taking the clue from system descriptions representative to nonlinear

dynamics literature [17]. Sampled-data modeling techniques of power electronic circuits presented in the textbook by Kassakian, Schlecht and Verghese [9] helped in this elaboration. The state variables of the investigated system are observed discretely at specific time instants in this method and it is obvious that the choice of sampling instant is not unique. A first version, known as stroboscopic sampling, was used by Banerjee and Chakrabarty [33], Chan and Tse [34], Marrero, Font and Verghese [35] in analyzing the current mode controlled converters. A second variant was proposed by Deane and Hamill in [17] and used by them in the study of the current mode controlled boost converter [30,31]. A third method was applied by Di Bernardo et al. in investigating the voltage-controlled buck converter [36,37,38,39].

Using these tools, researchers focused on the nonlinear dynamics of specific converters under PWM control. The voltage-controlled buck converter and the current mode controlled boost converter have received high research attention: the former because it exhibits a wealth of nonlinear phenomena and the latter because it is easy to obtain a closed form expression of the map, facilitating the analysis.

Numerical and experimental bifurcation diagrams of the voltage-controlled buck converter were presented by Deane and Hamill [17]. Fossas and Olivar investigated the stability of the periodic solutions, obtaining the conditions of instability [18]. Banerjee noted that multiple attractors coexisting with the main attractor are responsible for the sudden expansion of the chaotic attractor by interior crisis [40]. Di Bernardo et al. explored the bifurcation sequence in detail and concluded that a period-5 orbit organizes the enlarged attractor in five zones [38,39].

The nonlinear map-based model of the current mode controlled boost converter in closed form was deduced first time by Deane by sampling the state variables at every switch-on instant [31]. The equivalent stroboscopic map was developed by Chan and Tse [34] and this stimulated research in two directions. Banerjee and Chakrabarty tried to obtain a more exact model by including parasitic elements such as the resistances of the inductor and the capacitor and proved that the model can still be deduced in closed form [41]. On the other hand, it was revealed that under certain reasonable assumptions the discrete-time model leads to a simple one-dimensional piecewise-linear map suitable for analytical investigation. The map was obtained under switch-on sampling by Deane and Hamill [30] and under stroboscopic sampling by Banerjee, Ott, Yorke and Yuan [42]. The bifurcation phenomena of this converter were analyzed in detail using these tools [34].

Nonlinear dynamics of other power converters were also studied. Tse proved that the boost converter in discontinuous conduction mode is characterized by a one-dimensional smooth (continuous and everywhere differentiable) map, and this system exhibits the bifurcation phenomena (such as repeated period-doublings) peculiar to such maps [43]. Bifurcation phenomena in current mode controlled Čuk converters were also investigated by Tse and Chan [44].

DC-DC converters received most attention in the first years of investigating nonlinear dynamics of power electronic systems, mainly because such phenomena were first discovered in this class of systems. Dobson et al. detected in 1992 and 1993 that thyristor circuits used to model Static Var Control show a new sort of bifurcation phenomenon in which switching times change discontinuously as a parameter is varied [45,46]. This switching time bifurcation cannot be predicted by the Jacobian matrix of the fixed point. It was also shown that discrete-time modeling of such systems can result in discontinuous-time maps having multiple attractors. The practical importance of investigating ferroresonance (a tuned circuit involving a saturating inductor) [47,48,49,50,51] was that it is used to regulate voltages, but unintended ferroresonance in power systems can generate excessive voltages and currents [52]. Nonlinear phenomena were also studied in some other (high-power) systems. Sütő, Nagy and Masada analyzed the current control of an induction motor drive [53]. Chaos, quasiperiodicity, subharmonics by period-doubling and various crises were detected by Magauer and Banerjee in a system controlled by the tolerance-band PWM technique [54]. Many interesting bifurcation phenomena in power electronic induction machine drive systems were noticed and studied by Kuroe and Hayashi [55].

The basic idea of all these investigations was to obtain a discrete-time model of the system studied and to analyze the noted phenomena in terms of standard bifurcation theory for smooth maps developed in Mathematics and Physics. This methodology worked well in many cases, but in some cases very atypical bifurcation phenomena were noticed, e.g., direct transition from a periodic trajectory to a chaotic one [34,44,56] and nonsmooth period-doubling [31,34]. These phenomena could not be explained in terms of the bifurcation theory. Banerjee, Ott, Yorke and Yuan proved that in most of these systems the discret-time model leads to piecewise-smooth maps and the atypical bifurcations occurring in such systems are part of a new class called border-collision bifurcation [42,57]. Mathematicians like Nusse and Yorke demonstrated earlier that characteristic bifurcations can appear in piece-wise smooth maps, but no physical examples were known at that time

[58,59]. Actually, power converters offered the first examples of physical systems characterized by piecewise-smooth maps and this renewed the interest in the theoretical analysis of these systems. Banerjee et al. recently created the conceptual framework for understanding and categorizing such bifurcations [60,61]. Some work done earlier by Feigin has been brought to the English-speaking world [62]. Many empirically detected bifurcation phenomena have now theoretical explanations by this knowledge.

It is clear now that all three types of maps (smooth, piecewise-smooth and discontinuous) occur in power electronics, therefore bifurcation theory developed for these classes of maps is useful in understanding why the behavior of a power electronic system changes from one type to another as a parameter is varied.

Because of the increased demand for better flexibility in high-current, high-power applications, there is a recently renewed interest in systems of interconnected converters. Bifurcation phenomena such as period-doubling, border-collision [63], Neimark-Sacker bifurcation [64] were detected in systems of parallel connected DC-DC converters.

Experiments assisted many of the theoretical analyses mentioned above. Experimental observations of the bifurcations in the voltage-controlled buck converter were given by Deane and Hamill [29,17]. The numerical study of the current mode controlled boost converter in discontinuous [43] and continuous [65] conduction mode by Tse et al. was supported by test results. Experimental investigations on the buck [32] and boost [33] converters have been done by Chakrabarty, Poddar and Banerjee.

Controlling chaos into periodic state is an ambition of nonlinear dynamics researchers ever since Ott, Grebogi and Yorke published their pioneering work in 1990 [66]. Various strategies were developed in Physics and Mathematics and applied in practical systems such as lasers. For power converters similar methods have also been developed. Experimental control of chaos in the buck [67] and boost [68] converters were reported by Poddar, Chakrabarty and Banerjee. An adaptive control technique was developed by Di Bernardo [69]. The time-delay stabilization of periodic trajectories in a current mode controlled boost converter was achieved by Batlle, Fossas and Olivar [70]. Hamill concluded in a 1995 review paper that power converters operating under controlled chaos instead of a stable periodic state, might have a better dynamic response [71] – just as fighter aircraft are designed to be open-loop unstable but are then stabilized by feedback, making them more agile than conventional designs. Although quantitative understanding of this possibility has still to emerge, stabilized chaotic power converters might react more quickly, e.g., in moving fast from one commanded output voltage to another.

Questions about the usefulness of nonlinear phenomena in power electronics have to be posed after their reasonable understanding. One possible field of application is reducing electromagnetic interference (EMI) in switch-mode power supplies, which are notorious generators of both conducted and radiated EMI, owing to the high rates of change of voltage and current which are necessary for efficient operation. Several electromagnetic compatibility regulations are coming into operation in the aviation sector, where the problem is especially acute. Efforts have been made to oppose the problem by spreading the power converters spectrum by pseudorandom modulation of the clock frequency [72,73]. The review paper by Hamill suggested first that this problem could also be charged by deliberately using chaos [71]. Marrero, Font and Verghese noticed then that "a potential advantage of chaotic operation is that the switching spectrum is flattened" [35]. In 1996 Deane and Hamill experimentally proved a reduction of the spectral peaks for a chaotically operated converter [74]. However, some theoretical issues had to be addressed for bringing this possibility into engineering practice. First, a theory to calculate the average values of state variables under chaos is required to formulate design procedures for converters operated in chaos. Second, a theory for predicting the structure of the power spectrum of the converter under chaotic operation is demanded. Third, since there are periodic windows in the parameter space of most chaotic systems and a slight unintended parameter alteration can get the system out of the chaotic regime, reliable chaotic converter operation must be assured. Since under certain reasonable assumptions current mode controlled DC-DC converters lead to piecewise-linear one-dimensional maps, they have been used for the first assaults on all these theoretical problems. Isabelle reasoned that these piecewise-linear maps can be approximated by a smaller class for which the computation of average values is tractable, known as Markov maps [75]. Marrero et al. elaborated further the idea. The second problem has been engaged for DC-DC converters which can be modeled by piecewise-linear one-dimensional maps. A method for computing the line spectrum at the switching frequency and its harmonics was developed by Deane, Ashwin, Hamill and Jefferies [76]. The method was extended to the continuous part of the spectrum by Baranovski, Mögel, Schwarz and Woywode [77,78]. For the third problem, there have been two approaches. The control of chaos was used to stabilize the chaotic regime by Bueno and Marrero [79]. On the other hand, the theory of robust chaos (the analytical condition under which there would be no periodic window or coexisting attractor in a chaotic system) was developed by Banerjee, Yorke and Grebogi and they demonstrated that current mode controlled converters meet this condition [80].

The main purpose of this Ph.D. thesis is to offer a systemic approach for applying the ideas of nonlinear dynamics in the control of power electronic systems, with an emphasis on chaotic behavior. The dissertation is organized as follows. Chapter 2 introduces the basic methods of the advanced theory of nonlinear dynamical systems and illustrates their application in power electronics by a feedback-controlled resonant DC-DC buck converter. As chopper circuits converting a DC input to a DC output at a lower voltage, buck converters are ones of the simplest but most useful power converters. Circuits closely related to them are used in many switched-mode power supplies. An application of current importance is the conversion of the standard 5V DC supply used in computers to the 3.3V or less required by processor chips like those from the Pentium family. A buck converter for this purpose can achieve a practical efficiency of 92%, while a linear regulator would be only 66% efficient, producing four times as much waste heat. Although the example is at a low power level, buck converters are also used at several kilowatts. The investigated buck converter belongs to a family of special resonant DC-DC converters and the various nonlinear phenomena and bifurcations exhibited by its behavior (all three classical routes to chaos have been identified) were first time detected by the author, who also introduced two methods for the analytical confirmation of this behavior by studying the stability.

Chapter 3 proposes first time four control strategies for this resonant DC-DC converter, in the sense of suppressing the unstable (chaotic, quasiperiodic and subharmonic) regimes from its behavior, hereby ensuring the stable periodic operation required by applications. The first two methods are inspired from the area of control engineering, while the last two use algorithms typical to chaotic systems. This chapter reports also the experimental setup.

Chapter 4 illustrates another application of nonlinear dynamics theory in power electronics by a special type of high frequency time-sharing inverter, designed mostly for induction heating applications. The nonlinear phenomena (subharmonic generation) in this system are also revealed first time by this study. One of the control strategies introduced in the previous chapter is successfully applied to remove the unstable regimes from the operation of the feedback-controlled inverter.

No prior knowledge of nonlinear systems is assumed. Experimental results back up the nonlinear phenomena discovered by computer aided simulations of the investigated systems. Appendixes are included to illustrate the software and experimental environment used throughout this study.

CHAPTER 2

ANALYSIS OF NONLINEAR DYNAMICS AND CHAOTIC BEHAVIOR OF A FEEDBACK-CONTROLLED RESONANT DC-DC CONVERTER

A resonant buck converter, whose output voltage is controlled by constant frequency PWM, is operated in symmetrical continuous conduction mode. A general review of the converters (section 2-1) is followed by the presentation of the configuration (section 2-2) and operation (section 2-3) of the system studied, including the basic steady-state relations and the description of the PWM control feedback loop. Phenomena in this nonlinear control loop are investigated by computer simulations (section 2-4). Quasiperiodic (subsection 2-4-1), period-doubling (subsection 2-4-2) and intermittency (subsection 2-4-2) route to chaos are detected first time in this converter as a result of varying the control gain. The observed bifurcation behavior is theoretically confirmed by the stability analysis of this variable structure, piecewise linear, nonlinear system. Two methods are introduced in order to perform the stability analysis: the first uses the Poincaré map function, while the second applies the Rácz method (section 2-5).

2-1 GENERAL REVIEW

The role of the DC-DC converters is to interface two DC systems and to control the power-flow between them. Their principal function is similar to the transformers' used in AC circuits, but the ratio of the output voltage/current and input voltage/current is continuously controllable by electric control signals. The voltage/current ratio can be smaller or bigger than unity. Often the input to these converters is an unregulated DC voltage, which is obtained by rectifying the line voltage, therefore, it will fluctuate due to changes in the line-voltage magnitude. The function of the converters is to convert the unregulated DC input into a controlled DC output at a desired voltage level. Their employment is very

extensive. The DC-DC converters are widely used in regulated switch-mode DC power supplies in sensors, controllers, transducers, computers, commercial electronics etc. They are also frequently used in DC motor drive applications, mainly in battery supplied vehicles and in electric cars, airplanes, spaceships, where on-board regulated DC power supplies are required. Their applications in plasma, arc, electron beam technologies, nuclear physics, solar energy conversion are also significant [8].

The usual building blocks of these converters are the electric switches, capacitors and inductors:

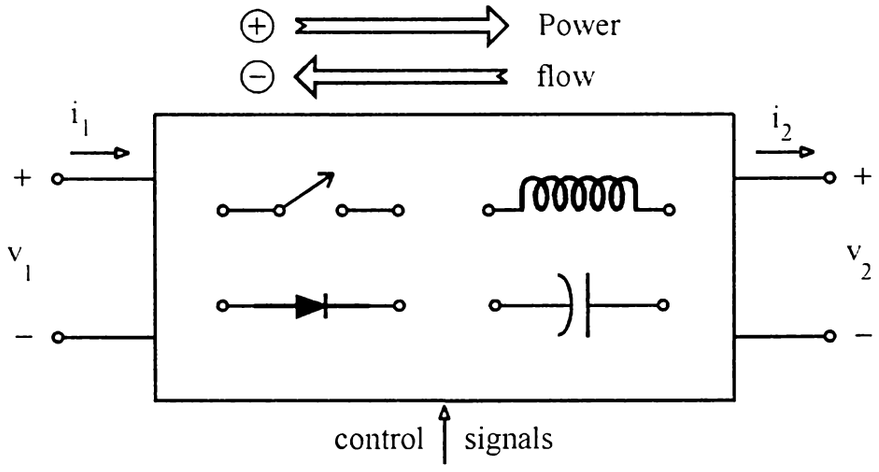

Figure 2-1 DC-DC converters

According to the direction of output current and voltage, the converters can operate in one-quadrant, two-quadrant and four-quadrant. Power flow is unidirectional at the first class and bidirectional at the other two. One directional power flow means that the only possible streaming direction of the power is from the input side towards the output side. Bidirectional power flow makes possible the streaming of the power in both directions between the input and output terminals. There is a direct path between the input and output terminals in direct converters, and there is no direct path among them in indirect converters.

Depending on the switching mode DC-DC converters can be hard-switched or soft-switched. Hard switching means that neither the voltage nor the current on the switch is zero at the initialization of the switching action. At soft switching converters the current and/or the voltage is zero in the switching moment. The power loss is significant at hard-switched converters even at high frequencies. The soft-switched converters (or resonant

converters) can be operated even at higher frequencies because of their smaller switching losses.

The basic converter topologies are the step-down and the step-up converters. The step-down or buck converters can only reduce the input voltage ($v_1 \geq v_2$ in Fig. 2-1), the step-up or boost converters can only increase the input voltage ($v_1 \leq v_2$ in Fig.2-1). The step-up/down (buck & boost) converters are combinations of the two basic topologies and can produce output voltage that can be higher or lower than the input voltage.

Converters have two principal shortcomings when their switches are operated in switch mode [8]:

- During the turn on and turn off time, high current and voltage appear simultaneously in and across the switches producing significant power losses in them, that is, high switching stresses. The power loss increases linearly with the switching frequency. To maintain a reasonable efficiency, the value of the switching frequency must be limited. However, it must be mentioned that by pushing the switching frequency to higher range the size and weight of the converters are reducible.
- The second shortcoming is the electromagnetic interference (EMI) generated by the large dv/dt and di/dt values of the switching variables.

Resonant converters can minimize these shortcomings. In these converters an *LC* circuit is always incorporated. Its resonant frequency can be either equal to the switching frequency or can substantially deviate. If they are identical then the unwanted harmonics are removed by the circuit. The switching frequency – in both cases – is one of the means for controlling the output power and voltage. Some advantages of the resonant converters over the conventional ones should be highlighted. These are the sinusoidal-like wave shapes, inherent filter action, reduced dv/dt, di/dt and EMI. In addition some resonant converters can accomplish zero current and/or zero voltage across the switches at the switching instant and reduce significantly the switching losses. An advantageous feature of the soft-switched resonant converters is the much lower switching stresses. However, it must be confessed that the price of it is the higher forward currents and reverse voltages the switches must endure. The resonant DC-DC converters are used in applications as induction heating, very high frequency DC-DC power supplies, sonar transmitters, ballast for fluorescent lamps, power supplies for laser cutting machines, ultrasonic generators, etc.

A new family of dual channel resonant switching DC-DC converters was introduced in 1989 on the 3rd European Conference on Power Electronics and Applications

[81]. These converters have strong similarities with the conventional buck, boost and buck&boost choppers in their configurations, but regarding the operation the differences are significant, The currents of the controlled switches are mostly sinusoidal. They are called Zero Voltage Turn-off Quasi-Resonant Converters (ZVT-QRC) because the voltage across the controlled switches are practically zero during their turn-off (assuming diodes on the output side). The switching elements can be SCRs, BJTs, IGBTs or other controllable switches at the input side, but the employment of diodes is also possible at the output side. The converters work on their resonant-frequency, determined by the inductor and capacitor elements. The frequency should be high, since in this manner the size and weight decrease. The range of the output power is broad, because the applied elements are produced from low power to high power (diodes, SCR-s, GTO-s etc.). Their output voltages can be changed in wide range and they can be either higher or lower than the input ones, depending on the configuration. One of the converters can work as a current generator too.

The advantageous features of the converters are as follows [81]:

- The converter is capable of interchanging a controlled part of the power drawn from the two DC power sources having different voltages by interconnecting the two channels of the converter through a switched capacitance, which transfers power from one part of the converter to the other one; hence, the ratio control of the two output power flows can provide either symmetrical or asymmetrical output voltages.
- It suits for DC uninterruptible power supply (UPS): one of the two sources can be removed (e.g., during battery change) without disturbing the power supply in the output side.
- Greatly reduced switching stress and loss in switching devices by turning them on and off either at zero voltage or current.
- Further reduction in switching stress and loss in switching devices by generating only or mainly sinusoidal voltages and currents.
- High or ultra high switching frequency with high bandwidth.
- Good efficiency.
- High power density.
- Considerable size and weight reduction.
- Low noise and EMI level.

The disadvantages [81]:

- 'Floating' output; no common ground terminal can be used between the input and output side.
- Larger forward currents and reverse voltages in and across the switching devices.
- Higher peak current on the inductors and peak voltage on capacitor(s).
- Complicated control circuitry is needed even in case of asymmetrical operation.

In this chapter, the converters are analyzed in steady-state. The switches are treated as being ideal, and the losses in the inductive and the capacitive elements are neglected. The DC input voltage to the converters is assumed to have zero internal impedance. It could be a battery source; however, in most cases, the input is a diode rectified AC line voltage with a large filter capacitance, as shown in Fig. 2-2 to provide a low internal impedance and a low-ripple DC voltage source. In the output stage of the converter, a small filter is treated as an integral part of the DC-DC converter. Looking at the applications of these converters, it is found that they are very often used with an electrical isolation transformer in the switch-mode DC power supplies and almost always without an isolation transformer in case of DC motor drives. Therefore, to discuss the circuits in a generic manner, only the nonisolated converters are considered, since the electrical isolation is an added modification. The output of the converter is assumed to supply a load that can be represented by an equivalent resistance, as is usually the case in switch-mode DC power supplies.

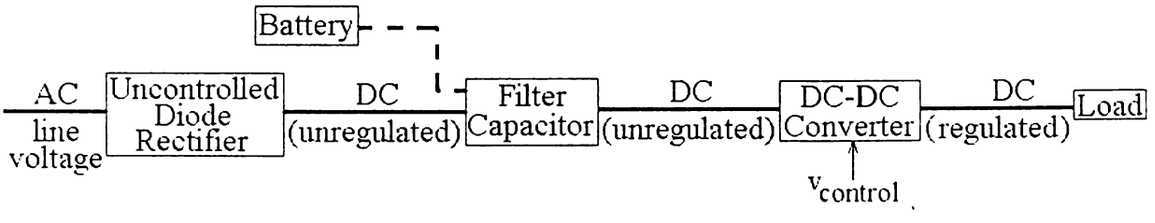

Figure 2-2 A DC-DC converter system

2-2 CONVERTER CONFIGURATION

The resonant converter family is built up on two basic blocks B_{to} (Fig. 2-3a) and B_{off} (Fig. 2-3b). Both have controlled switches S_1 and S_2 and one inductance L. The controlled switches can conduct current flowing to point P in B_{to} and flowing off point P in B_{off}.

The general configuration of the converters is shown in Fig 2-4 where two switched capacitances C and βC are used beside the building blocks. A common feature of the different versions is that they transmit power from input to output through two channels, the so-called positive and negative ones, coupled by these resonating capacitors.

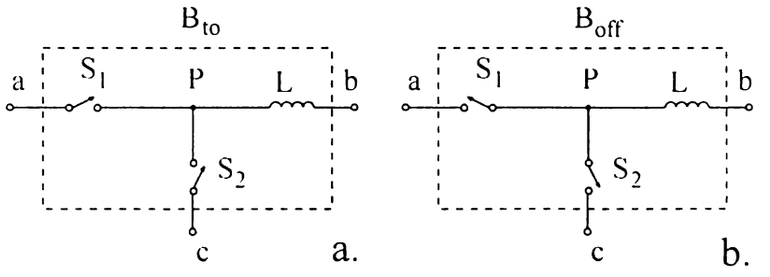

Figure 2-3 Basic building blocks

The capacitances across the input and output terminals for short-circuiting the high frequency components of the input and output currents are not shown. Table 2-1 summarizes the set-up of the three configurations by the two building blocks and their connections to terminals x, y and z. The names of the configurations are the same as those of the corresponding choppers: buck, boost and buck&boost. Suffixes i and o refer to input and output while suffixes p and n refer to positive and negative, respectively.

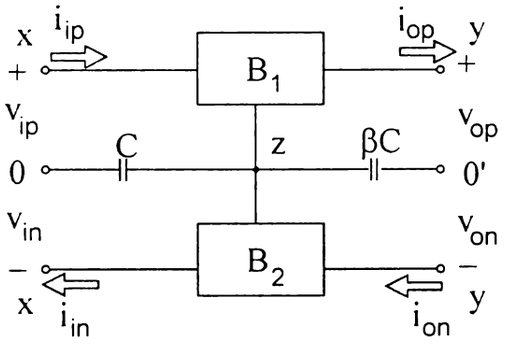

Figure 2-4 General configuration of the converters

Table 2-1 Set up of the converters

	x	*y*	*z*	B_1	B_2
Buck	a	b	c	B_{to}	B_{off}
Boost	b	c	a	B_{off}	B_{to}
B&B	c	a	b	B_{to}	B_{off}

Using Fig. 2-3, Fig. 2-4 and Table 2-1, the three configurations are shown in Fig. 2-5.

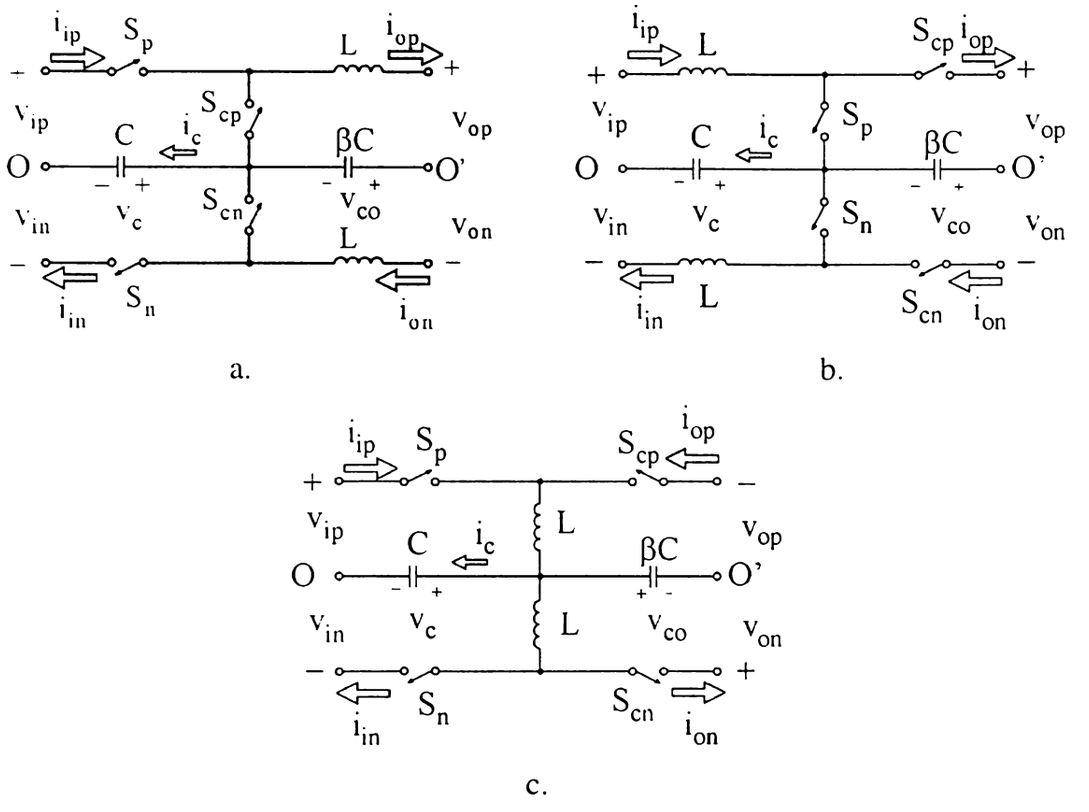

Figure 2-5 Configurations of buck (a), boost (b) and buck & boost (c) converters

Four different converter versions can be derived from any of these configurations, therefore, altogether twelve different versions are available [81]. The first three configurations have a single resonant circuit with energy storage elements L and C. They are called *resonant converters* (RC). The RC configurations can readily be obtained by replacing the capacitor βC with short circuit in the buck and in the buck & boost converters and with an interrupt in the boost converter. The next three configurations have double resonant circuits with components L, C, βC. They are called *double resonant converters* (DRC). Both RCs and DRCs can contain either controlled switches (three configurations) or diodes (three configurations) in place of clamping switches S_{cp} and S_{cn}.

Our investigation is restricted to the buck configuration depicted in Fig. 2-6 (including the output filter and load). This version applies controlled switches (IGBTs, BJTs, MOSFETs or other switches) conducting current in the direction of arrow (e.g., to point P for the positive channel). The configuration corresponds to a RC converter, with a single resonant circuit (the capacitance βC has been replaced by short circuit).

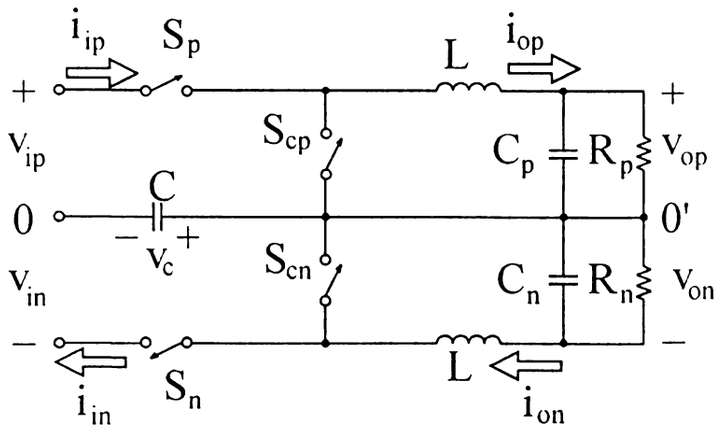

Figure 2-6 Resonant buck converter

2-3 CONVERTER OPERATION

The assumptions used are as follows:

- Idealized and lossless circuit components.
- Constant and smooth input ($v_{ip} > 0$, $v_{in} > 0$) and output ($v_{op} > 0$, $v_{on} > 0$) voltages.
- Steady-state operation.
- Neglected commutation times.

The controlled switches within one channel are always in complementary states (i.e., when S_p is on, S_{cp} is off and vice versa). By turning-on switch S_p, a sinusoidal current pulse i_{ip} is developed from $\omega t = 0$ to α_p ($\omega = 1/\sqrt{LC}$) in circuit S_p, L, v_{op}, C and v_{ip} (Fig. 2-7). The currents are $i_{ip}=i_{op}=i_{cp}$ in interval $0 \le \omega t \le \alpha_p$. The capacitor voltage v_c swings from v_{cn} to v_{cp} ($v_{cn} < 0$). By turning-on switch S_{cp} at α_p the choke current commutes from S_p to S_{cp}. The energy stored in the choke at $\omega t = \alpha_p$ is depleted in the interval $\alpha_p < \omega t < \omega T_s$ where $T_s = 1/f_s$ is the switching period. In the discontinuous current conduction mode (DCM) of operation the stored energy is entirely depleted in interval $\alpha < \omega t < \alpha_{ep}$, where α_{ep} denotes the extinction angle of the inductor current. In DCM the current is zero between α_{ep} and ωT_s (Fig. 2-7). In the continuous-conduction mode (CCM) of operation the inductor current flows continuously: $i_{op}>0$ (Fig. 2-8). The inductor current i_{op} decreases in both cases in a linear fashion. After turning-on S_{cp} the capacitor voltage v_c stops changing. It keeps its value v_{cp} (Fig. 2-7, 2-8). The same process takes place at the negative

side resulting in a negative current pulse and condenser voltage swing after turning-on S_n at the beginning of the next half cycle at $\omega T_s/2$ (Fig. 2-7, 2-8) [82].

The converter can operate both in symmetrical and in asymmetrical mode. The symmetrical operation illustrated in figures above requires identical components of the two channels and identical load resistance R. It can be considered as a particular case of the more general asymmetrical operation. In symmetrical case the commutation angles (α_p and α_n), the input voltages (v_{ip}, v_{in}), the output voltages (v_{op}, v_{on}) and the peak condenser voltages (v_{cp} and $|v_{cn}|$) are identical. In general $v_{ip} \neq v_{in}$; $v_{op} \neq v_{on}$; $v_{cp} \neq -v_{cn}$; $\alpha_p \neq \alpha_n$ and $\alpha_{ep} \neq \alpha_{en}$. There is no energy exchange between the positive and the negative channels in the symmetrical case. In asymmetrical operation the energy exchange between the two channels is accomplished by the switched capacitor.

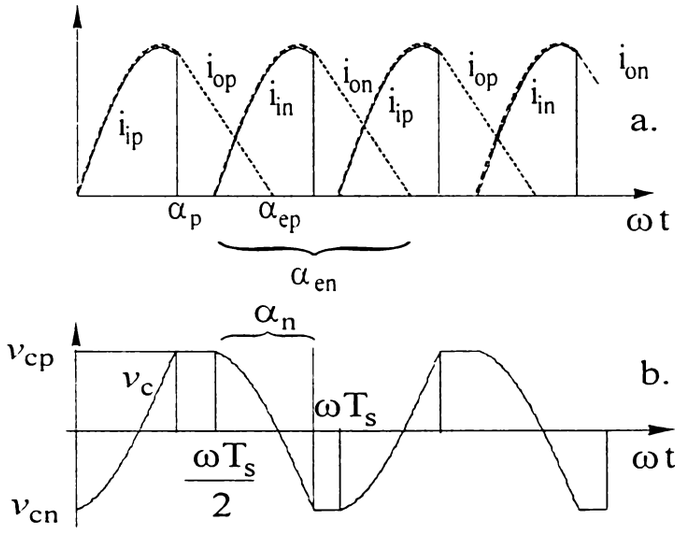

Figure 2-7 Time functions of input and output (inductor) currents (a) and condenser voltage (b) in DCM

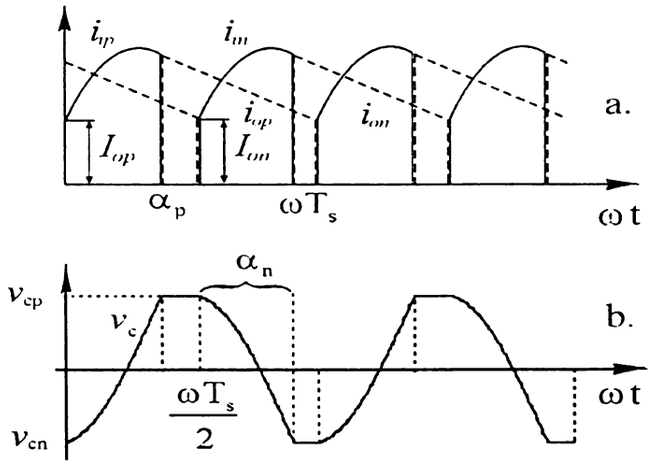

Figure 2-8 Time functions of input and output (inductor) currents (a) and condenser voltage (b) in CCM

The input variables directly set by us are v_{ip}, v_{in}, α_p, α_n, f_s and R. The input voltages v_{ip}, v_{in} and the load resistance R are usually given, but the selection of the switching angles α_p, α_n and the switching frequency f_s depends on the control. Condition $f_s \le f_r$ must hold, where $f_r = 1/(2\pi\sqrt{LC})$ is the resonant frequency. The reason is simple. The change of condenser voltage v_c in one direction must be completed before its change gets started in the opposite direction (Fig. 2-7, 2-8). Switch S_p and S_n must not be turned on simultaneously, $\alpha_p, \alpha_n \le \omega T_s / 2$ must hold, the two input currents may flow only in separate intervals. The output variables determined by the set of input variables are v_{op}, v_{on}, v_{cp}, v_{cn}.

2-3-1 BASIC STEADY-STATE RELATIONS

Assuming symmetrical continuous conduction mode, the current time functions in the chokes are [83]

$$i_o(\omega t) = I_o \cos\omega t + I_k \sin\omega t \tag{2-1}$$

in the interval $0 \le \omega t \le \alpha$, and

$$i_o(\omega t) = I_o \cos\alpha + I_k \sin\alpha - \frac{V_o/2}{Z}(\omega t - \alpha) \tag{2-2}$$

in the interval $\alpha \le \omega t \le \omega T_s$, where $I_o = i_o(\omega t = 0)$ (Fig. 2-8), $V_{op} = V_{on} = V_o / 2$ are the ripple free instantaneous output voltages, $Z = \sqrt{L/C}$ is the characteristic impedance, furthermore

$$I_k = \frac{V_c - (V_o/2) + (v_i/2)}{Z} \tag{2-3}$$

where $V_c = v_{cp} = -v_{cn}$ (Fig. 2-8) and $v_i / 2 = v_{ip} = v_{in}$.

The choke current is the same at $\omega t = 0$ and at $\omega t = \omega T_s$

$$i_o(\omega t = 0) = i_o(\omega t = \omega T_s) = I_o \tag{2-4}$$

The capacitor voltage change is the result of current $i_c = i_o$ in interval $0 \le \omega t \le \alpha$

$$Z\int_0^{\alpha} i_o \, d(\omega t) = 2V_c \tag{2-5}$$

Substituting (2-1) into (2-5)

$$Z[I_o \sin\alpha + I_k(1-\cos\alpha)] = 2V_c \tag{2-6}$$

and (2-2) into (2-4)

$$I_o = \frac{I_k \sin\alpha - \frac{V_o}{2}\cdot\frac{\omega T_s - \alpha}{Z}}{1-\cos\alpha} \tag{2-7}$$

Let us substitute now I_o from (2-7) into (2-6)

$$-I_k + \frac{V_c}{Z} + \frac{V_o}{4Z}(\omega T_s - \alpha)\frac{\sin\alpha}{1-\cos\alpha} = 0 \tag{2-8}$$

The output voltage is on the basis of (2-8) and (2-3)

$$V_o = \frac{v_i}{1 + \frac{\omega T_s - \alpha}{2}\cdot\frac{\sin\alpha}{1-\cos\alpha}} \tag{2-9}$$

2-3-2 THE PWM SWITCH CONTROL

In DC-DC converters, the average DC output voltage must be controlled to equal a desired level, though the input voltage and the output load may fluctuate. The analytical relationship (2-9) deduced above reveals that for a given input voltage the output voltages are controlled by the on durations α_p, α_n of the controlled switches. One of the methods for controlling the switches employs switching at a constant frequency and adjusting the on duration of the switch to control the output voltage. In this method, called *pulse-width modulation* (PWM) switching, the switch duty ratio, defined as the ratio of the on duration to the switching time period, is varied.

For controlling the output voltage

$$v_o = v_{op} + v_{on} \tag{2-10}$$

by PWM switching a feedback control loop is applied (Fig. 2-9a). The control signal voltage v_{con} is obtained through proportional control - by amplifying the error signal (the difference between the actual output voltage v_o and its desired value v_{ref}) - and is compared to a repetitive sawtooth waveform (Fig. 2-9b) [82].

When the amplified error signal v_{con} is greater than the sawtooth waveform, the switch control signal (Fig. 2-9c) becomes high and the selected switch turns on. Otherwise, the switch is off. The controlled switches are S_p and S_n (the switches within one channel are in complementary states) and they are controlled alternatively, i.e., the switch control signal for the switch in one channel is generated in one period of the sawtooth wave and

for the switch in the other channel in the next period. Hence, the period of the sawtooth wave is half of the switching period: $T_r = T_s / 2$.

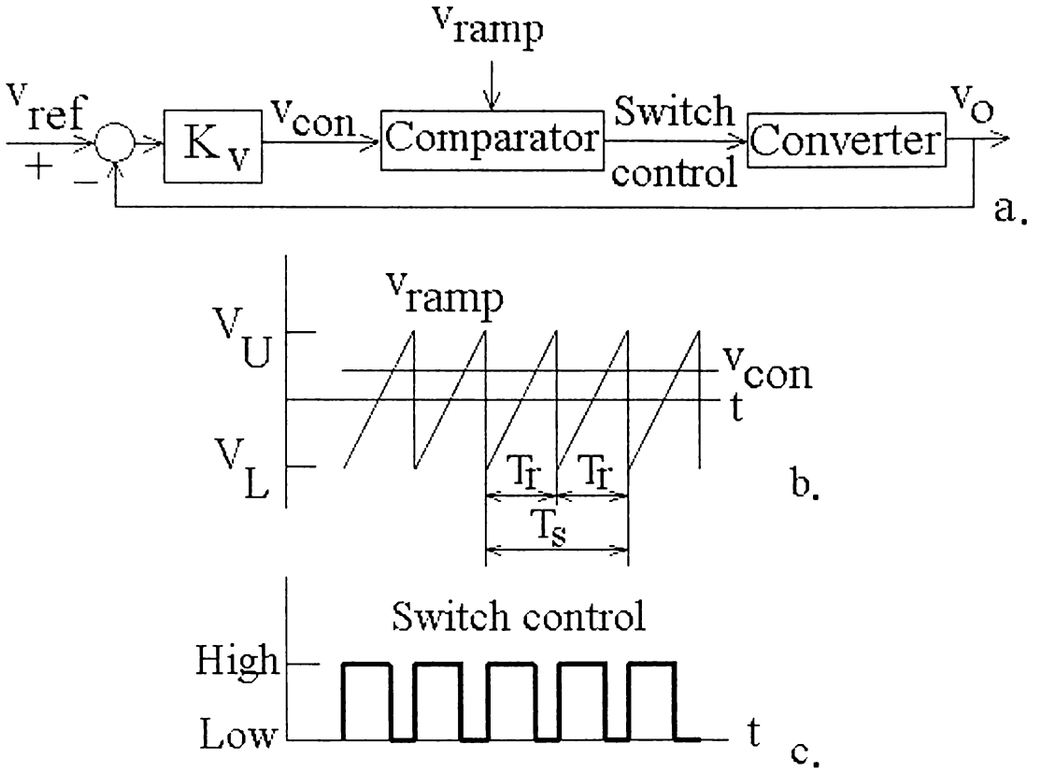

Figure 2-9 PWM switching control loop: block diagram (a), comparator signals (b) and switch control signals (c)

2-4 STEADY-STATE ANALYSIS

The main objective of the following study is the investigation of the phenomena in the presented feedback loop, in steady-state, in order to discover the various possible behaviors of this nonlinear dynamic system. Since the voltage gain K_V of the proportional controller in the PWM switching loop is a design parameter that can be changed at will, the presentation will be restricted to the effect of variation of this parameter, but the methods and the results remain valid in case of other parameters (parameters of PWM switching, load, DC input and reference voltages).

The study proposed assumes the calculation of the system variables. The independent energy storage elements are: two series inductances, two load capacitances and one series capacitance, altogether five elements, with five state variables defining the *state*

space: output voltages v_{op} and v_{om}, condenser voltage v_c, choke currents i_{op} and i_{om}. A usual mode of investigation and presentation is to begin with theory and analytical study, followed by simulations and/or experiments. However, it was emphasized in the previous chapter that, very often, simulations and experiments have been more useful when they preceded analysis in studying nonlinear dynamics of physical systems. This study reflects this practical mode of investigation, i.e., it starts with a series of computer simulation studies which identify important bifurcation phenomena. This will be followed by an analytical study of the system which establishes formally the possibility of bifurcation.

The values of parameters and variables used in the analysis presented in this chapter are specified in Appendix A. Those belonging to the converter basic configuration were chosen to ensure $f_s / f_r = 1$ and symmetrical CCM in open loop operation.

The computer simulations were performed in MATLAB environment. MATLAB programs and Simulink models were developed for the calculation of the state variables of the nonlinear system. The Simulink models for the converter configuration with the PWM switching are drawn in Appendix B.

2-4-1 QUASIPERIODIC ROUTE TO CHAOS

2-4-1-1 POINCARÉ MAPS

One of the most important steps in investigating the nonlinear phenomena in any physical dynamical system is deciding how to describe its dynamics. DC-DC converters are most naturally modeled as piecewise linear systems of ordinary differential equations. These are continuous-time models and can be used to obtain an analytical and numerical description of the dynamics of the physical systems. However, it was revealed in the previous chapter that when one's aim is to understand the nature of the nonlinear phenomena exhibited by these systems, there are severe limitations of these models. The use of alternative, discrete-time models for these continuous-time dynamical systems, can be very useful.

One of the most useful methods of discretization involves the so-called *Poincaré map*, due to French scientist Henri de Poincaré [1]. The use of appropriate system discretizations by Poincaré maps will be defined in this section in order to perform the study of nonlinear phenomena in the converter behavior.

The systems of concern are the continuous-time dynamical systems. An nth-order continuous-time deterministic dynamical system is defined by a system of ordinary differential equations of the form:

$$\dot{x}(t) = f(x(t), t), \quad x(t_0) = x_0 \tag{2-11}$$

where $\dot{x} = dx/dt$, $x(t) \in \Re^n$ is the state at time t and $f : \Re^n \rightarrow \Re^n$ is called the *vector field*.

> ***Poincaré map:*** A technique that transforms an nth-order continuous-time system into an $(n-1)$th-order discrete-time system.

The Poincaré map's usefulness lies in the reduction of the order and in the fact that the *limit sets* (the state space equivalent of the steady-state) of the Poincaré map correspond to the limit sets of the underlying continuous-time system, as it will be shown through this chapter.

The standard technique of the Poincaré map from the theory of dynamical systems is defined for *autonomous systems*.

> ***Autonomous continuous-time system:*** A differential equation $\dot{x} = f(x)$ where the vector field does not depend on time. Since the vector field does not depend on time, the initial time may always be taken as $t_0 = 0$. The solution that passes through x_0 at time 0 is denoted by $\theta_t(x_0)$ and is called *trajectory*.

The conversion of the continuous-time dynamical system to a discrete-time dynamical system is carried out by using the concept of *Poincaré section*. For an n-dimensional continuous-time dynamical system a Poincaré section is an $(n-1)$-dimensional hyperplane in the state space which is intersected transversally by the trajectories. Considering a third-order system with the *limit cycle* (the limit set of a periodic solution) shown in Fig. 2-10, the Poincaré map is the set of points in the Poincaré plane produced by the trajectory by crossing the surface from one direction. The selection of Poincaré plane is arbitrary, but it requires advance knowledge of the position of a limit cycle [84].

The standard definition of the Poincaré map just presented gets a special interpretation for *non-autonomous systems*.

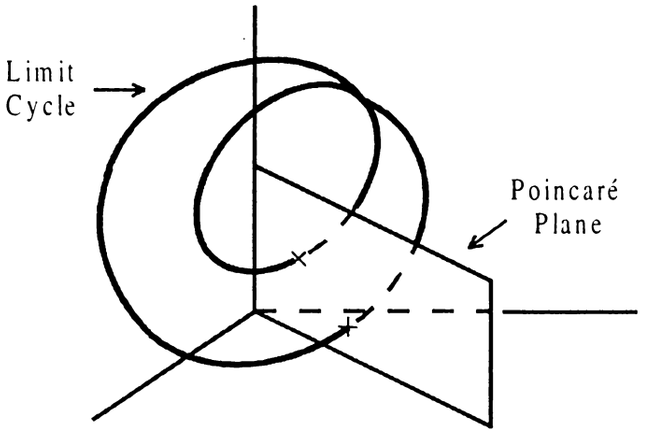

Figure 2-10 Poincaré map in the Poincaré plane

> ***Non-autonomous continuous-time system:*** A differential equation $\dot{x} = f(x,t)$ where the vector field depends on time. The solution (trajectory) that passes through x_0 at time t_0 is denoted by $\theta_t(x_0, t_0)$.

If there exists a $T > 0$ such that $f(x,t) = f(x,t+T)$ for all x and t, then the non-autonomous system is said to be *time periodic* with period T.

A non-autonomous nth-order time-periodic continuous system with period T may be transformed into an $(n+1)$th-order autonomous continuous system by appending time as an additional state variable: $x_{n+1} = t$. The resulting autonomous system is given by

$$\begin{aligned} \dot{x} &= f(x, x_{n+1}), & x(t_0) &= x_0 \\ \dot{x}_{n+1} &= 1, & x_{n+1}(t_0) &= t_0 \end{aligned} \tag{2-12}$$

and is periodic with period T, since f is time periodic with period T. The solution of (2-12) is

$$\begin{bmatrix} x(t) \\ x_{n+1}(t) \end{bmatrix} = \begin{bmatrix} \phi_t(x_0, t_0) \\ t \bmod T \end{bmatrix} \tag{2-13}$$

where the modulo function restricts $0 \le x_{n+1} < T$.

Due to (2-12) a time-periodic non-autonomous system can be considered a special case of an autonomous system and using the standard definition, a n-dimensional Poincaré section can be defined by

$$\Sigma = \{(x, x_{n+1}) \in \Re^n \times \Re_+ : x_{n+1} = t_0\} \tag{2-14}$$

Every T seconds, the trajectory (2-14) intersects Σ. The resulting Poincaré map $P : \Sigma \to \Sigma\ (\Re^n \to \Re^n)$ is defined by

$$x_{k+1} = P(x_k) = \phi_{t_0+T}(x_k, t_0) \tag{2-15}$$

and it can be thought of as a sampling of a single trajectory every T seconds, i.e.,

$$P^m(x_k) = \phi_{t_0+mT}(x_k, t_0), \quad m = 0, 1, \ldots \tag{2-16}$$

where $P^m = P(P(\ldots(P(\bullet))\ldots))$ is called the mth iterate of P and denotes P applied m times to the argument of the map.

This Poincaré map is similar to the action of a stroboscope flashing with period T.

> ***The Poincaré map for time-periodic non-autonomous systems*** is equivalent to sampling the trajectory at a rate equal to the forcing frequency.

The converter configuration studied is a time-period non-autonomous system with period equal to the switching period T_s. To produce a Poincaré map, one selects, say, two state variables, samples them once every switching cycle, and plots them as points in the plane of the two state variables. Examples will be shown through the following sections, where the Poincaré maps will be very useful in identifying the various steady-state behaviors.

2-4-1-2 BIFURCATION DIAGRAMS

Consider an nth-order continuous-time system

$$\dot{x}(t) = f_\mu(x(t), t), \quad x(t_0) = x_0 \tag{2-17}$$

whose vector field $f_\mu : \Re^n \to \Re^n$ is parameterized by a *control parameter* μ. As μ changes, the steady-state of the system changes, too. A small perturbation in μ typically produces small quantitative changes in the steady-state. E.g., changing slightly μ could change the position of the steady-state in state space slightly, along with its shape or size when the limit set is not an *equilibrium point* (corresponding to a stationary steady-state). But there exists also the possibility that a small change in μ may cause a limit set to undergo a qualitative change.

> ***Bifurcation:*** A qualitative change in a limit set as a parameter is infinitesimally perturbed. Examples are the creation or disappearance of a limit set and the change in stability type of a limit set.

Bifurcation value: A parameter value at which a bifurcation occurs. A system is structurally unstable at a bifurcation value.

A *structurally stable* vector field F is one for which sufficiently close vector fields F' have equivalent dynamics, that is, there exists a continuous invertible function which transforms F into F'. The set of bifurcation values is the set of parameter values μ at which the system is not structurally stable.

While state space, Poincaré maps, time- and frequency-domain measurements are useful for characterizing steady-state behaviors, nonlinear dynamics offers several other tools for summarizing qualitative information concerning bifurcations. One of the most useful ways for the presentation of the information is the so-called *bifurcation diagram*.

Bifurcation diagram: A plot that indicates the steady-state behavior of a system over a range of parameter values.

This diagram is a plot of the position of the limit sets versus the bifurcation parameter μ. In this way the bifurcation diagram shows the various states and the sudden changes of the system in steady-state (the bifurcations) as a result of the variations of one system parameter [85].

If it is desired to show by a bifurcation diagram how the behavior of a time-periodic non-autonomous system varies with some parameter, the Poincaré map, as defined at the end of the previous subsection, may be further simplified by selecting just a single state variable for observation. The Poincaré map is thereby reduced to a one-dimensional object and the second dimension of the plane can be employed to sweep the parameter over its range of interest. The resulting plot represents the bifurcation diagram and allows qualitative changes of behavior to be appreciated at a glance [86].

Accordingly, to generate this kind of diagram for the converter, the output voltage v_o was sampled and stored, in steady-state, at the start of every switching cycle ($v_{ok}=v_o(kT_s)$). With sufficient number of sets of steady-state data the bifurcation diagram can be obtained by plotting vertically the sampled output voltage whereas the voltage gain K_V is varied horizontally as a control parameter [82].

Such a representative bifurcation diagram, which reveals a first bifurcation in the behavior of the system, about $K_V \approx 4.5$, is shown in Fig. 2-11.

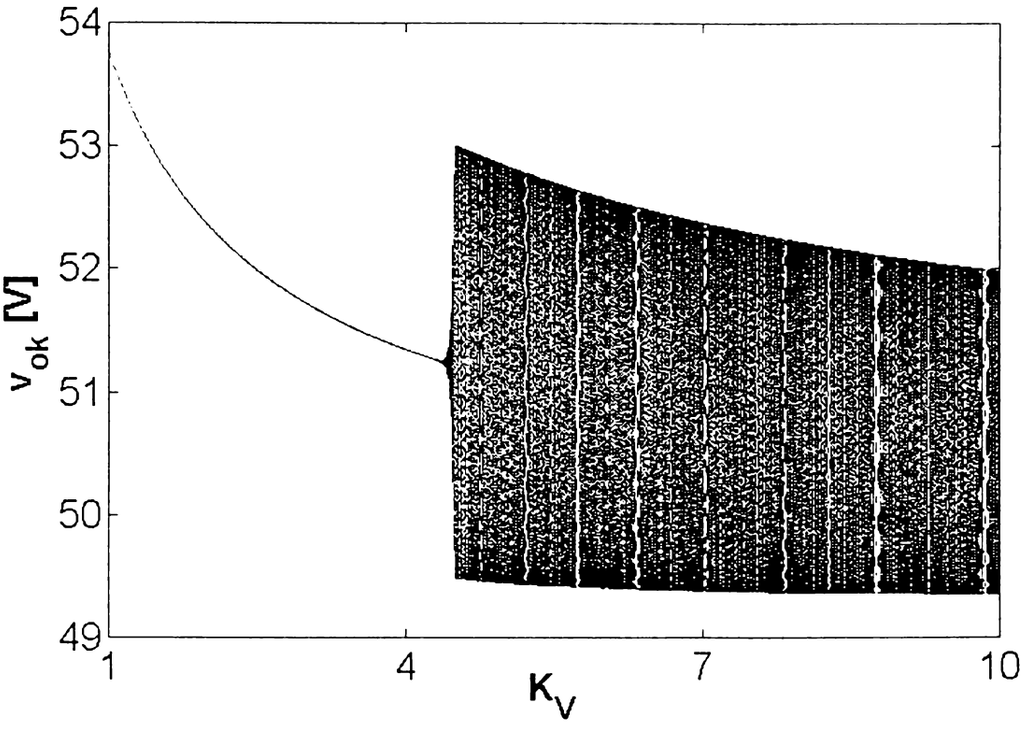

Figure 2-11 Bifurcation diagram

2-4-1-3 PERIODIC STEADY-STATE

Below the bifurcation value $K_V \approx 4.5$, there is just one single sampled value $v_{ok}=v_o(kT_s)$ for a given controller gain K_V in the bifurcation diagram from Fig. 2-11, i.e., the output voltage v_o repeats itself in each switching period T_s. This state is called *period-1*.

> ***Period-1 behavior:*** A solution of a time-periodic non-autonomous system that repeats itself with the forcing period.

The Poincaré Map Normal periodic operation - presented in Fig. 2-8 - sustains in this region and all state variables are periodic time waveforms with period T_s. As it was mentioned above, if the sampling time is chosen properly, the Poincaré map behaves similarly to a stroboscope, i.e., sampling with the switching period T_s, a periodic steady-state of the converter is represented as a single point provided that the initial transient is omitted (unless otherwise stated, all Poincaré maps are assumed to be for steady-state). This point is a *fixed point* for the Poincaré map. Fig. 2-12 presents the Poincaré map for the period-1 operation in the plane of output voltage $v_{ok}=v_o(kT_s)$ vs. inductor current $i_{opk}=i_{op}(kT_s)$ at $K_V = 2$.

> ***Fixed point:*** x^* is a fixed point of the map P if $x^* = P(x^*)$.

Period-1 behavior: A fixed point of the Poincaré map of a time-periodic non-autonomous system indicates a period-1 solution.

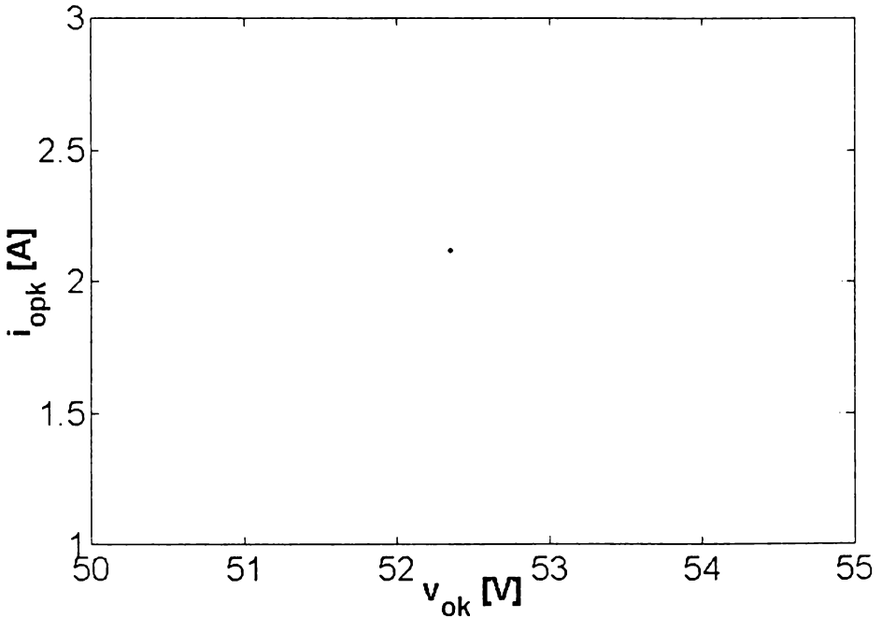

Figure 2-12 Poincaré map for period-1 operation ($K_V = 2$)

Time Domain The choke current i_{op} and the condenser voltage v_c are plotted in Fig. 2-13 and Fig. 2-14, at $K_V = 2$. The period-1 state is clearly visible in these figures. The control voltage v_{con} hits the ramp wave once per ramp cycle (Fig. 2-15).

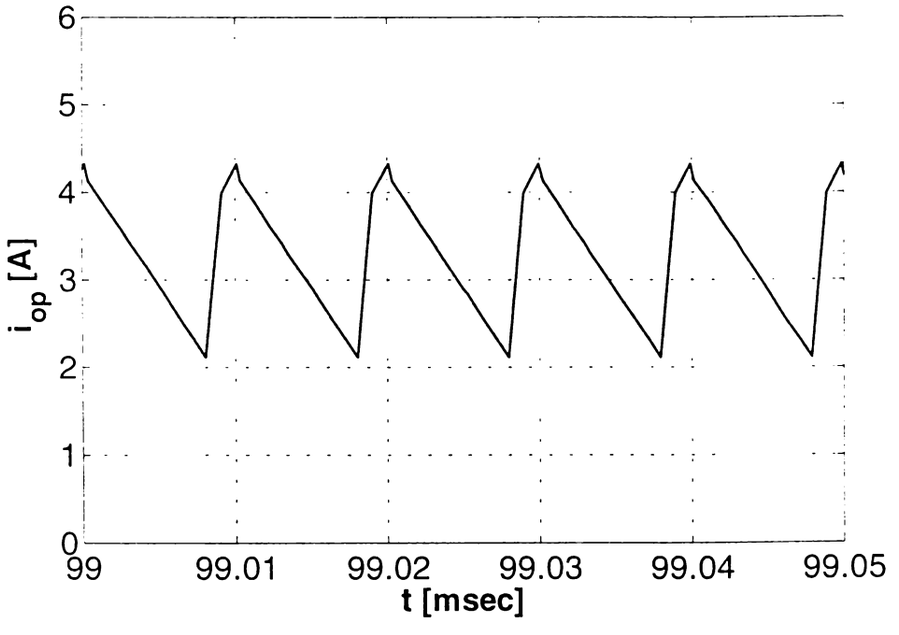

Figure 2-13 Inductor current in period-1 operation ($K_V = 2$)

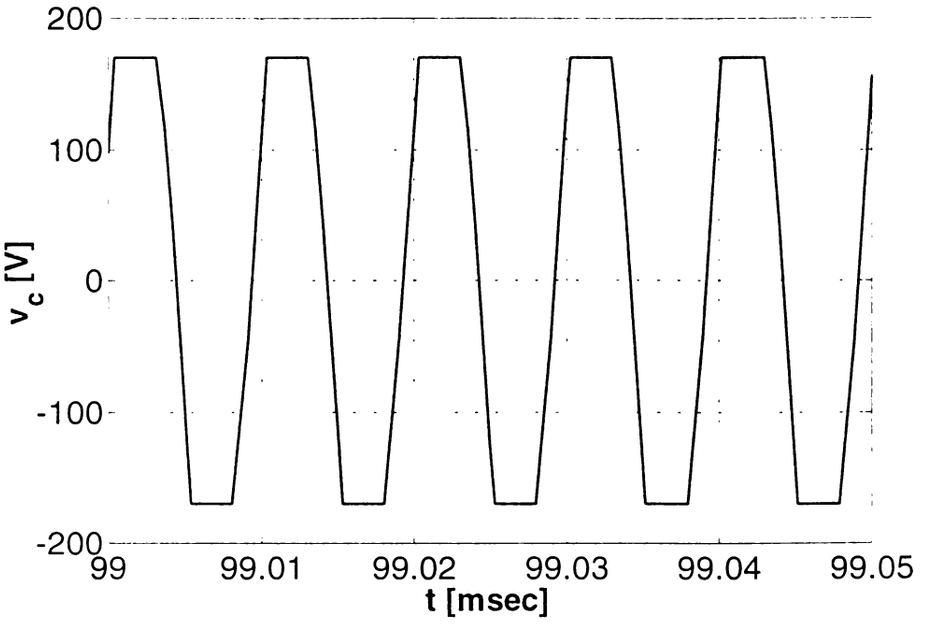

Figure 2-14 Condenser voltage in period-1 operation ($K_V = 2$)

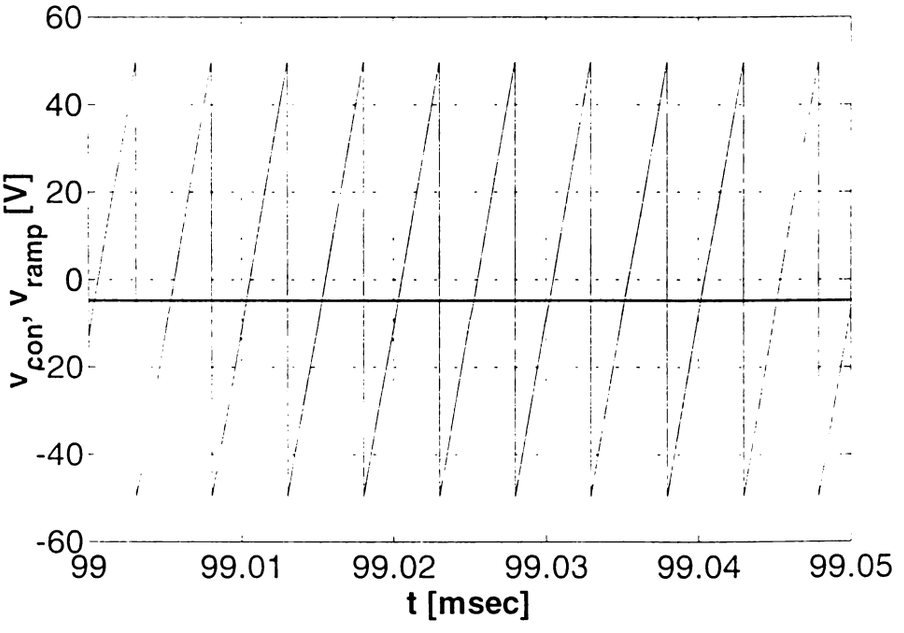

Figure 2-15 Control voltage in period-1 operation ($K_V = 2$)

Frequency Domain The spectrum of the periodic condenser voltage waveform in Fig. 2-14, at $K_V = 2$, is plotted in Fig. 2-16. The spectrum of a period-1 solution contains spikes at integer multiples of the forcing (switching) frequency $f_s = 1/T_s$.

State Space By plotting the solution (or *trajectory*) of the system in state–space the *state portrait* is obtained. The steady-state will be represented in the state space by the limit set, which in case of periodic behavior is the *limit cycle*, the closed curve traced out by the trajectory over one period. The trajectory keeps circulating along this limit cycle

while in steady-state. A limit cycle trajectory corresponding to $K_V = 2$ is presented in Fig. 2-17 in the three-dimensional state space defined by the output voltage of the positive channel v_{op}, the condenser voltage v_c and the choke current i_{op}.

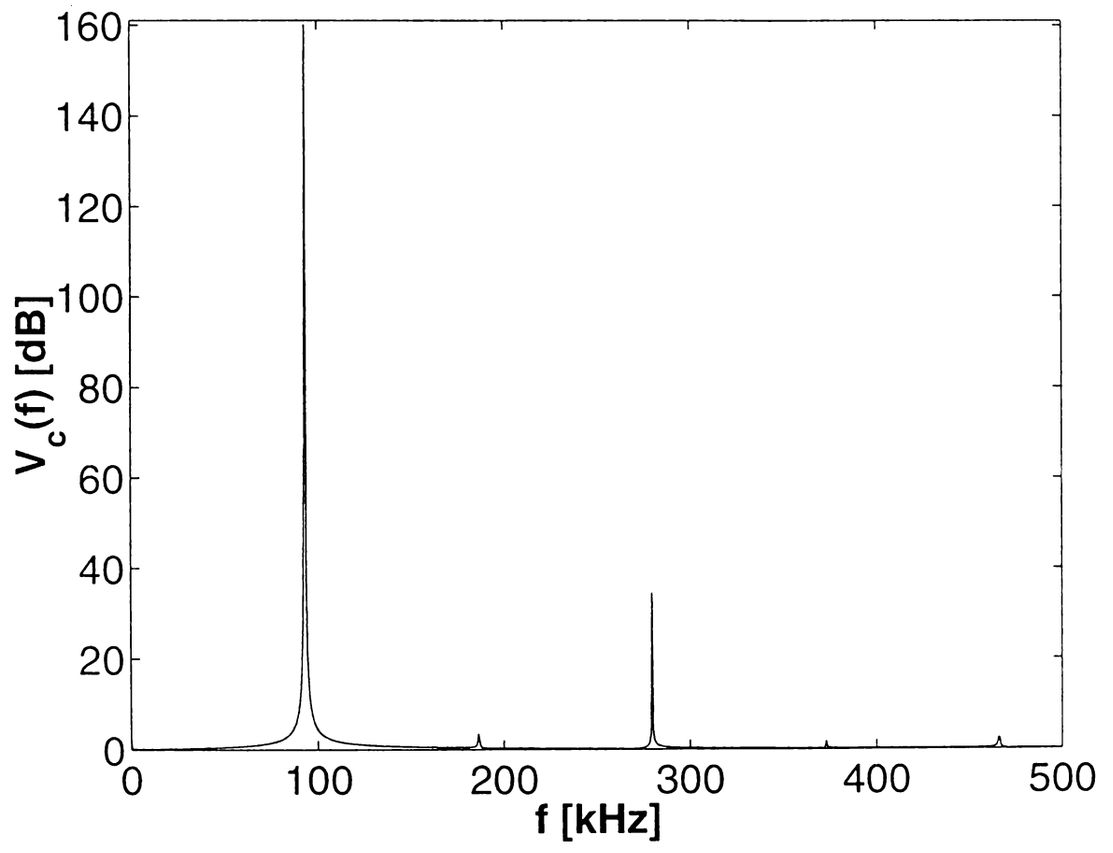

Figure 2-16 Spectrum of condenser voltage in period-1 operation ($K_V = 2$)

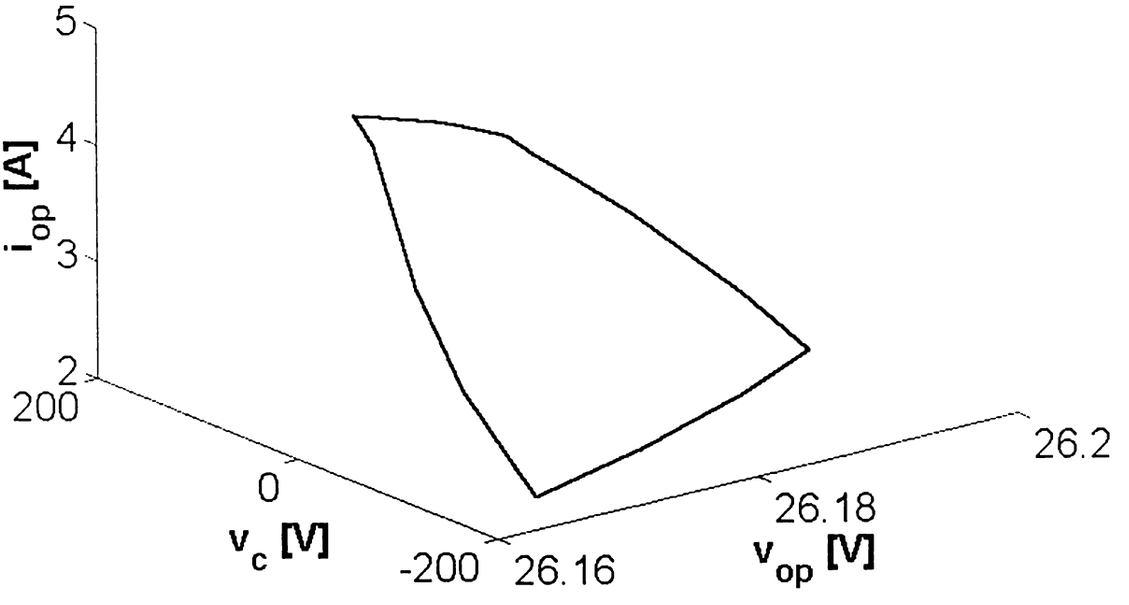

Figure 2-17 Limit cycle in period-1 operation ($K_V = 2$)

2-4-1-4 QUASIPERIODIC STEADY-STATE

The Poincaré Map When the controller gain exceeds the bifurcation value $K_V \approx 4.5$ there is no direct way to identify the new class of steady-state behavior on the basis of the mess of points representing it in the bifurcation diagram from Fig. 2-11. This can be more readily achieved by means of the Poincaré map. The Poincaré map for $K_V = 6$ is presented in Fig. 2-18, again in the reference frame i_{opk} vs. v_{ok}. This Poincaré map is a set of separate points along a closed curve so densely populated that it looks like a curve. Similar Poincaré maps are shown in reference frame of condenser voltage $v_{ck}=v_c(kT_s)$ vs. output voltage v_{ok} in Fig. 2-19 and inductor current i_{opk} vs. condenser voltage v_{ck} in Fig. 2-20, respectively. It will be proved that this type of Poincaré maps corresponds to a *quasiperiodic* solution [86].

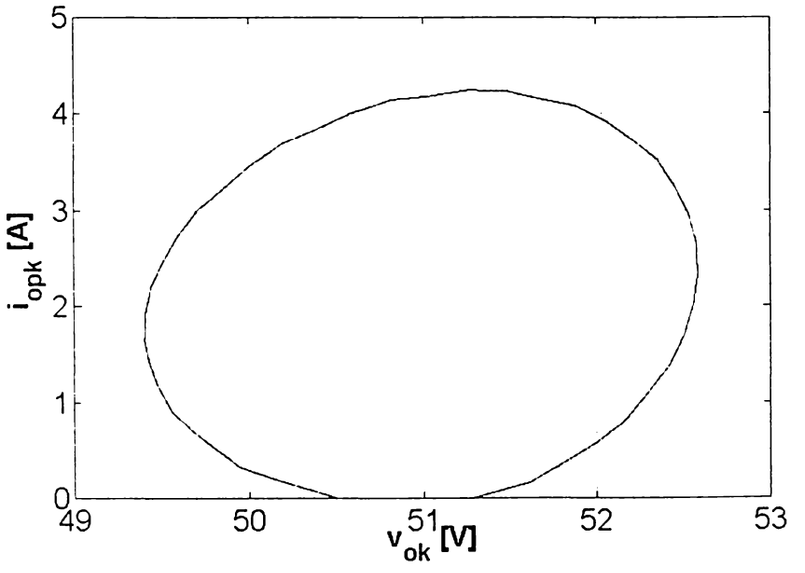

Figure 2-18 Poincaré map in quasiperiodic state ($K_V = 6$)

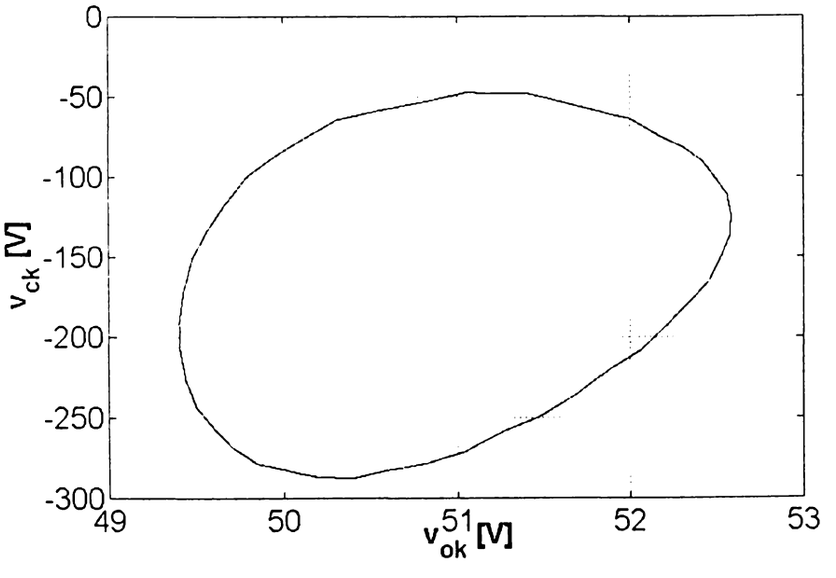

Figure 2-19 Poincaré map in quasiperiodic state ($K_V = 6$)

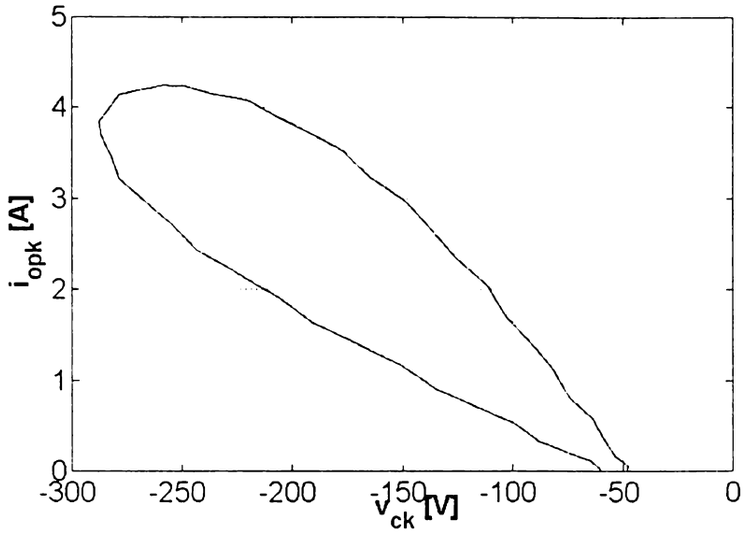

Figure 2-20 Poincaré map in quasiperiodic state ($K_V = 6$)

A quasiperiodic solution is one which may be expressed as a countable sum of periodic functions $x(t) = \sum_i x_i(t)$, where x_i has period T_i and frequency $f_i = 1/T_i$. There is also a finite set of *base frequencies* $\{ \hat{f}_1, \ldots, \hat{f}_m \}$ with two properties:

- It is linearly independent, i.e., there does not exist a non-zero set of integers $\{k_1, \ldots, k_m\}$ such that $k_1 \hat{f}_1 + \ldots + k_m \hat{f}_m = 0$.
- It forms a finite integral base for the f_i, i.e., for each i, $f_i = \left| k_1 \hat{f}_1 + \ldots + k_m \hat{f}_m \right|$ for some integers $\{k_1, \ldots, k_m\}$.

> ***Quasiperiodic behavior:*** A solution of the system that can be written as the sum of a countable number of periodic functions each of whose frequencies is an integer combination of incommensurate frequencies taken from a finite base set.

The base frequencies are not defined uniquely, but m is. A quasiperiodic function with m base frequencies is called *m-periodic* [84].

In a continuous-time dynamical system, a two-periodic trajectory lies on a two-torus $T^2 = S^1 \times S^1$, where each circle S^1 represents one of the base frequencies (Fig. 2-21b). Consider a trajectory traveling on the torus looping in the $\omega_1 = 2\pi/T_1$ direction with period T_1 and in the $\omega_2 = 2\pi/T_2$ direction with period T_2 (Fig. 2-21a). The equations describing the motion of the trajectory are:

$$x_1 = (R + r\sin\omega_2 t)\cos\omega_1 t$$

$$x_2 = r\cos\omega_2 t \qquad (2\text{-}18)$$

$$x_3 = (R + r\sin\omega_2 t)\sin\omega_1 t$$

where x_1, x_2 and x_3 are the state space coordinates, t is the time, larger radius R corresponds to the rotation about the origin and radius r corresponds to that about the cross section (Fig. 2-21c). If T_1 and T_2 are commensurate, there exist positive integers p and q such that $pT_1 = qT_2$. Therefore, the trajectory will close on itself in pT_1 seconds since it has to make exactly p loops in the first direction and exactly q loops in the second (Fig. 2-22a would not change if the simulations were run longer). The result of the motion in state space will be a limit cycle with period pT_1. This type of behaviour is called *frequency-locked* or *phase-locked motion*. If T_1 and T_2 are incommensurate, there are no such p and q and the trajectory never closes on itself (Fig. 2-22b would become more densely filled in if the simulations were run longer). Not every point of the torus will lie on the trajectory, since a trajectory is a curve and the two-torus a surface, but because the trajectory repeatedly passes arbitrarily close to every point on the torus, the two-torus is considered the limit set of the two-periodic behavior.

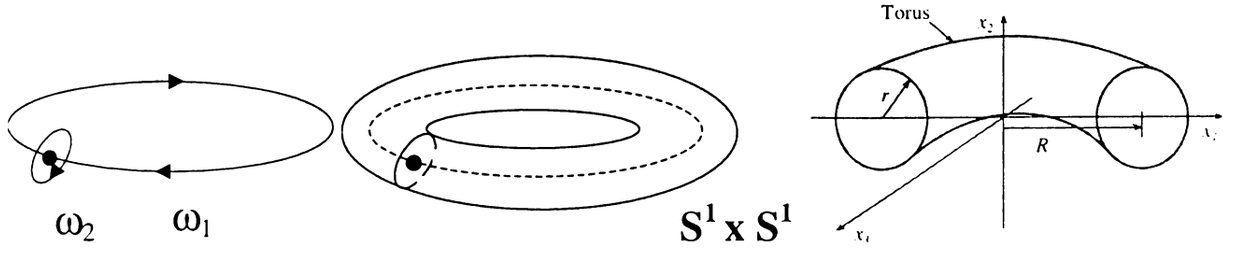

a. b. c.

Figure 2-21 Two-periodic behavior corresponds to motion on a two-torus

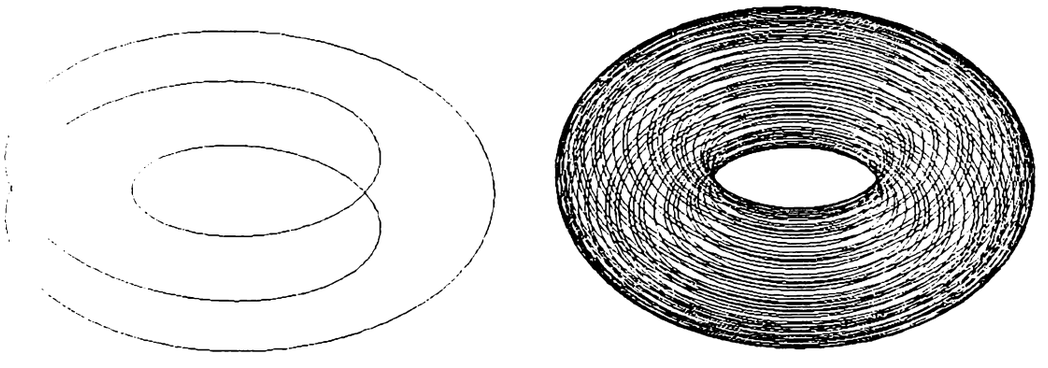

a. b.

Figure 2-22 a. Periodic trajectory with $T_1 = 2$ and $T_2 = 3$;

b. Two-periodic trajectory with $T_1 = 1$ and $T_2 = \sqrt{2}$.

In time-periodic non-autonomous systems two-periodic behavior can occur as a result of the "conflict" between the natural frequency of the system and the forcing frequency, not rationally related to the first one. Consider a two-periodic solution $\phi_t(x)$ of a time-periodic non-autonomous system with frequency base $\{f_1, f_f\}$, where f_f is the forcing frequency. Using coordinates (θ_1, θ_2) on the torus, $\phi_t(x)$ can be written as $x(t) = F(\theta_1(t),\theta_2(t))$ where $F : S^1 \times S^1 \rightarrow \Re^n$ and

$$\begin{bmatrix} \theta_1(t) \\ \theta_2(t) \end{bmatrix} = \begin{bmatrix} 2\pi f_1 t \bmod 2\pi \\ 2\pi f_f t \bmod 2\pi \end{bmatrix} \tag{2-19}$$

The action of the Poincaré map is to sample $\phi_t(x)$ every $1/f_f$ seconds:

$$\begin{bmatrix} \theta_1(k/f_f) \\ \theta_2(k/f_f) \end{bmatrix} = \begin{bmatrix} 2\pi k f_1 / f_f \bmod 2\pi \\ 0 \end{bmatrix}, \quad k = 0, 1, \ldots \tag{2-20}$$

Because f_1 and f_f are incommensurate, $\theta_1(k/f_f)$ is not periodic and will repeatedly come arbitrarily close to every point in $[0, 2\pi)$ as $k \rightarrow \infty$. Therefore, in the (θ_1, θ_2) coordinate system, the Poincaré map is the circle defined by $\theta_2 = 0$. In the original Euclidean coordinates, the Poincaré map is a closed curve.

> ***Quasiperiodic behavior:*** If the underlying flow exhibits two-periodic behavior, the Poincaré map consists of a closed curve.

Accordingly, the Poincaré maps presented in Fig. 2-18, Fig. 2-19 and Fig. 2-20 permit to identify immediately the quasiperiodic (two-periodic) behavior of the converter when the controller gain just exceeds the bifurcation value $K_V \approx 4.5$.

Time Domain In the time domain, quasiperiodic signals may look like amplitude modulated waveforms. The time function of condenser voltage v_c and control voltage v_{con} are plotted in Fig. 2-23 and Fig. 2-24 at $K_V = 6$. The time waveform of the condenser voltage is clearly amplitude modulated. The "carrier" frequency is the forcing (switching) frequency provided by the sawtooth signal. In addition, a natural frequency of the system is developed and acts as a modulating frequency [82]. It can be seen from the succession of the peak values that the condenser voltage is not periodic. Because the two frequencies are incommensurate, the resulting signal is two-periodic. The control voltage v_{con} changing with the natural frequency of the system hits the ramp wave once per ramp cycle (Fig. 2-24). The forcing (switching) frequency generated by the ramp wave is present in the small ripple of the control voltage.

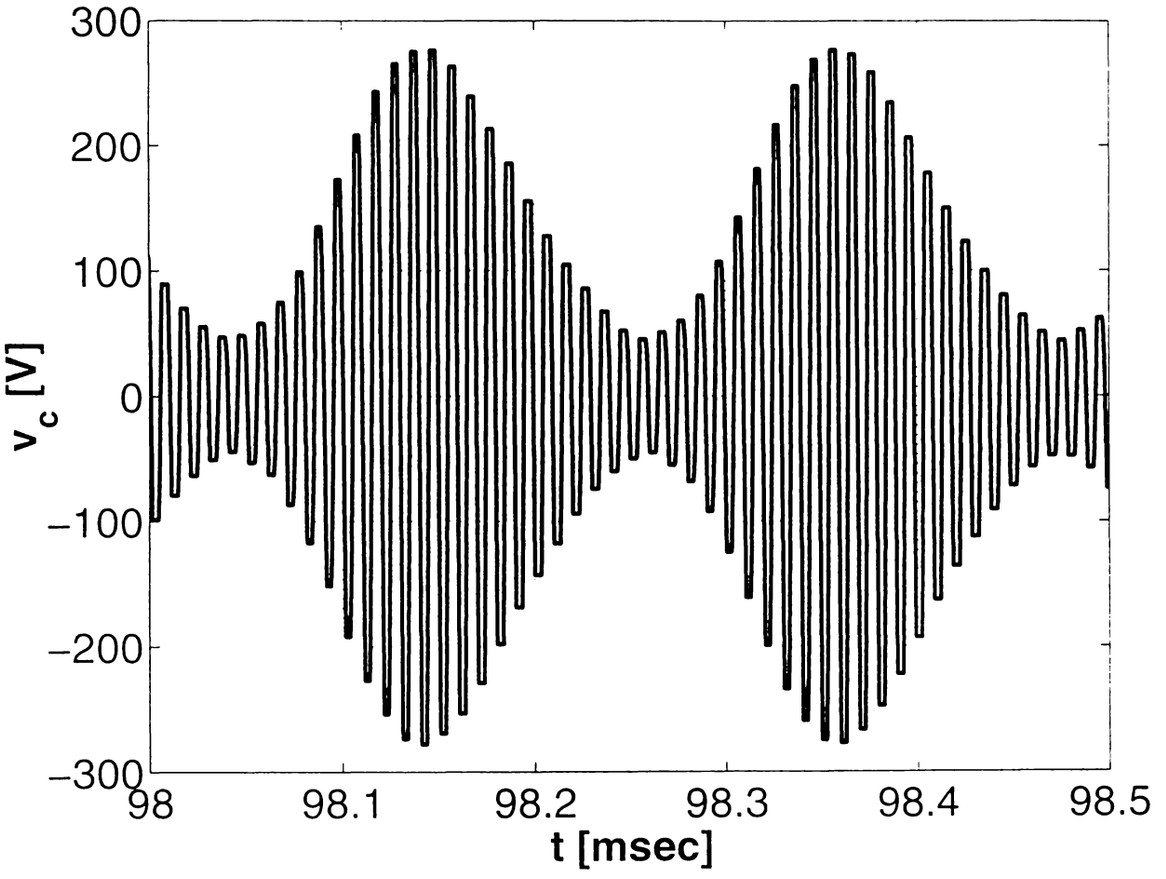

Figure 2-23 Condenser voltage in quasiperiodic state ($K_V = 6$)

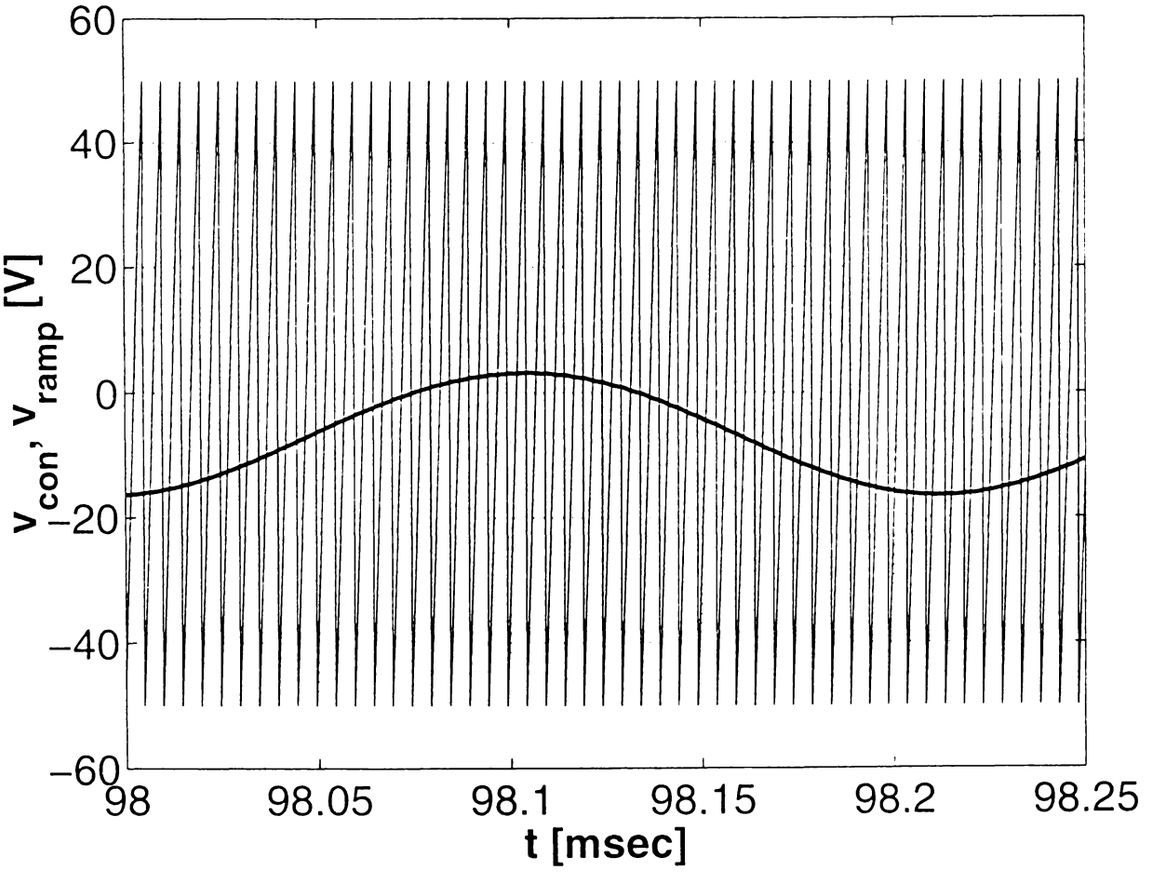

Figure 2-24 Control voltage in quasiperiodic operation ($K_V = 6$)

Frequency Domain The spectrum of the quasiperiodic condenser voltage waveform in Fig. 2-23, at $K_V = 6$, is plotted in Fig. 2-25. The spectrum consists of the spectrum of the forcing (switching) frequency $f_s = 1/T_s$ (Fig. 2-16) plus side-spikes spaced at integer multiples of the natural frequency. Therefore, the spectrum of a quasiperiodic signal consists of spikes at the various sum and difference frequencies of the base set. Theoretically, a quasiperiodic spectrum can be distinguished from a periodic one because the quasiperiodic spikes are not spaced at integer multiples of one frequency. In practice, because it is impossible to determine if a measured value is rational or irrational, a spectrum that appears to be quasiperiodic can be in fact periodic with a very long period.

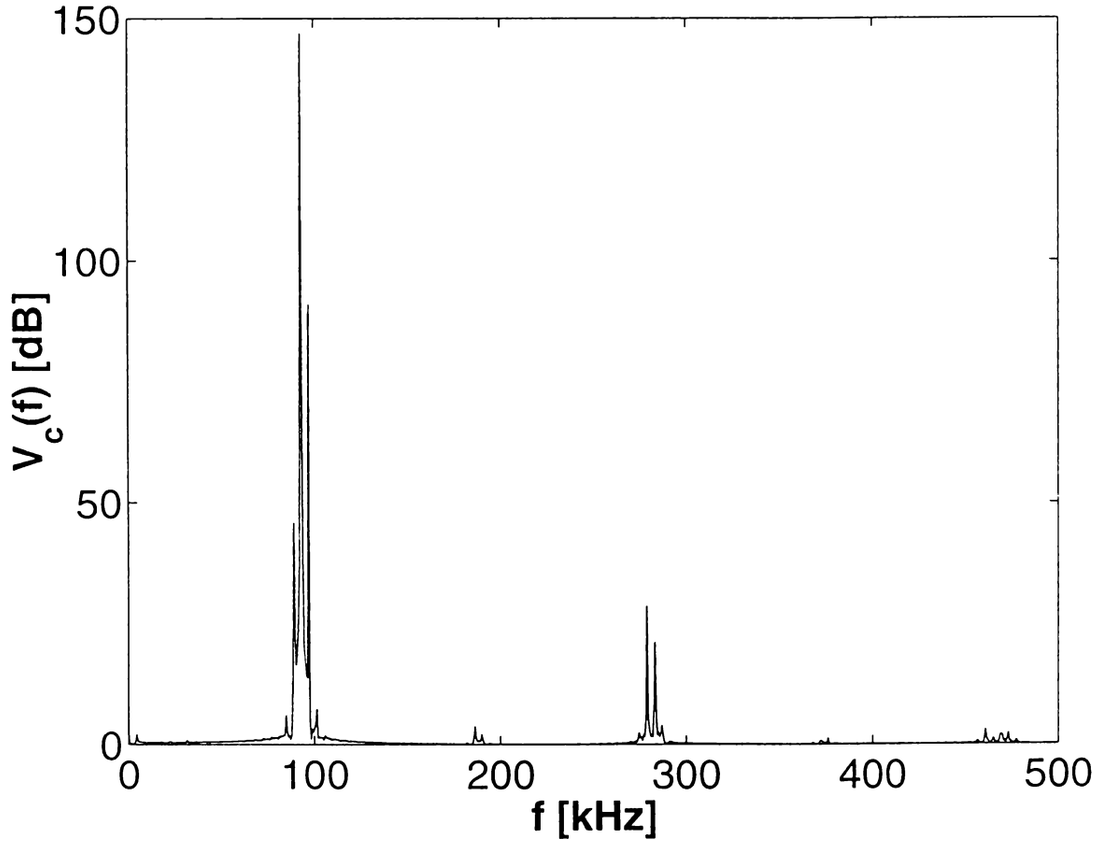

Figure 2-25 Spectrum of condenser voltage in quasiperiodic operation ($K_V = 6$)

State Space The steady-state trajectory corresponding to $K_V = 6$ is presented in Fig. 2-26 in the three- dimensional state space defined by choke current i_{op}, condenser voltage v_c and output voltage v_o. It is visible that the limit set is a torus, denoting once again the two-periodic behavior. Because the frequencies of the rotations in the two directions are incommensurate, the trajectory never closes on itself and if the simulations were run longer the surface of the torus would become more densely filled in [83].

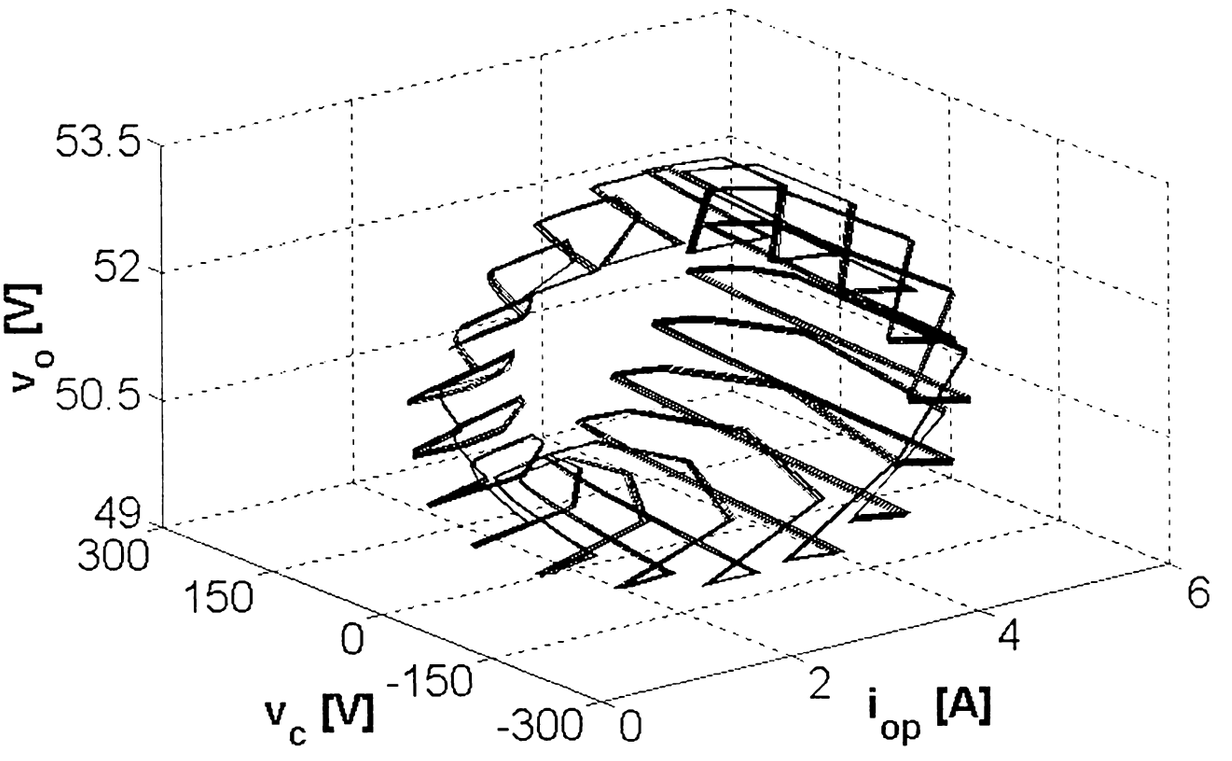

a.

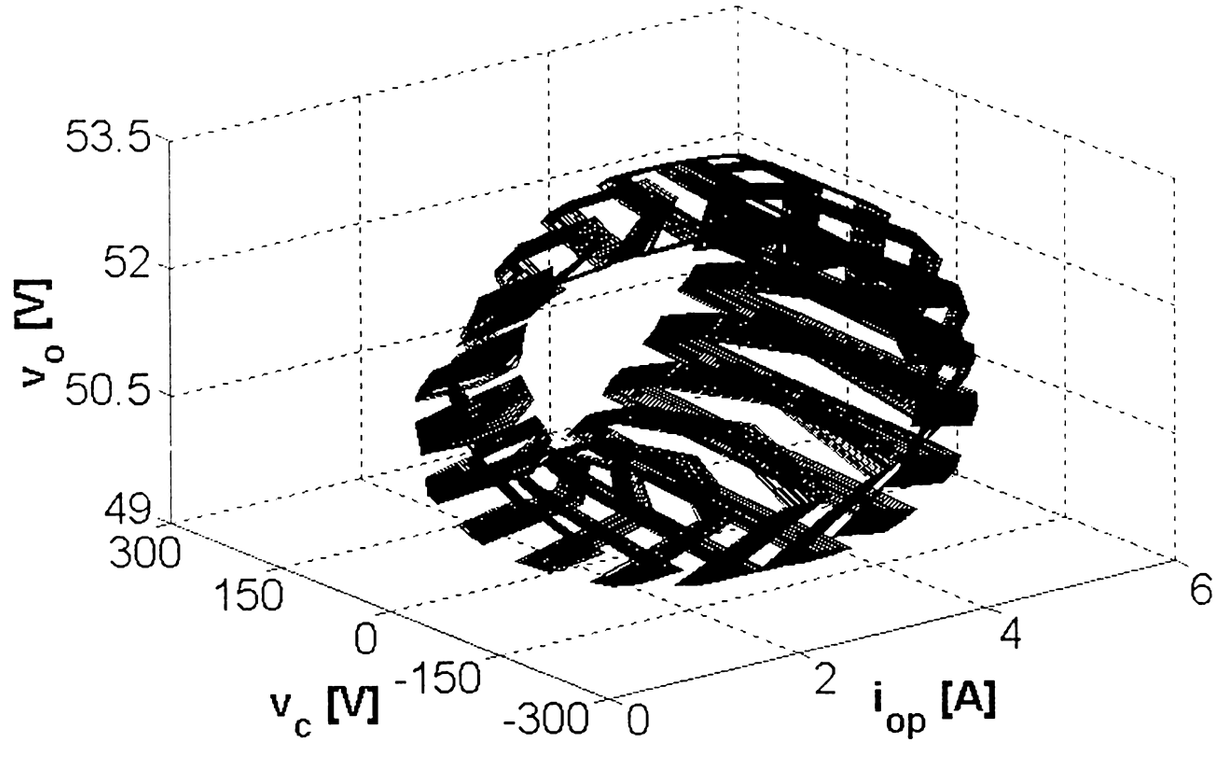

b.

Figure 2-26 State space trajectory in quasiperiodic steady-state (K_V = 6) with longer run in *b* than in *a*

2-4-1-5 THE NAIMARK-SACKER BIFURCATION

Consider a continuous-time dynamical system with a complex-conjugate pair of eigenvalues of an equilibrium point. From standard linear control theory, while the real part of the eigenvalues is negative, the system will be stable. Suppose that when a control parameter of the system increases through a bifurcation value, the pair of complex conjugate eigenvalues passes through the imaginary axis. If such a situation occurs in a linear system, it will become unstable. For a nonlinear system, a stable limit cycle is born and this scenario represents *a Hopf bifurcation* [84].

> ***Hopf Bifurcation:*** A Hopf bifurcation occurs in a continuous-time system when a complex-conjugate pair of eigenvalues of the linearization of the vector field at an equilibrium point passes through the imaginary axis, thereby creating a limit cycle.

In the discrete-time analogue of the Hopf bifurcation, an invariant closed curve is created as a stable fixed point loses stability when its complex-conjugate pair of eigenvalues passes through the unit circle. Since discrete-time models are obtained by making Poincaré section in the state space of continuous time systems, it is useful to investigate what happens in a continuous-time dynamical system when a Hopf bifurcation occurs in its Poincaré map. Before the bifurcation, the Poincaré map is a fixed point, hence in the continuous time system it corresponds to a stable limit cycle. The Poincaré map becomes a closed loop due to the Hopf bifurcation and this corresponds to a two-periodic trajectory. Hence, a Hopf bifurcation in the Poincaré map can be interpreted as a transition of the continuous-time system from a periodic behavior to a quasiperiodic one. This is called a *Naimark-Sacker bifurcation* [85].

> ***Naimark-Sacker bifurcation:*** When a limit cycle undergoes a Naimark-Sacker bifurcation, motion on a two-torus results.

As proved in the previous sections, precisely this state of affairs occurs in the converter when the controller gain is increased above the bifurcation value $K_V \approx 4.5$: below this value normal periodic operation sustains and all state variables are changing with the switching period; in addition another frequency develops by the Naimark-Sacker bifurcation and the system exhibits quasiperiodic state [87].

2-4-1-6 CHAOS

The quasiperiodic operation pertains to a relatively large range of the controller gain, approximately from $K_V \approx 4.5$ up to $K_V \approx 60$. The quasiperiodic states could been easily identified by calculating the three Poincaré maps of Fig. 2-17, Fig. 2-18 and Fig. 2-19. In all cases each Poincaré map looked like a closed curve, denoting a quasiperiodic behavior. By increasing further the controller gain a totally different type of Poincaré maps is obtained, corresponding hence to a state that is none of the previous found. It was revealed already the possibility that in the conflict between the forcing frequency and the natural frequency, neither wins and quasiperiodic state is developed. Another possibility is *chaos*, which can be defined as "none of the above" from a practical point of view [88].

> ***Chaos:*** A bounded steady-state behavior in a deterministic dynamical system, which is not an equilibrium point, not periodic, and not quasiperiodic.

The Poincaré Map Fig. 2-27 shows the Poincaré map in chaotic behavior at $K_V = 70$ in reference frame of condenser voltage $v_{ck}=v_c(kT_s)$ vs. output voltage $v_{ok}=v_o(kT_s)$. The Poincaré maps for chaotic systems are distinctive and quite beautiful. Looking at Fig. 2-27, it can be seen that the map lies, indeed, in a bounded region of the state space but it does not lie on a simple geometrical object, as in the case of periodic and quasiperiodic behavior. Chaotic state appears in the Poincaré map as a set of highly organized points reflecting a multilayered structure and order, with a fractal dimension [84].

> ***Chaos:*** The Poincaré map of a chaotic steady-state is not a simple, geometrical object. Unlike the Poincaré maps of the other limit sets, it exhibits a fine, highly organized structure underlying the chaotic behavior.

Time Domain Using Poincaré maps can be the best way to distinguish chaotic from quasiperiodic solutions. They appear much the same and there is no direct way to distinguish the chaotic state from the quasiperiodic one on the basis of the mess of points representing them in a bifurcation diagram. Frequently it is difficult to separate them from time history as well. A chaotic waveform of the output voltage v_o at $K_V = 70$ is presented in Fig. 2-28. It can be seen that the chaotic signal is, indeed, bounded and not periodic. It is difficult to tell whether it is not quasiperiodic, but, however, it looks more random (random behavior in a deterministic system may be surprising at first, but pseudorandom number generators

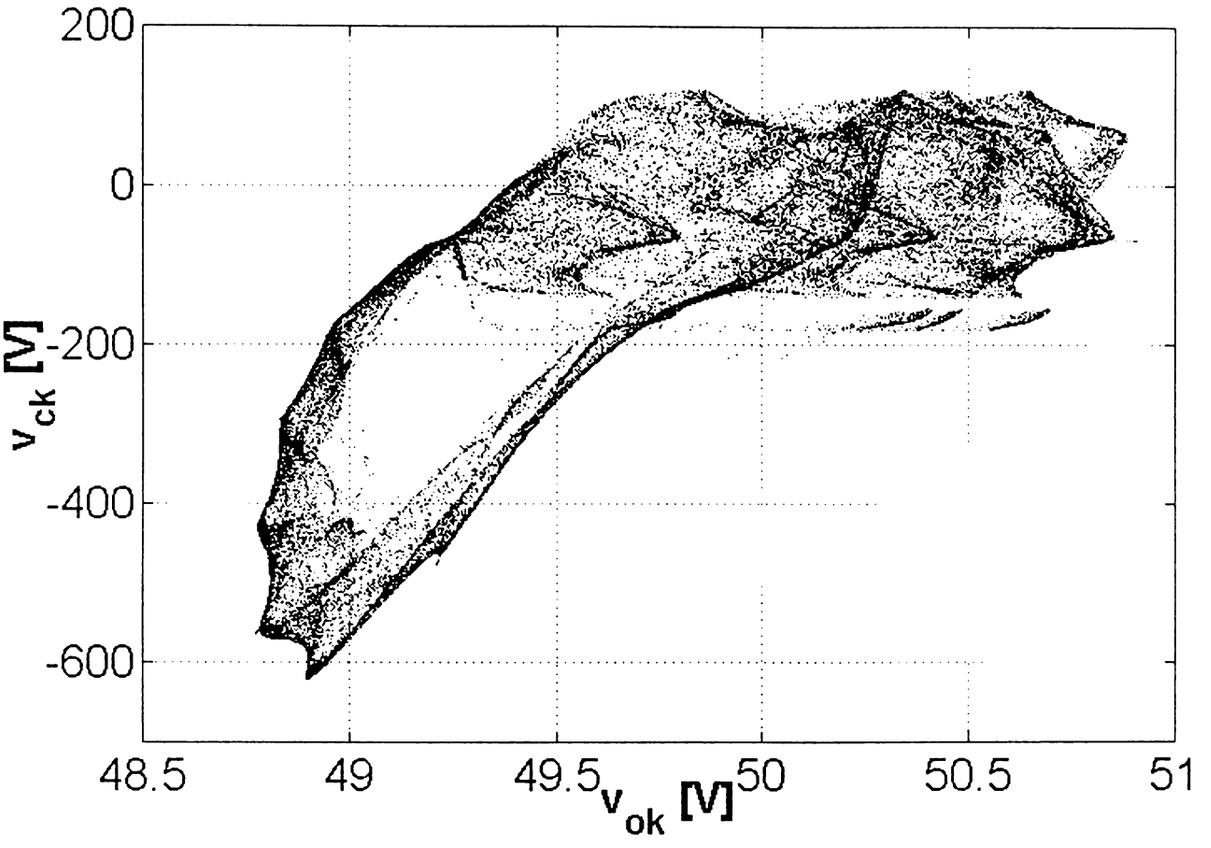

Figure 2-27 Poincaré map for chaotic operation ($K_V = 70$)

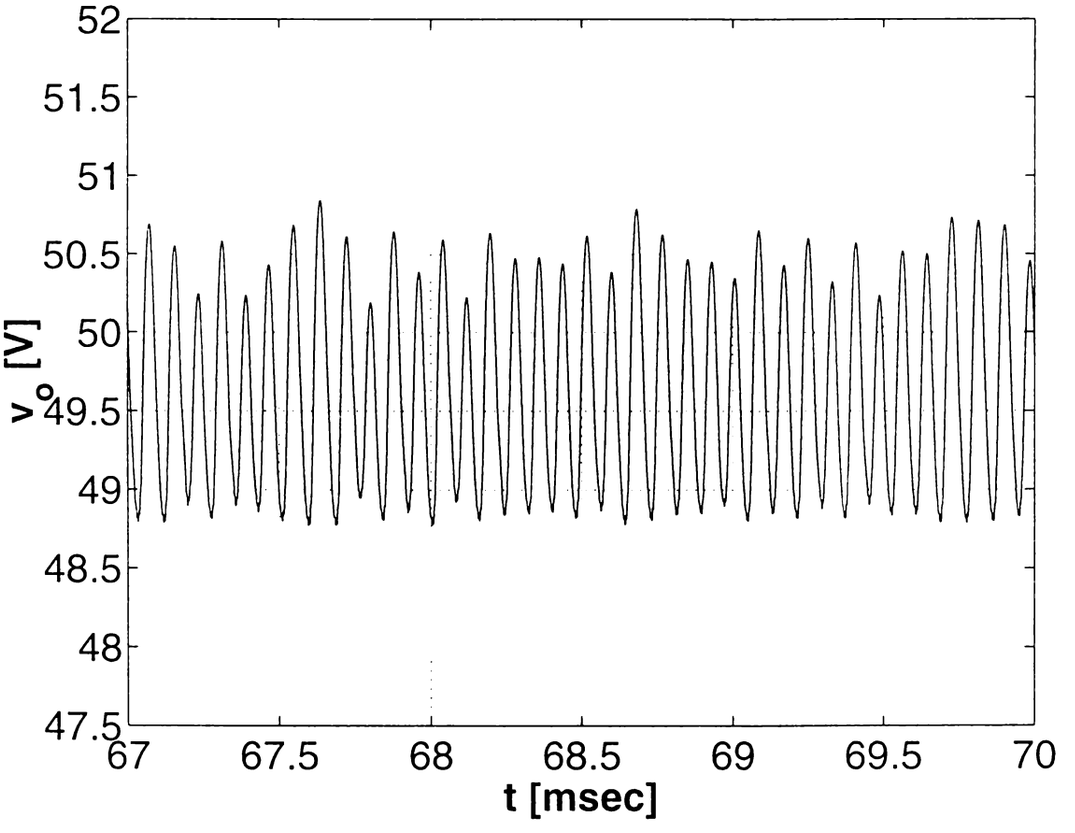

Figure 2-28 Chaotic waveform of the output voltage ($K_V = 70$)

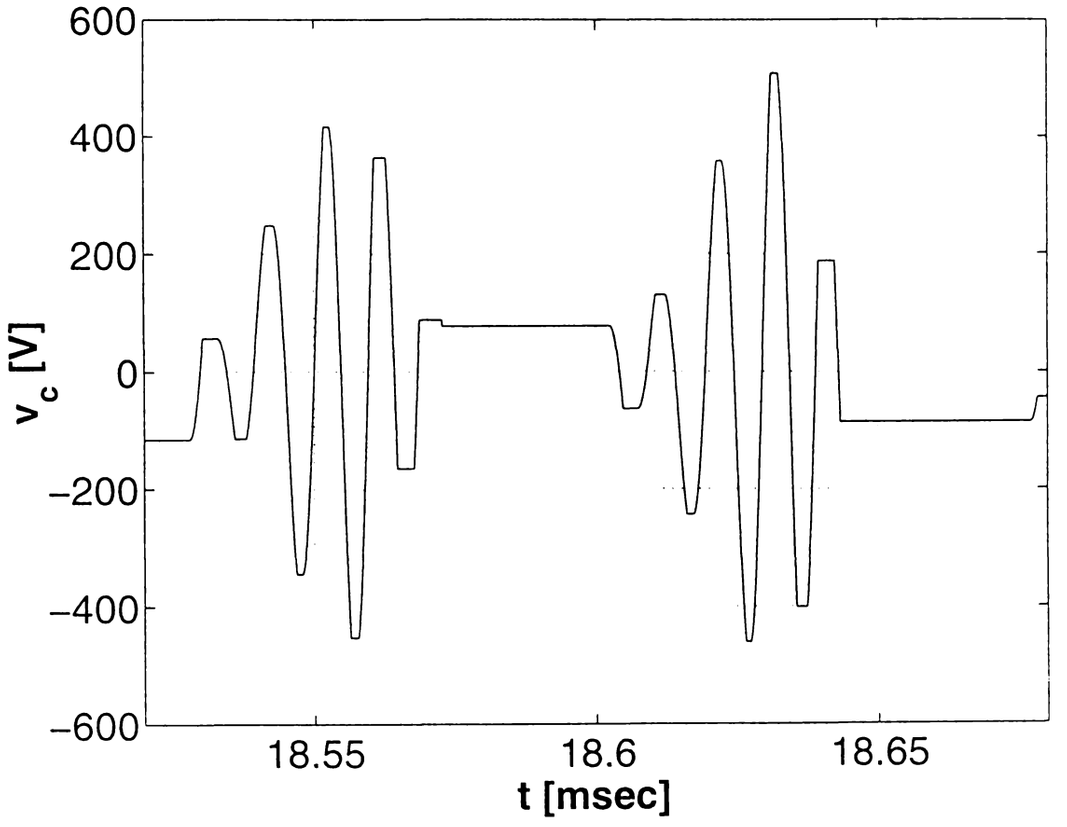

Figure 2-29 Condenser voltage in chaotic operation ($K_V = 70$)

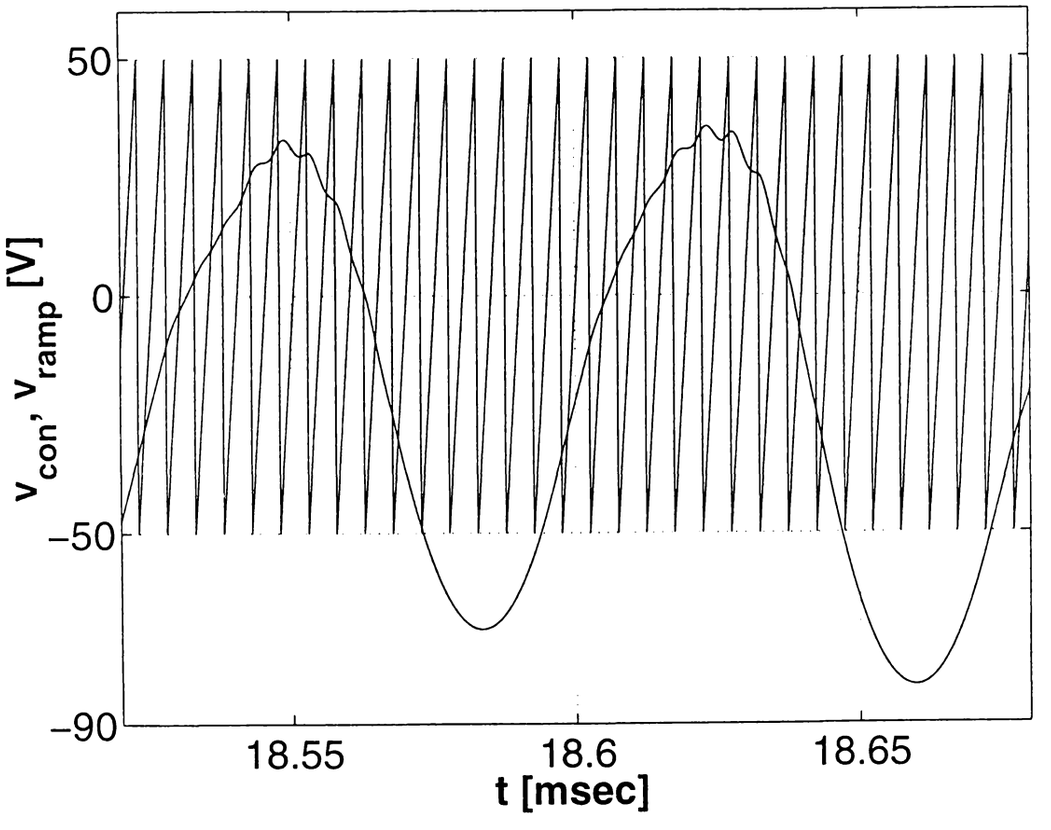

Figure 2-30 Control voltage in chaotic operation ($K_V = 70$)

are simple examples). The time function of the condenser voltage in chaotic operation is plotted in Fig. 2-29. In chaotic operation the control voltage v_{con} fails to hit the ramp wave in its every cycle (Fig. 2-30).

> ***Chaos:*** In the time domain, a chaotic trajectory looks "random".

Sensitive dependence on initial conditions Two chaotic waveforms of the output voltage, started from almost identical initial conditions, are presented in Fig. 2-31 at K_V = 70. It can be clearly noticed that the small differences in initial conditions are persistently magnified by the dynamics of the system so that the trajectories diverge until they become uncorrelated. This represents the *sensitive dependence on initial conditions*, which is a very important criterion of chaos [84].

> ***Sensitive dependence on initial conditions:*** Nearby trajectories diverge and soon become uncorrelated.

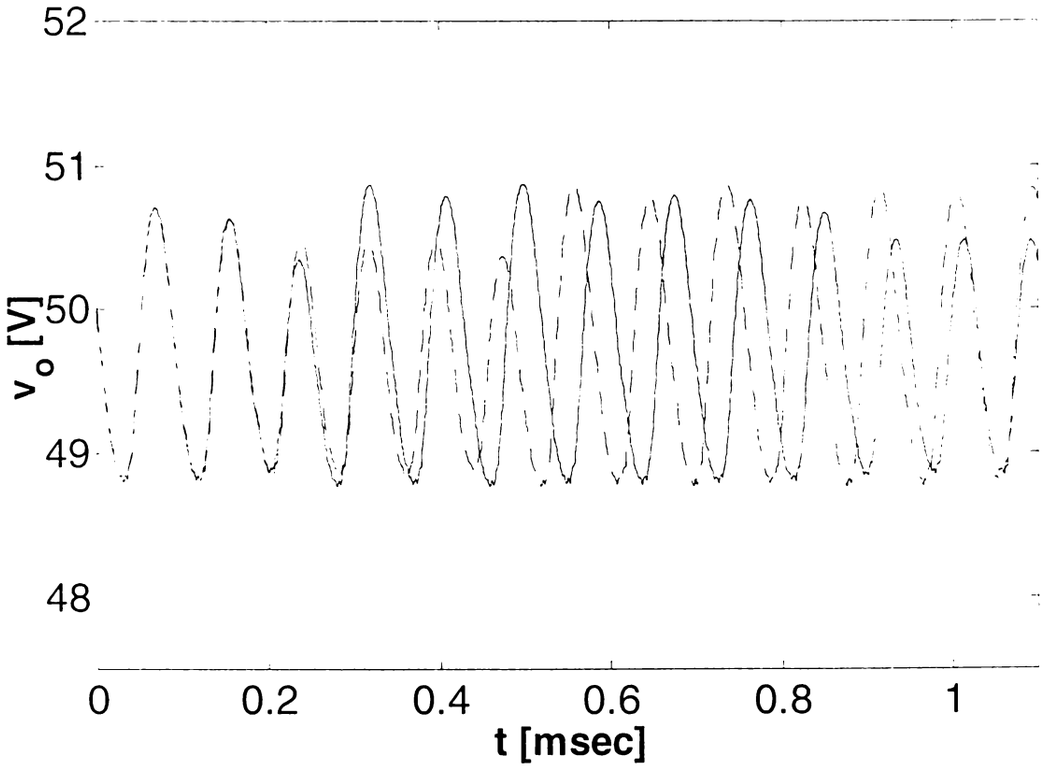

Figure 2-31 Sensitive dependence on initial conditions: two chaotic waveforms of the output voltage (K_V = 70). The initial conditions differ by 0.04%.

Predictive power There is a very important implication of this sensitive dependence on initial conditions. There is always noise in a physical system or computational noise in a

simulation. In addition, initial conditions cannot be specified or measured with infinite accuracy. These errors, although small, will make chaotic systems to be unpredictive beyond a short time frame. In order to specify what is meant by an unpredictive deterministic system, consider one observer A observing a dynamical system at time t_A and an other observer B observing the same system at time $t_B > t_A$. Observer A can also predict the state of the system at t_B if he knows the initial condition at t_A. The system is called *predictive* if observer A – using observation and prediction – knows more precisely the state of the system at t_B than observer B, using only observation. These systems can be thought of as *information sinks*, because information is lost with time. On the contrary, the system is called *unpredictive* if observer B knows more precisely the state of the system at time t_B than observer A. These systems represent *information sources*, since information is gained with time. Sensitive dependence on initial conditions is exhibited by an unpredictive system and vice versa. According to the definitions above, an expanding system, i.e., a system whose all trajectories diverge one another, is unpredictive. Thus, *stretching* mechanism leads to an unpredictive system. In addition, because expanding trajectories become unbounded, *folding* mechanism is required to achieve a steady-state.

> ***Unpredictive system:*** Later observations convey more information about the state of the system than earlier ones (observations are more accurate than predictions). It is equivalent to sensitive dependence on initial conditions. Two mechanisms are required for continuous-time systems to be unpredictive: stretching and folding [84].

Shadowing Theorem There is another important implication of the sensitive dependence on initial conditions, which arises in numerical computations, by taking into account the combined influence of round-off errors in numerical computations and the property of divergence of nearby trajectories for chaotic behavior. Under such conditions, how can numerical computations of trajectories be trusted to give us reliable results? (In experimental measurements the noise plays the role of round-off errors and leads to the same problem.) For a chaotic system even small numerical errors will be amplified in time and the results could depend critically on the computational procedures, losing their generality. The comforting answer to these doubts is given by the *shadowing theorem*, which states that the computed trajectory shadows some possible trajectory of the system. This is illustrated in Fig. 2-32, where the upper picture shows an exact trajectory started

from x_0 and described by the time series values $x_0, x_1, x_2, \ldots, x_k$, and a computed trajectory started from $y_0 = x_0 + \varepsilon_0$ and characterized by the obtained time series values $y_0 = x_0 + \varepsilon_0$, $y_1 = x_1 + \varepsilon_1$, $y_2 = x_2 + \varepsilon_2, \ldots, y_k = x_k + \varepsilon_k$. For a chaotic behavior $|\varepsilon|$ grows exponentially and the two trajectory diverge until, for all practical purposes, they become uncorrelated. Shadowing theorem says that there is a starting point z_0 in the ball of radius ε about x_0 that gives rise to an exact trajectory whose all time series values $z_0, z_1, z_2, \ldots, z_k$ stay in the balls of radius ε about y_k (lower picture from Fig. 2-32). So, the exact trajectory passing through the z_k points shadows the computed trajectory, which in this way is a good characterization of the system's behavior [85].

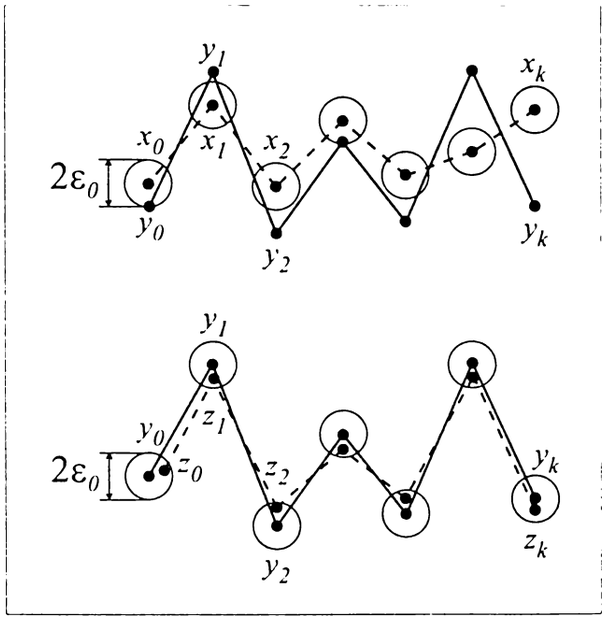

Figure 2-32 Shadowing theorem

Frequency Domain The spectrum of the condenser voltage waveform in Fig. 2-30, at $K_V = 70$, is plotted in Fig. 2-33. The spectrum is different from the corresponding periodic (Fig. 2-16) or quasiperiodic (Fig. 2-25) one. It still have spikes indicating the predominant frequencies but also has a broad-band, noise-like component, which is a characteristic exhibited by all chaotic systems.

> ***Chaos:*** The spectrum may have spikes, but always has a continuous, broad, "noise-like" nature.

The route to chaos described so far represents the *quasiperiodic (torus breakdown) route to chaos* [86].

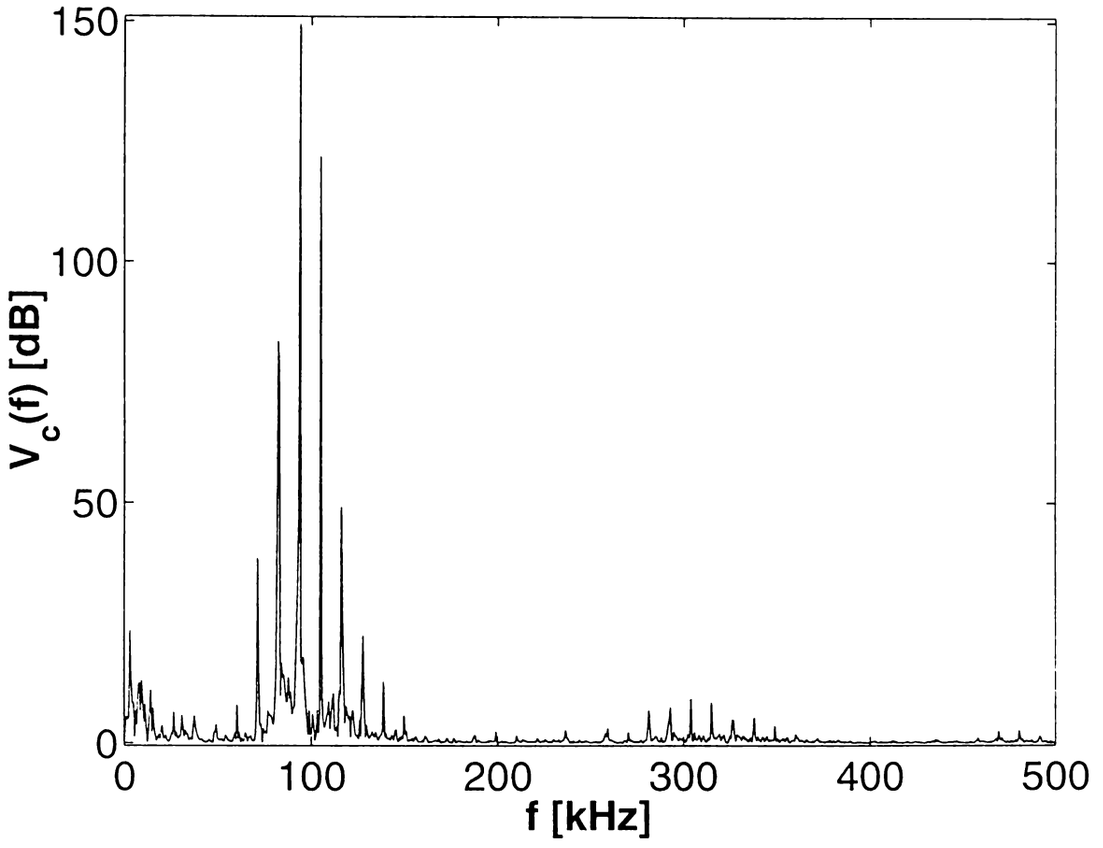

Figure 2-33 Spectrum of condenser voltage in chaotic operation (K_V = 70)

> ***Quasiperiodic route to chaos:*** As a result of the alteration in a parameter the system changes from periodic to quasiperiodic state through a Naimark-Sacker bifurcation. Later, by changing further the parameter the quasiperiodic state turns into a chaotic one.

2-4-2 PERIOD-DOUBLING ROUTE TO CHAOS

Another type of bifurcation behavior that is present in the system studied is the periodic-doubling route to chaos [82]. This is the most frequent route and can be readily identified from a bifurcation diagram. Such a representative bifurcation diagram for the converter configuration is shown in Fig. 2-34.

2-4-2-1 SUBHARMONIC STEADY-STATE

Starting from left in the bifurcation diagram of Fig. 2-34, the chaotic region suddenly changes with the increase of K_V into a region with nine consecutive distinct v_{ok} values.

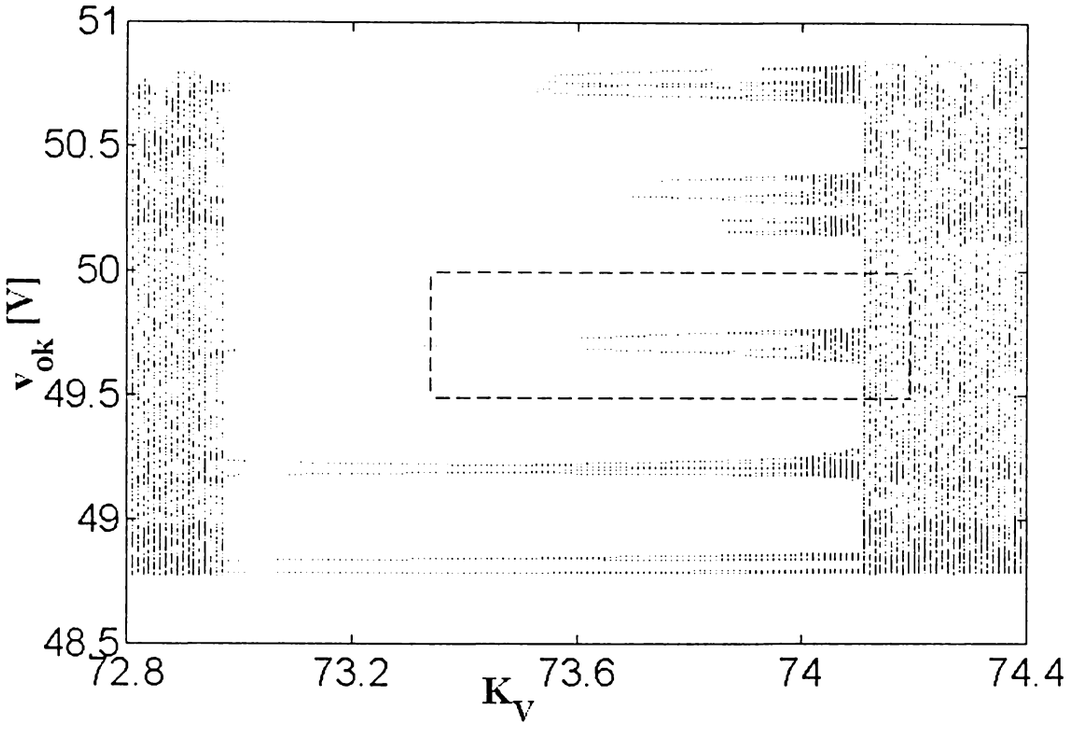

Figure 2-34 Bifurcation diagram of the period-doubling route to chaos

Hence, the output voltage v_o is periodic in this state and repeats itself after 9 switching cycles or 18 periods of the sawtooth wave. This state is called period-9 and corresponds to a frequency-locked or phase-locked motion, in which the solution could synchronize with some multiple of the forcing frequency. Beside quasiperiodicity and chaos, this is the third possibility in the conflict between the forcing frequency and the natural frequency. Using terminology borrowed from Fourier analysis, a period-K solution with $K > 1$ is called a *Kth-order subharmonic periodic state* [84].

> ***Subharmonic behavior:*** A periodic solution of a time-periodic non-autonomous system whose period is an integer multiple (>1) of the forcing period.

Such *periodic windows* (regions of periodic behavior between regions of chaotic behavior) appear frequently in chaotic systems [86]. It is hard to see in Fig. 2-11, but even within the region where quasiperiodic behavior exists, periodic windows appear, where the steady-state phase-locks onto a subharmonic.

The Poincaré Map The period of the state variables in the converter is $9*T_s$ in period-9 state. As it was defined previously, the Poincaré map behaves similarly to a periodically flashing stroboscope. Therefore, sampling with the switching period T_s, the period-9 state

of the converter will appear as a set of nine points in the Poincaré map. This points represents a *period-9 closed orbit* for the Poincaré map. Fig. 2-35 presents the Poincaré map for the period-9 operation in the plane of output voltage $v_{ok}=v_o(kT_s)$ vs. inductor current $i_{opk}=i_{op}(kT_s)$ at $K_V = 73.2$.

Closed orbit: The sequence $\{ x_1^*, ..., x_K^* \}$ is a period-K closed orbit of the map P if $x_{k+1}^* = P(x_k^*)$ for $k = 1, \ldots, K-1$, and $x_1^* = P(x_k^*)$.

Subharmonic behavior: A period-K subharmonic of a time-periodic non-autonomous system appears as a period-K closed orbit of the Poincaré map.

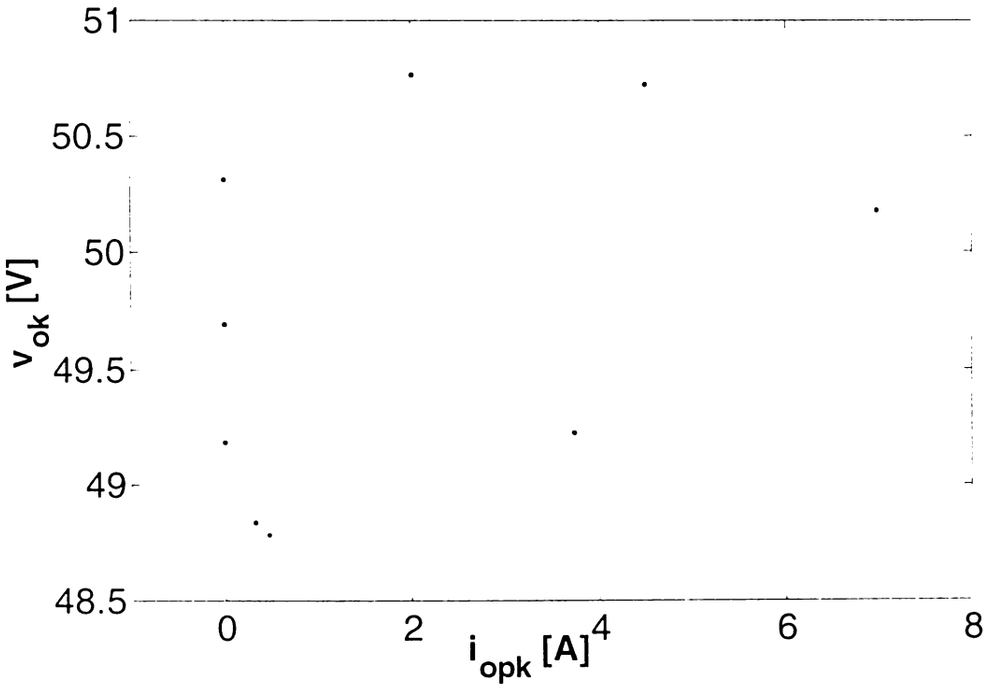

Figure 2-35 Poincaré map for period-9 operation ($K_V = 73.2$)

Time Domain The time functions of condenser voltage v_c and control voltage v_{con} are plotted in Fig. 2-36 and Fig. 2-37 at $K_V = 73.2$. The period-9 subharmonic state is clearly visible in all figures. During the period-9 operation v_{con} fails to hit the ramp wave in its every cycle (Fig. 2-37).

Frequency Domain The spectrum of the period-9 condenser voltage waveform in Fig. 2-36, at $K_V = 73.2$, is plotted in Fig. 2-38. The spectrum of a Kth-order subharmonic signal contains spikes spaced at integer multiples of $f_s = 1/KT_s$.

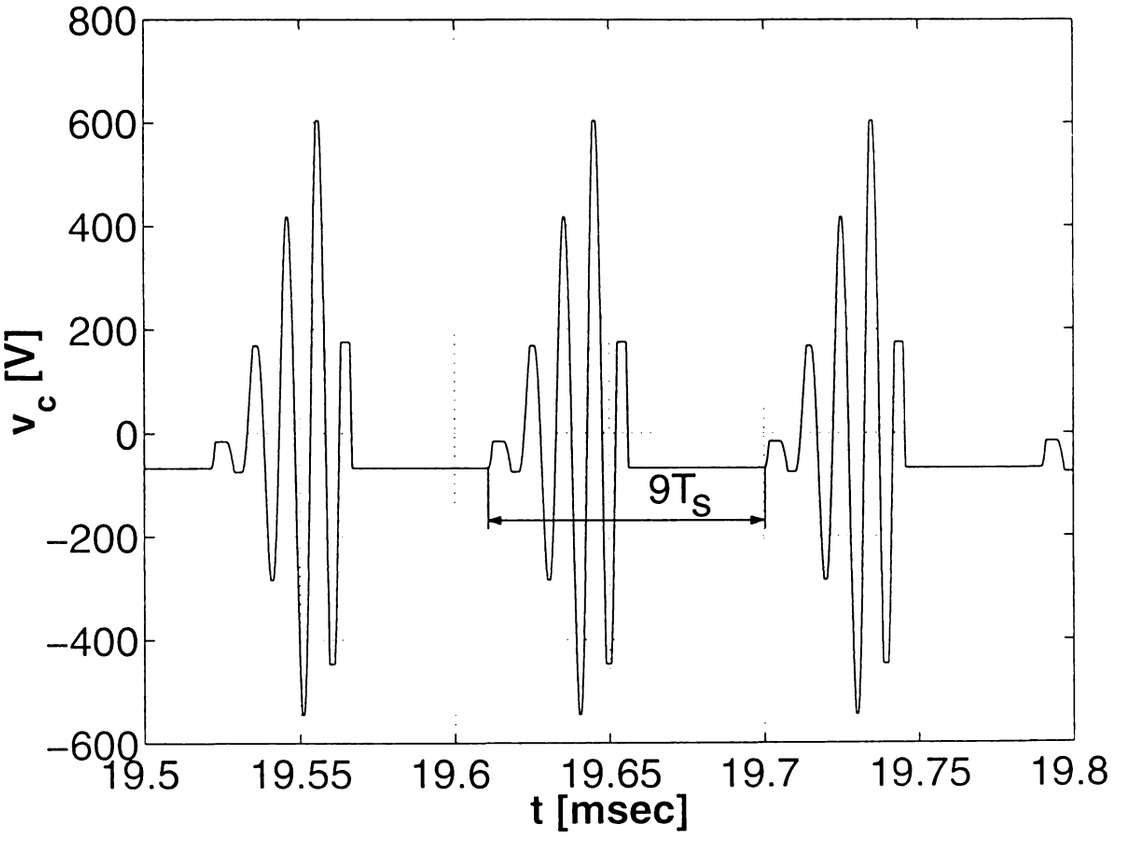

Figure 2-36 Condenser voltage in period-9 operation ($K_V = 73.2$)

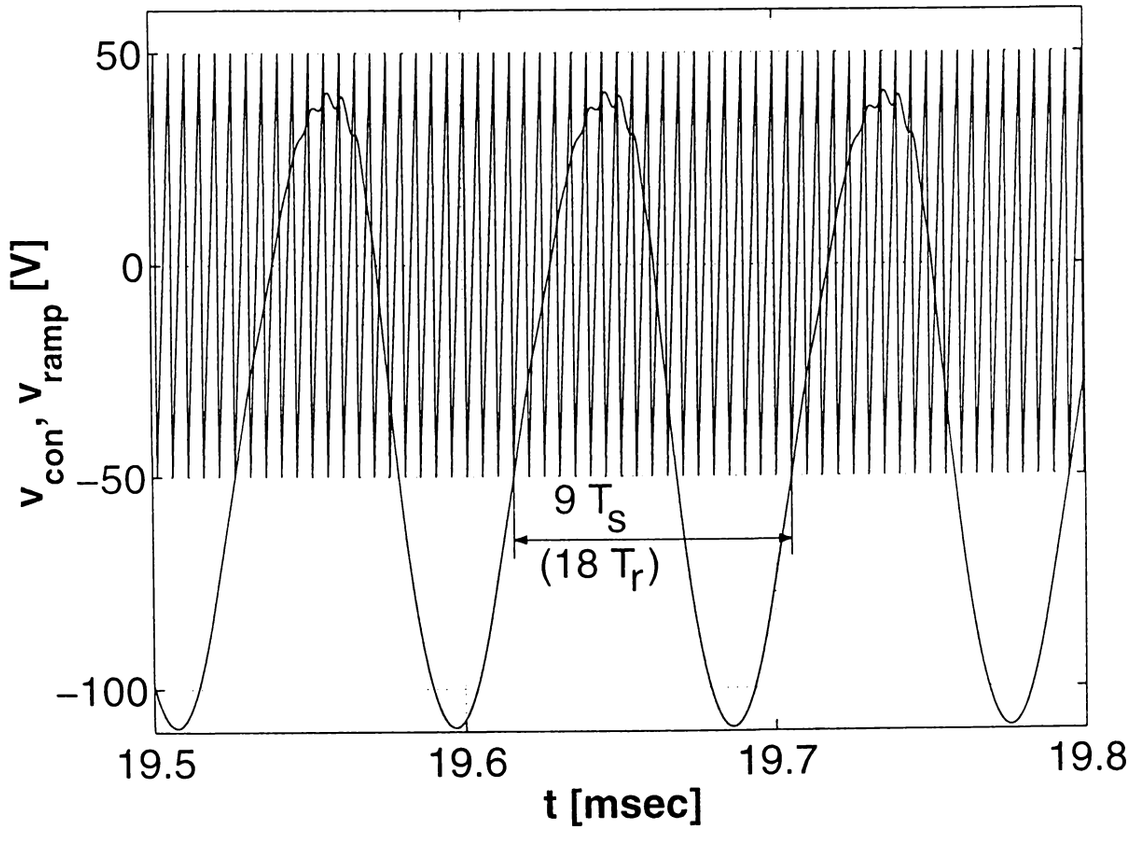

Figure 2-37 Control voltage in period-9 operation ($K_V = 73.2$)

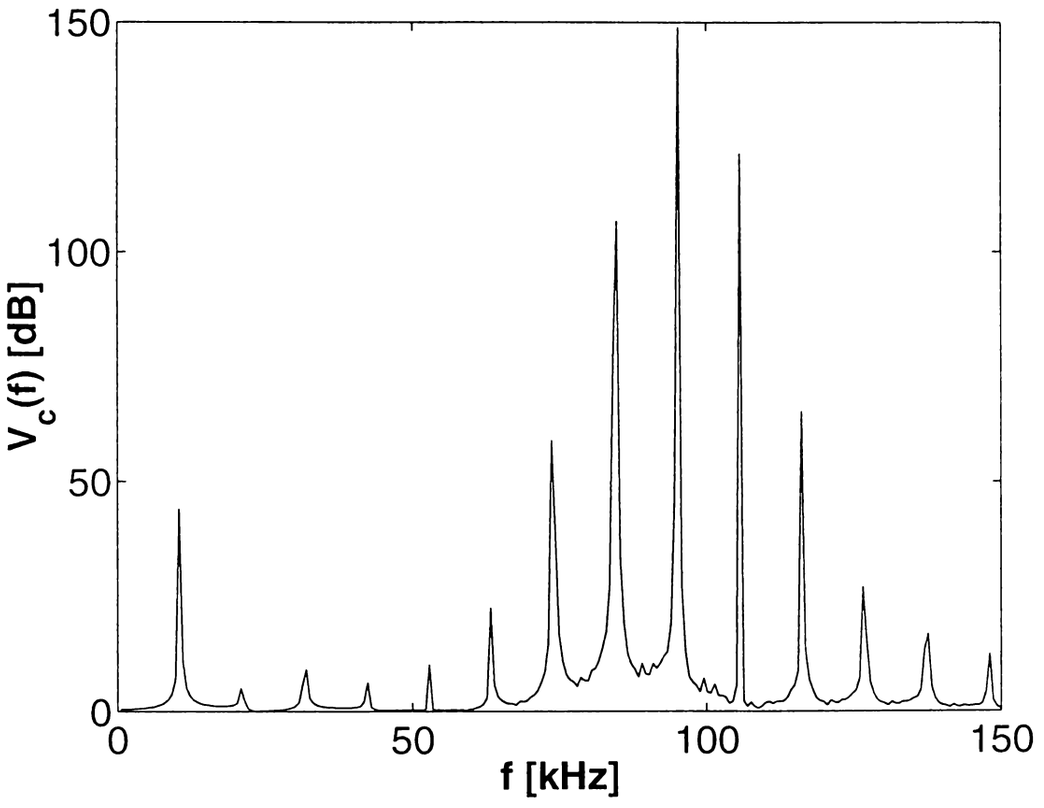

Figure 2-38 Spectrum of condenser voltage in period-9 operation (K_V = 73.2)

State Space The limit cycle corresponding to the period-9 steady-state is presented in Fig. 2-35 at K_V = 73.2 in the plane of output voltage v_o vs. inductor current i_{op}. The points belonging to the Poincaré map (Fig. 2-35) are also marked.

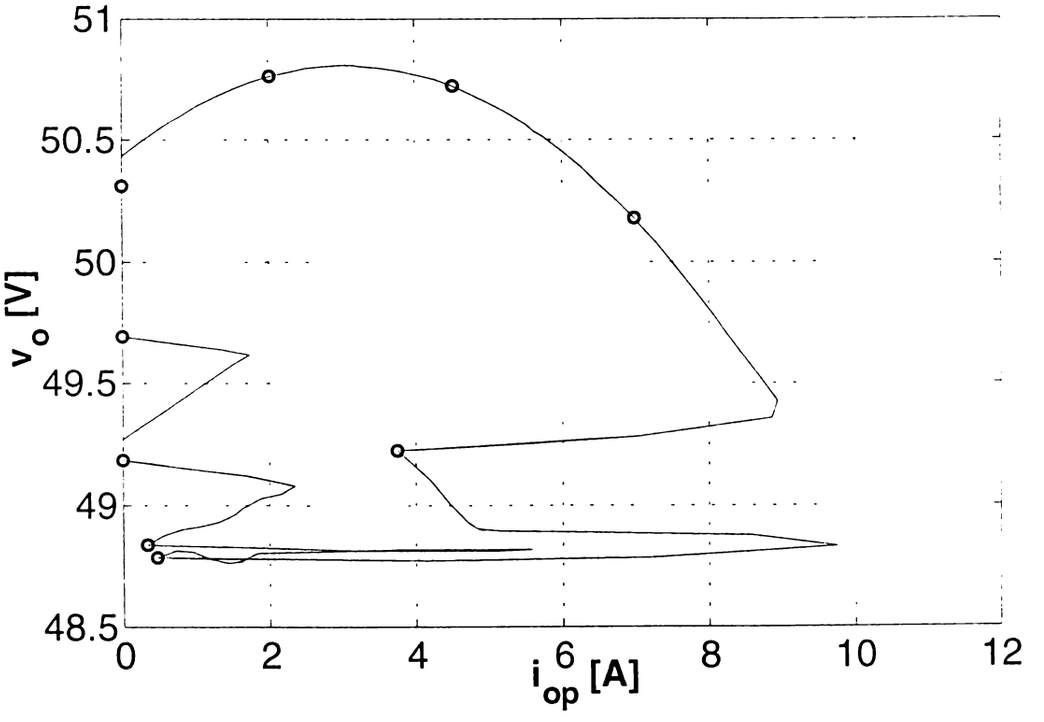

Figure 2-35 Limit cycle in period-9 operation (K_V = 73.2)

2-4-2-2 PERIOD-DOUBLING BIFURCATION

A little above K_V = 73.5 a bifurcation can be noticed in the diagram depicted in Fig. 2-31: the 9[th]-order subharmonic periodic steady-state changes into an 18[th]-order one. This is called *period-doubling (flip) bifurcation* [85].

> ***Period-doubling bifurcation:*** A period-K solution changes into a period-$2K$ solution.

The first period doubling is followed by a cascade of other period doublings generating the subharmonics with order $9*2^n$ where n = 1, 2, ... Increasing further the controller gain Kv a little above 74, the smear of points in the bifurcation diagram (Fig. 2-31) indicates that the period-doubling bifurcations accumulate at a bifurcation value at which chaotic state develops again. The chaotic behavior can be readily identified again by means of the Poincaré map. Such a representative map is presented in Fig. 2-36 at K_V = 74.2, in the plane of output voltage $v_{ok}=v_o(kT_s)$ vs. choke current $i_{opk}=i_{op}(kT_s)$.

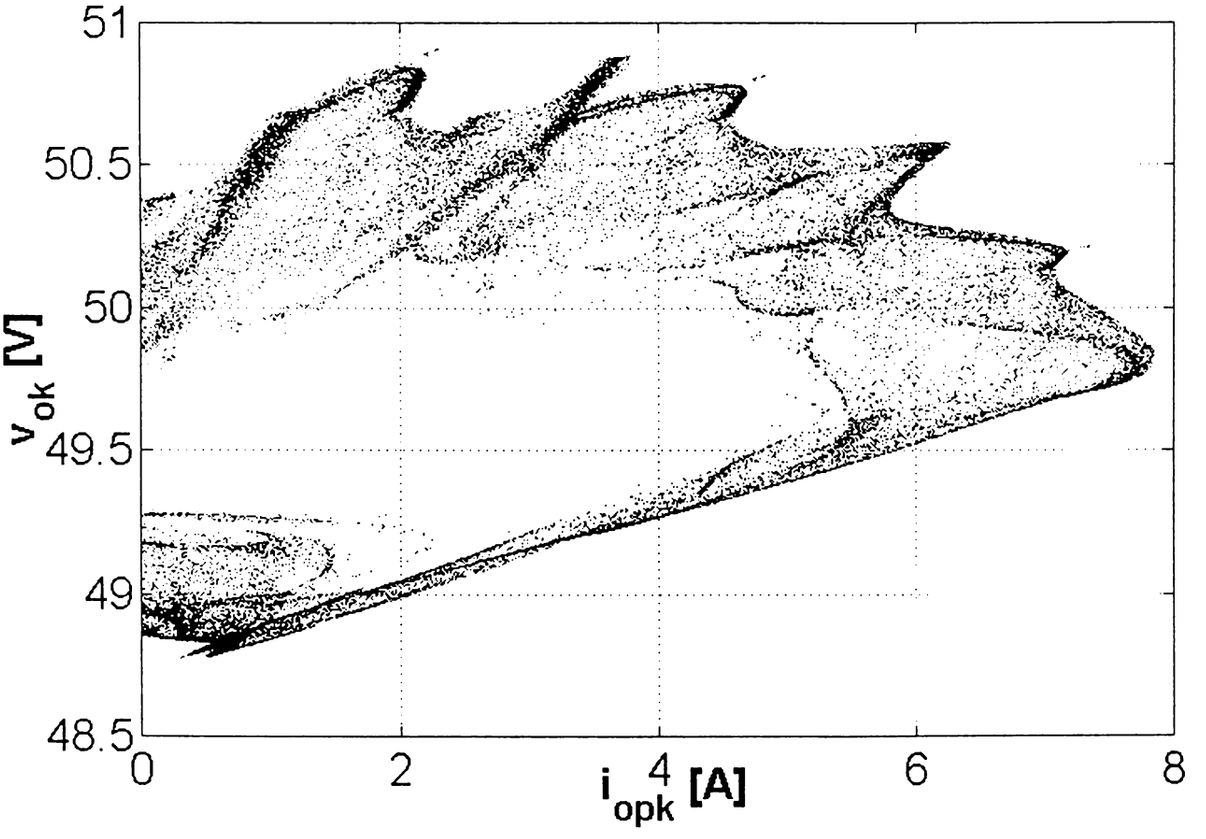

Figure 2-36 Poincaré map for chaotic operation (K_V = 74.2)

Chaos Revisited: State Space The chaotic steady-state trajectory corresponding to K_V = 74.2 is presented in Fig. 2-37 in the plane defined by choke current i_{op} and output

voltage v_o. As it was already revealed by the Poincaré map, the limit set of the chaotic behavior is a complicated geometrical structure, which is called *strange attractor*.

> ***Strange attractor:*** The geometrical object in state space to which chaotic trajectories are attracted.

During its wandering over the strange attractor in Fig. 2-37, the unclosed trajectory repeatedly and randomly comes on an infinite number of limit cycles very similar to that of the subharmonic behavior plotted in Fig. 2-35 (if the simulations were run longer the attractor would become more densely filled in, but not uniformly, as was the case of the quasiperiodic limit set). This is a very important and useful feature common to chaotic systems [86].

> ***Strange attractor:*** A chaotic attractor typically has embedded within it an infinite number of unstable periodic trajectories.

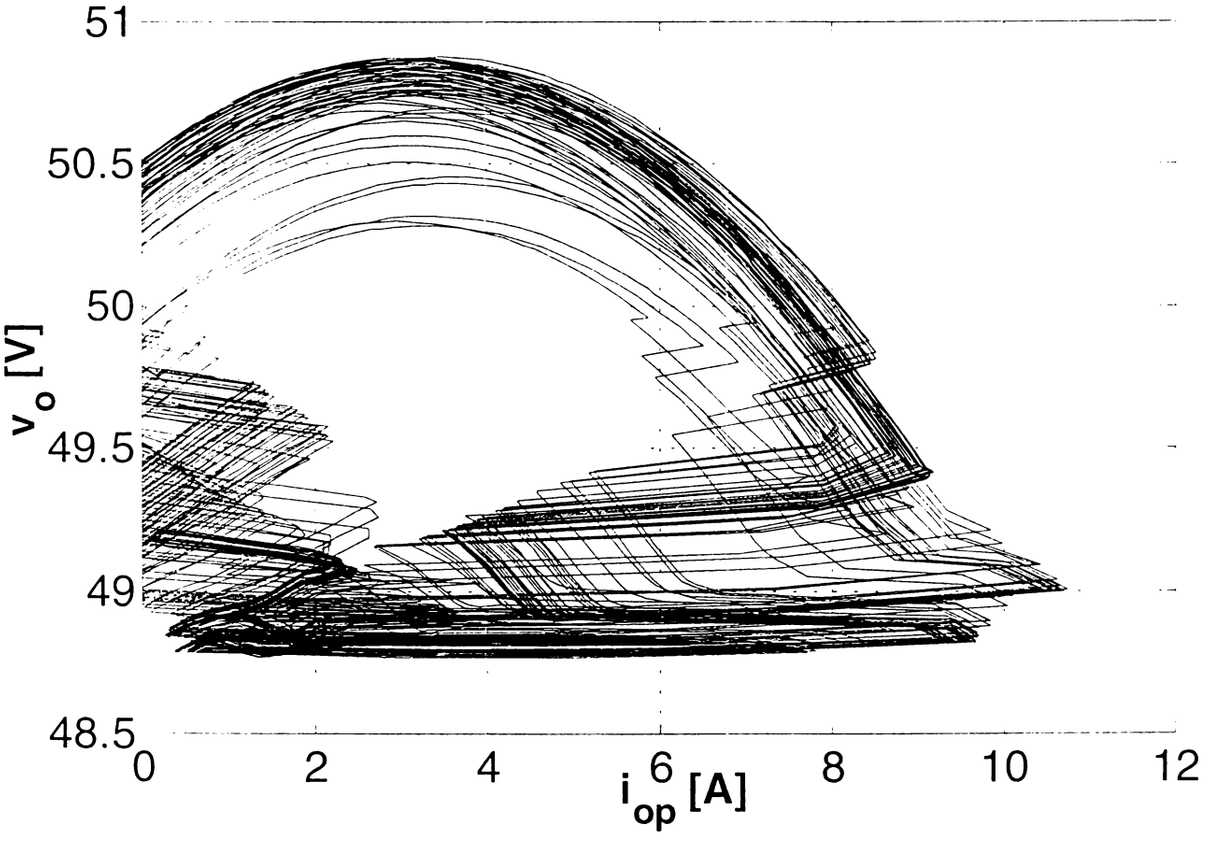

Figure 2-37 Chaotic state space trajectory ($K_V = 74.2$)

It is worth to mention another very important feature common to chaotic systems, resulting also from state space behavior. An important consequence of the uniqueness of

the solution $\theta_t(x_0)$ of an autonomous continuous-time system $\dot{x} = f(x)$ is that a trajectory of the dynamical system cannot go through the same point twice in two different directions. In particular, no two trajectories may cross each other and this is called the *noncrossing property*. Taking into account the noncrossing property and the assumption of a bounded region of state space in which the trajectories live, the *Poincaré-Bendixson theorem* states that there are only two possibilities for the trajectory of a two-dimensional autonomous continuous-time dissipative system: it approaches after the transient process either an equilibrium point or a limit cycle (in contrast with the strange attractor, these and the quasiperiodic limit sets are called *classical attractors* and they are associated with some geometrical forms). Only a two-dimensional space is separated by a curve into a region „inside" and a region „outside", hence a trajectory starting inside the limit cycle can never get out and vice-versa. Furthermore, the Poincaré-Bendixson theorem leads to an important result: chaotic behavior cannot occur in a one- or two-dimensional autonomous continuous-time system [88]. It is obvious that chaos cannot arise in linear systems either.

> ***Chaos:*** Nonlinearity and at least three state variables are needed in autonomous continuous-time systems for chaos.

Due to (2-12) a time-periodic non-autonomous continuous-time system can be converted into an autonomous continuous-time system by appending time as an additional state variable, therefore, at least two state variables are needed in non-autonomous continuous-time systems for chaos. In discrete time, even first-order maps can exhibit chaotic behavior.

The route to chaos identified in this section represents the *period-doubling route to chaos*. A period-doubling route to chaos displays a quite surprising behavior because it is governed by a universal scaling law which holds in the vicinity of the bifurcation point to chaos. Defining the ratio δ of successive interval lengths δ_k, in each of which holds a period-2^{k+1} state (Fig. 2-38), a universal constant called the *Feigenbaum number* δ is obtained in the limit as $k \to \infty$ [85].

> ***Feigenbaum number:*** $\delta = \lim_{k \to \infty} \frac{\delta_k}{\delta_{k+1}} = 4.66920161...$ (Fig. 2-38)

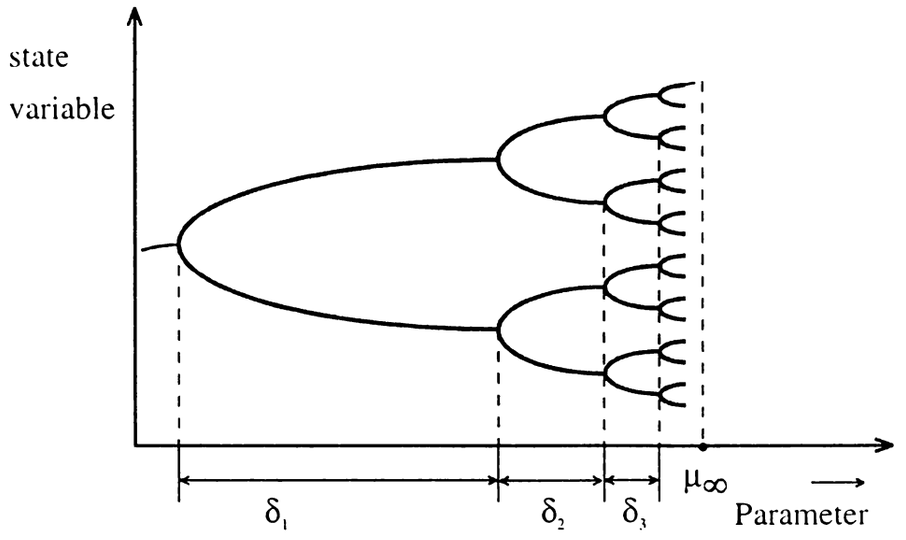

Figure 2-38 Scenario of period doubling

Feigenbaum's number is a universal constant in the theory of chaos like other fundamental numbers, e.g., π, e, and the golden mean ratio $(\sqrt{5}-1)/2$. For the converter the period-doubling scenario can be seen better in Fig. 2-39, which shows in magnified form the window encircled by dotted line in Fig. 2-31. Denoting the first bifurcation point by λ_0, the next one by λ_1 etc., the values of the first several bifurcation points are in Table 2-2. Table 2-1 contains also δ_1 and δ_2. The δ values are not far from the Feigenbaum constant.

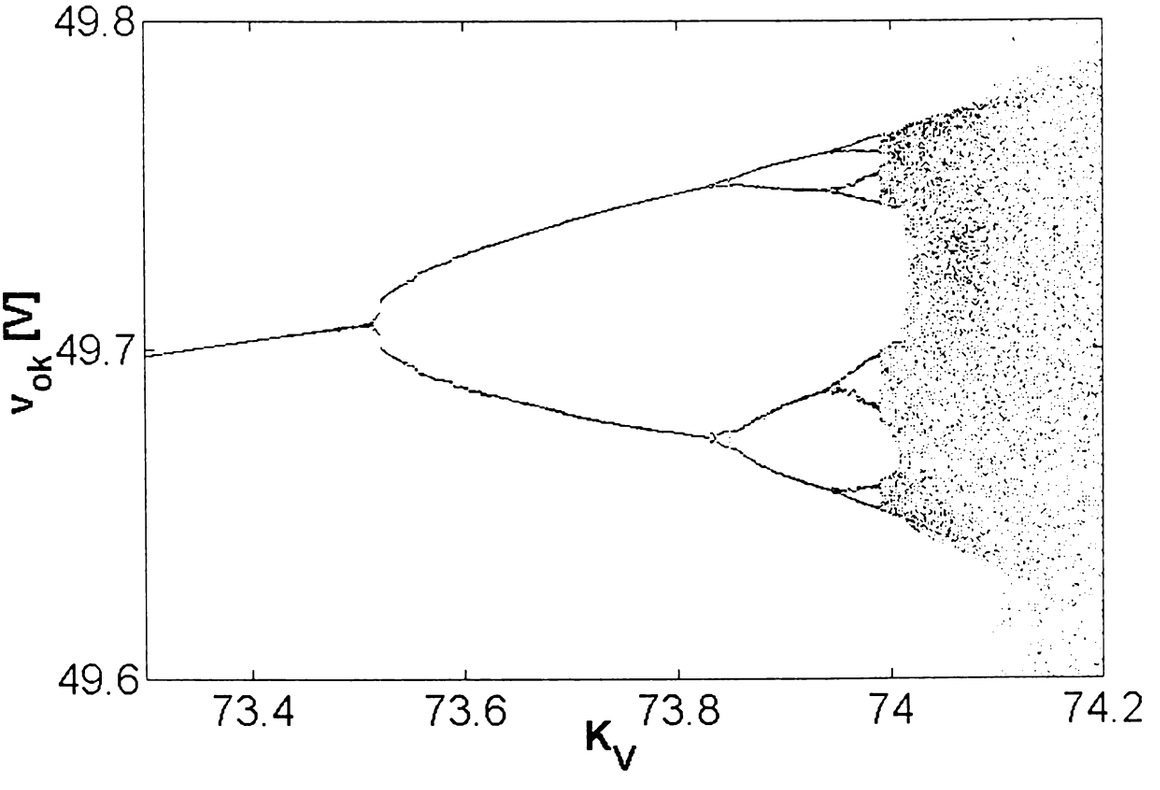

Figure 2-39 Enlarged part of the bifurcation diagram in Fig. 2-31

TABLE 2-2 Bifurcation Points in Fig. 2-39

k	λ_k	δ_k
0	73.501	
1	73.841	4.0476
2	73.925	4.2000
3	73.945	

Period-doubling route to chaos: A cascade of period-doubling bifurcations that accumulate at a parameter value for which the system becomes chaotic. The rate of convergence of the bifurcation values is a universal constant independent of the system.

2-4-3 INTERMITTENCY ROUTE TO CHAOS

The last type of bifurcation behavior that is present in the studied converter configuration is the intermittency route to chaos. In the diagram presented in Fig.2-32 it corresponds to the bifurcation from period-9 subharmonic state to the chaotic state by decreasing the controller gain K_V. Intermittency is best characterized in the time domain: after the bifurcation, a time waveform is characterized by long intervals of regular motion (called *laminar phases*) and short bursts of irregular motion. Such a representative fragment from the time waveform of the output voltage v_o is depicted in Fig. 2-40, at $K_V = 72.97$. The period of the oscillations during the laminar phases is equal to that of the system just before the bifurcation, in period-9 operation. Decreasing the controller gain further the laminar phases become shorter and the bursts become more frequent, until the regular intervals disappear completely. The fully developed chaotic state is illustrated again by the Poincaré map in Fig. 2-41, in the plane of choke current i_{opk} vs. condenser voltage v_{ok}, at $K_V = 72.8$.

Intermittency route to chaos: After a bifurcation, a trajectory alternates between periodic motion and bursts of chaotic behavior. Changing the system parameter further the duration of chaotic states become more and more longer, until chaos is fully developed at some distance from the bifurcation point [85].

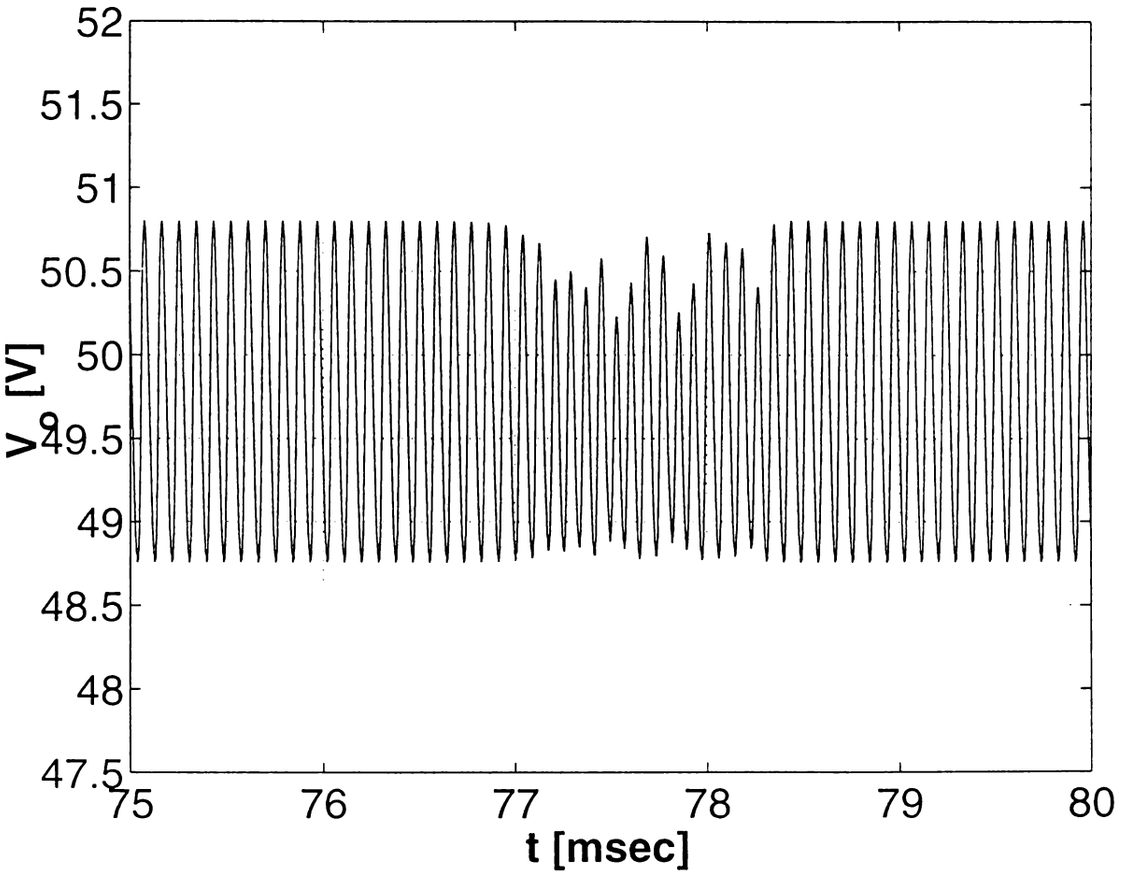

Figure 2-40 Time waveform of the output voltage during intermittency route to chaos ($K_V = 72.8$)

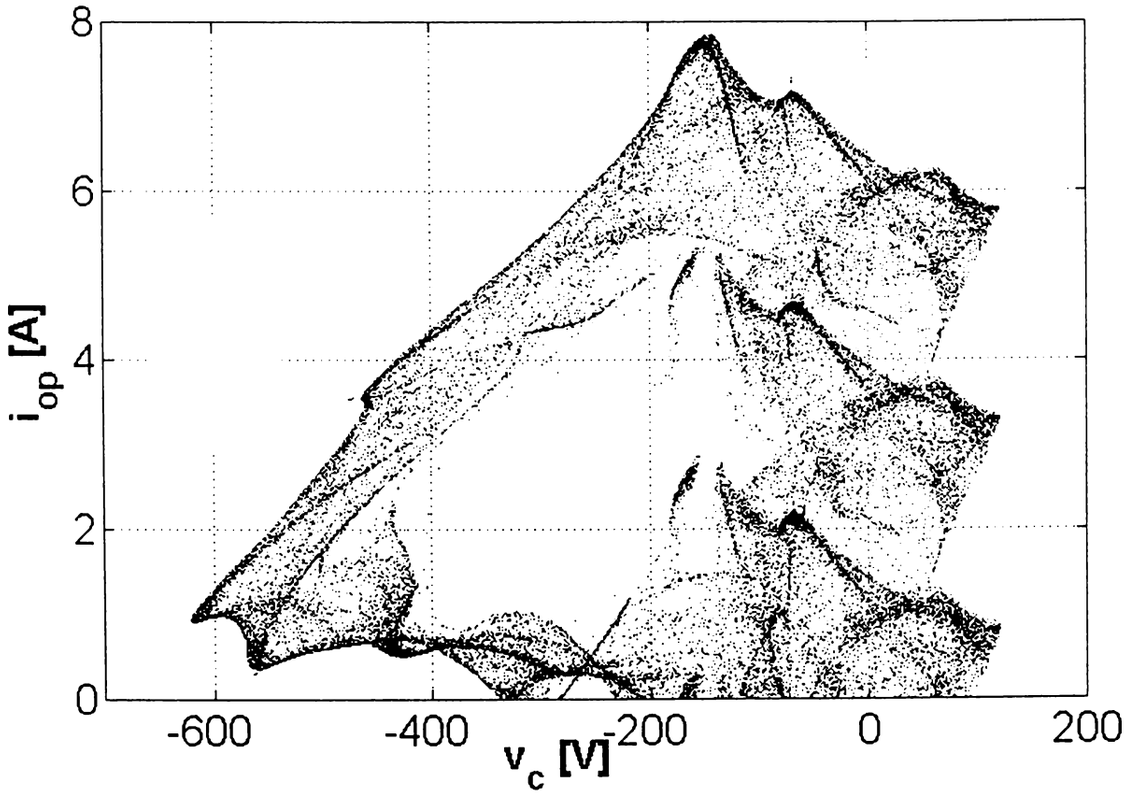

Figure 2-41 Poincaré map for chaotic operation ($K_V = 72.8$)

The studied converter configuration was able to exhibit all three classical routes to chaos. These scenarios can be useful because it is often difficult to conclude from experimental data alone whether irregular behavior is due to measurement noise or to underlying chaotic dynamics. If, upon adjusting a control parameter, one of the three prototype routes to chaos is observed, this indicates that the dynamics might be chaotic.

2-5 STABILITY ANALYSIS OF THE FEEDBACK-CONTROLLED CONVERTER

Computer simulation studies presented in the previous sections revealed important bifurcation phenomena when adjusting the gain of the proportional control in the PWM switching loop. Hence, the following study is concerned with system stability in conjunction with the design of the feedback control loop, i.e., it tries to establish formally the possibility of bifurcation as a result of varying K_V.

2-5-1 THEORETICAL BACKGROUND: STABILITY OF A PERIODIC SOLUTION

As presented in subsection 2-4-1-2, in normal operation the converter exhibits period-1 behavior. Periodic time functions describe the waveforms of the state variables, with period T_s (Fig. 2-8, Fig. 2-9). It was also emphasized that one of the most useful method for investigating continuous-time nonlinear systems involves the discretization technique represented by the Poincaré map. It was shown that for a non-autonomous system the Poincaré map is defined by the sampling of the trajectory at a rate being equal to the switching frequency. Consequently, assuming that the period of the periodic state is the same as that of the switching frequency, the period-1 state corresponds to a fixed point x^* in the Poincaré map denoted by P in the state space. Therefore, the stability of the period-1 state is the same as the stability of the fixed point in the Poincaré map. In the succeeding discussion of stability, „fixed point" can be replaced everywhere by „period-1 solution".

Therefore the stability is determined by the local behavior of the Poincaré map near the fixed point x^*. If all sufficiently small alterations around x^* tends toward 0 with time, then x^* and the limit cycle are *asymptotically stable*, the trajectories are attracted onto the

limit cycle. x^* and the limit cycle are *unstable* if any sufficiently small alteration increases with time and the trajectories move away the initial limit cycle [89].

> ***Stable:*** A limit set is stable if all nearby trajectories stay nearby.

> ***Asymptotically stable:*** A limit set is asymptotically stable if all nearby trajectories are attracted, i.e., they approach the limit set as $t \to \infty$.

> ***Unstable:*** A limit set is unstable if all nearby trajectories are repelled (except of course those lying on the limit set).

The Poincaré map function relates the consecutive points in the Poincaré map, their coordinates in state space separated by one switching period T_s from each other in time:

$$x_{n+1} = P(x_n) \tag{2-21}$$

and at the fixed point $x^* = P(x^*)$.

In particular, the local behavior of the Poincaré map in the neighborhood of the fixed point x^* is governed by its linearization near that fixed point:

$$\Delta x_{n+1} = J_P(x^*)\,\Delta x_n \tag{2-22}$$

where

$$J_P(x^*) = \left.\frac{dP(x)}{dx}\right|_{x^*} \tag{2-23}$$

is the Jacobian matrix of the Poincaré map function $P(x_n)$, evaluated at the fixed point x^*. Substituting $J_P(x^*)$ by its eigenvalues λ_i and right u_{ir} and left u_{il} eigenvectors, the linear map becomes:

$$\Delta x_{n+1} = \left[\sum_{i=1}^{n} \lambda_i u_{ir} u_{il}^T\right] \Delta x_n \tag{2-24}$$

The eigenvalues λ_i are called *characteristic multipliers* or *Floquet multipliers* of the periodic solution.

> ***Characteristic multipliers:*** The characteristic multipliers of a periodic solution are the eigenvalues of the linearization of the Poincaré map at the corresponding fixed point. They give the amount of expansion and contraction near the periodic solution during one period.

From linear system theory, the position of the characteristic multipliers in the complex plane determines the stability of the fixed point (Fig. 2-42). The fixed point and the limit cycle are asymptotically stable if and only if all eigenvalues of the linearization (2-24) have modulus less than unity, i.e., they lie inside the unit circle; if any characteristic multiplier has modulus greater than unity, i.e., it lies outside the unit circle, the limit cycle is unstable. The characteristic multipliers are real in a *node* and complex-conjugate pairs in a *focus*. The trajectories approach an asymptotically stable limit cycle in an aperiodic way if the fixed point is a *stable* (or *attractor*) *node* and in a spiral way for a *stable* (or *repellor*) *focus*. They diverge aperiodically from an unstable limit cycle if the fixed point is an *unstable* (or *repellor*) *node* and spiral away in case of an *unstable* (or *repellor*) *focus*. If the fixed point is a *saddle point*, the trajectories approach the limit cycle in one direction and diverge in another one (in higher dimensional case saddle point can contains also focus, i.e., complex eigenvalues). Generic fixed points just presented remain structurally stable as long as none of their characteristic multipliers lies on the unit circle. Such fixed points those have no characteristic multipliers on the unit circle are called *hyperbolic* [84].

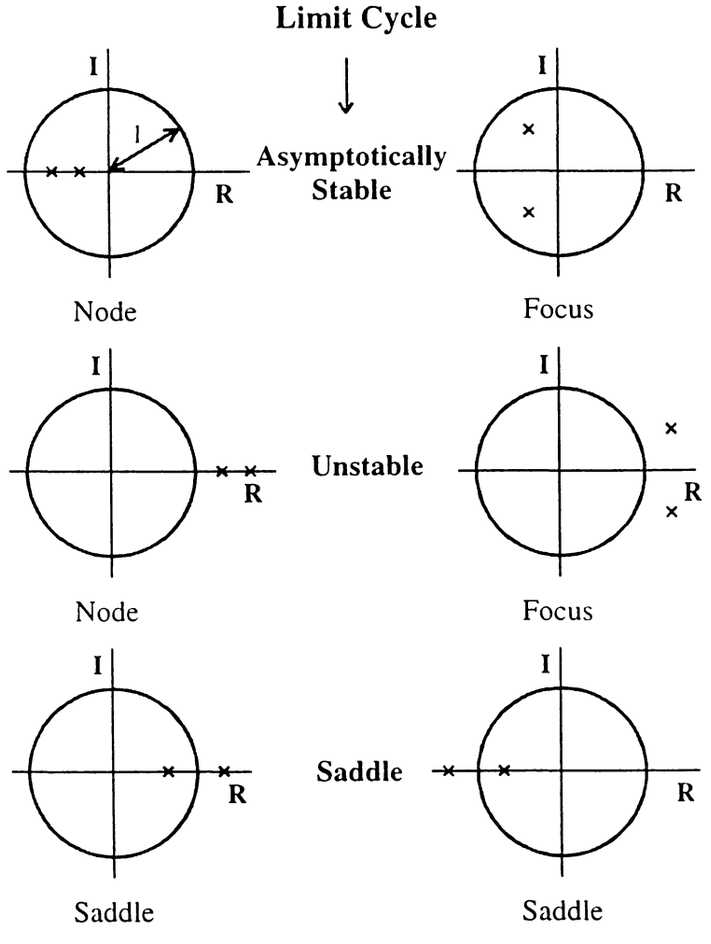

Figure 2-42 The position in the complex plane of the characteristic multipliers for the two-dimensional case

Hyperbolic periodic solution: None of the characteristic multipliers of a hyperbolic periodic solution has magnitude 1. Hyperbolic periodic solutions are generic and structurally stable.

Stability of a periodic solution: A hyperbolic periodic solution is asymptotically stable if and only if all its characteristic multipliers lie inside the unit circle. It is unstable if any of the characteristic multipliers lies outside the unit circle.

2-5-2 THE FEEDBACK CONTROLLED CONVERTER: A VARIABLE STRUCTURE, PIECEWISE LINEAR, NONLINEAR SYSTEM

The studied resonant converter is a *variable structure, piecewise linear, nonlinear dynamical* system [89]. The structure of the active circuit varies during the periodic steady-state operation (Fig. 2-8). The *structures* change periodically during the operation. One *period* corresponds to the switching cycle T_s and it is divided into two *subperiods* (semiperiods in time) by the repeated succession of two structures presented in Fig. 2-43. The correspondence between the circuits in Fig. 2-43 and the active parts of the converter configuration (Fig. 2-6) during one switching period is shown in Table 2-3. The time sequence of structure changes is outlined in Fig. 2-44. The durations of the same structure in the two subperiods are equal in periodic state due to the symmetrical operation investigated (Appendix A): $\alpha_p = \alpha_n = \alpha$.

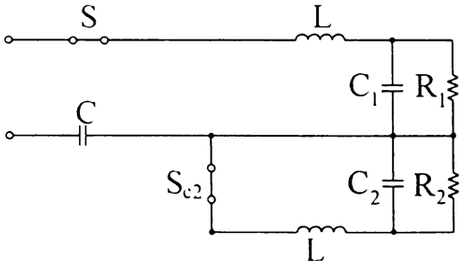

STRUCTURE1: $\omega t \in [0, \alpha_p]$

$\omega t \in [\omega T_s/2, \omega T_s/2 + \alpha_n]$

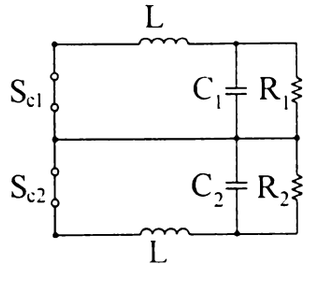

STRUCTURE 2: $\omega t \in [\alpha_p, \omega T_s/2]$

$\omega t \in [\omega T_s/2 + \alpha_n, \omega T_s]$

Figure 2-43 Converter structures during a subperiod

Table 2-3 The connection between the converter and the structures in Fig. 2-43 during one switching period

	ONE SWITCHING PERIOD			
	SUBPERIOD I		SUBPERIOD II	
	STRUCTURE 1	STRUCTURE 2	STRUCTURE 1	STRUCTURE 2
S	S_p	-	S_n	-
S_{c1}	-	S_{cp}	-	S_{cn}
S_{c2}	S_{cn}	S_{cn}	S_{cp}	S_{cp}
C_1	C_p	C_p	C_n	C_n
C_2	C_n	C_n	C_p	C_p
R_1	R_p	R_p	R_n	R_n
R_2	R_n	R_n	R_p	R_p

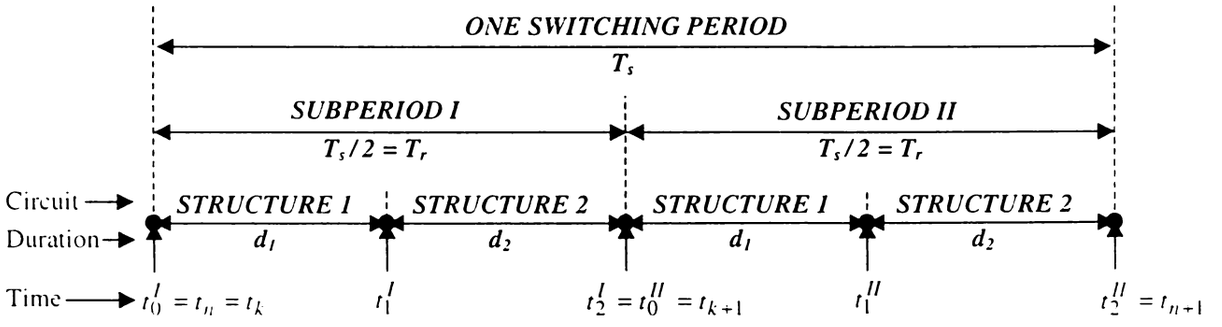

Figure 2-44 The time sequence of structure changes

Since each structure has linear dynamics, the resonant converter is a *piecewise linear* system. On the other hand, the whole system, the feedback controlled converter is nonlinear due to the dependence of commutation angles α_p, α_n on the state variable v_o. The linear state equations of the structures in subperiod I, using Table 2-3, are as follows [91]:

Structure 1:

$$\begin{aligned}
\frac{dv_{op}}{dt} &= -\frac{1}{R_p C_p} v_{op} + \frac{1}{C_p} i_{op} \\
\frac{dv_{on}}{dt} &= -\frac{1}{R_n C_n} v_{on} + \frac{1}{C_n} i_{on} \\
\frac{dv_c}{dt} &= \frac{1}{C} i_{op} \\
\frac{di_{op}}{dt} &= -\frac{1}{L} v_{op} - \frac{1}{L} v_c + \frac{1}{L} v_{ip} \\
\frac{di_{on}}{dt} &= -\frac{1}{L} v_{on}
\end{aligned} \tag{2-25}$$

Equations (2-25) can be rewritten in the dimensionless form:

$$\begin{aligned}
\frac{dx_1}{d\tau} &= -ax_1 + bx_4 \\
\frac{dx_2}{d\tau} &= -ax_2 + bx_5 \\
\frac{dx_3}{d\tau} &= \pi x_4 \\
\frac{dx_4}{d\tau} &= -\pi(x_1 + x_3 - 1) \\
\frac{dx_5}{d\tau} &= -\pi x_2
\end{aligned} \tag{2-26}$$

where

$$\begin{aligned}
&x_1 = \frac{v_{op}}{v_i/2}, x_2 = \frac{v_{on}}{v_i/2}, x_3 = \frac{v_c}{v_i/2}, x_4 = \frac{Z \cdot i_{op}}{v_i/2}, x_5 = \frac{Z \cdot i_{on}}{v_i/2}, \tau = \frac{t}{T_r} \\
&a = \frac{T_r}{T_o}, b = \frac{\pi T_c}{T_o} = \frac{\pi C}{C_o}, T_o = RC_o, T_C = RC, Z = \sqrt{L/C}
\end{aligned} \tag{2-27}$$

and $v_i/2 = v_{ip} = v_{in}, C_o = C_p = C_n, R = R_p = R_n, T_r = T_s/2 = \pi\sqrt{LC}$ (Appendix A).

The state model of structure 1 is hereby:

$$\dot{x} = A_1 \cdot x + B_1; \quad x = \begin{bmatrix} x_1 \\ x_2 \\ x_3 \\ x_4 \\ x_5 \end{bmatrix}; \quad A_1 = \begin{bmatrix} -a & 0 & 0 & b & 0 \\ 0 & -a & 0 & 0 & b \\ 0 & 0 & 0 & \pi & 0 \\ -\pi & 0 & -\pi & 0 & 0 \\ 0 & -\pi & 0 & 0 & 0 \end{bmatrix}; \quad B_1 = \begin{bmatrix} 0 \\ 0 \\ 0 \\ \pi \\ 0 \end{bmatrix} \tag{2-28}$$

Structure 2:

State equations:

$$\begin{aligned}
\frac{dv_{op}}{dt} &= -\frac{1}{R_p C_p} v_{op} + \frac{1}{C_p} i_{op} \\
\frac{dv_{on}}{dt} &= -\frac{1}{R_n C_n} v_{on} + \frac{1}{C_n} i_{on} \\
\frac{dv_c}{dt} &= 0 \\
\frac{di_{op}}{dt} &= -\frac{1}{L} v_{op} \\
\frac{di_{on}}{dt} &= -\frac{1}{L} v_{on}
\end{aligned} \tag{2-29}$$

The state model of structure 2 in dimensionless form:

$$\dot{x} = A_2 \cdot x; \quad x = \begin{bmatrix} x_1 \\ x_2 \\ x_3 \\ x_4 \\ x_5 \end{bmatrix}; \quad A_2 = \begin{bmatrix} -a & 0 & 0 & b & 0 \\ 0 & -a & 0 & 0 & b \\ 0 & 0 & 0 & 0 & 0 \\ -\pi & 0 & 0 & 0 & 0 \\ 0 & -\pi & 0 & 0 & 0 \end{bmatrix} \tag{2-30}$$

Subperiod II consists of the same structure series as subperiod I containing structure 1 and structure 2, with the same parameters, due to the symmetrical configuration. By utilizing the periodicity of the structure series, the values of the five state variables at the end of subperiod I, $x(t_2^I)$, can be transformed back to structure 1 used in subperiod I by a periodicity or transformation matrix T^{-1}, that is:

$$x_b(t_0^{II}) = T^{-1} \cdot x(t_2^I) \tag{2-31}$$

where suffix b refers to the back transformation. Now the same structures, structure 1 and 2 and the same state variables are used even in subperiod II as in subperiod I. The transformation matrix is:

$$T = T^{-1} = \begin{bmatrix} 0 & 1 & 0 & 0 & 0 \\ 1 & 0 & 0 & 0 & 0 \\ 0 & 0 & -1 & 0 & 0 \\ 0 & 0 & 0 & 0 & 1 \\ 0 & 0 & 0 & 1 & 0 \end{bmatrix} \tag{2-32}$$

$x_b(t_0^{II})$ is considered as the initial condition of the state variables in structure 1 for subperiod II. The result of the back transformation is ($v_i / 2 = 1$):

$$\begin{aligned} &\left[v_{op}(t_0^{II}) \quad v_{on}(t_0^{II}) \quad v_c(t_0^{II}) \quad Z \cdot i_{op}(t_0^{II}) \quad Z \cdot i_{on}(t_0^{II})\right]^T = \\ &= \left[v_{on}(t_2^I) \quad v_{op}(t_2^I) \quad -v_c(t_2^I) \quad Z \cdot i_{on}(t_2^I) \quad Z \cdot i_{op}(t_2^I)\right]^T \end{aligned} \tag{2-33}$$

Suffix b has been omitted in eq. (2-33). At the beginning of subperiod II, $v_{op}(t_0^{II})$ starts from $v_{on}(t_2^I)$ and increases a little bit as a result of the current pulse i_{op} starting from $i_{on}(t_2^I)$. The capacitor voltage v_c swings over from $-v_c(t_2^I)$ to the positive values as a result of the positive current i_{op} flowing in C. There is no need to write new equations in

subperiod II, the same equations can be used as in subperiod I. The same back transformation has to be used at the end of each succeeding subperiod [89].

The procedure can be applied both in periodic steady-state and in transient state. In periodic steady-state due to the periodicity (Fig. 2-8):

$$x(t_2^I) = T \cdot x(t_0^I) \tag{2-34}$$

As it was mentioned above, the system within each subperiod is piecewise linear and the PWM-controlled feedback converter becomes a *nonlinear system* due to the dependence of the structure change instants (the turn-on time of the switches) on the state variable, the output voltage.

2-5-3 STABILITY ANALYSIS USING POINCARÉ MAP FUNCTION

It has been shown that the stability of the feedback control loop including the converter in periodic operation is determined by the eigenvalues of the Jacobian matrix of the Poincaré map function at the corresponding fixed point [eq. (2-22)]. Since we have proved in the previous subsection that the dynamics of the entire switching period is fully characterized by that of one subperiod, with transformation (2-31) applied at its end, we are interested in a discrete-time map that relates the state variables over one subperiod. This discrete-time map function f can be expressed in the following form:

$$x_{k+1} = f(x_k, \delta_1) \tag{2-35}$$

where at the beginning of each T_s switching period k takes the value of the number of periods $k = n$ and the dimensionless interval is $\delta_1 = d_1 / T_r$ of structure 1 (Fig. 2-44). δ_1 determines unanimously the dimensionless interval $\delta_2 = d_2 / T_r$ of structure 2. One subperiod lasts one period of the sawtooth waveform $T_r = T_s / 2$ (Fig. 5), therefore:

$$\delta_2 = 1 - \delta_1 \tag{2-36}$$

By applying in cascade the solutions of differential equations (2-28) and (2-30), map function f can be written as follows:

$$x_{k+1} = f(x_k, \delta_1) = \Phi_2(1-\delta_1) \cdot \left\{ \Phi_1(\delta_1) \cdot x_k + \left[\Phi_1(\delta_1) - I \right] \cdot A_1^{-1} \cdot B_1 \right\} \tag{2-37}$$

where

$$\Phi_1(\delta_1) = e^{A_1 \delta_1} \; ; \; \Phi_2(1-\delta_1) = e^{A_2(1-\delta_1)} \tag{2-38}$$

are the transition matrixes of the two structures, respectively, as well as one particular solution of (2-28) is

$$x_p = -A_1^{-1} \cdot B \tag{2-39}$$

obtained from (2-28) by substituting $\dot{x} = 0$. By using (2-28) and calculating $x_p = -A_1^{-1} \cdot B_1 = -\frac{adjA_1}{|A_1|} \cdot B_1$, the result is: $x_1 = 0, x_2 = 0, x_3 = \frac{v_c}{v_i/2} = 1, x_4 = 0$ and $x_5 = 0$. This result as one possible particular solution can easily be deduced by physical consideration without any calculation as well. I is the identity matrix.

Our next aim is to express the feedback relation that connects the duration δ_1 and the state vector x_k. The PWM control terminates the structure 1 of one subperiod at δ_1 when the difference between the control voltage v_{con} and the sawtooth waveform v_{ramp} becomes zero (Fig. 2-9). In dimensionless form:

$$\begin{aligned} e(x_k, \delta_1) &= \frac{v_{con}(\delta_1) - v_{ramp}(\delta_1)}{v_i/2} = \\ &= K_V \cdot [v_{ref}^* - x_1(\delta_1) - x_2(\delta_1)] - V_L^* - (V_U^* - V_L^*) \cdot \delta_1 = \\ &= K_V \cdot v_{ref}^* - k^T \cdot x(\delta_1) - V_L^* - (V_U^* - V_L^*) \cdot \delta_1 = \\ &= K_V \cdot v_{ref}^* - k^T \cdot \left\{\Phi_1(\delta_1) \cdot x_k + [\Phi_1(\delta_1) - I] \cdot A_1^{-1} \cdot B_1\right\} - V_L^* - (V_U^* - V_L^*) \cdot \delta_1 = \\ &= 0 \end{aligned} \tag{2-40}$$

where $v_{ref}^* = \frac{v_{ref}}{v_i/2}, V_L^* = \frac{V_L}{v_i/2}, V_U^* = \frac{V_U}{v_i/2}, k^T = [K_V \quad K_V \quad 0 \quad 0 \quad 0]$. Relations (2-10), (2-27) and the solution of (2-28) were used in (2-40).

On the basis of eq. (2-37) after back transformation:

$$x_{k+1,b} = T^{-1} \cdot x_{k+1} = T^{-1} \cdot f[x_k, \delta_1(x_k)] \tag{2-41}$$

At the end of subperiod II after back transformation:

$$x_{k+2,b} = x_{n+1} = T^{-1} \cdot x_{k+2} = T^{-1} \cdot f[x_{k+1,b}, \delta_1(x_{k+1,b})] \tag{2-42}$$

The Poincaré map function F belonging to f, i.e., to one subperiod, from (2-41) and (2-42) is

$$x_{k+1,b} = F(x_k) \tag{2-43}$$

In period-1 steady-state $x_n = x_k = x_{k+1,b} = x_{k+2,b} = x^*$ where x^* is the fixed point. From the previous three equations:

$$x^* = T^{-1} \cdot f[x^*, \delta_1(x^*)] = F(x^*) \tag{2-44}$$

The Jacobian matrix J_F of map function F defined in (2-43) and (2-44) takes the following form:

$$\begin{aligned} T \cdot J_F(x^*) &= \left.\frac{df(x,\delta_1)}{dx}\right|_{x^*} = \left[\frac{\partial f}{\partial x} + \frac{\partial f}{\partial \delta_1}\left(\frac{d\delta_1}{dx}\right)^T\right]_{x^*} = \\ &= \left[\frac{\partial f}{\partial x} - \frac{\partial f}{\partial \delta_1}\left(\frac{\partial e}{\partial \delta_1}\right)^{-1}\left(\frac{\partial e}{\partial x}\right)^T\right]_{x^*} \end{aligned} \tag{2-45}$$

The derivatives of f can be calculated from (2-37), (2-38):

$$\frac{\partial f}{\partial x} = \Phi_2(1-\delta_1)\cdot\Phi_1(\delta_1) \tag{2-46}$$

$$\begin{aligned} \frac{\partial f}{\partial \delta_1} &= \frac{\partial \Phi_2(1-\delta_1)}{\partial \delta_1}\cdot\left\{\Phi_1(\delta_1)\cdot x_k + [\Phi_1(\delta_1)-I]\cdot A_1^{-1}\cdot B_1\right\} + \\ &+ \Phi_2(1-\delta_1)\cdot\frac{\partial\left\{\Phi_1(\delta_1)\cdot x_k + [\Phi_1(\delta_1)-I]\cdot A_1^{-1}\cdot B_1\right\}}{\partial \delta_1} = \\ &= -\Phi_2(1-\delta_1)\cdot A_2\cdot x(\delta_1) + \Phi_2(1-\delta_1)\cdot\frac{\partial x(\delta_1)}{\partial \delta_1} = \\ &= \Phi_2(1-\delta_1)\cdot\left(-\dot{x}_{2,start} + \dot{x}_{1,end}\right) \end{aligned} \tag{2-47}$$

where $\dot{x}_{1,end}$ and $\dot{x}_{2,start}$ are the velocities of state vector x at the end of structure 1 [eq. (2-28)], and at the beginning of structure 2 [eq. (2-30)], respectively.

The derivatives of e are obtained from (2-40) using also the solution of (2-28):

$$\begin{aligned} \frac{\partial e}{\partial \delta_1} &= -k^T\cdot\frac{\partial\left\{\Phi_1(\delta_1)\cdot x_k + [\Phi_1(\delta_1)-I]\cdot A_1^{-1}\cdot B_1\right\}}{\partial \delta_1} - (V_U^* - V_L^*) = \\ &= -k^T\cdot\frac{\partial x(\delta_1)}{\partial \delta_1} - (V_U^* - V_L^*) = -k^T\cdot\dot{x}_{1,end} - (V_U^* - V_L^*) \end{aligned} \tag{2-48}$$

$$\left(\frac{\partial e}{\partial x_k}\right)^T = -k^T\cdot\Phi_1(\delta_1) \tag{2-49}$$

Substituting all the derivatives expressed in (2-46) – (2-49) into (2-45), the Jacobian matrix of map function F is:

$$
\begin{aligned}
J_F(x^*) &= T^{-1}\cdot\Phi_2(1-\delta_1)\cdot\Phi_1(\delta_1)\big|_{x^*} - \\
&\quad - T^{-1}\cdot\left.\frac{\Phi_2(1-\delta_1)\cdot(\dot{x}_{1,end}-\dot{x}_{2,start})\cdot k^T\cdot\Phi_1(\delta_1)}{k^T\cdot\dot{x}_{1,end}+V_U^*-V_L^*}\right|_{x^*} = \\
&= T^{-1}\cdot\Phi_2(1-\delta_1)\cdot\left[I-\frac{\dot{x}_{1,end}-\dot{x}_{2,start}}{k^T\cdot\dot{x}_{1,end}+V_U^*-V_L^*}\cdot k^T\right]\cdot\Phi_1(\delta_1)\Big|_{x^*} = \\
&= T^{-1}\cdot\Phi_2(1-\delta_1)\cdot M\cdot\Phi_1(\delta_1)\big|_{x^*}
\end{aligned}
\tag{2-50}
$$

The equations from (2-35) up to (2-44) are the same for the next subperiod starting by state variable $x_{k+1,b}$ and ending by $x_{k+2,b} = x_{n+1}$. Therefore, the stability of the converter is unambiguously determined by the Jacobian matrix $J_F(x^*)$ expressed in (2-50) [83].

For small deviations around the fixed point x^*

$$\Delta x_{k+1,b} = J_F(x^*)\cdot\Delta x_k = J_F(x^*)\cdot\Delta x_n \tag{2-51}$$

and

$$\Delta x_{n+1} = \Delta x_{k+2,b} = J_F(x^*)\cdot\Delta x_{k+1,b} = J_F{}^2(x^*)\cdot\Delta x_n \tag{2-52}$$

Using the Jacobian matrix J_P related for a full period [eq. (2-22)]

$$\Delta x_{n+1} = J_P(x^*)\cdot\Delta x_n = J_P{}^{n+1}(x^*)\cdot\Delta x_0 \tag{2-53}$$

From the last two relations:

$$\Delta x_{n+1} = J_F{}^{2(n+1)}(x^*)\cdot\Delta x_0 \tag{2-54}$$

The absolute values of the eigenvalues of J_F or J_P must be smaller than 1 for stable operation. Since the eigenvalues of J_F are the square roots of those of J_P, their positions, as compared to the unit circle, lead to the same conclusion. Therefore, the eigenvalues of J_F are used for the stability study and a MATLAB program was developed in order to compute them.

To calculate the eigenvalues of J_F the value δ_1 must be determined. An iterative algorithm was used to this end [83]. The initial value $\delta_{1,in}$ was obtained from the steady-state relations derived in subsection 2-3-1, where the filter capacitor at the output was assumed to be very large, as it is normally the case in applications requiring a nearly ripple free instantaneous output voltage V_o. The corresponding steady-state duty ratio $\delta_{1,in}$ was determined by the PWM control (Fig. 2-9b):

$$\delta_{1,in} = \frac{\alpha}{\pi} = \frac{K_v(v_{ref}-V_o)-V_L}{V_U-V_L} \tag{2-55}$$

The average output voltage V_o can be expressed from (2-9) by taking into consideration that $f_s / f_r = 1$:

$$V_o = \frac{v_i}{1 + \frac{\pi - \alpha/2}{tg(\alpha/2)}} \tag{2-56}$$

Substituting V_o from (2-56) into (2-55), $\delta_{1,in} = d_1 / T_r = \alpha / \pi$ was calculated from the transcendental equation.

The accurate value δ_1 deviates from $\delta_{1,in}$ due to the ripple in v_o. It has been shown that in periodic steady-state $x_k = T^{-1} \cdot f(x_k, \delta_{1,ac})$, where $\delta_{1,ac}$ is the accurate value giving the accurate meeting point of v_{con} and v_{ramp} within period T_r (Fig. 2-9b), i.e., satisfying eq. (2-40). The iteration for the calculation of $\delta_{1,ac}$ starts by substituting $\delta_{1,in}$ in eq. (2-37) and calculating x_k, i.e., the first approximation of the time functions v_o or v_{con} from relation:

$$x_k = [T - \Phi_2(1-\delta_1) \cdot \Phi_1(\delta_1)]^{-1} \cdot \Phi_2(1-\delta_1) \cdot [\Phi_1(\delta_1) - \underline{I}] \cdot A_1^{-1} \cdot B_1 \tag{2-57}$$

Knowing v_{con}, the meeting point of v_{con} and v_{ramp} provides the new value for δ_1 in the next iteration step. By setting a limit ε for the deviation in δ_1 in two consecutive iteration steps in such a way that $\frac{|\delta_{1,i} - \delta_{1,i-1}|}{\delta_{1,i}} < \varepsilon$, $\delta_{1,ac}$ can be approximated at will, where i is the number of iteration steps.

The calculation of matrix

$$M|_{x^*} = \left[I - \frac{\dot{x}_{1,end} - \dot{x}_{2,start}}{k^T \cdot \dot{x}_{1,end} + V_U^* - V_L^*} \cdot k^T \right]_{x^*} \tag{2-58}$$

requires the velocity of state vector at the end of structure 1 ($\dot{x}_{1,end}$) and that at the start of structure 2 ($\dot{x}_{2,start}$), which are defined by the state models of the two structures, by eq. (2-28) and (2-30), respectively. The state vector $x(\delta_1)$ is needed for the calculation both for $\dot{x}_{1,end} = A_1 \cdot x(\delta_1) + B_1$ and $\dot{x}_{2,start} = A_2 \cdot x(\delta_1)$. It can be determined from the solution of eq.(2-28) [see eq.(2-37)]:

$$x(\delta_1) = \Phi_1(\delta_1) \cdot x_k + [\Phi_1(\delta_1) - I] \cdot A_1^{-1} \cdot B_1 \tag{2-59}$$

Knowing all terms in matrix J_F, its eigenvalues can be calculated e.g. by MATLAB. The developed MATLAB program is listed in Appendix C.

2-5-4 STABILITY ANALYSIS USING THE RÁCZ METHOD

The Rácz method is applied in this second approach to determine the Jacobian matrix J_F of map function F. The basic idea of this method is illustrated in Fig. 2-45. Recall again that in steady state the system exhibits a periodic behavior, its trajectory in state space reaches a limit cycle, whose stability can be determined by modifying slightly the trajectory in the vicinity of this limit cycle. Initially, before the change in the trajectory, the system reaches the switching hypersurface of the limit cycle at time t_m in $P(t_m)$ and the trajectory suddenly changes due to this switching (solid line in Fig. 2-45). As an effect of the alteration Δx the trajectory is modified (dashed line in Fig. 2-45). The new trajectory reaches at time t_m the point P_1 and the alteration of the state vector at this time is $\Delta x_{m,end}(t_m)$. The switching hypersurface is reached by this modified trajectory at $t_m+\Delta t_m$ in P_2. The "distance" between P_1 and P_2 is $\dot{x}_{m,end}\Delta t_m$, where $\dot{x}_{m,end}$ is the velocity vector at the end of the structure m. The alteration of the state vector on the hypersurface is $\Delta x_{m,end}(t_m+\Delta t_m)$. After the switching, the velocity vector at the start of the structure $m+1$ is $\dot{x}_{m+1,start}$. Since each structure is a linear one, the point $P_2(t_m+\Delta t_m)$ of the trajectory can be projected "back in time" to t_m by extending the trajectory at the start of the structure $m+1$ toward "negative time" along the velocity vector $\dot{x}_{m+1,start}$. Point $P_3(t_m)$ at distance $-\dot{x}_{m+1,start}\Delta t_m$ from P_2 is obtained in this way and the virtual alteration of the state vector becomes $\Delta x_{m+1,start}(t_m)$. This mathematical abstraction is useful since by applying it, the trajectory will start in structure $m+1$ at the same instant t_m as in the case of the original trajectory [89].

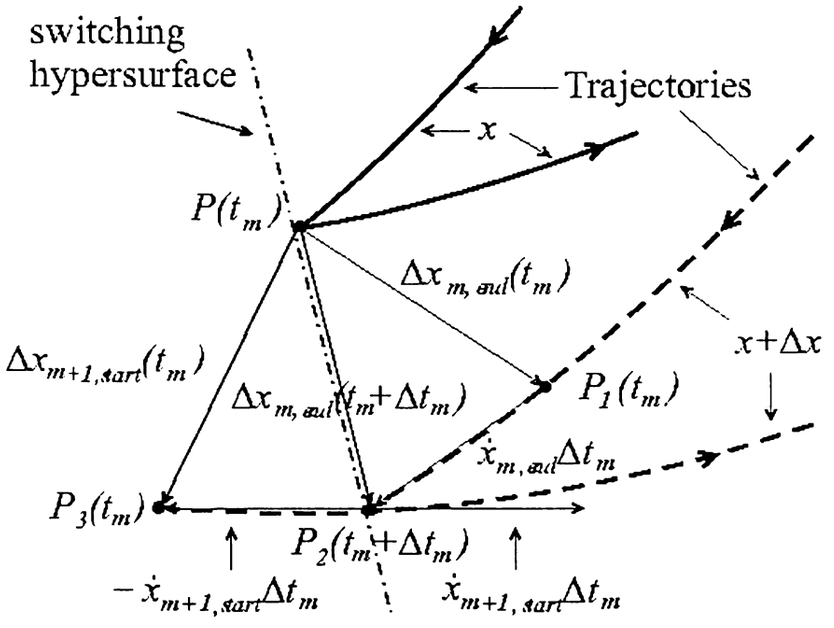

Figure 2-45 The Rácz method

Applying Fig. 2-45 for the feedback-controlled converter in periodic steady-state, a first switching instant t_m within a subperiod corresponds to the transition from structure 1 into structure 2 (Fig. 2-44) at the dimensionless moment δ_1. The aim is to determine a relation between the real and virtual alterations of the dimensionless state vector at time δ_1: $\Delta x_{1,end}(\delta_1)$ and $\Delta x_{2,start}(\delta_1)$. From triangles PP_1P_2 and PP_2P_3 the following relationship is obtained ($m = 1$):

$$\Delta x_{2,start}(\delta_1) = \Delta x_{1,end}(\delta_1) + (\dot{x}_{1,end} - \dot{x}_{2,start}) \cdot \Delta\delta_1 \tag{2-60}$$

The switching condition between structure 1 and structure 2 is represented by eq. (2-40). For the initial trajectory in point $P(\delta_1)$:

$$K_V \cdot v_{ref}^* - k^T \cdot x(\delta_1) - V_L^* - (V_U^* - V_L^*) \cdot \delta_1 = 0 \tag{2-61}$$

and for the modified trajectory, in $P_2(\delta_1+\Delta\delta_1)$:

$$K_V \cdot v_{ref}^* - k^T \cdot [x(\delta_1) + \Delta x_{1,end}(\delta_1 + \Delta\delta_1)] - V_L^* - (V_U^* - V_L^*) \cdot (\delta_1 + \Delta\delta_1) = 0 \tag{2-62}$$

Subtracting (2-62) from (2-61):

$$k^T \cdot \Delta x_{1,end}(\delta_1 + \Delta\delta_1) + (V_U^* - V_L^*) \cdot \Delta\delta_1 = 0 \tag{2-63}$$

From triangle PP_1P_2:

$$\Delta x_{1,end}(\delta_1 + \Delta\delta_1) = \Delta x_{1,end}(\delta_1) + \dot{x}_{1,end} \cdot \Delta\delta_1 \tag{2-64}$$

Substituting (2-64) into (2-63):

$$k^T \cdot [\Delta x_{1,end}(\delta_1) + \dot{x}_{1,end} \cdot \Delta\delta_1] + (V_U^* - V_L^*) \cdot \Delta\delta_1 = 0 \tag{2-65}$$

By expressing $\Delta\delta_1$ from (2-65) and substituting it into (2-60) results the relationship we are looking for:

$$\Delta x_{2,start}(\delta_1) = \left[I - \frac{\dot{x}_{1,end} - \dot{x}_{2,start}}{k^T \cdot \dot{x}_{1,end} + V_U^* - V_L^*} \cdot k^T \right] \cdot \Delta x_{1,end}(\delta_1) = M \cdot \Delta x_{1,end}(\delta_1) \tag{2-66}$$

Since for small variations during linear structure 1:

$$\Delta x_{1,end}(\delta_1) = e^{A_1\delta_1} \cdot \Delta x_{1,start} = \Phi_1(\delta_1) \cdot \Delta x_{1,start} \tag{2-67}$$

eq. (2-66) becomes:

$$\Delta x_{2,start}(\delta_1) = M \cdot \Phi_1(\delta_1) \cdot \Delta x_{1,start} \tag{2-68}$$

Equation (2-68) makes the connection between the (virtual) alterations of the state vector at the start of the first and the second structure.

The next structure switching, at the end of structure 2, into subperiod II, is a forced one. It is independent of the state variables and is imposed by the end of one period of the sawtooth waveform (Fig. 2-44, Fig. 2-9). Therefore this switching instant and the beginning of the next structure it is invariant to the modification of the initial periodic trajectory, i.e., there is no need to apply the mathematical abstraction from Fig. 2-45.

For small variations during linear structure 2 (using also (2-36)):

$$\Delta x_{2,end} = e^{A_2(1-\delta_1)} \cdot \Delta x_{2,start}(\delta_1) = \Phi_2(1-\delta_1) \cdot \Delta x_{2,start}(\delta_1) \tag{2-69}$$

Applying (2-68) and (2-69) in cascade for the entire subperiod:

$$\Delta x_{2,end} = \Phi_2(1-\delta_1) \cdot M \cdot \Phi_1(\delta_1) \cdot \Delta x_{1,start} \tag{2-70}$$

Equation (2-70) represents the linearization of the discrete-time map function f defined in (2-35) ($x_{1,start} = x_k$; $x_{2,end} = x_{k+1}$). The linearization of the Poincaré map function F belonging to f is obtained after back transformation [eq. (2-41)]:

$$\Delta x_{k+1,b} = T^{-1} \cdot \Delta x_{k+1} = T^{-1} \cdot \Phi_2(1-\delta_1) \cdot M \cdot \Phi_1(\delta_1) \cdot \Delta x_k \tag{2-71}$$

The Jacobian matrix of of map function F, evaluated at the fixed point x^*, is therefore:

$$J_F(x^*) = T^{-1} \cdot \Phi_2(1-\delta_1) \cdot M \cdot \Phi_1(\delta_1)\Big|_{x^*} \tag{2-72}$$

This coincides with the expression obtained through the first method in eq. (2-50) and will lead to the same results after following the iterative algorithm for determining δ_1 described already in the first method.

2-5-5 CALCULATION RESULTS OF THE STABILITY ANALYSIS

The loci of the eigenvalues are presented in Fig. 2-46 for three values of the control gain: for K_v = 2 with +-mark, corresponding to the periodic behavior analyzed in subsection 2-4-1-3, for K_v = 4.5 with o-mark and for K_v = 6 with x-mark, corresponding to the quasiperiodic operation analyzed in subsection 2-4-1-4. It can be clearly seen that a complex-conjugate pair of eigenvalues passes through the unit circle as the control gain is increased. This phenomenon is numerically detailed in Table 2-5. It confirms the Naimark-Sacker bifurcation discovered by computer simulations in section 2-4-1. According to the stability condition, as long as the eigenvalues lie inside the unit circle, the periodic steady-state solution is asymptotically stable. When a complex-conjugate pair of eigenvalues gets outside the unit circle, the periodic solution loses stability and, as we proved through

section 2-4, spawns a quasiperiodic solution, which turns into a chaotic one by increasing further the control gain. The locus of the eigenvalues in chaotic operation is plotted in Fig. 2-47, at K_V = 70 [90].

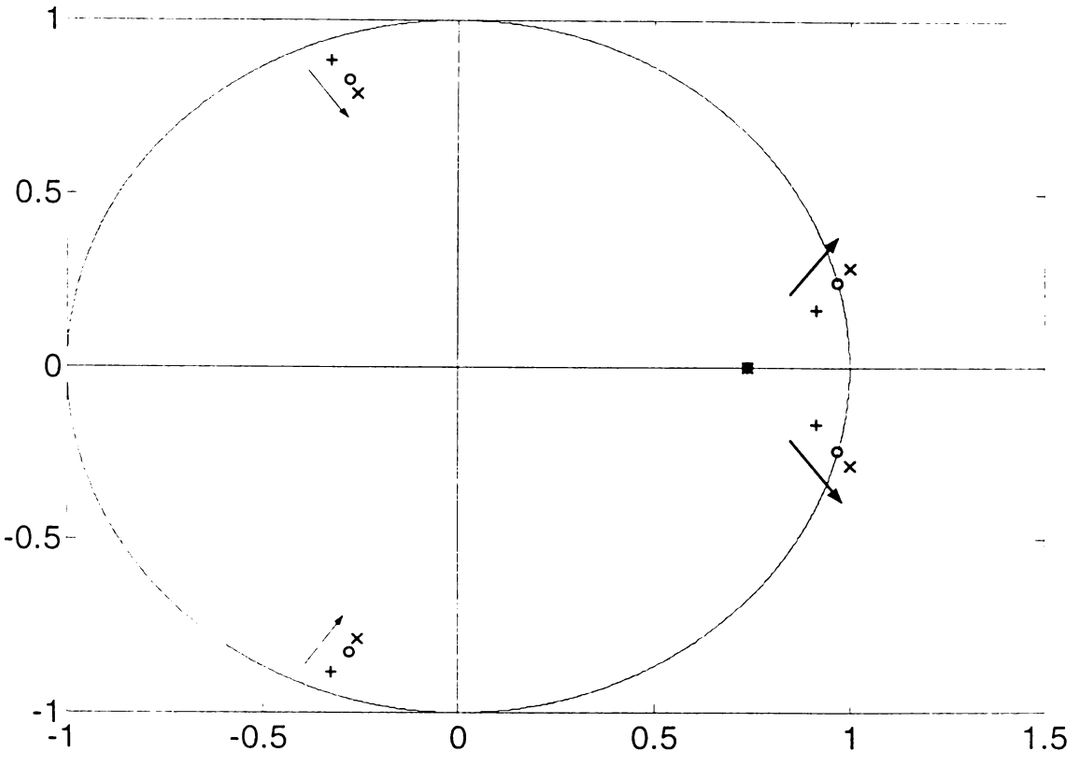

Figure 2-46 Loci of eigenvalues as the controller gain varies. Arrows indicate increasing controller gain.

Table 2-5 Complex-conjugate eigenvalues during the Naimark-Sacker bifurcation

K_V	*Pair of Characteristic Multipliers*	*Modulus*	*Stability of Periodic Solution*
2	0.915 ± 0.163i	0.930	Asymptotically stable (period-1)
3	0.937 ± 0.197i	0.958	Asymptotically stable (period-1)
4	0.959 ± 0.228i	0.986	Asymptotically stable (period-1)
4.5	**0.970 ± 0.243i**	**1.000**	**Structurally unstable: Naimark-Sacker bifurcation**
5	0.980 ± 0.258i	1.014	Unstable (2-periodic)
6	1.001 ± 0.286I	1.042	Unstable (2-periodic)

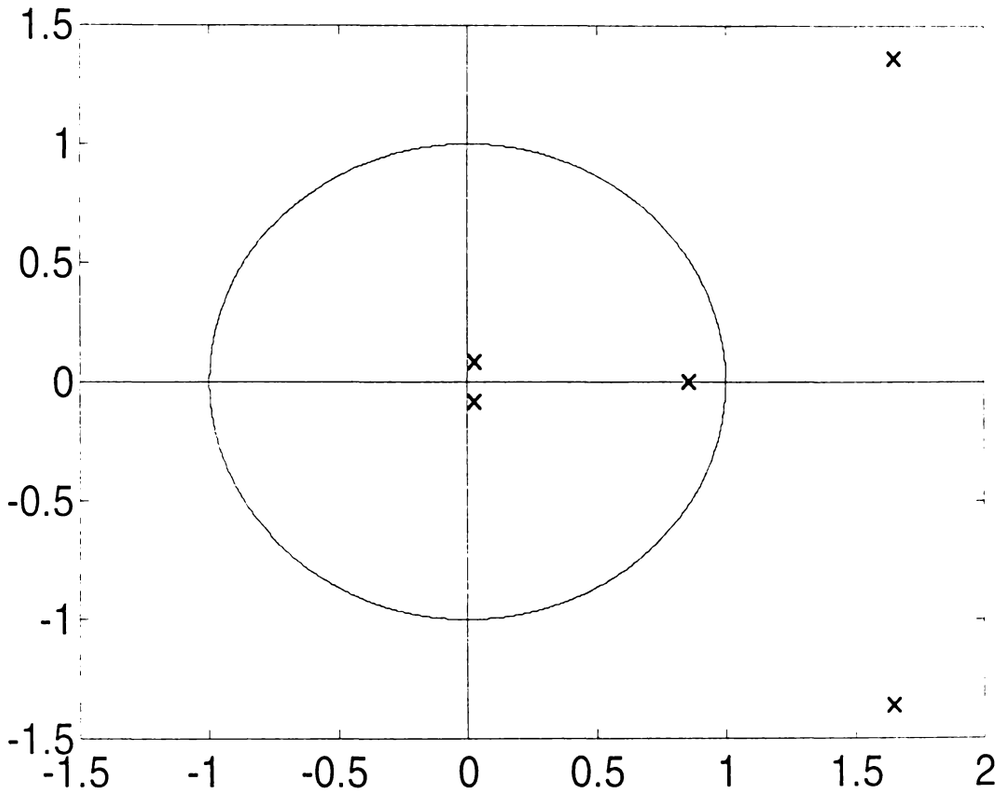

Figure 2-47 Locus of eigenvalues in chaotic operation ($K_v = 70$)

The stability analysis presented in this section confirmed the bifurcation value of the gain K_V and the asymptotically stable region below this value. All the methods introduced in this chapter can be also applied to study the effects of other system parameters beside this gain, in order to have a practical overall picture of the converter behavior, to help the designing engineer and to search for stable periodic regions and settings.

CHAPTER 3

CONTROL STRATEGIES FOR THE UNSTABLE REGIMES OF THE RESONANT DC-DC CONVERTER

In the previous chapter unstable regimes (chaotic, quasiperiodic, subharmonic) were depicted by computer simulation and confirmed by stability analysis in the operation of a resonant DC-DC converter, whose output voltage is feedback-controlled by PWM switching. Since the control should be designed for the required stable operation, the object of the study (section 3-1) is represented by the suppression of these unstable dynamics, hereby extending the required stable period-1 operation and avoiding any bifurcation within the operating range. Four distinct control strategies are introduced first time for this converter. The first two achieve the control objectives by the insertion of feedback controllers into the configuration. The first control method deals with the use of series linear compensation in the generation of the control voltage and applies the stability analysis to tone its parameters (section 3-2). The second one employs a fuzzy controller with dynamics, which is tuned using the pseudo-fuzzy features of the correspondent conventional control (section 3-3). The last two control strategies try to stabilize one of the many unstable periodic trajectories embedded in a chaotic attractor. The third control technique applies the Ott-Grebogi-Yorke algorithm to perform a discrete-time control by time- and state-dependent small perturbations of an accessible system parameter (section 3-4). The fourth control method is based on time-delay autosynchronization and uses a control signal formed with the difference between the current state of the system and the state of the system delayed by one period of the unstable periodic trajectory one wants to stabilize (section 3-5). The results obtained by computer simulation are confirmed by tests performed on an experimental setup comprising the power stage and its control implemented on a DSP board (section 3-6).

3-1 OBJECTIVES OF CONTROL

Power electronic system controls should be designed for the required stable operation [8]. In particular, for DC-DC converters, the use of a feedback control must guarantee stable period-1 operation at the switching frequency and any subharmonic, quasiperiodic or chaotic operation is considered undesirable and should be avoided. For the resonant DC-DC converter introduced in the previous chapter (Fig. 2-6), the switch control is achieved by a feedback PWM process, as in most commercial DC-DC converters (Fig. 2-9). Bifurcations and chaos have been detected in the range of variation of the parameters and they have been analyzed through the previous chapter in the case of changing the control gain used to obtain the control voltage from the error signal. The stable period-1 operation was found to be restricted to gains less than a certain bifurcation value.

The main control improvement objective will be therefore the suppression of the unstable dynamics (being it chaotic, quasiperiodic or subharmonic), hereby extending the stable period-1 operation and avoiding any bifurcation within the operating range. Any method that allows the converter to operate for a larger range of the parameters has potential advantages. Since for consistency, the problem will be tackled for the case of the control gain, extending the stable operation toward the region of higher gains may result in smaller steady-state error (as denoted by Fig. 2-11) and faster dynamical response of the system [92,93].

The objective fixed above is a steady-state design problem from the conventional point of view, since it does not take into consideration the dynamical response of the system [91]. However, power electronics applications demand high performance, i.e., the fastest possible response and small transient disturbances. Therefore, in conjunction with the avoidance of bifurcation, the conventional control that refers to shaping the dynamical response is also considered when appropriate [94].

It was already revealed that the nonlinear character of the converter configuration (determined mainly by its variable structure) complicates its analysis, particularly from a stability and control point of view. Switching makes the state derivatives discontinuous and basic tools such as linearization do not apply directly. Nonlinear systems of this type actually still have serious limitations for mathematics and control theory. When chaos is added to the picture, it becomes even more difficult to deal with the actual time-domain and frequency-domain behavior of the system. It was shown that Poincaré maps can be

used to get a view of how the system evolves over time, but the action at any particular moment remains essentially unpredictable. Consequently, design tools are not readily available. Four distinct control strategies will be introduced in this chapter:

- Linear compensation
- Fuzzy control
- Control of chaos using the *OGY* technique
- Time-delay autosynchronization

3-2 LINEAR COMPENSATION

The PWM switching for controlling the output voltage of the investigated resonant DC-DC converter was achieved by comparing a repetitive sawtooth waveform with a control signal obtained through a feedback loop. So far the part of the control applied to obtain the control signal v_{con} was a proportional one, since it has been typically achieved by an amplifier with a constant gain K_V (Fig. 2-9a). The control signal was simply related to the error signal by this proportional constant.

In this section is studied the possibility to meet the control objectives set in the introductory section by using other basic linear controller operations in addition to the simple multiplication by a constant [95]. The analysis will be exemplified for a controller with transfer function $H_c(s)$, whose physical implementation is a simple task [91]:

$$H_c(s) = K_V \cdot \frac{T_1 s + 1}{T_2 s + 1} \tag{3-1}$$

The main design objective is to determine values of the time constants T_1, T_2 so that the stable steady-state period-1 operation is extended and conserved over the range of variation of the gain K_V. Therefore, the steady-state stability of the resulting control system, depicted in Fig. 3-1, is investigated in the following.

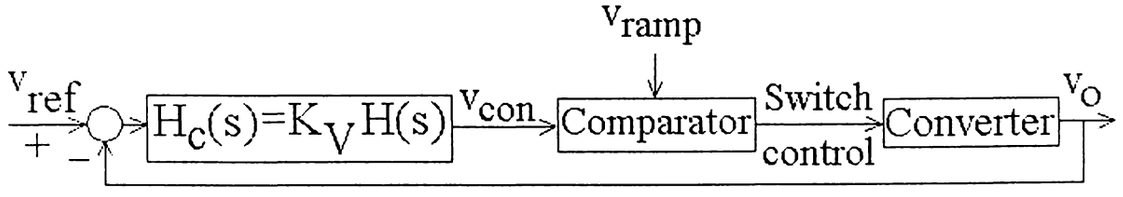

Figure 3-1 Block diagram of control system with linear compensation

This will be done in the same way as was in section 2-5 for the proportional control. The stability criterion that has to be applied was deduced in subsection 2-5-1. The series of two linear structures during a switching semiperiod was depicted in subsection 2-5-2. The main difference from the proportional control case is due to the additional state variable introduced by the controller. If this state variable is the output of the controller (i.e., the control signal voltage v_{con}), the corresponding state equation can be obtained from the control law (3-1) by expressing the error signal at the controller input as the difference between the actual output voltage v_o (2-10) and its desired value v_{ref}. Taking into consideration the zero time derivative of a constant reference signal and substituting the time derivatives of the positive and negative channel output voltages with their state equations deduced in (2-44) or (2-48), the additional state equation results as follows:

$$\frac{dv_{con}}{dt} = \frac{K_V}{T_2}\left(\frac{T_1}{R_pC_p}-1\right)\cdot v_{op} + \frac{K_V}{T_2}\left(\frac{T_1}{R_nC_n}-1\right)\cdot v_{on} - \\ -\frac{K_VT_1}{C_pT_2}\cdot i_{op} - \frac{K_VT_1}{C_nT_2}\cdot i_{on} - \frac{1}{T_2}\cdot v_{con} + \frac{K_V}{T_2}\cdot v_{ref} \tag{3-2}$$

Using the dimensionless variables and parameters defined in (2-46) and (2-40), the additional state equation can be written in dimensionless form:

$$\frac{dx_6}{d\tau} = K_V\cdot(a\cdot m-n)\cdot(x_1+x_2)-K_V\cdot b\cdot m\cdot(x_4+x_5)-n\cdot x_6+K_V\cdot n\cdot v_{ref}^{*} \tag{3-3}$$

where $x_5 = \dfrac{v_{con}}{v_i/2}$ is the additional dimensionless state variable and

$$m=\frac{T_1}{T_2}, n=\frac{T_r}{T_2} \tag{3-4}$$

are the dimensionless design parameters.

Consequently, the state models of the system during a subperiod are obtained by appending (3-3) to the converter structures models (2-28) and (2-30), respectively:

Structure 1:

$$\dot{x} = A_1 \cdot x + B_1 \cdot u; \quad x = [x_1 \quad x_2 \quad x_3 \quad x_4 \quad x_5 \quad x_6]^T; \quad u = \begin{bmatrix} 1 & v_{ref}^* \end{bmatrix}^T;$$

$$A_1 = \begin{bmatrix} -a & 0 & 0 & b & 0 & 0 \\ 0 & -a & 0 & 0 & b & 0 \\ 0 & 0 & 0 & \pi & 0 & 0 \\ -\pi & 0 & -\pi & 0 & 0 & 0 \\ 0 & -\pi & 0 & 0 & 0 & 0 \\ K_V(am-n) & K_V(am-n) & 0 & -K_V bm & -K_V bm & -n \end{bmatrix}; \tag{3-5}$$

$$B_1 = \begin{bmatrix} 0 & 0 & 0 & \pi & 0 & 0 \\ 0 & 0 & 0 & 0 & 0 & K_V n \end{bmatrix}^T$$

Structure 2:

$$\dot{x} = A_2 \cdot x + B_2 \cdot u; \quad x^T = [x_1 \quad x_2 \quad x_3 \quad x_4 \quad x_5 \quad x_6]; \quad u^T = \begin{bmatrix} 1 & v_{ref}^* \end{bmatrix};$$

$$A_2 = \begin{bmatrix} -a & 0 & 0 & b & 0 & 0 \\ 0 & -a & 0 & 0 & b & 0 \\ 0 & 0 & 0 & 0 & 0 & 0 \\ -\pi & 0 & 0 & 0 & 0 & 0 \\ 0 & -\pi & 0 & 0 & 0 & 0 \\ K_V(am-n) & K_V(am-n) & 0 & -K_V bm & -K_V bm & -n \end{bmatrix}; \tag{3-6}$$

$$B_2 = \begin{bmatrix} 0 & 0 & 0 & 0 & 0 & 0 \\ 0 & 0 & 0 & 0 & 0 & K_V n \end{bmatrix}^T$$

As proved in subsection 2-5-2, the dynamics of the entire switching period can be fully characterized by the dynamics of one subperiod, modeled above, by applying back transformation (2-31) at its end. By utilizing the periodicity of the additional state variable in steady-state, the completed transformation matrix (2-32) becomes:

$$T = T^{-1} = \begin{bmatrix} 0 & 1 & 0 & 0 & 0 & 0 \\ 1 & 0 & 0 & 0 & 0 & 0 \\ 0 & 0 & -1 & 0 & 0 & 0 \\ 0 & 0 & 0 & 0 & 1 & 0 \\ 0 & 0 & 0 & 1 & 0 & 0 \\ 0 & 0 & 0 & 0 & 0 & 1 \end{bmatrix} \tag{3-7}$$

With this kind of system description, any of the two methods introduced in section 2-5 can be applied for determining the stability of the control system. Only the differences will be detailed here. Using for example the analysis based on the Poincaré map function, described in subsection 2-5-3, the difference (beside the new system models (3-5), (3-6) and transformation matrix (3-7), of course) appears when determining the feedback relation corresponding to (2-40) that connects the duration δ_1 and the state vector x_k:

$$\begin{aligned} e(x_k,\delta_1) &= \frac{v_{con}(\delta_1)-v_{ramp}(\delta_1)}{v_i/2} = k^T\cdot x(\delta_1)-V_L^*-(V_U^*-V_L^*)\cdot\delta_1 = \\ &= k^T\cdot\left\{\Phi_1(\delta_1)\cdot x_k+\left[\Phi_1(\delta_1)-I\right]\cdot A_1^{-1}\cdot B_1\right\}-V_L^*-(V_U^*-V_L^*)\cdot\delta_1 = 0 \end{aligned} \tag{3-8}$$

where $k^T=[0\quad 0\quad 0\quad 0\quad 0\quad 1]$.

Consequently, the derivatives of $e(x_k, \delta_1)$ involved in the Jacobian matrix of the Poincaré map function F expressed in (2-45) are changed as follows:

$$\begin{aligned} \frac{\partial e}{\partial\delta_1} &= k^T\cdot\frac{\partial\left\{\Phi_1(\delta_1)\cdot x_k+\left[\Phi_1(\delta_1)-I\right]\cdot A_1^{-1}\cdot B_1\right\}}{\partial\delta_1}-(V_U^*-V_L^*) = \\ &= k^T\cdot\frac{\partial x(\delta_1)}{\partial\delta_1}-(V_U^*-V_L^*) = k^T\cdot\dot{x}_{1,end}-(V_U^*-V_L^*) \end{aligned} \tag{3-9}$$

$$\left(\frac{\partial e}{\partial x_k}\right)^T = k^T\cdot\Phi_1(\delta_1) \tag{3-10}$$

Similarly to (2-50), the Jacobian matrix of the Poincaré map function F, evaluated at the fixed point x^*, results in:

$$\begin{aligned} J_F(x^*) &= T^{-1}\cdot\Phi_2(1-\delta_1)\cdot\left[I-\frac{\dot{x}_{1,end}-\dot{x}_{2,start}}{k^T\cdot\dot{x}_{1,end}-(V_U^*-V_L^*)}\cdot k^T\right]\cdot\Phi_1(\delta_1)\Big|_{x^*} = \\ &= T^{-1}\cdot\Phi_2(1-\delta_1)\cdot M\cdot\Phi_1(\delta_1)\Big|_{x^*} \end{aligned} \tag{3-11}$$

The rest of the stability investigation, i.e., the iterative determination of δ_1, is the same as it was in subsection 2-5-3, taking into account, of course, the modified system models (3-5), (3-6) and transformation matrix (3-7). A MATLAB program for the stability analysis of the control system can be developed in accordance with above.

The stability investigation procedure just presented permits to solve the design problem of controller (3-1). Having a controller gain K_V for which the proportional control investigated in the previous chapter led to an unstable (quasiperiodic, subharmonic or chaotic) converter operation - i.e., some of the eigenvalues resulted from the stability study in subsection 2-5-3 lie outside the unit circle - the dimensionless parameters m, n of the

linear compensation (3-1) can be tuned using the method just described, in such a way that all the eigenvalues are "moved" inside the unit circle, replacing hereby the unstable behavior with the desired asymptotically stable period-1 converter operation.

Such a solution is represented by $m = \frac{T_1}{T_2} = \frac{T/10}{T/100} = 10, n = \frac{T_r}{T_2} = \frac{T_r}{T/100} = 2.3$,

where T = 215 μsec represents the additional natural period of the system developed in quasiperiodic steady-state (Fig. 2-23, Fig. 2-24) [92]. The other parameter values remain those specified in Appendix A. The effect of the resulting linear compensation (3-1) on the system stability can be seen from Fig. 3-2 at K_V = 6, since the initially quasiperiodic behavior, with eigenvalues plotted in Fig. 2-46 with x-mark, is replaced by the asymptotically stable period-1 operation, with all eigenvalues inside the unit circle. The same effect can be observed from Fig. 3-3 at K_V = 70 on the initially chaotic behavior, with eigenvalues plotted in Fig. 2-47.

Results of computer simulations, showing the dynamical response of the converter control system, are presented in the following. The controller gain is K_V = 70, which for a purely proportional control leads to a chaotic behavior, as shown in subsection 2-4-1-6. The reference voltage v_{ref} is changed stepwise from 40V to 50V and back in Fig. 3-4. The rise time is 0.3 msec and the fall time is 0.16 msec. The start-up transient process can be seen in Fig. 3-5. The overshoot was reduced, even avoided, by introducing two limiters in the loop. Limiter 1 confines the extreme value of the control voltage v_{con} in both directions, to V_U and V_L, respectively (Fig. 3-6). The other limiter (not shown in Fig. 3-6) turns on the controlled switches whenever $|v_c|$ would pass the value $2v_i$ prior v_{con} would reach v_{ramp}.

Simulations to test the robustness of this control configuration under changes in the parameters of the system were also performed [96,97]. Fig. 3-7 shows the result of a simulation where the load R is changed stepwise successively from 8Ω to 10Ω and 15Ω, then back to 10Ω and 8Ω, each phase lasting 200 switching periods. It can be seen that the sudden changes in the load only introduce a short fluctuation in the output voltage. The same conclusion is obtained when changing stepwise the input voltage $v_{ip} = v_{in}$ successively from 100V to 110V and to 120V, then back to 220V to 200V, each phase lasting again 200 switching periods (Fig. 3-8). These results show that the domain of control does not vary too much under this kind of changes.

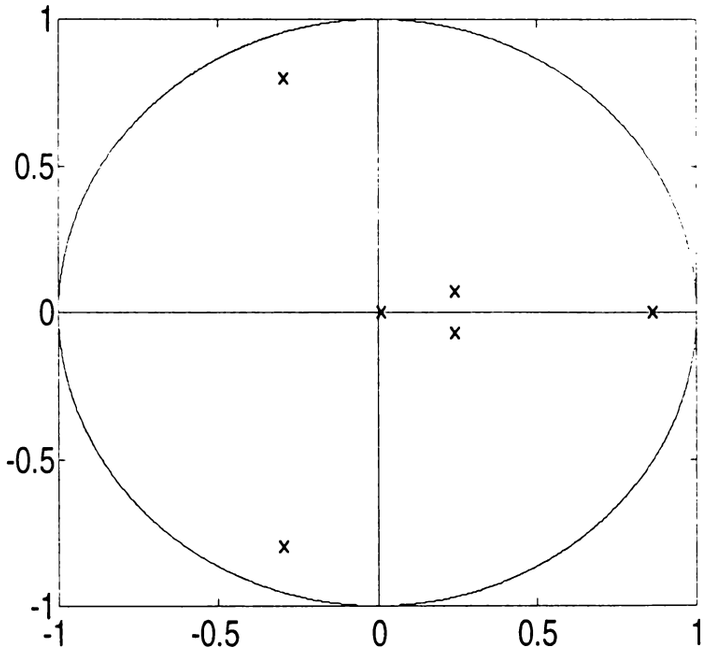

Figure 3-2 Locus of eigenvalues for the control system with linear compensation ($K_V = 6$)

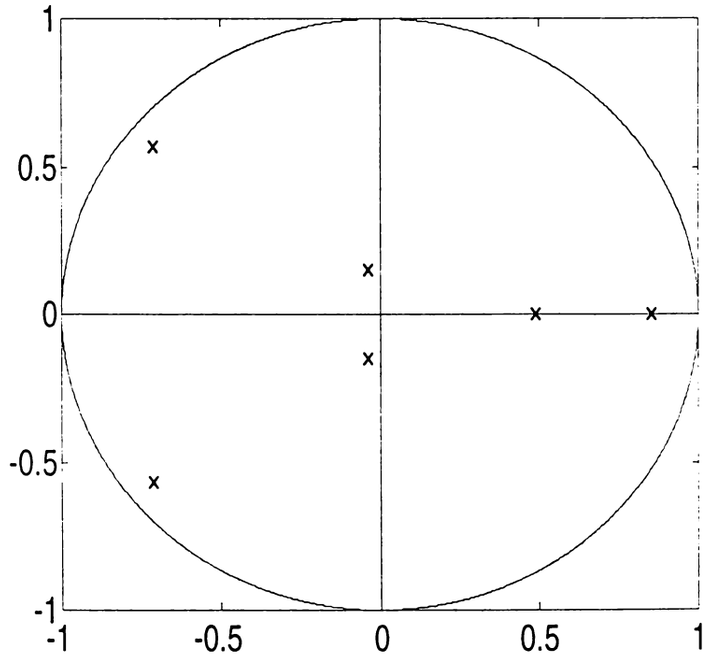

Figure 3-3 Locus of eigenvalues for the control system with linear compensation ($K_V = 70$)

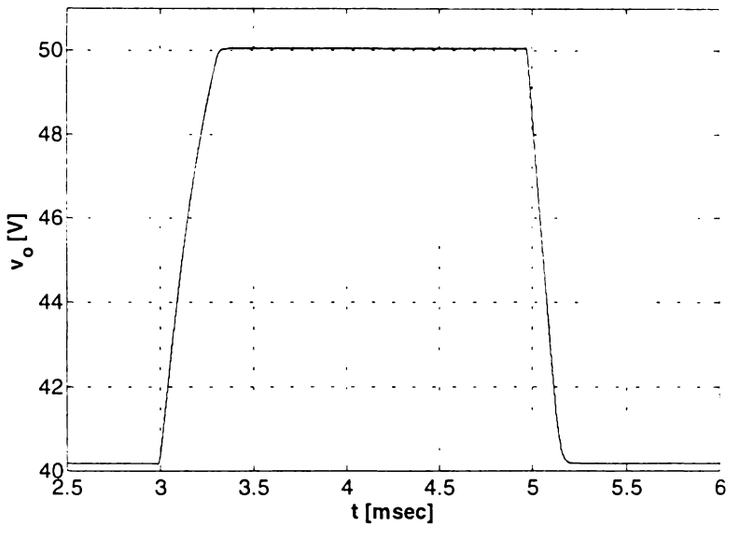

Figure 3-4 Control system response when the reference voltage is changed stepwise up and down

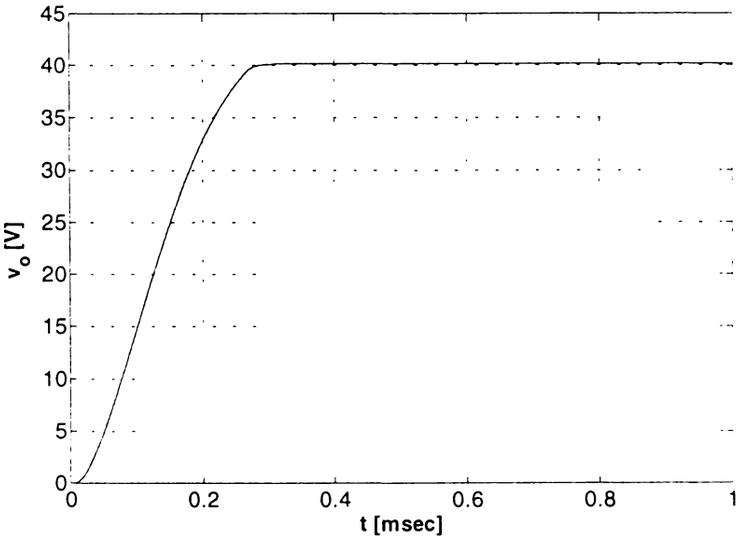

Figure 3-5 Start-up transient process

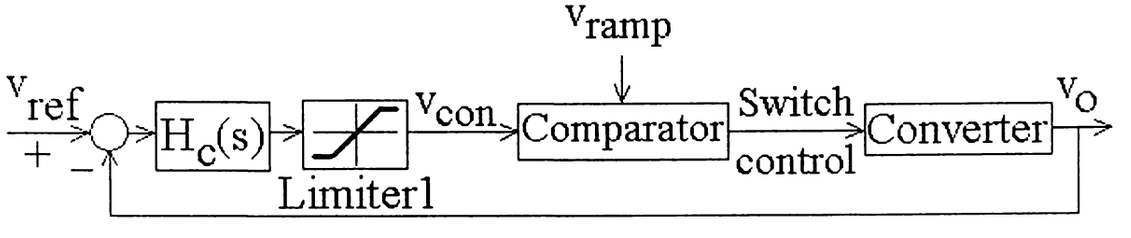

Figure 3-6 Block diagram of control loop with linear compensation and limiter

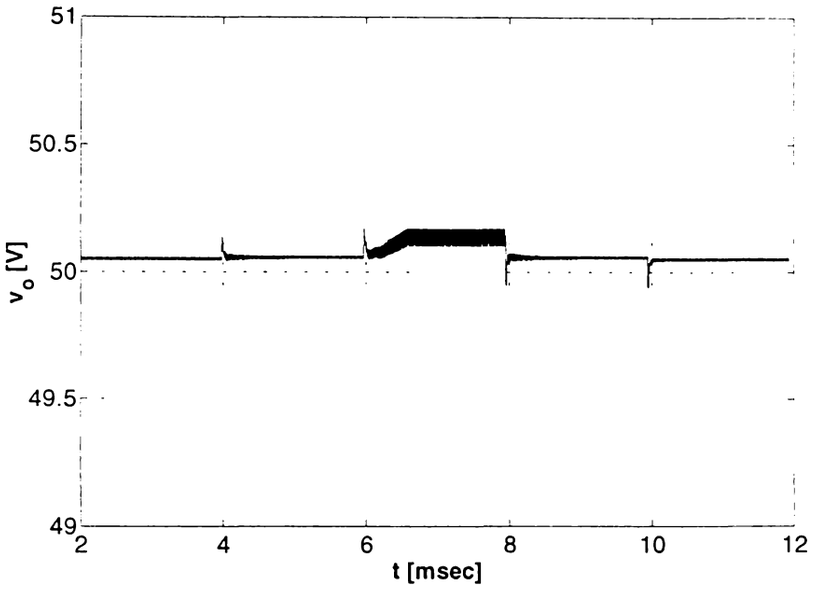

Figure 3-7 Control system response when the load is changed stepwise up and down

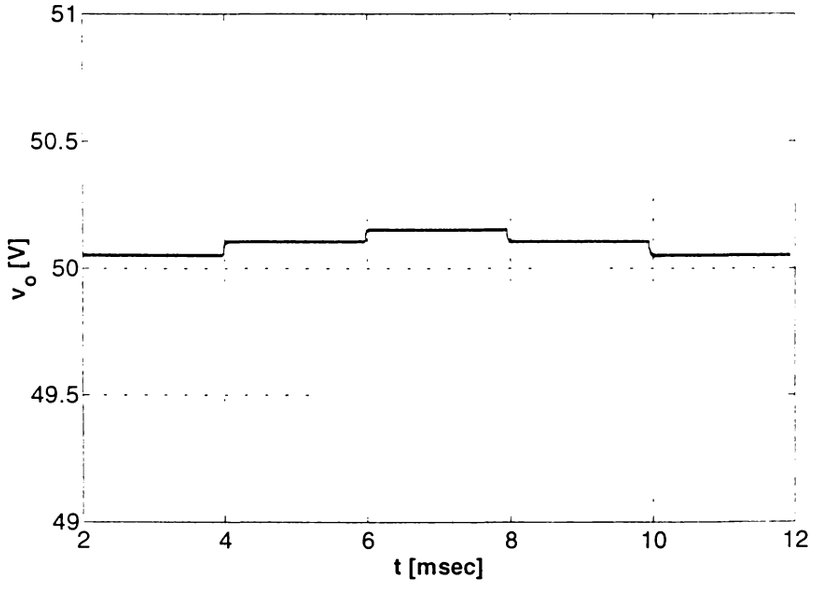

Figure 3-8 Control system response when the input voltages of the converter are changed stepwise up and down

The stability study above investigated the effects of derivative control on the initially unstable (chaotic) regimes of the feedback-controlled converter. In the same way can be analyzed other basic controller operations, e.g., the integral control, which reduces the steady-state error to zero, provided that the final system is stable, of course.

3-3 FUZZY CONTROL

In some situations, e.g., in controlling plants with functional nonlinearities that are difficult to model, the *fuzzy control* can be a viable alternative to the classical control, since fuzzy controllers have some advantages which can be attractive to the practitioner engineer [99]:

- The fuzzy control can be strongly based on the experience of a trained "expert" human operator, therefore the fuzzy controller vs. a conventional one can model more accurately this experience.
- The design of the fuzzy control system does not require a complex mathematical apparatus (at least in the first phase).
- The process implementation can be relatively simple.

Despite some disadvantages:

- The fuzzy solution does not guarantee superior performance with respect to a conventional control solution
- The stability and robustness ensured by the rule base are not analytically guaranteed

the advantages mentioned above offer a pragmatic attraction to the field of fuzzy control.

Although the resonant buck converter, as the controlled plant, can be easily modeled as a piecewise linear system, the nonlinear features of the resulting variable structure system actually still imply serious limitations for conventional control theory (it becomes even more difficult to deal with the actual time-domain and frequency-domain behavior of the system when chaos is added to the picture). For that reason, a fuzzy logic based control strategy can be an alternative way to meet the control objectives set in the introductory section for the studied converter configuration and it will be presented in this section.

The fuzzy control is based on *fuzzy controllers* (or *fuzzy logic controllers*) characterized by a generally speaking nonlinear input-output static map that can be modified according to the needs. Since the fuzzy controllers are controllers without dynamics, the performance of the resulting *fuzzy control systems* (automatic control systems with fuzzy controllers) can be enlarged by extending the fuzzy controller with dynamic modules, obtaining the so-called *fuzzy controllers with dynamics*. Both the input and output signals of the fuzzy controller can be subject to dynamic (analog or digital) processing, i.e., the dynamic processing takes place outside the strictly speaking fuzzy

controller which remains nonlinear and without dynamics. The fuzzy controller must have at least one input corresponding to the control error [100].

By taking into consideration the very good control features of the linear PI controller:

- Zero steady-state control error required by most applications,
- Improvement of control system dynamics (alleviation of settling time and overshoot) by canceling the large time constants of the controlled plant,
- Positive practical experience gained in implementing the linear PI controller,

a PI based fuzzy controller is used and presented in detail in order to control the initially unstable (chaotic) regimes of the converter configuration. The usefulness of the fuzzy controllers with dynamics with quasi-PI behavior is that they can be systematically developed by starting from the well-known features of a basic linear PI controller. As mentioned before, the dynamic (integrating) effect can be introduced on the output of the fuzzy controller (resulting the standard version of the PI fuzzy controller with output integration) or on the input of the fuzzy controller (resulting the standard version of the PI fuzzy controller with input integration). Only the first version is subject to the present study and the block diagram of the resulting fuzzy control system is presented in Fig. 3-9. This control version is characterized by the fact that the dynamics is introduced by the numerical differentiation of the amplified control error e under the form of its increment Δe, and by the numerical integration of the increment of control signal Δv_{con} [101].

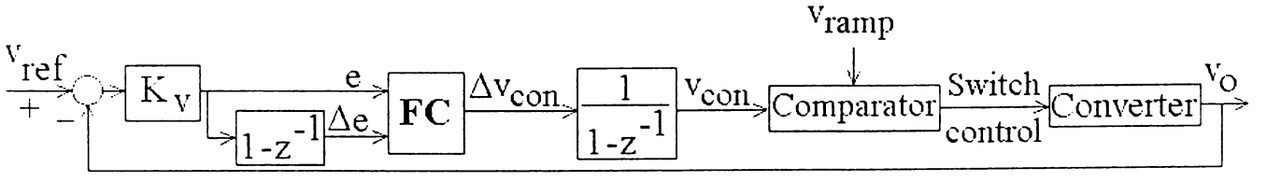

Figure 3-9 Block diagram of fuzzy control system

The design of the fuzzy controller FC starts by expressing the PI quasi-continuous digital control algorithm in its incremental version:

$$\Delta v_{con} = K_P \cdot \Delta e + K_I \cdot e = K_P \cdot (\Delta e + q \cdot e) \tag{3-12}$$

The parameters K_P, K_I and q are functions of those ones belonging to the conventional continuous-time PI controller:

$$H_{PI}(s) = k \cdot (1 + \frac{1}{T_i \cdot s}) \tag{3-13}$$

by the following relationships:

$$K_P = k \cdot (1 - \frac{T}{2 \cdot T_i}), \quad K_I = \frac{k \cdot T}{T_i}, \quad q = \frac{K_I}{K_P} = \frac{2 \cdot T}{2 \cdot T_i - T} \tag{3-14}$$

where T is the sampling time.

Using eq. (3-12) and the representation of the increment of the control voltage Δv_{con} in the state plane from Fig. 3-10, the pseudo-fuzzy features of the PI quasi-continuous digital control algorithm in its incremental version are obtained:

- There is a "zero control signal increment line" $\Delta v_{con} = 0$, with equation:

$$\Delta e + q \cdot e = 0 \tag{3-15}$$

- With regard to this line: $\Delta v_{con} > 0$ in the upper half-plane and $\Delta v_{con} < 0$ in the lower one.
- The distance from any point of the state plane to the "zero control signal increment line" corresponds to the absolute value of the increment of the control voltage $|\Delta v_{con}|$.

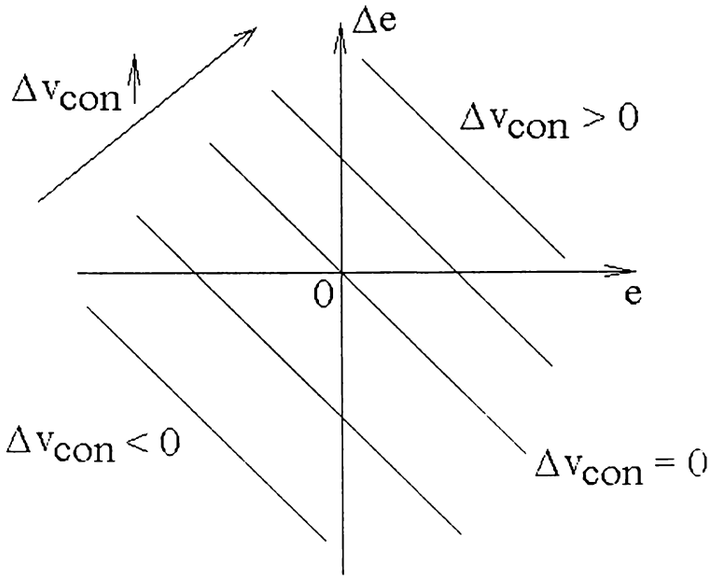

Figure 3-10 State plane representation corresponding to eq. (3-12)

As a matter of principle, the operation of the fuzzy controller involves the following sequence of operations [104]:

- *Fuzzification*: The crisp input information (the control error and its increment) is "converted" into a fuzzy representation. For the fuzzy controller studied the fuzzification is solved as shown in Fig. 3-11:

- for the input variables e, Δe: five linguistic terms are chosen as *antecedent sets* (BN - Big Negative, SN - Small Negative, Z - Zero, SP - Small Positive, BP - Big Positive) with triangular shaped membership functions arranged in regular Ruspini partition (the sum of the membership functions gives 1 in any place).
- for the output variable Δv_{con}: five linguistic terms are chosen as *consequent sets*, with regularly distributed singleton type membership functions.

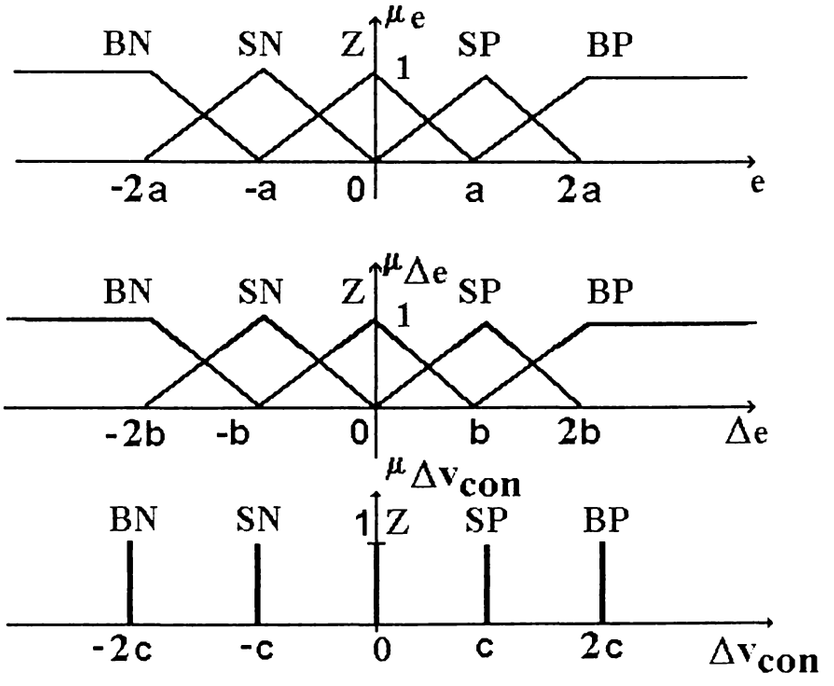

Figure 3-11 Membership functions of the fuzzy controller

- *Fuzzy inference*: The "fuzzified" information is processed on the basis of a set of rules (the *rule base*) of the form

  IF (antecedent) **THEN** (consequent)

  that have to be well stated in order to control the given plant. The rule base of the fuzzy controller investigated is built by taking into consideration the previously described pseudo-fuzzy features of the PI quasi-continuous digital control algorithm. The complete rule base can be synthetically presented by means of the decision table in Table 3-1. It can be noticed that

  IF e is zero **AND** Δe is zero **THEN** Δv_{con} is zero

  which is in accordance with the fact that the output of the fuzzy controller is the increment of the control signal: in steady-state the control signal is constant, therefore its increment is zero.

Table 3-1 Decision table of the fuzzy controller

Δv_{con}		e				
		BN	SN	Z	SP	BP
Δe	BN	BN	BN	BN	SN	Z
	SN	BN	BN	SN	Z	SP
	Z	BN	SN	Z	SP	BP
	SP	SN	Z	SP	BP	BP
	BP	Z	SP	BP	BP	BP

The principles of evaluation of the rule base are called *inference engine* and the result is the fuzzy set of the increment of control signal (the *fuzzy control signal*). The fuzzy controller presented uses the MAX-MIN inference [102].

- *Defuzzification*: The fuzzy control signal is converted into a crisp signal value, with well-specified physical nature, directly usable at the actuator level. For the fuzzy controller studied the center of gravity method was used in order to obtain the effective value of the increment of the control voltage Δv_{con} [103].

The specific parameters of the fuzzy controller are a, b and c and the following steps have been proceeded for the establishment of their concrete values [99]:

- The following relationship is valid along the "zero control signal increment line":

$$q = -\frac{\Delta e}{e} = \frac{b}{a} \tag{3-16}$$

- The following condition is fulfilled along the "constant control signal increment line" $\Delta v_{con} = c$:

$$c = \Delta v_{con} = K_P \cdot (\Delta e + q \cdot e) = K_P \cdot b \tag{3-17}$$

- The previous equation results in:

$$c = K_P \cdot q \cdot a = K_I \cdot a \tag{3-18}$$

- One of the parameters, namely c, was chosen, and the other two parameters, a and b, resulted from (3-17) and (3-18).

By applying this method, the parameters of the basic PI controller (3-13), k and T_i, are taken into consideration in tuning the parameters of the fuzzy controller, a, b, and c (for tuning the PI controller, it can be used, e.g., the method introduced in the previous section, based on the stability investigation).

In order to perform the analysis of the just presented fuzzy control system by computer simulation, the fuzzy controller was included in the Simulink model of the converter configuration as a MATLAB function, listed in Appendix D. The implementation of the fuzzy controller through an own program was preferred to the use of the MATLAB's fuzzy toolbox. Simulations using the toolbox might overtax the computing resources available in terms of memory and CPU time, since it processes the whole information, not only the useful one. The developed program is specific for the required type of application, therefore the simulation time is significantly decreased [105].

Results of computer simulations, showing the dynamical response of the fuzzy control system, are presented in the following. The controller gain is $K_V = 70$, which for a purely linear proportional control leads to a chaotic behavior, as depicted in subsection 2-4-1-6. The other parameter values remain those specified in Appendix A. The reference voltage v_{ref} is changed stepwise from 40V to 50V and back in Fig. 3-12. The rise time is 0.5 msec and the fall time is 0.3 msec. The start-up transient process can be seen in Fig. 3-13. Comparing these results with those of the conventional linear control applied in the previous section (Fig. 3-4, Fig. 3-5), it can be seen that while the steady-state error is improved, the rise time of the response is a little slower (this is not surprising, since the PI based control is essentially a low-pass filter which attenuates high-frequency signals). The same conclusions are valid when simulations are performed to test the robustness of the fuzzy control configuration under changes in the parameters of the system (load, input voltages).

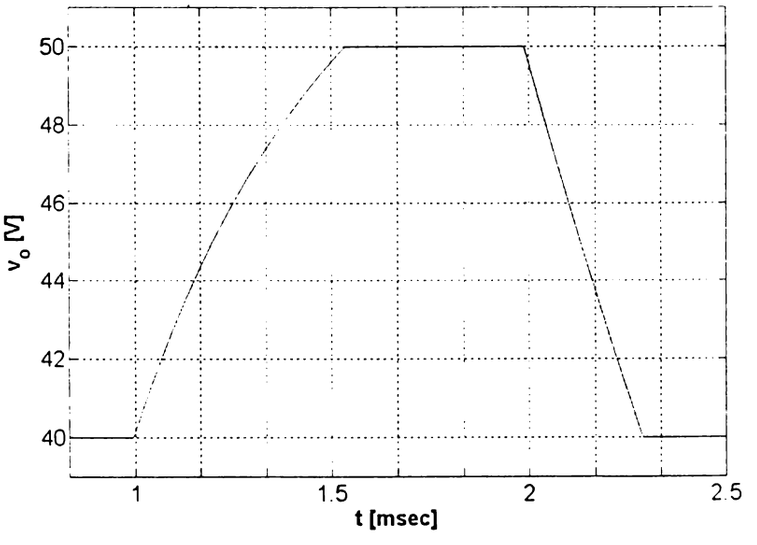

Figure 3-12 Fuzzy control system response when the reference voltage is changed stepwise up and down

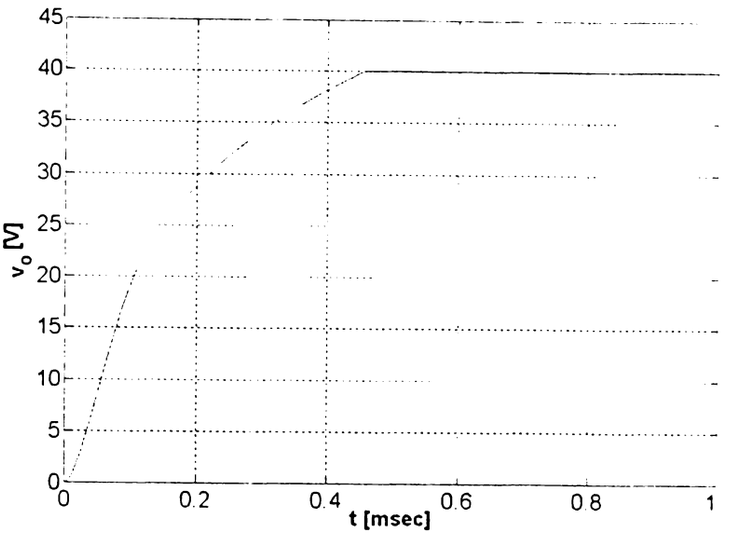

Figure 3-13 Start-up transient process

3-4 CONTROL OF CHAOS USING THE *OGY* TECHNIQUE

The previous two sections detected a first class of control strategies, inspired from the area of control engineering, which make use of feedback controllers to solve the problem of controlling unstable operation including chaos, in the sense of suppressing chaotic regimes in the investigated resonant DC-DC converter. They have been shown to be very useful to achieve the control goal while guaranteeing satisfactory robustness to parameter perturbations. A quite different approach to the control of a chaotic dynamical system was proposed by Ott, Grebogi and Yorke (*OGY*) [66]. They demonstrated that given a chaotic attractor, one can obtain a desired attracting time-periodic trajectory by making only *small* time- and state- dependent perturbations in an *accessible* system parameter. The key observation is that a chaotic attractor typically has embedded within it an infinite number of unstable periodic trajectories, as it was illustrated in Fig. 2-37 for the studied converter.

> ***Basic idea:*** A trajectory on a chaotic attractor comes arbitrarily close an infinite number of different unstable periodic trajectories. With a small control signal, one should be able to stabilize any of these periodic solutions [88].

Since only small parameter changes can be performed, new trajectories with very different properties from the existing ones cannot be created. Thus, the approach is to determine first some of the low-period unstable periodic trajectories embedded in the chaotic attractor and to choose one which can improve the system performance. Finally, the control attempts to program the small parameter adjustments so as to stabilize this unstable periodic trajectory.

This makes OGY's approach quite different from other previously published methods on controlling chaos. They demonstrated their method numerically by controlling the Hénon map. Far from being a numerical curiosity that requires experimentally unattainable precision, the OGY method can be widely implemented in a variety of systems. In this section is designed the control of chaotic behavior in the examined resonant DC-DC converter, based on the method of OGY.

3-4-1 THEORETICAL BACKGROUND

The OGY method assumes only the following four points [85]:

- The dynamics of the system can be represented as arising from an n-dimensional nonlinear discrete-time function of the form

$$x_{k+1} = P(x_k, p) \tag{3-19}$$

  where p is some accessible system parameter. In the (typically) case of continuous-time systems this map is constructed via some form of sampling, e.g., by introducing the Poincaré map.
- There is a maximum small perturbation Δp^* in the parameter p by which it is acceptable to vary p from the nominal value p^*.
- For the value of p^* there is a chaotic attractor of the underlying system which contains a specific periodic trajectory around which one wishes to stabilize the dynamics.
- The position of this periodic trajectory is a function of p, but the local dynamics about it do not vary much with the allowed small changes in p.

Note that while the dynamics is assumed to arise from a map, one needs no model for the global dynamics. These assumptions would seem to allow for the control of any chaotic system for which a faithful Poincaré section can be constructed, e.g., from experimental data. For simplicity the presentation is restricted to a two-dimensional map P.

A fixed point $x_F(p)$ of the map (3-19) of the system is defined by:

$$x_F(p) = P(x_F(p), p) \tag{3-20}$$

therefore it moves with the parameter p by:

$$\frac{dx_F(p)}{dp} = \left.\frac{\partial P}{\partial x}\right|_{x_F(p),p} \cdot \frac{dx_F(p)}{dp} + \left.\frac{\partial P}{\partial p}\right|_{x_F(p),p} \tag{3-21}$$

Let $x^*(p^*)$ denote the unstable fixed point of the map P existing for the parameter value p^* and corresponding to that periodic trajectory on the attractor which one wants to stabilize. From (3-21) results:

$$\left.\frac{\partial P}{\partial p}\right|_{x^*,p^*} = \left.\frac{dx_F}{dp}\right|_{p^*} - \left.\frac{\partial P}{\partial x}\right|_{x^*,p^*} \cdot \left.\frac{dx_F}{dp}\right|_{p^*} \tag{3-22}$$

or

$$b = (I - A)\cdot g \tag{3-23}$$

where $g = \left.\frac{dx_F}{dp}\right|_{p^*}$, $A = \left.\frac{\partial P}{\partial x}\right|_{x^*,p^*}$, $b = \left.\frac{\partial P}{\partial p}\right|_{x^*,p^*}$.

In the close neighborhood of the desired fixed point $x^*(p^*)$ we can assume with good accuracy that the dynamics of map P is linear and can be expressed by the first-order approximation of (3-19):

$$\Delta x_{k+1} = \left.\frac{\partial P}{\partial x}\right|_{x^*,p^*} \cdot \Delta x_k + \left.\frac{\partial P}{\partial p}\right|_{x^*,p^*} \cdot \Delta p_k = A\cdot\Delta x_k + b\cdot\Delta p_k \tag{3-24}$$

Substituting (3-23) in (3-24):

$$\Delta x_{k+1} = A\cdot\Delta x_k + (I - A)\cdot g\cdot\Delta p_k \tag{3-25}$$

Matrix A may be determined using a measured chaotic time series x_k with $p = p^*$ and analyzing its behavior close to the fixed point x^*. Furthermore, the stable and unstable eigenvalues λ_s, λ_u and corresponding eigenvectors e_s, e_u of this matrix can be found and they determine the stable and unstable manifolds in the neighborhood of the fixed point.

To control the chaos, the parameter p is adjusted at each iteration (so instead of p we have p_k) in such a way that the iterates of the map P are confined to a small neighborhood of the desired fixed point $x^*(p^*)$. When an iterate falls near the desired trajectory, parameter p is changed from its nominal value p^* by Δp_k, thereby changing the location of the trajectory and its stable manifold, such that the *next* iterate will be forced back toward the stable manifold of the *original* trajectory for $p = p^*$. Fig. 3-14 illustrates the method for the case of a saddle fixed point located at $x^*(p^*)$ [88].

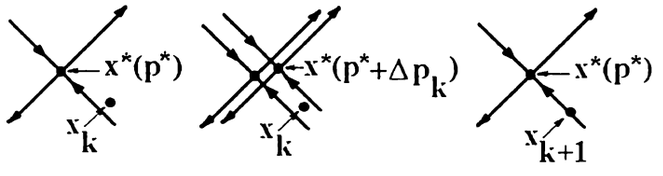

Figure 3-14 Schematic of the OGY control algorithm:

a. The kth iterate x_k falls near the desired fixed point $x^*(p^*)$.

b. Turn on the perturbation of p to move the fixed point.

c. The next iterate is forced onto the stable manifold of $x^*(p^*)$.
Turn off the perturbation.

Assume that x_k falls near the desired fixed point $x^*(p^*)$ so that (3-25) applies. The choice of Δp_k is attempted in such a way that Δx_{k+1} lies along the stable manifold of fixed point. Let $\Delta p_k = c^T \cdot \Delta x_k$ and (3-25) becomes:

$$\Delta x_{k+1} = A \cdot \Delta x_k + (I - A) \cdot g \cdot c^T \cdot \Delta x_k = \left[A + (I - A) \cdot g \cdot c^T\right] \cdot \Delta x_k \tag{3-26}$$

c^T must be picked so that Δx_{k+1} falls on the stable eigenvector e_s of matrix A, which can be rewritten as:

$$A = \lambda_u e_u f_u^T + \lambda_s e_s f_s^T \tag{3-27}$$

where f_u and f_s are the contravariant basis vectors, defined by $f_u^T e_u = f_s^T e_s = 1$ and $f_u^T e_s = f_s^T e_u = 0$. Note that Δx_{k+1} lies along e_s if $f_u^T \Delta x_{k+1} = 0$. Thus, dotting (3-26) with f_u^T and expressing A with (3-27) the following equation is obtained:

$$f_u^T \cdot [\lambda_u e_u f_u^T + \lambda_s e_s f_s^T + (I - \lambda_u e_u f_u^T + \lambda_s e_s f_s^T) \cdot g \cdot c^T] \cdot \Delta x_k = 0, \forall \Delta x_k \tag{3-28}$$

Using the definition of the contravariant basis vectors, (3-28) results in:

$$\lambda_u \cdot f_u^T + (1 - \lambda_u) \cdot f_u^T \cdot g \cdot c^T = 0 \tag{3-29}$$

which leads to the following equation for c^T:

$$c^T = \frac{\lambda_u}{(\lambda_u - 1) \cdot f_u^T \cdot g} \cdot f_u^T \tag{3-30}$$

Therefore the *OGY control law* is:

$$\Delta p_k = \frac{\lambda_u \cdot f_u^T \cdot \Delta x_k}{(\lambda_u - 1) \cdot f_u^T \cdot g} \tag{3-31}$$

where $\Delta p_k = p_k - p^*, \Delta x_k = x_k - x^*$ and $g = \left.\frac{dx_F}{dp}\right|_{p^*}$.

The control (3-31) is only activated if the resulting change in the parameter Δp_k is less than the maximal allowed disturbance Δp^*; otherwise Δp_k is set to zero. Note that the parameter value $p_k = p^* + \Delta p_k$ should be updated only when the trajectory crosses the surface of section that generates map P (e.g., the Poincaré section). However, the trajectory may not be brought to the fixed point because of nonlinearities not included in (3-31). In this case the trajectory will move away and continue to move chaotically as if there was no control. Eventually (due to ergodicity of the uncontrolled attractor) the trajectory will fall near enough to the desired fixed point that attraction to it is obtained.

The above procedure specifying the control Δp_k is a special case of the general technique known as "pole placement" in the theory of control systems. For an n-dimensional map $P(x, p)$,linearization around fixed point $x^*(p^*)$ and nominal parameter value p^* yields $\Delta x_{k+1} = A \cdot \Delta x_k + B \cdot \Delta p_k$, where $\Delta x_k = x_k - x^*$, $\Delta p_k = p_k - p^*$, $A = \left.\frac{\partial P}{\partial x}\right|_{x^*, p^*}$, $B = \left.\frac{\partial P}{\partial p}\right|_{x^*, p^*}$. For a linear control in general $\Delta p_k = C^T \cdot \Delta x_k$, thus $\Delta x_{k+1} = \left(A + B \cdot C^T\right) \cdot \Delta x_k$ and C^T is chosen so that the matrix $A' = A + B \cdot C^T$ is stable (i.e., has eigenvalues of magnitude less than 1). If A and B satisfy the controllability condition, then the pole placement technique allows one to determine a control vector C^T that yields any set of eigenvalues that could be chosen for the matrix A'. Equation (3-31) corresponds to the choice wherein the unstable eigenvalue of A is made zero, while the stable eigenvalue is unaltered by the control.

The OGY method employs a discrete-time feedback control system: it requires a permanent analysis of the state of the system and the changes of the parameter are discrete in time since the method deals with a (generally Poincaré) map. The main advantages of the OGY technique are [85]:

- Extremely general, extending to any system whose dynamics can be characterized by a nonlinear map and relying only on the universal feature of infinitely many unstable periodic trajectories embedded within chaotic attractors.
- Solid theoretical foundation.
- No model of system dynamics required.
- Control can be achieved even with imprecise measurements of the eigenvalues and eigenvectors.
- The computations required at each iterate are minimal.
- Any accessible system parameter can be used as a control parameter.
- Just one parameter to vary and variations are small.
- At least in theory, different periodic trajectories embedded in a chaotic attractor can be stabilized for the *same* system in the *same* parameter range.

Some disadvantages are the following [85]:

- Local control scheme.
- Model derived from measurements; high resolution and large data set required.
- Chaotic transient before settling into the desired periodic state.

- Noise may destabilize the controlled periodic trajectory resulting in occasional chaotic bursts.

3-4-2 CONTROL SETUP

In order to control the chaotic operation of the investigated converter configuration, the data used by the OGY algorithm were time-series of the inductor current from the positive channel $i_{op}(t)$ (Fig. 2-6). Accordingly to the construction of the Poincaré map (see Chapter 2), the current is sampled and stored, in steady-state, at the start of every switching cycle. By considering the sampled state variable as arising from iterates of a map, $i_{op,k}=i_{op}(kT_s)$, the control theory introduced above can be applied directly. Since the bifurcation behavior of the converter, as detected through the study presented in Chapter 2, arose as an effect of alteration of voltage gain K_V, this parameter is selected to be varied to achieve control, i.e., $p = K_V$. The parameter region is chosen such that the converter operates in the chaotic state identified in subsection 2-4-1-6 for $K_V = p^* = 70$ (Appendix A).

In Fig. 3-15a is plotted the obtained first return map. The approximate location $i_{op,F}$ of a fixed point of the map, corresponding to an unstable periodic trajectory of the system, is found by noting that any fixed point must lie along the $i_{op,k+1} = i_{op,k}$ line in the plot of the first return map. Next are identified all pairs of iterates *both* of which fell within an imposed close neighborhood of the desired fixed point i_{op}^* corresponding to that periodic trajectory which one wants to stabilize. The result is shown in Fig. 3-15b.

To these pairs of iterates is fitted the approximate local *linear* map A (e.g., using the least squares method), where:

$$x_{k+1} - x^* = A \cdot \left(x_k - x^*\right), \; x_{k+1} = \begin{bmatrix} i_{op,k+2} \\ i_{op,k+1} \end{bmatrix}, \; x_k = \begin{bmatrix} i_{op,k+1} \\ i_{op,k} \end{bmatrix}, \; x^* = \begin{bmatrix} i_{op}^* \\ i_{op}^* \end{bmatrix} \tag{3-32}$$

Knowing A, the stable and unstable eigenvalues λ_s, λ_u and eigenvectors e_s, e_u can be extracted. Actually only λ_u and the unstable contravariant basis vector f_u^T given by $f_u^T e_u = 1$ and $f_u^T e_s = 0$ are needed.

Next, $p = K_V$ is slightly changed and another set of data is collected. Founding again the location of the fixed point allows the calculation of

$$g = \frac{dx^*}{dp} \approx \frac{\Delta x^*}{\Delta K_V} \tag{3-33}$$

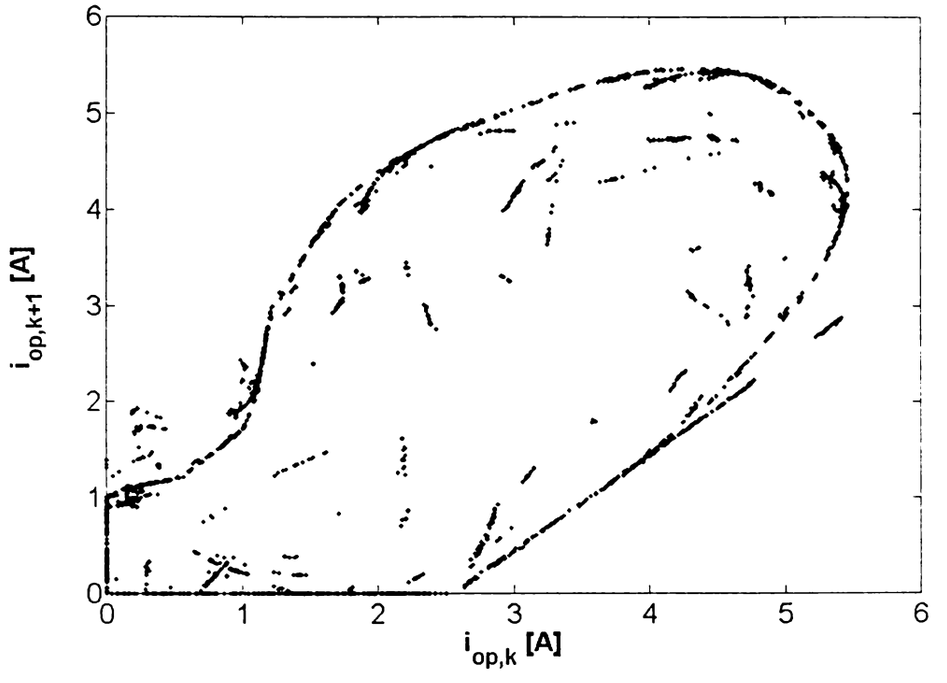

a.

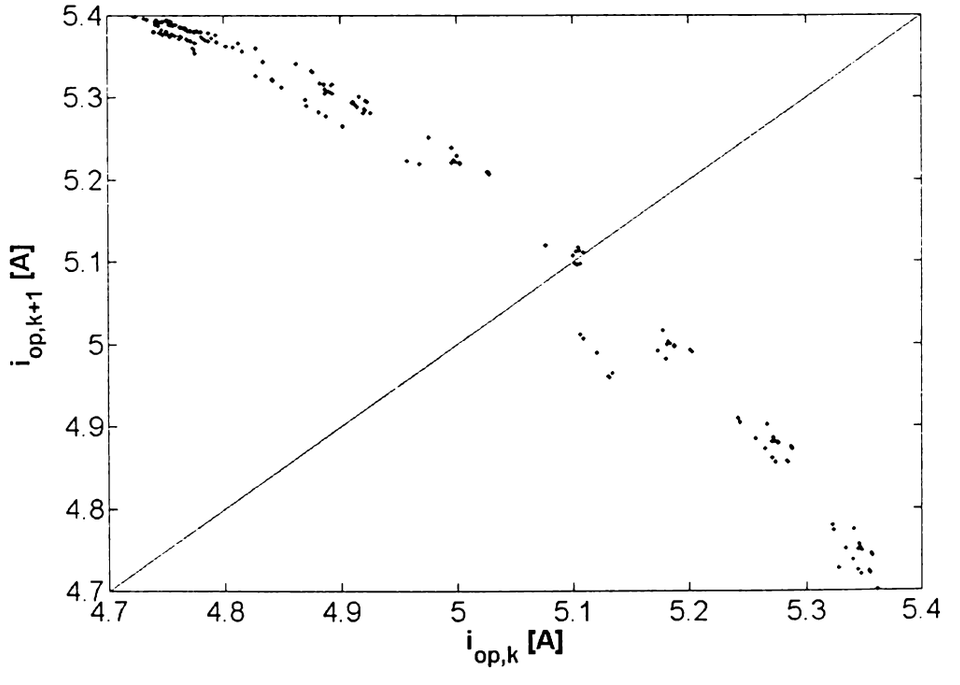

b.

Figure 3-15 The first return map for the uncontrolled system (a) and the magnified neighborhood of the desired fixed point (b).

To control the chaotic behavior of the converter, $p = p^*$ with a maximum allowed perturbation $\Delta p^* = 0.1 \cdot p^*$ is set. The control law defined by (3-31) is applied in steady-state as long as the resulting perturbation

$$\Delta p_k = \frac{\lambda_u \cdot f_u^T \cdot \left(x_k - x^*\right)}{\left(\lambda_u - 1\right) \cdot f_u^T \cdot g} = k^T \cdot \left(x_k - x^*\right) \tag{3-34}$$

is within Δp^* of p^*; otherwise it is set to zero. Since noise and errors in determining x^*, λ_u, f_u^T and g, as well as any inaccuracies due to the linear approximation, prevent from getting the next iterate exactly on the stable manifold, a new Δp_k is calculated for each iterate. Note that k^T of (3-34) can be computed at the start of the run, therefore the calculations at each iterate are very simple (for experimental application, the change in K_V can be effectively instantaneous in relation to the sampling period T_s).

For the parameter setup mentioned at the beginning of this subsection, the values obtained were i_{op}^* = 5.305 A, λ_u = -1.193, $f_u^T = [-0.837 \quad 0]$ and g = 0.001. Fig. 3-16 shows the response of the converter control system. The first 500 iterations are of the response of the converter without the control based on the OGY technique, which is initiated after iteration 500 and stabilizes the trajectory nearly instantaneous (less than 50 iterations, i.e., 0.5 msec).

Although the details vary, the analysis and the results apply to any other accessible control parameter of the converter.

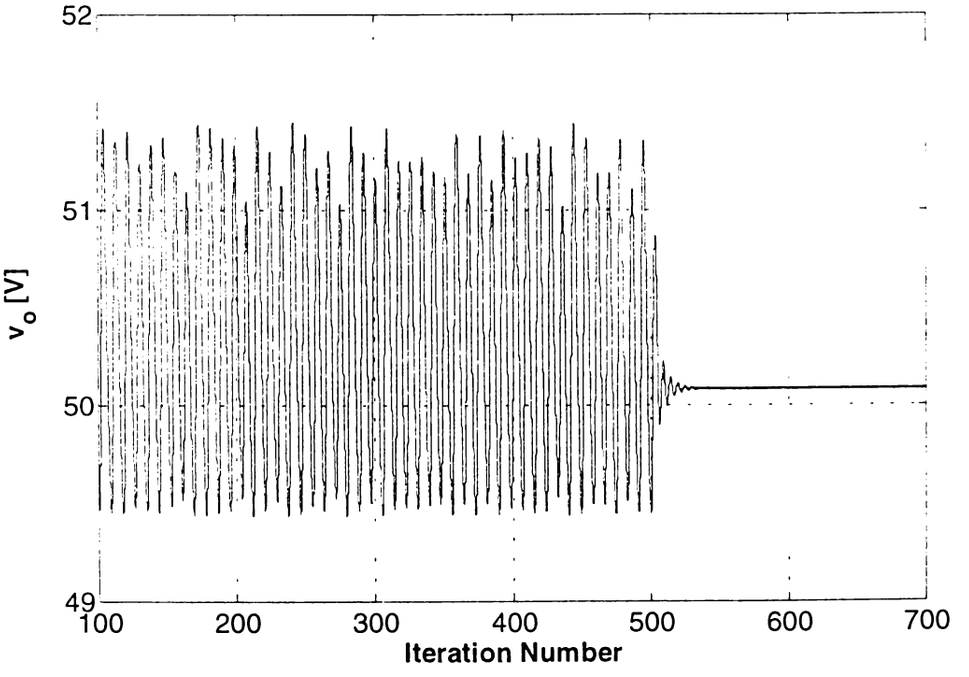

Figure 3-16 Converter response with control based on OGY method initiated after 500 switching cycles

3-5 TIME-DELAY AUTOSYNCHRONIZATION

Control of unstable regimes (in the sense of suppressing them) in the given nonlinear dynamical system was achieved in the previous sections either by the insertion of controllers into the configuration or by time- and state-dependent small perturbations of an accessible system parameter. A particular, discrete-time case of the later was just applied above and it pointed out that the many unstable periodic trajectories embedded in a chaotic attractor can be used to produce regular behavior to the advantage of control of nonlinear systems in which chaotic oscillations are present but undesirable. A different, continuous-time method from this class of strategies of control such that the feedback perturbation vanishes on the target trajectory, was proposed by Pyragas [106]. The method is based on the construction of a special form continuous-time perturbation which does not change the form of the desired unstable periodic trajectory, but under certain conditions can stabilize it. The variant discussed here, called *time-delay autosynchronization*, is based on a self-controlling delayed feedback by involving a control signal formed with the difference between the current state of the system and the state of the system delayed by one period of the unstable periodic trajectory one wants to stabilize [70].

In this section is addressed the problem of stabilizing the unstable periodic trajectories of the investigated resonant converter by means of time-delay autosynchronization. Recall that the PWM control of this converter is achieved by comparing a sawtooth waveform with the control signal v_{com} obtained by amplifying the error signal, i.e., the difference between the actual output voltage of the converter v_o and its desired value v_{ref} (Fig. 2-9). The proposed time-delay autosynchronization control (Fig. 3-17) forms the control voltage v_{com} by adding to the amplified error signal a term proportional to the difference between the present output voltage $v_o(t)$ of the converter and its past value $v_o(t - T_s)$:

$$v_{TDAS}(t) = \eta \cdot [v_o(t) - v_o(t - T_s)] \tag{3-35}$$

where η is a dimensionless feedback gain. The switching period T_s corresponds to the period of the desired periodic trajectory for a stable period-1 operation. Notice that $v_{TDAS}(t) = 0$ when the system evolves on a period-1 solution and thus the time-delay autosynchronization control effort vanishes on the target trajectory.

The main property of the time-delay autosynchronization control is that it transforms the natural unstable behavior of the converter without time-delay

autosynchronization (being chaotic, quasiperiodic or subharmonic) into a stable period-1 dynamics provided that the parameter η belongs to a given trajectory-dependent range. Despite some disadvantages [85]:

- One must store a sample of the system's state for a time length equal to the period of the target trajectory (the possibility of variable delay, the market availability and the low cost recommend the implementation of the delay by means of a digital memory)
- The mathematical computations to find out that range of parameter which stabilizes the trajectory can be quite imposing (a method was proposed in [70])

once this parameter range is known, the time-delay autosynchronization control has the following major advantages [85]:

- The only information needed about the target trajectory is its period
- The time-delay autosynchronization signal is generated by a minimal information processing
- No model of system dynamics required

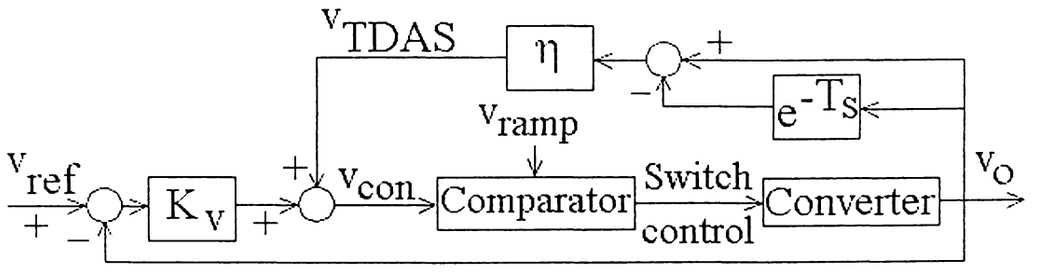

Figure 3-17 Block diagram of control system with time-delay autosynchronization

Results of several computer simulations of the dynamical response of the time-delay controlled converter are reported in the following for voltage gain K_V = 70, which corresponds to a natural chaotic behavior of the converter configuration, as revealed in subsection 2-4-1-6 (the other parameter values remain those specified in Appendix A). The simulations were performed with η = -50. In Fig. 3-18 the time-delay autosynchronization was switched on after 500 switching periods have elapsed. Notice that the collapse of the chaotic state to the stabilized period-1 trajectory is nearly instantaneous (less than 30 switching periods, i.e., 0.3 msec).

Simulations to test the robustness of the time-delay autosynchronization under perturbations of the parameters of the system were also performed. Fig. 3-19 shows the

response of the converter when the load R is changed stepwise successively from 8Ω to 10Ω and 15Ω, then back to 10Ω and 8Ω, each phase lasting 100 switching periods. It can be seen that the sudden changes in the load only introduce a short fluctuation in the output voltage. The same conclusion is obtained when changing stepwise the input voltage v_{ip} = v_{in} successively from 100V to 110V and to 120V, then back to 220V to 200V, each phase lasting again 100 switching periods (Fig. 3-20). These results show that a proper value of η does not vary too much under this kind of changes and it can be used without regard to the exact value of the load, which may be advantageous from an implementation point of view.

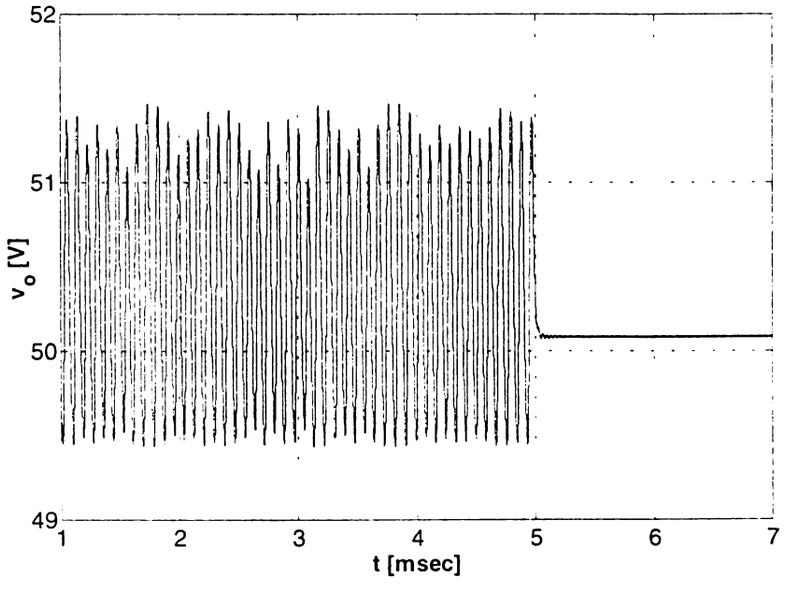

Figure 3-18 Converter response with time-delay autosynchronization initiated after 500 switching cycles

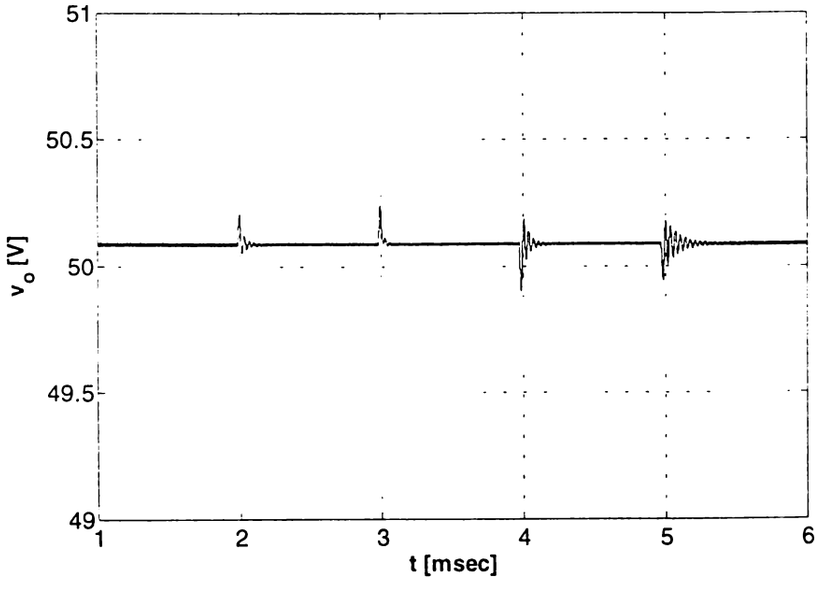

Figure 3-19 Control system response when the load is changed stepwise up and down

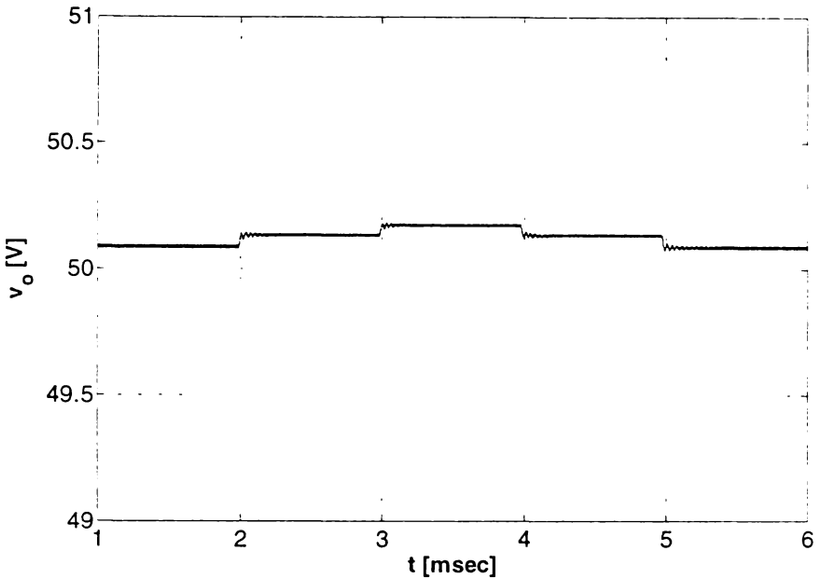

Figure 3-20 Control system response when the input voltages of the converter are changed stepwise up and down

3-6 EXPERIMENTAL SETUP AND TEST RESULTS

In order to verify the theoretical analysis and simulation results presented so far, the controlled converter configuration was constructed at the Laboratory of Group of Electrical Engineering, Department of Automation and Applied Informatics, Budapest University of Technology and Economics, Hungary.

3-6-1 THE POWER STAGE

A configurable experimental circuit that allows the study of the twelve resonant converters introduced in section 2-2 was built at the laboratory mentioned above. The circuit does not contain the control loop, which can be externally attached. The resonant frequency of 45kHz was chosen to avoid high-frequency problems and to permit the implementation of the control loop by using dSPACE 1102 DSP board available in the laboratory equipment.

Concerning the electric switches of the circuit, MOSFETs (IRF740) and diodes (BYT79) were applied. The series connection of one MOSFET and one diode corresponds to the directional switches in Fig 2-3. To provide smooth output voltage an electrolyte and a low ESR tantalum type capacitors are connected in parallel. The resonating capacitor is of the same tantalum type. Contrary to the ideal inductance assumed in the theoretical model and analysis, the inductors have an inherent series resistance of L_{DC} = 0.1 Ω. The

circuit was designed for a power range up to 100W.

Due to the different source potentials of the MOSFETs, the electrical isolation was accomplished by transformer in case of power supplies of the driver circuits and by opto-coupler in case of switching signals.

As presented in section 2-3, the inputs of the converter as controlled plant are represented by the control pulses of the switches, acting as actuating signals (Fig. 2-9a). The switches S_p and S_{cp} (S_n and S_{cn}) (Fig. 2-6) within one channel are in complementary states, that is, when S_p is on S_{cp} is off and vice-versa. Only the pulse train for the controlled switches S_p and S_n (Fig. 2-9c) is acquired from the control device and the pulses are selected alternatively by means of a steering flip-flop. The pulses for S_{cp} and S_{cn} are generated by a driver circuit, which in order to avoid the commutation problem (i.e., both switches are turned off), also provides a small overlap among the switching signals.

The controlled output of the converter is represented by its output voltage. A disadvantageous feature of the buck configuration investigated is the floating output ground potential, preventing the direct acquisition of the output voltage by the DSP board implementing the control. The problem was overcome by using an additional circuit on the output of the converter, which delivers a voltage proportional with the difference between the potential of the output terminals. The proportional factor ensures the acquired voltage to remain in the input voltage range of the DSP's ADC (see subsection 3-4-2-1).

The values of the components of the experimental converter are specified in Appendix E.

3-6-2 THE CONTROL DEVICE

3-6-2-1 THE DIGITAL SIGNAL PROCESSOR

The control of the above depicted power stage was achieved by using the *DS1102 Floating-Point Controller Board*. It is a Digital Signal Processor (DSP) board included in the hardware line of dSPACE, a company that specializes in real-time hardware and software products. The DS1102 is a stand-alone board system specifically designed for development of high-speed multivariable digital controllers and real-time simulations in various fields and also well suited for general digital signal processing and related tasks. It is based on the *TMS320C31* third generation floating-point DSP, a high performance member of Texas Instruments' TMS320 family of VLSI digital signal processors. It builds the main processing unit, providing fast instruction cycle time for numeric intensive algorithms and performing parallel multiply and ALU operations on integers or floating-

point numbers in a single cycle. The TMS320C31 supports a large address space with various addressing modes allowing the use of high-level languages for application development. Some key features of the TMS320C31 are [107]:

- 60 MHz clock rate and 33.33 ns single cycle instruction execution time
- Two 1K x 32-bit dual access on-chip data RAM blocks
- 64 x 32-bit instruction cache
- 32-bit instruction and data words, 24-bit addresses
- 40/32-bit floating-point / integer multiplier and ALU
- Eight 40-bit accumulators
- Two independent address arithmetic units
- 2- and 3-operand instructions
- On-chip bidirectional 15Mbaud serial link
- DMA controller for concurrent DMA and CPU operation
- Four external interrupt lines
- Two 32-bit on-chip timers/event counters

The DSP has been supplemented by a set of on-board peripherals frequently used in digital control systems. Analog to digital and digital to analog converters, a DSP-microcontroller based digital-I/O subsystem and incremental sensor interfaces make the DS1102 an ideal single board solution for a broad range of digital control tasks. The available blocks are [107]:

- 4-Channel ADC
- 16-Bit Digital Input
- 16-Bit Digital Output
- 4-Channel DAC
- 4/6-Channel PWM
- 2-Channel Encoder Position Measurement
- 2-Channel Encoder Delta Position Measurement
- 1-Channel Encoder Counter Reset
- 1-Channel Encoder Index Search
- Hardware Interrupt

This subsection details in the following only those DS1102 features which were used for the control interface with the resonant converter. The controlled signal, the output

voltage of the converter, is acquired through an ADC channel. The DS1102 contains two types of ADCs [107]:

- Two 16-bit 250kHz sampling A/D converters with integrated sample/holds. Each of the ADCs contains a 16-bit successive approximation (SAR) type AD converter and a sample/hold circuit. The converter achieves a conversion time of 4μs.
- Two 12-bit 800kHz sampling successive approximation A/D converters with integrated sample/hold circuits and digitally controlled offset calibration units. Each converter achieves a conversion time of 1.25μs.

The input range of all ADCs is ±10V. Since dSPACE functions reading data from input devices automatically scale their output data to floating-point values within the range of −1 - +1, the scaling between the analog input voltage and the output of the ADC is 10:1.

As recalled in the previous subsection, the control device provides the pulse train for the PWM controlled switches S_p and S_n (Fig. 2-9). To this end is used the high-precision PWM operating mode of DS1102, where six output lines are available for PWM generation with variable duty cycle and constant frequency [107]. The possible frequency range is 0.01Hz - 1MHz. The PWM resolution is 40nsec for PWM frequencies above approximately 385Hz, and 160 nsec otherwise. The input value to control the duty cycle must be scaled to range 0 - 1, representing a duty cycle of 0 - 100%. This value is calculated by the digital control as a result of the comparation between the control signal computed by the control algorithm and the sawtooth waveform (Fig. 2-9b).

3-6-2-2 THE SOFTWARE ENVIRONMENT

The DS1102 controller board is inserted directly into a host *PC*. At present, all dSPACE boards conform to the half length or full length ISA slot size. The ISA slot enables the host PC to download the executable to the target processor board at a higher bandwidth than is possible over the ISA backplane. The ISA bus is also used for downloading new parameters and for passing collected data back to the host computer.

This PC setup is used in combination with code generated by the *Real-Time Workshop*. The Real-Time Workshop, for use with MATLAB and Simulink, produces code directly from *Simulink* models and automatically builds the program that can be run in real-time on the target processor [108]. Executing code generated from the Real-Time Workshop on a particular target in real-time requires target-specific code, which includes I/O device drivers and an interrupt service routine. Other components, such as a communication link with Simulink, are required if the ability to download parameters on-

the-fly to the target hardware is needed. The key software component that provides this support is the dSPACE *Real-Time Interface to Simulink* (RTI), with special versions available for various dSPACE processor boards, including the DS1102 used [109]. The RTI connects MATLAB, Simulink and Real-Time Workshop development software with dSPACE hardware to form an integrated, ready-to-use development environment for real-time applications, by providing an automatic and seamless implementation of Simulink models on dSPACE real-time systems for controller prototyping.

The development and test session for the real-time control of the converter based on DS1102 and RTI comprised the following steps:

- Use of MATLAB, Simulink and the dSPACE I/O board library added to Simulink to design the real-time application and to specify the I/O hardware setup. Simulink block diagrams of the control algorithms implemented on DS1102 are elementals of the diagrams of the controlled converter used through the study performed by computer simulations. They have been completed with I/O device drivers as appropriate for the model and for DS1102. Simulink includes a set of preconfigured blocks for I/O device drivers associated with particular dSPACE hardware [110,111].
- Use of Real-Time Workshop to generate C code for the real-time application and to start the RTI. The RTI runs through all the necessary steps to prepare the application for the real-time test, and as a last step downloads the converter control onto DS1102 via the ISA bus.
- Start of dSPACE TRACE tool for recording the time histories of variables in the real-time application. This data can be transferred into the MATLAB workspace for further analysis and visualization.
- Start of dSPACE COCKPIT tool for experiment control, real-time parameter tuning and signal monitoring. The dSPACE COCKPIT program provides a virtual instrument panel on the host PC, with a graphical interface for the interactive modification of the parameters while the generated code executes on a dSPACE board, including the DS1102 used. It is possible to modify or display all variables represented as single-precision floating point or integer variables in the processor board's memory. COCKPIT has two operation modes, edit mode and animation mode. The layout of an instrument panel is created in edit mode. Various instruments can be chosen to build a screen layout that meets the user's requirements. Output is performed with instruments like numeric displays, gauges or moving bars. Variables can be modified with sliders, various buttons or numeric input from the keyboard. By starting the animation mode,

the interaction with the underlying real-time processor board is initiated. While animation mode is active, the variables of the currently running converter control are read and displayed on the screen and the parameters of the control can be modified by user action on input controls [112].

During the development process of the real-time test it is necessary to run through these different steps several times. As the RTI manages the transition from the Simulink model to the real-time test fully automatically, the user needs not concern himself with the details of the implementation and the system is ready for a new test within seconds.

3-6-3 EXPERIMENTAL RESULTS

The values of the parameters and variables of the experimental setup are listed in Appendix E. Fig. 3-21 shows the corresponding global bifurcation diagram obtained by computer simulation for a wide variation range of the gain K_V relating the control voltage to the error signal (Fig. 2-9a). This complex bifurcation behavior detected by simulations was described in Chapter 2. The experiments verified the behavior revealed by simulations. The oscilloscope traces of the condenser voltage v_c and choke current i_{op} are shown in Fig. 3-22 in chaotic operation (at $K_V = 40$), in Fig. 3-23 in quasiperiodic operation (at $K_V = 10$) and in Fig. 3-24 in subharmonic operation (at $K_V = 7.3$). Quantitatively the simulation and test results are in good agreement. The main source of deviations is the assumption of ideal components used both in the derivation of the relations and in the simulations. Parasitic elements (the equivalent series resistance of the inductor, the forward voltages of the semiconductors) are always present in the practical circuit and they affect its behavior, but they do not affect the bifurcation structure. They were only found to shift the bifurcation points and are not essential to the phenomena reported. For example, the Naimark-Sacker bifurcation occurs in the practical circuit for an upper value of the gain, about $K_V = 7$, than in the simulation model ($K_V = 3.6$ in Fig. 3-21).

Test results also supported the simulations when the control algorithms introduced in this chapter were implemented on DS1102 in order to suppress the unstable regimes illustrated above. The oscilloscope traces of the condenser voltage v_c and choke current i_{op} in such a stabilized period-1 behavior are shown in Fig. 3-25. There is at least one point that makes these digital implementations non-optimal. Since for simplicity the comparation between the control signal generated by the digital control algorithm and the sawtooth waveform (Fig. 2-9) is implemented also on DS1102 and the result is used by the PWM outputs as the duty ratio of the switches control pulses, only one sample of the system state

per ramp period is used. However, the control performs very well. Even more accurate results can be expected by using an external comparator circuit and increasing the number of state samples per ramp period in the control algorithm.

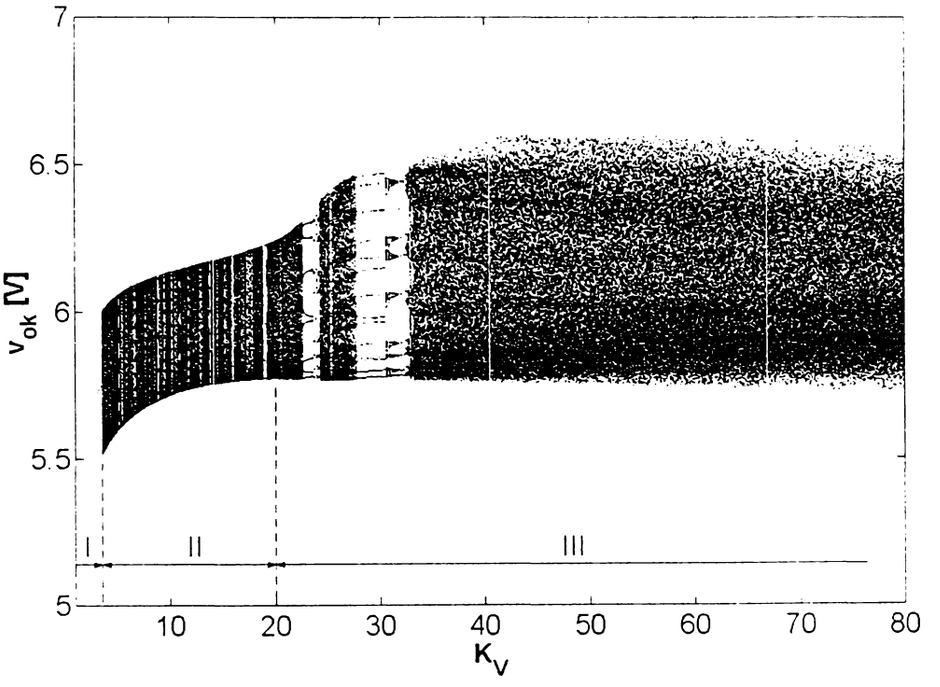

Figure 3-21 Bifurcation diagram: I = Periodic range
II = Quasiperiodic and subharmonic range
III = Chaotic and subharmonic range

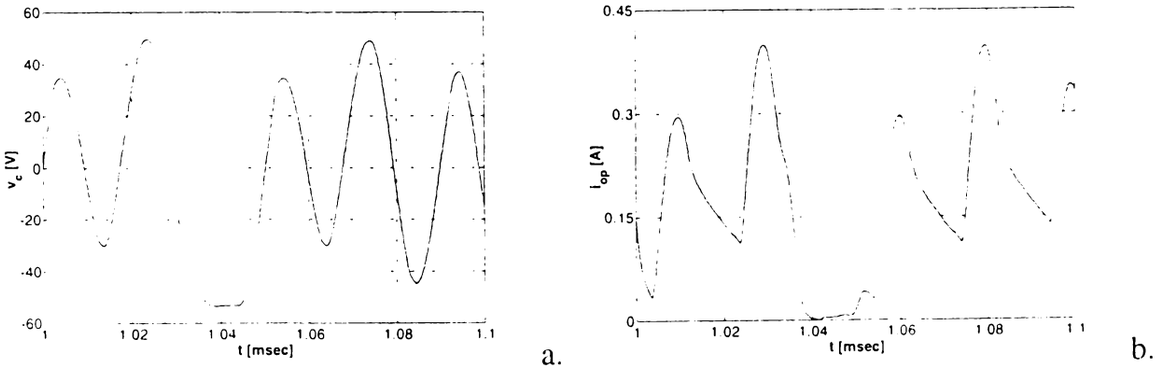

Figure 3-22 Oscilloscope traces of the condenser voltage (a) and choke current (b) in chaotic operation ($K_V = 40$)

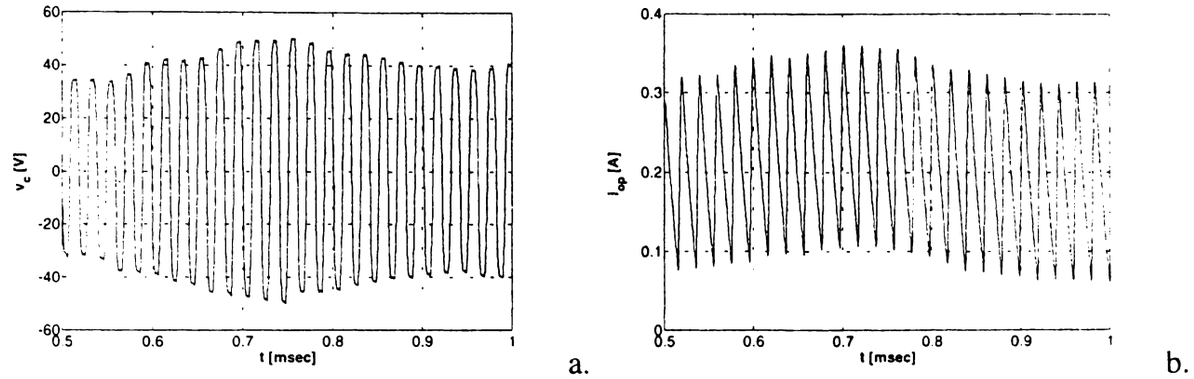

a. b.

Figure 3-23 Oscilloscope traces of the condenser voltage (a) and choke current (b) in quasiperiodic operation ($K_V = 10$)

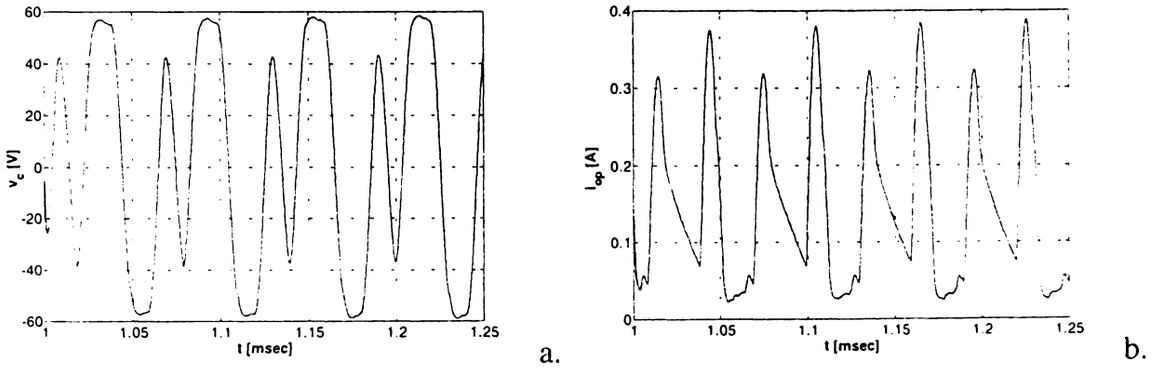

a. b.

Figure 3-24 Oscilloscope traces of the condenser voltage (a) and choke current (b) in subharmonic (period-2) operation ($K_V = 7.3$)

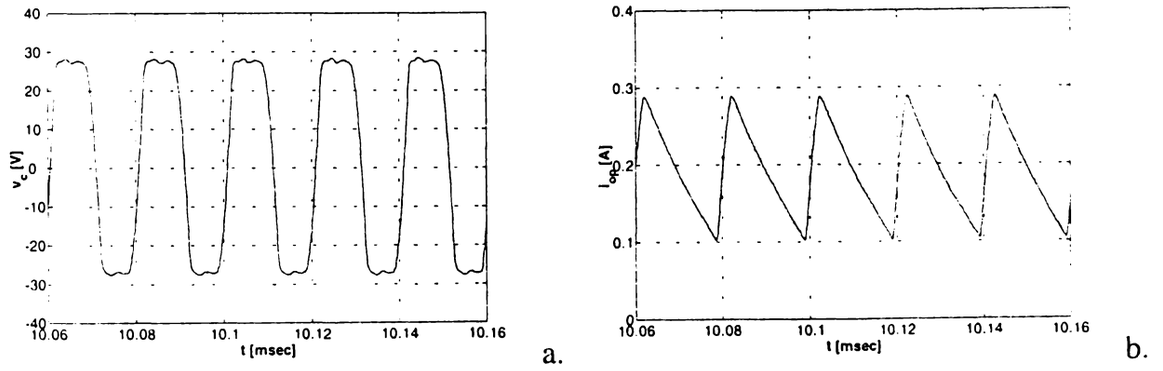

a. b.

Figure 3-25 Oscilloscope traces of the condenser voltage (a) and choke current (b) in stabilized period-1 operation

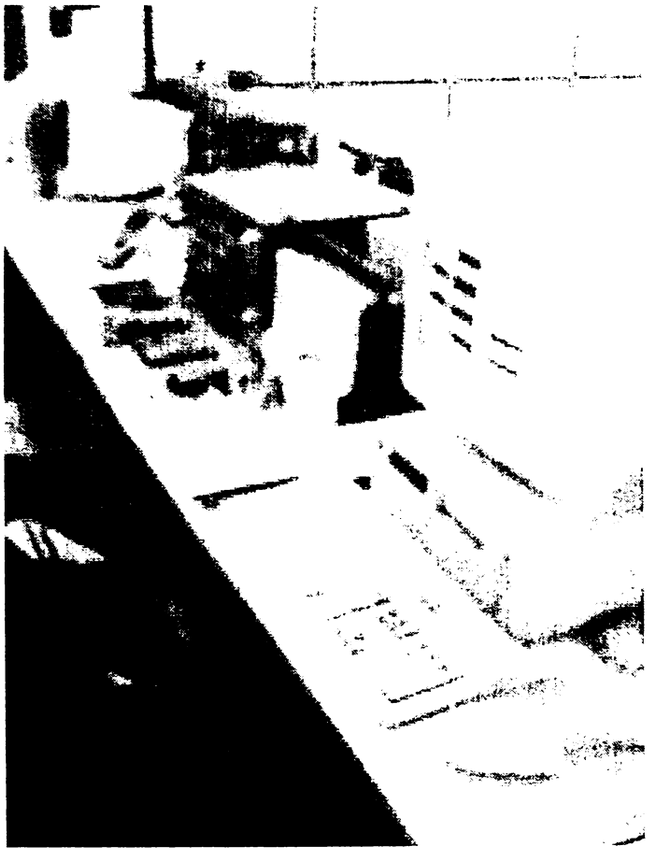

Figure 3-26 Experimental setup of the controlled converter

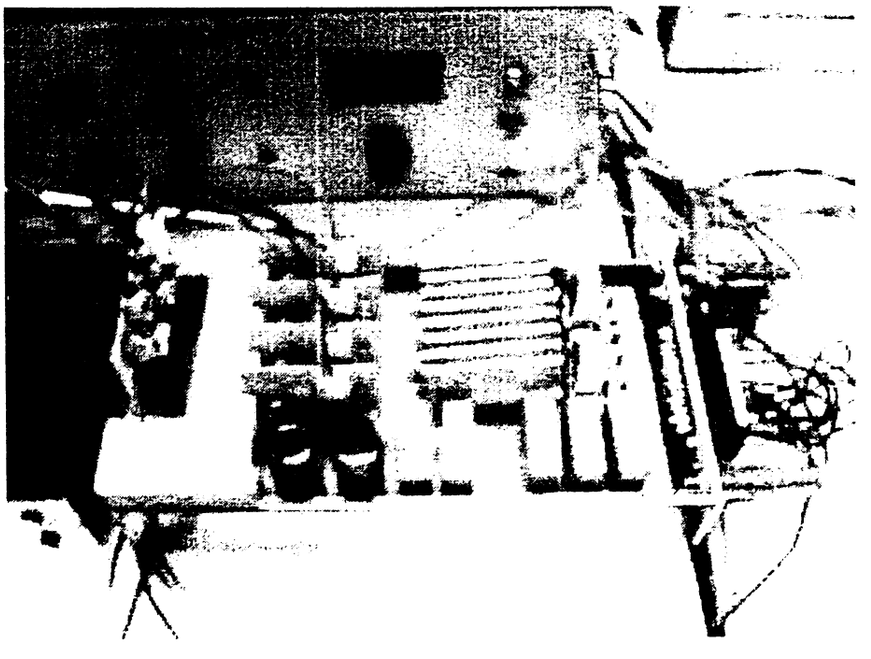

Figure 3-27 Experimental dual-channel resonant DC-DC converter circuit

CHAPTER 4

ANALYSIS OF NONLINEAR DYNAMICS AND CONTROL OF A HIGH FREQUENCY TIME-SHARING INVERTER

A short introduction of a special type of high frequency time-sharing thyristor inverter (section 3-1) is followed by the presentation of the basic configuration of the inverter (section 3-2) and by the description of the mode of operation of this configuration (section 3-3). The basic configuration is extended in order to obtain the complete inverter structure that still benefits from the time-sharing principle (section 3-4). The steady-state analysis of the inverter with open loop control includes the analysis in time-domain (comprising an approximate mathematical study and an analysis by simulation on an exact model), followed by the analysis in frequency-domain and state-space, performed by computer simulations (section 3-5), first time for this inverter. A feedback loop control structure is introduced and its steady-state behavior is investigated (section 3-6). The control by time-delay autosynchronization is proposed in order to remove the detected subharmonic regimes and to ensure the stable period-1 operation (section 3-7). Some experimental results are presented (section 3-8).

4-1 SHORT INTRODUCTION

This chapter is concerned with a special type of high frequency thyristor inverter, characterized by time-sharing operation and used mostly in induction heating applications [113]. The aim of the study is to present the solution used in designing the configuration, to highlight the interesting features of the nonlinear dynamics of the inverter and to introduce the appropriate control.

The upper frequency of most high frequency, conventional inverter circuits is limited by the dynamic parameters as the turn-off time of the controlled switches e.g.

thyristors. The turn-off time barrier can be broken by special inverter configuration applying the principle of time-sharing. The practical inverter circuit discussed here uses this principle to enable the circuit turn-off time to be extended over two half-cycles of the output voltage [114].

It will be shown how methods specific to nonlinear dynamics can be used to provide an overall practical picture of the strange behavior of the inverter, despite its complexity and difficult modeling. This study of the effects of system parameters on the inverter behavior helps the designing engineer to search for stable periodic regions and settings (the numerical results of severe peak stress of power devices, such as controlled switches and series capacitors are also included). A feedback control solution will be also developed in order to avoid the unstable regimes of the inverter behavior, extending hereby the stable operation required in applications.

4-2 BASIC INVERTER CONFIGURATION

The purpose of this section is to introduce the basic configuration of this special type, high frequency time-sharing, thyristor inverter,. Fig. 4-1 shows the inverter configuration in its simplest form [115]:

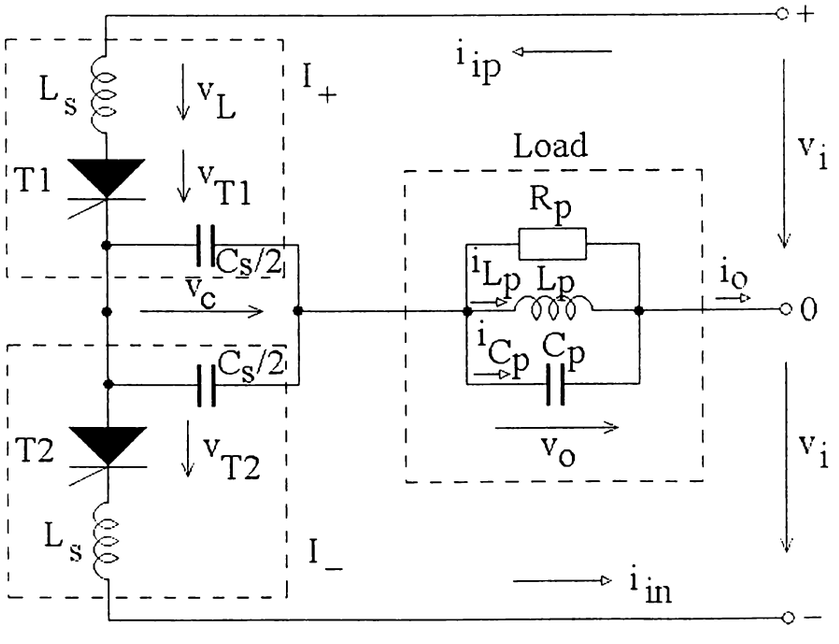

Figure 4-1 The basic configuration of the inverter

The inverter consists of two so-called subinverters, encircled by dotted lines. I_+ and I_- are the so-called positive and negative subinverter, respectively. Each subinverter has one thyristor, one choke L_s and one condenser $C_s/2$. The parallel oscillatory circuit L_p-C_p-R_p represents the load. The supply is provided by a center-tapped DC voltage source.

In order to explain the fundamental features of the mode of action of the inverter, the following assumptions are introduced:

- The DC supply voltage is constant and smooth.
- The thyristors used are supposed to be ideal.
- The resonant frequency of the series and the parallel oscillatory circuits are equal with each other, i.e., $L_s C_s = L_p C_p$.

4-3 INVERTER OPERATION

The basic operation of the inverter can be understood by the time functions of Fig. 4-2:

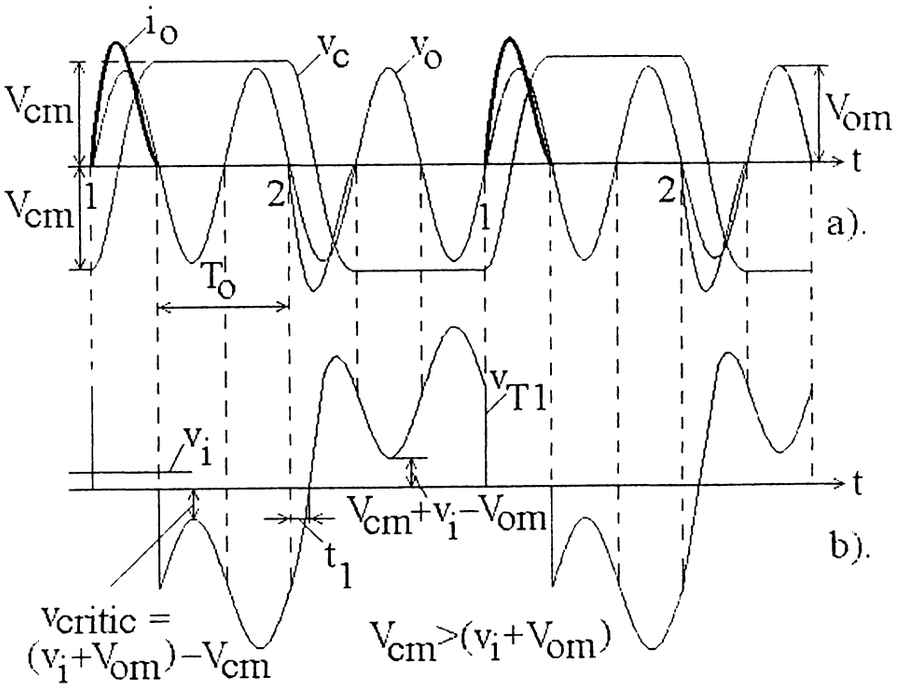

Figure 4-2 Time functions in basic operation

In Fig. 4-2a the sinusoidal output voltage v_o, the inverter output current pulses i_o and the condenser voltage v_c can be seen. Thyristors $T1$ and $T2$ are alternatively fired at the

instants located at every sixth zero crossings on the positive and on the negative slope of the output voltage, respectively. After firing a thyristor, an output current pulse i_o is flowing into the load which changes the polarity of the series condenser voltage v_c, for instant from $-V_{cm}$ to V_{cm}. By knowing the time functions of v_c, v_o and v_i, thyristor voltage v_{T1} is known as well and is drawn in Fig. 4-2b. When a thyristor is reverse-biased, its voltage is (Fig. 4-1):

$$v_T = v_i \mp (v_C + v_o)$$

The sign " – " and " + " refers to the thyrirstor voltage in the positive and in the negative subinverter, respectively. As long as inequality $V_{cm} > v_i + V_{om}$ or $v_{critic} < 0$ holds true as in the case of Fig. 4-2, the thyristor turn-off time is a little bit longer than two half cycles of the output voltage. It is more than four times longer than the theoretical maximum of the turn-off time in the conventional high frequency inverters [116].

4-4 EXTENSION OF BASIC INVERTER CONFIGURATION

The presented basic configuration provides energy to the load only in every third half cycle, therefore the output voltage is damped exponentially between two successive current pulses. By applying two more positive and two more negative subinverters, that is altogether three positive and three negative subinverters, a time-sharing inverter configuration can easily be built up which provides output current pulses in every half cycle of the output voltage [115].

Fig. 4-3 presents the configuration having three positive and three negative subinverters. Here the respective input and output terminals of the subinverters are paralleled. The numbering of the subinverters corresponds to the firing order. Each subinverter pair works in the same way as it was previously described, except that for instance the time functions of the variables belonging to subinverter pair I_{3+} and I_{6-} are delayed by one period with respect to those of subinverter pair I_{1+} and I_{4-}. The same holds for subinverter pair I_{5+} and I_{2-} with respect to subinverter pair I_{3+} and I_{6-}. The frequency of the variables within a subinverter is one-third of the output frequency. The smaller frequency provides longer turn-off time.

The power circuit of the inverter is shown in Fig. 4-4. In general, by increasing the number of subinverters pairs, the turn-off time can be extended at will.

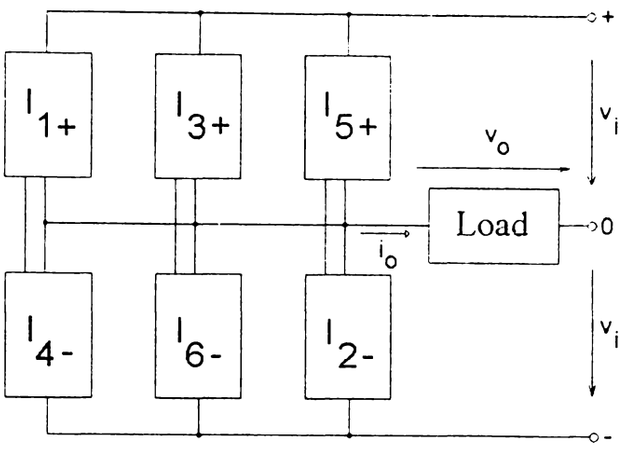

Figure 4-3 Time – sharing inverter configuration with 6 subinverters

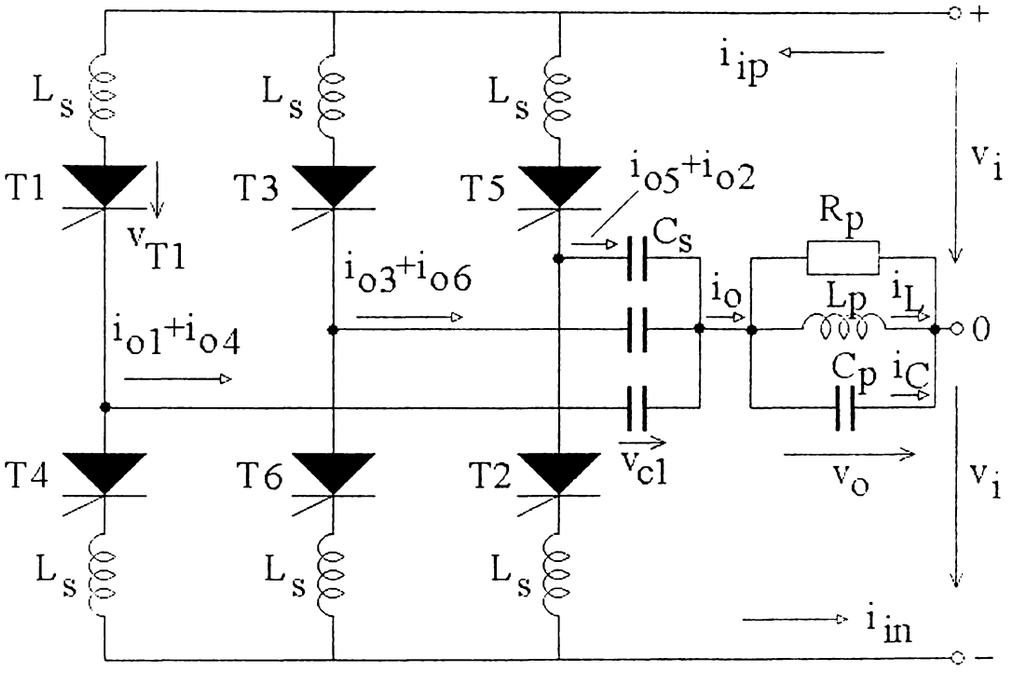

Figure 4-4 The power circuit of the time - sharing inverter

4-5 STEADY-STATE ANALYSIS OF INVERTER BEHAVIOR

The main objective of the study performed in this section is the calculation of the inverter variables in steady state. This is carried out in two steps. The approximate analysis applies simple mathematics. It discovers an operation region that cannot be described any longer by maintaining the approximations. To understand phenomenon in this strange region a more accurate model and simulation tool are needed in the second step [117].

Per unit system is used. The units are as follows:

Voltage: V_{om}, peak value of output voltage v_o.

Current: $C_S \omega_S V_{om}$, where $\omega_S = 1/\sqrt{L_S C_S}$.

Time: $1/\omega_P$, where $\omega_P = 1/\sqrt{L_P C_P}$.

4-5-1 ANALYSIS IN TIME DOMAIN

4-5-1-1 APPROXIMATE ANALYSIS

The load was substituted by a sinusoidal voltage source of constant amplitude and frequency equal to the natural frequency of the parallel resonant circuit [115]. This approximation is justified because the inverter output current i_o is only a fraction of the current in the compensating capacitor or in the load coil. These approximately sinusoidal circulating reactive currents determine practically alone the output voltage v_o. Due to this assumption the energy storage elements of the load are omitted. The subinverters are uncoupled on the load side by voltage source v_o and on the source side by v_i, respectively. They can be analyzed independently. Each subinverter contains only two energy storage elements (two time constants): the choke L_s and the condenser C_s.

Knowing voltages v_i and v_o, the time functions of the subinverter currents can be calculated, provided that the initial condition of the series condenser voltage v_{c1} and the thyristor firing angle α in the reference frame of the output voltage v_o is given. On the basis of approximation introduced the relations can be developed as follows [117]:

The voltage balance equation for example for subinverter 1 in per unit is:

$$\frac{1}{\Omega}\frac{di_{o1}}{dt} + \Omega \int i_{o1}\,dt = v_i - v_o , \tag{4-1}$$

where $\Omega = \omega_S/\omega_P$.

Using the Laplace transformation, eq. (4-1) can be rewritten as follows:

$$I_{o1} = L[i_{o1}] = -\frac{sV_o - sV_i - V_{cm}}{\Omega[1 + (s/\Omega)^2]} \tag{4-2}$$

where $V_o=L[v_o]$, $V_i=L[v_i]$ and $-V_{cm}=v_c(0)$ is the initial condition for the series capacitor C_S, i.e., its voltage at $t = 0$. Assuming

$$v_o = V_{om}\sin(t + \alpha) \tag{4-3}$$

$$L[v_o] = V_o = V_{om}\frac{s \cdot \sin\alpha + \cos\alpha}{1 + s^2} \tag{4-4}$$

$$L[v_i] = V_i = \frac{v_i}{s} \tag{4-5}$$

and substituting eq. (4-4) and (4-5) into (4-2) and calculating its inverse Laplace transform. the result is for $\Omega \neq 1$

$$i_{o1} = -V_{om}D_1 \cos(t+\alpha) + V_{om}D_1[\cos\alpha\cos\Omega t - \Omega\sin\alpha\sin\Omega t] - (v_i + V_{cm})\sin\Omega t \tag{4-6.1}$$

and for $\Omega = 1$

$$i_{o1} = -0.5V_{om}[\sin\alpha\sin t + t\sin(t+\alpha)] - (v_i + V_{cm})\sin t \tag{4-6.2}$$

where

$$D_1 = \frac{\Omega}{\Omega^2 - 1} \tag{4-7}$$

The current i_{o1} decays to zero at extinction angle α_e:

$$i_{o1}(\alpha_e) = 0 \tag{4-8}$$

The voltage change across capacitor C_S produced by the total i_{o1} current pulse is

$$2V_{cm} = \Omega \int_0^{\alpha_e} i_{o1}\,dt \tag{4-9}$$

The average value of the input power

$$P_i = \frac{1}{\pi} \int_0^{\alpha_e} v_i i_{o1}\,dt \tag{4-10}$$

From the last two equations for lossless inverter the average value of the output power

$$P_o = P_i = \frac{2}{\pi}\frac{v_i V_{cm}}{\Omega} \tag{4-11}$$

By giving α, v_i and P_o and knowing Ω, the value V_{cm} and α_e can be calculated from (4-11) and (4-6) observing (4-8). The equations were solved iteratively by computer programs in order to provide the steady-state values of the variables.

α_e versus α with parameter P_o are plotted in Fig. 4-5 and Fig. 4-6 for $\Omega = \omega_S/\omega_P = 1$ and $\Omega = 1.5$, respectively. α_e is the current conduction angle in a subinverter, α is the firing angle of a thyristor (Fig. 4-7 and Fig. 4-8) and P_o is the average output power [eq. (4-11)]. Remember that per unit system is used. Beside the curves $V_{cm} = v_i$ and $V_{cm} = V_{om} + v_i = 1 + v_i$, two other so-called limit curves plotted in Fig. 4-5, Fig. 4-6, Fig. 4-9 and Fig. 4-10 too, have to be mentioned. They are denoted by α_{e2} and α_{e3}. Along curves α_{e2} and α_{e3} the current pulse i_{o1} has two (Fig. 4-7) and three (Fig. 4-8) extreme values, one maximum and one minimum (Fig. 4-7) and two maximum and one minimum (Fig. 4-8), respectively.

Assuming small output power P_o, e.g. $P_o = 0.02$ and increasing α from negative value up to $\alpha \cong 35^\circ$, the curve $P_o = 0.02$ reaches the limit curve α_{e2} (Fig. 4-5). The current pulse i_{o1} extincts at $\alpha_e = \alpha_{e2}$ with zero derivative, $di_{o1}/dt = 0$, in a similar way as in Fig. 4-7. Increasing α further by $d\alpha$, a second current pulse develops in time $\omega t > \alpha_{e2}$ like in Fig. 4-8 and the extinction angle jumps from $\alpha \cong 80^\circ$ up to $\alpha \cong 280^\circ$. Decreasing now α along curve $P_o = 0.02$, the curve reaches the limit curve α_{e3} around $\alpha \cong 0^\circ$ where the current pulse touches the time axis with zero derivative at $\omega t = \alpha_{ee}$ in a similar way as in Fig. 4-8. The current pulse has two maximum and one minimum value. Decreasing α further by $d\alpha$ the second current pulse is lost and α_e jumps back around $\alpha_e \cong 65^\circ$ (Fig. 4-5). Keeping P_o = const., a hysteresis loop develops in the function $\alpha_e(\alpha)$. The width of this hysteresis loop along axis α is getting smaller as the value P_o is increased (Fig. 4-5, Fig. 4-10). It can be shown that the width of the hysteresis loop becomes zero at $\alpha = 1.22$, $P_o = 0.275$ (Fig. 4-10). Increasing further the value P_o above $P_o = 0.275$, the curves P_o = const. reach the limit curve α_{e2} in the smaller α_e region at smaller α value than they meet the limit curve α_{e3} in the higher α_e region (Fig. 4-9 and Fig. 4-10). As an example the current pulse i_{o1} belonging to point 21 at limit curve α_{e2} (Fig. 4-9) is shown in Fig. 4-7 and the other current pulse i_{o1} belonging to point 22 at limit curve α_{e3} (Fig. 4-9) is shown in Fig. 4-8. The output power $P_o = 0.7$ in both cases.

One of the most interesting results is that by using the approximate model described no steady-state solution can be found for the current pulse and other variables e.g. between points 21 and 22 in Fig. 4-9. The laboratory tests verified this theoretical conclusion.

Similar phenomena can be observed at other Ω frequency ratios (Fig. 4-6).

The most serious problem in the design of time-sharing inverter is the severe peak stress of power devices. Although the detailed design considerations are out of the scope of this study, three of the most significant numerical results are presented. The positive peak voltage stress of the controlled switches V_{Tm+}, the peak voltage of the series capacitors V_{cm} and the input voltage v_i are shown in Fig. 4-11, Fig. 4-12 and Fig. 4-13 in various operation conditions, respectively. It can be concluded that the firing angle α has to be around zero or in the negative region near zero. The peak value of the controlled switched voltage V_{Tm+} and that of the capacitor voltage V_{cm} can be kept at resonable level by selecting the suitable value of the rated output power P_o. Furthermore, the input voltage v_i is maintained around its maximum value in order to reduce the input current [116].

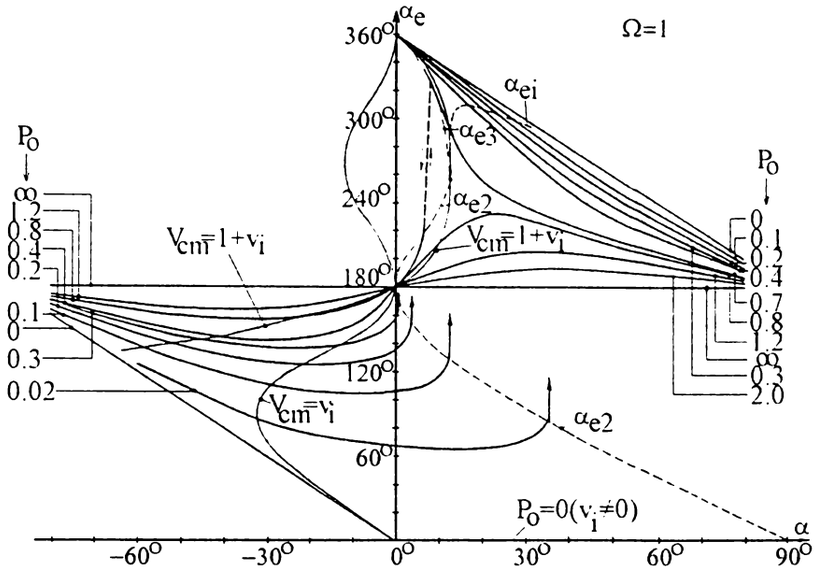

Figure 4-5 Current conduction angle α_e vs. firing angle α for Ω = 1

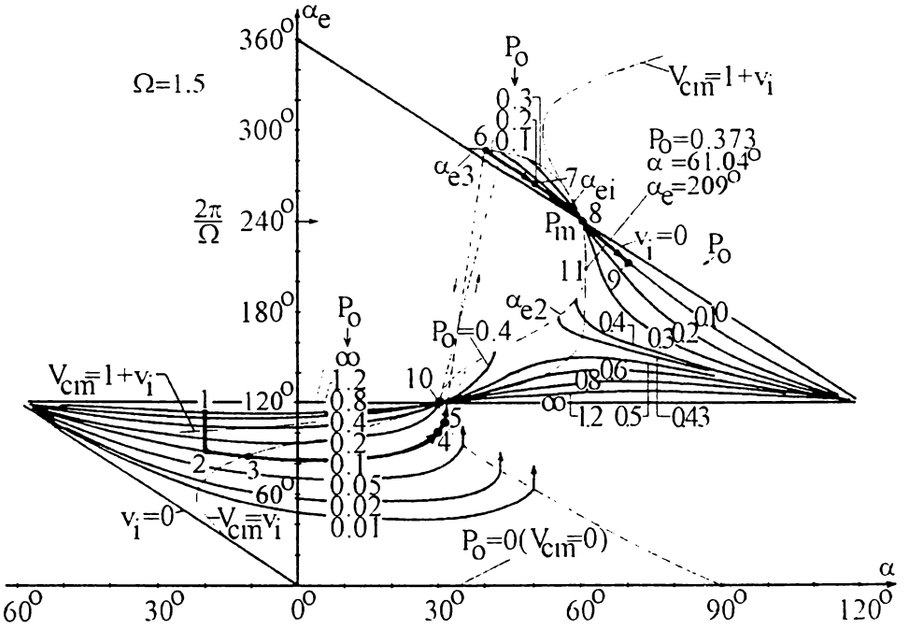

Figure 4-6 Current conduction angle α_e vs. firing angle α for Ω = 1.5

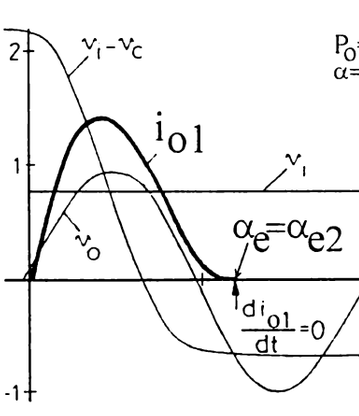

Figure 4-7 Time functions at point 21 in Fig. 4-9

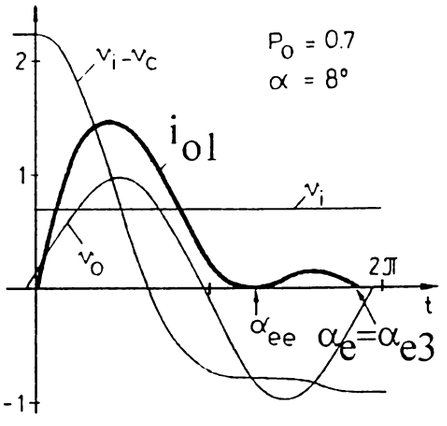

Figure 4-8 Time functions at point 22 in Fig. 4-9

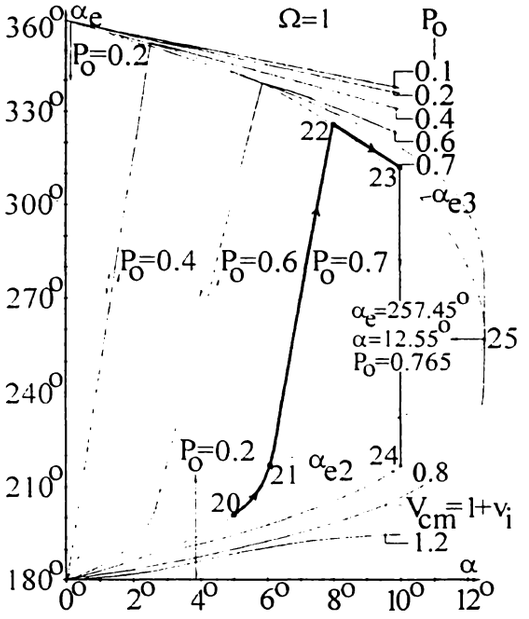

Figure 4-9 Enlarged $\alpha_e(\alpha)$ characteristics

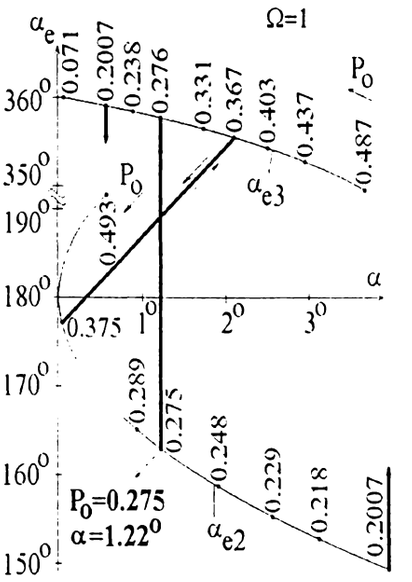

Figure 4-10 Enlarged α_{e2} and α_{e3} limit curves

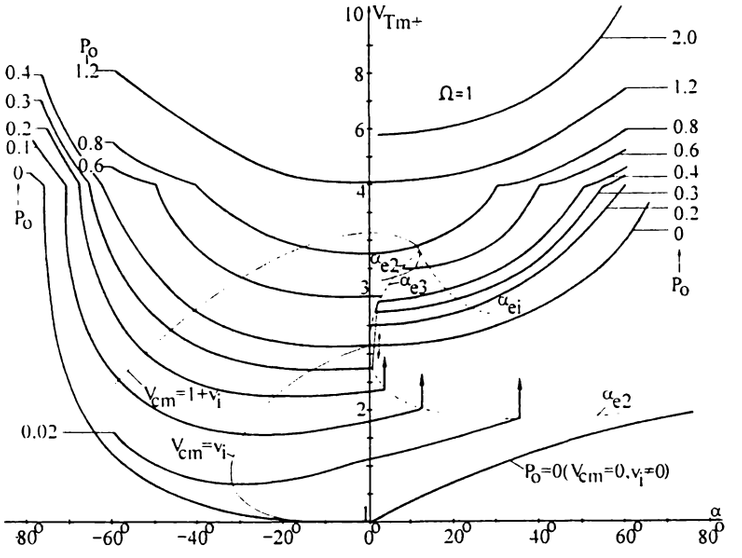

Figure 4-11 Positive peak voltage stress of the controlled switches V_{Tm+} vs. firing angle α

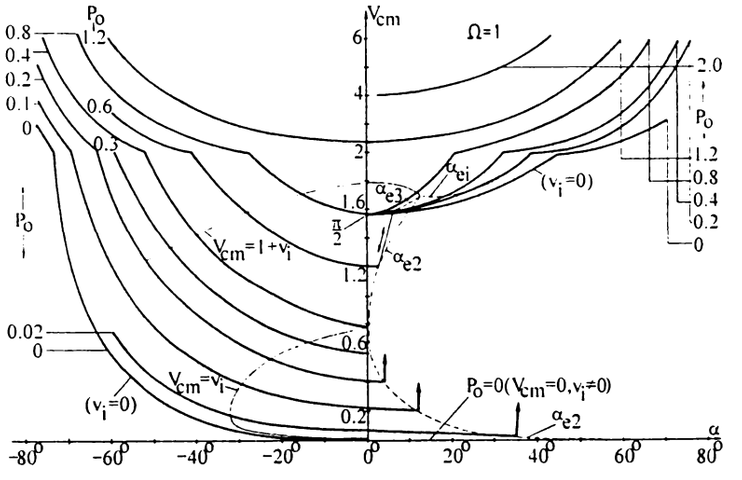

Figure 4-12 Peak voltage of the series capacitors V_{cm} vs. firing angle α

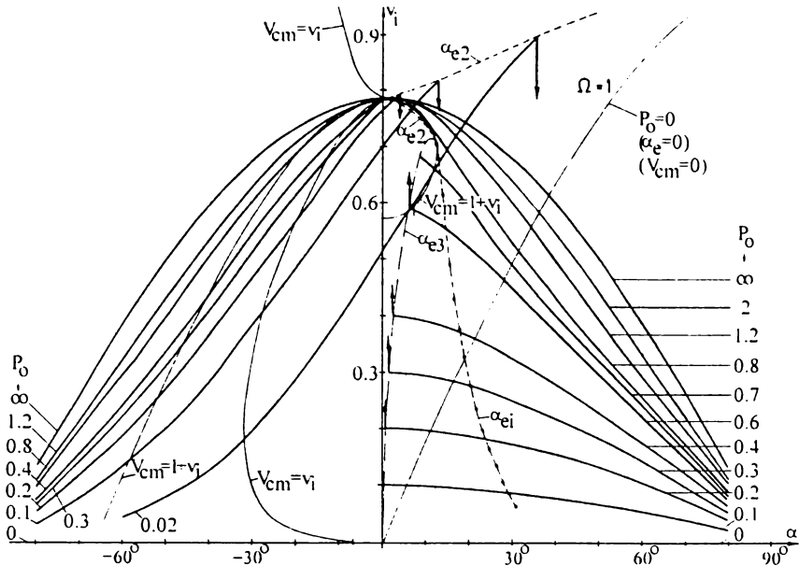

Figure 4-13 Input voltage v_i vs. firing angle α

4-5-1-2 ACCURATE ANALYSIS

To elucidate the phenomena in the region of firing angle $\alpha_2(\alpha_{e2}) \le \alpha \le \alpha_3(\alpha_{e3})$ discovered by the approximate analysis in the previous section a more accurate model in which the load is substituted by $C_p - L_p - R_p$ connected in parallel must be used for the inverter. The subinverters operate no longer independently of each other. The independent energy storage elements are: six L_s series inductances, three C_s series capacitances, one L_p inductance and one C_p capacitance, altogether eleven elements, with eleven state variables (eleven time constants) [116].

The accurate analysis was performed by simulation in MATLAB environment, using Simulink models for the calculation of the state variables of the nonlinear system. The developed Simulink models are drawn in Appendix F. The numerical values of the parameters and variables used in the study presented in this chapter are listed in Appendix G.

There is a great amount of information obtained by simulation describing the complex behavior. One of the most useful ways for the presentation of the results is the bifurcation diagram, defined in subsection 2-4-1-2. The bifurcation diagram shows the various states and the sudden changes or bifurcations of the system in steady state as a result of the variations of one system parameter.

To generate this kind of diagram, the peak values of the output voltage V_{om} were sampled, stored and plotted as a function of the control parameter T_o, where T_o is the period between two consecutive firing pulses in the positive or in the negative subinverters

(Fig. 4-2, Fig. 4-14). The system has been restarted from zero initial condition for each point of the bifurcation diagram in Fig. 4-15.

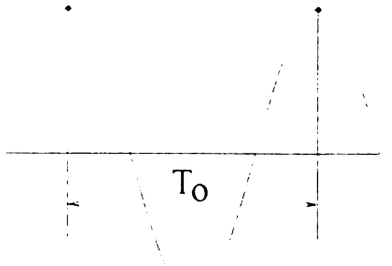

T_o = period of firing pulses =
= sampling period of v_o

Figure 4-14 Construction of bifurcation diagram

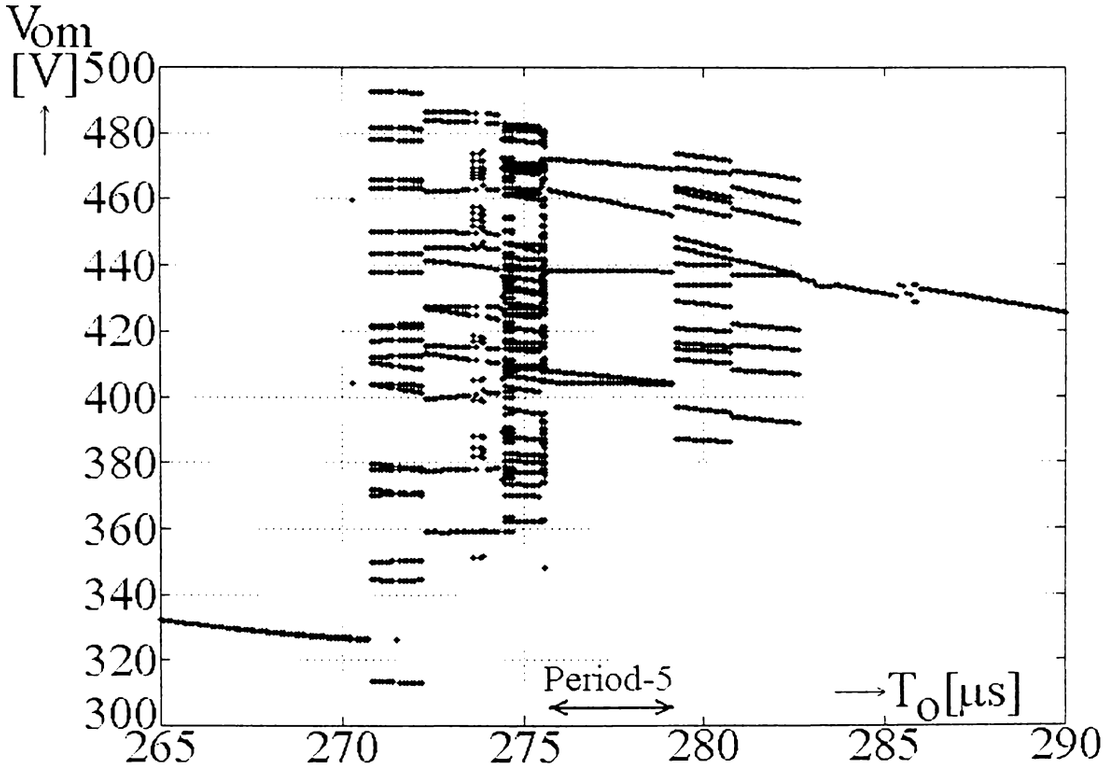

Figure 4-15 Bifurcation diagram (R_p = 0.8Ω; zero initial condition)

Having just one single value V_{om} for a given T_o, the output voltage v_o repeats itself in each period T_o. This is the period-1 state. The frequency of v_c and v_{T1} of subinverter variables is one third of the frequency of the output voltage v_o (Fig. 4-2). Similarly, state "period-5" is developed for example at firing period T_o = 277μsec. Now there are five consecutive distinct V_{om} values. v_o is still periodic, it repeats itself after $5T_o$ elapses (Fig. 4-16). The period of the variables – e.g. current i_{o1} – in the subinverters is $3T_5 = 15T_o$ in period-5 (Fig. 4-16). The same frequency division occurs in subharmonic states among the frequencies of the output variables and those of the subinverter variables as in normal operation.

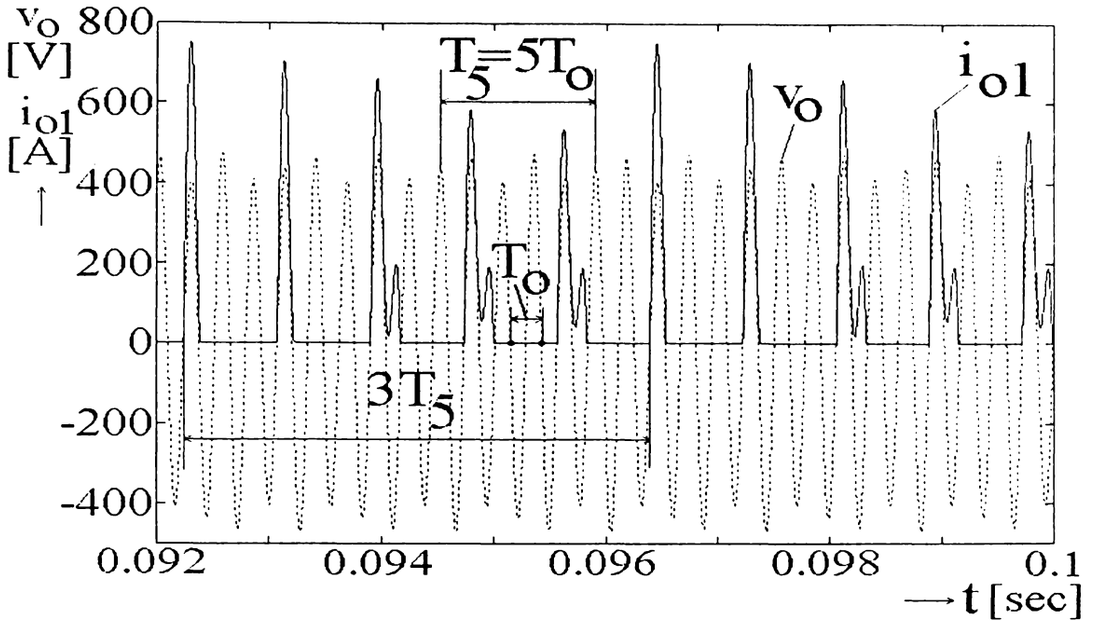

Figure 4-16 Time functions for $v_o(t)$ and $i_{o1}(t)$ at T_o = 277 μs in period-5 state

One of the subinverter current i_{o1} with short and long conduction angle α_e is shown also in Fig. 4-16. The current has either one or three extreme values (see Fig. 4-7 and Fig. 4-8 too).

The peak value V_{om} is changing between 400-470V at T_o = 277μs. Taking the average value 435V, the output power P_o = 0.58p.u.

Regions period-9, period-16 etc. can also be distinguished in the bifurcation diagram. Consequently the inverter generates subharmonic 5^{th}, 9^{th}, 16^{th} etc. as the firing period T_o is varied.

All states have been calculated from the previous neighboring state for the bifurcation diagrams in Fig. 4-17, Fig. 4-18 and Fig. 4-19 instead of starting the system from zero initial condition. The calculation proceeded in both directions, as it can be seen in the figures, where the calculation proceeded from left to right in Fig. 4-17 and from right to left in Fig. 4-18. The superposition of Fig. 4-17 and 4-18 is shown in Fig. 4-19.

Increasing R_p the subharmonic range shrinks (Fig. 4-20) and finally it disappears (Fig. 4-21). The system has been restarted from zero initial condition in the simulations in Fig. 4-20 and Fig. 4-21.

In Fig. 4-22 all states have been calculated from the previous neighboring state, for R_p = 2.4 Ω and the bifurcation diagram with curve *a* was obtained. The calculation proceeded from left to right in the lower curve *a* and from right to left in the upper curve *a*. The subharmonic range disappeared but a hysteresis loop was developed similarly to Fig.

4-10 where the hysteresis loop can be observed at $P_o < 0.276$. Again using $V_{om} = 435$V, the output power for the lower part of the diagram is $P_o = 0.19$ p.u.

Reducing R_p at 0.4 Ω, curve *b* in Fig. 4-22 was obtained. Calculating with V_{om} = 350V, the output power P_o = 1.34 p.u. Smooth curve and regular, periodic operation was found similarly to the result produced by using the approximate model. Both the subharmonic range and the hysteresis loop disappear. Zero initial conditions were used in the calculation of each point of curve *b*.

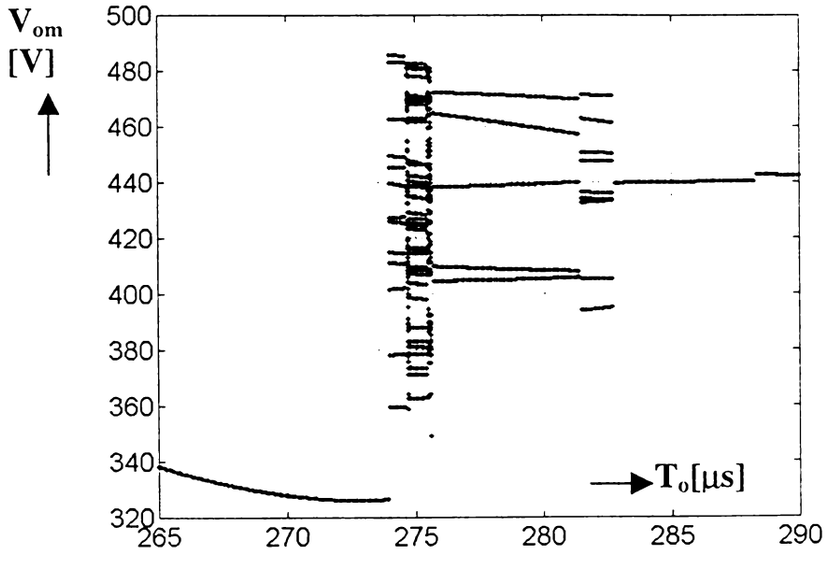

Figure 4-17 Bifurcation diagram (R_p = 0.8Ω; increasing T_o with previous neighboring state as initial condition)

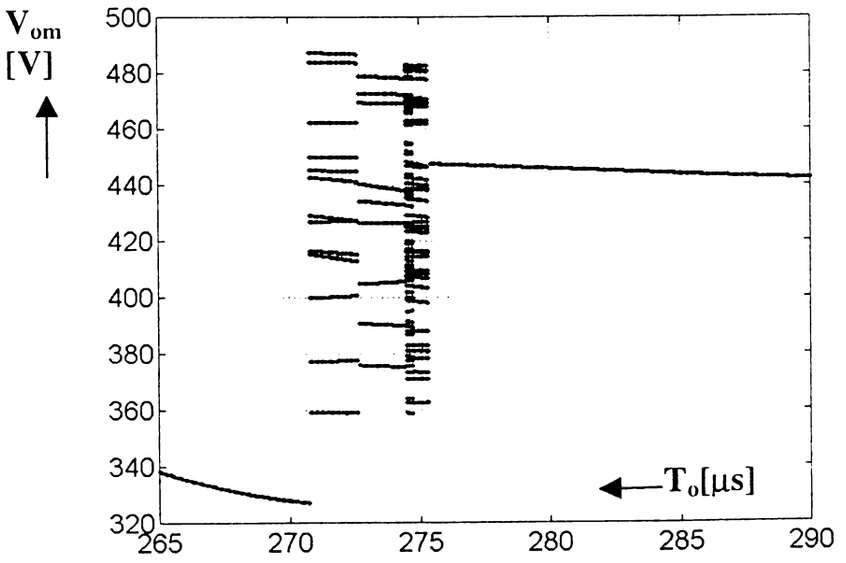

Figure 4-18 Bifurcation diagram (R_p = 0.8Ω; decreasing T_o with previous neighboring state as initial condition)

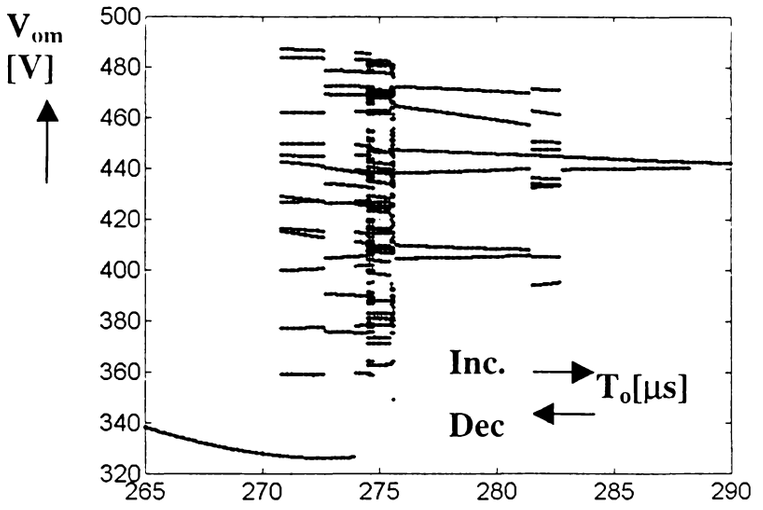

Figure 4-19 Bifurcation diagram (R_p = 0.8Ω; T_o varied in both directions, with previous neighboring state as initial condition)

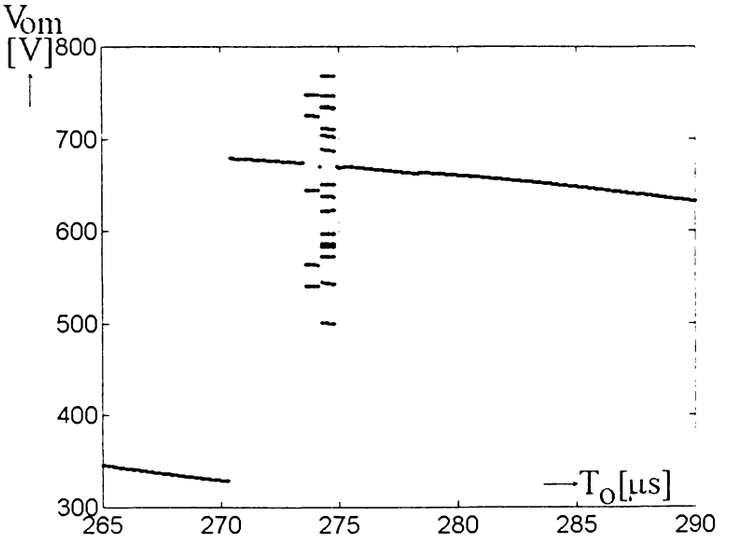

Figure 4-20 Bifurcation diagram (R_p = 1.2Ω; zero initial condition)

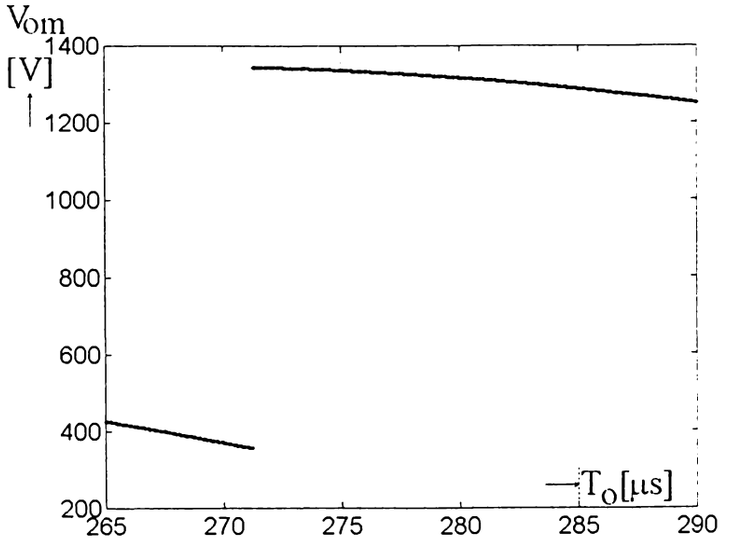

Figure 4-21 Bifurcation diagram (R_p = 2.4Ω; zero initial condition)

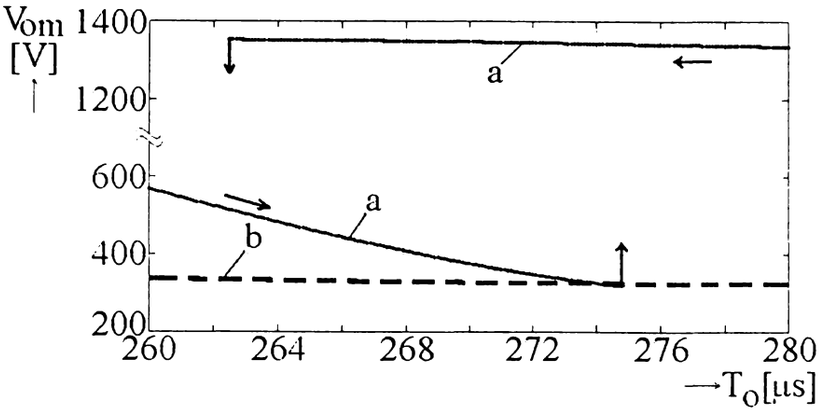

Figure 4-22 Bifurcation diagram (previous neighboring state as initial condition; R_p = 2.4Ω for curve *a*; R_p = 0.4Ω for curve *b*)

4-5-2 ANALYSIS IN FREQUENCY DOMAIN

The output voltage of the inverter is a periodic signal in each state in Fig. 4-15. Fourier spectra in period-5 at T_o = 277μs and in period-9 at T_o = 282μs are shown in Fig. 4-23 and in Fig. 4-24, respectively.

As a first approximation the output voltage in period-5 and in period-9 is an amplitude modulated signal in which the carrier frequencies are f_5 and f_9 and the modulating frequencies are f_2 and f_4, respectively, where $f_2 = f_0 / 2$ and $f_4 = f_0 / 4$. T_5 and T_9 are the periods in the fifth and in the ninth subharmonic state, respectively.

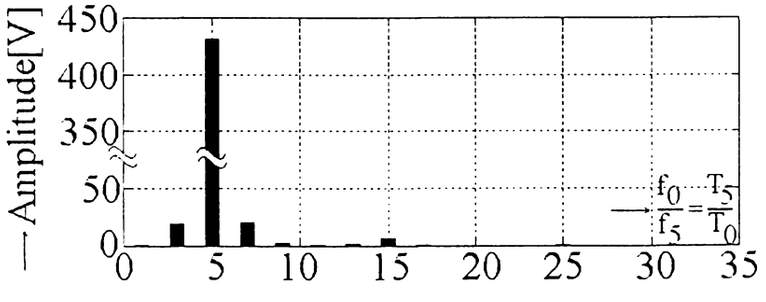

Figure 4-23 Fourier spectrum for output voltage in state period-5

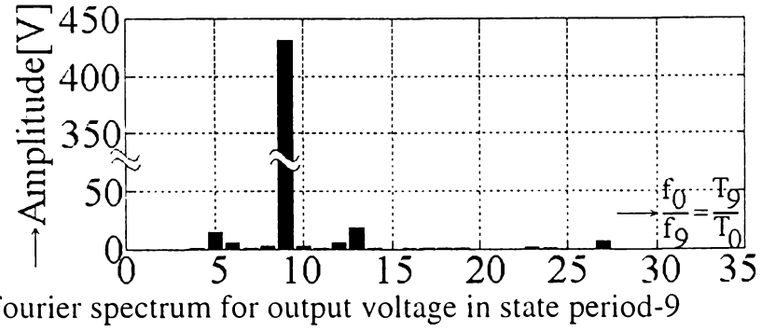

Figure 4-24 Fourier spectrum for output voltage in state period-9

4-5-3 ANALYSIS IN STATE SPACE

By plotting the first time derivative of the output voltage as a function of v_o the limit cycle is obtained in the state-plane. The trajectory is depicted for period-1, at T_o = 300μsec, starting at $dv_o / dt = 0$ and $v_o = 0$, in Fig. 4-25. It can clearly be seen how the state trajectory reaches the periodic orbit depicted in Fig. 4-26. Another limit cycles are shown in Fig. 4-27 and Fig. 4-28 for period-5 and period-9, respectively.

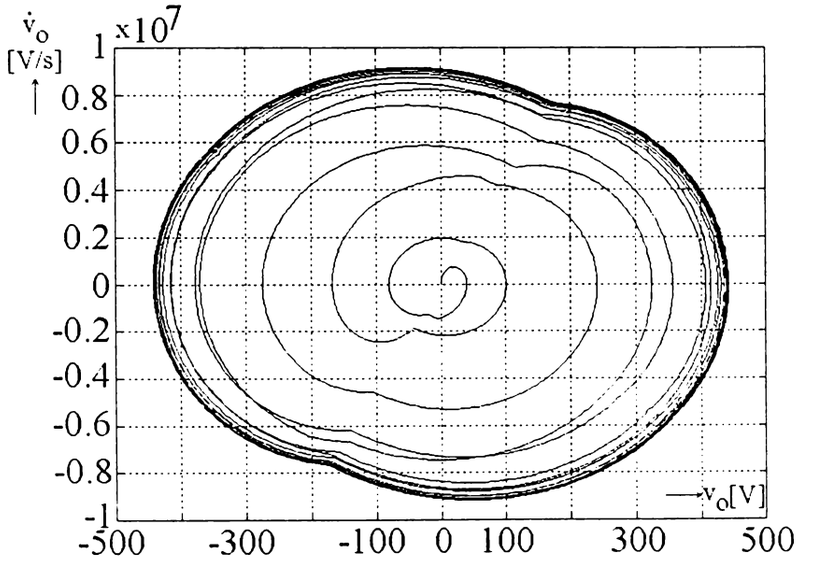

Figure 4-25 State-space trajectory with transient for period-1 behavior

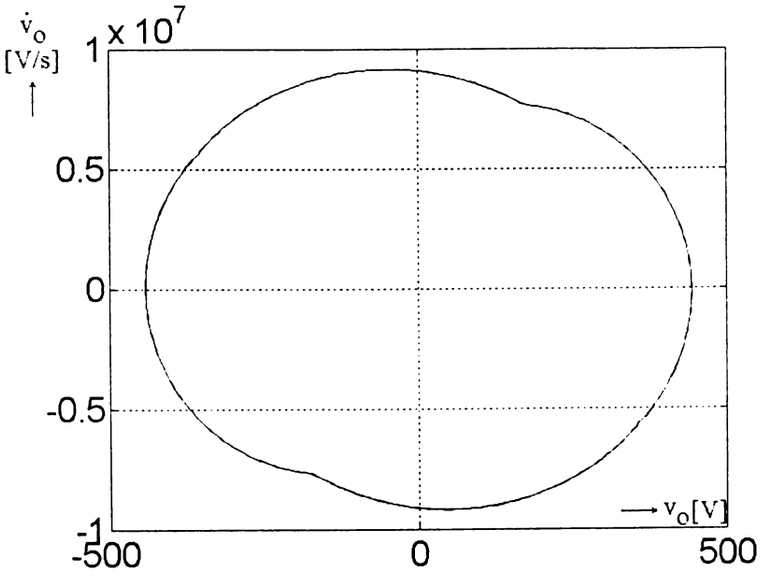

Figure 4-26 Limit cycle for period-1 behavior

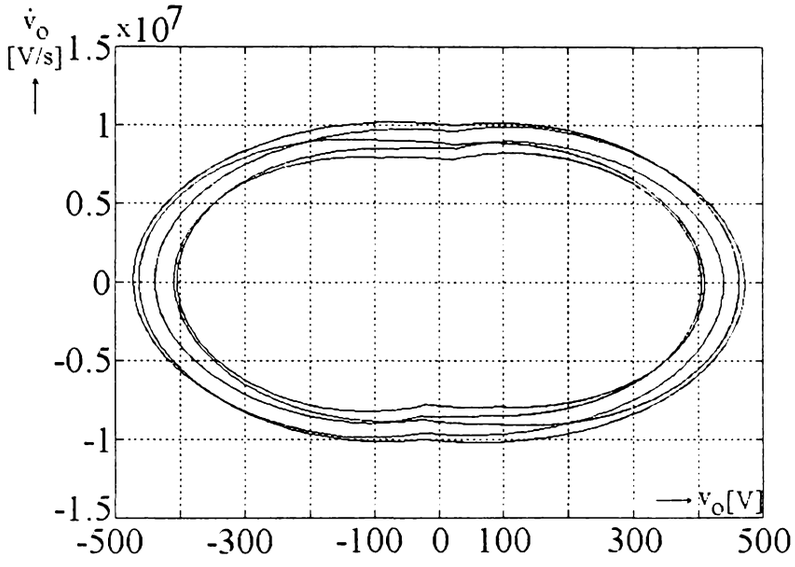

Figure 4-27 Limit cycle for period-5 behavior

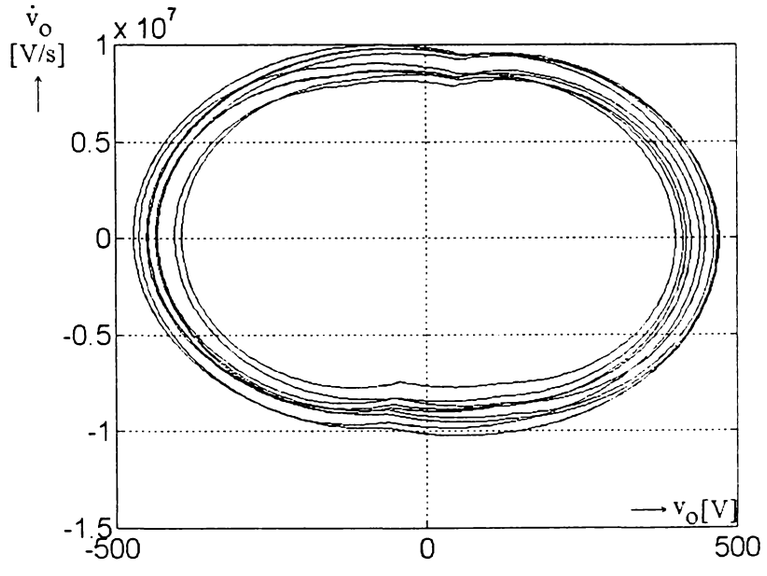

Figure 4-28 Limit cycle for period-9 behavior

4-6 STEADY-STATE ANALYSIS OF FEEDBACK CONTROL LOOP

A self-control structure is obtained by applying a feedback control loop. Now the approximately sinusoidal output voltage v_o is compared with a DC control voltage and the thyristors are alternatively fired at the crossing points of the two curves (Fig. 4-29) [115].

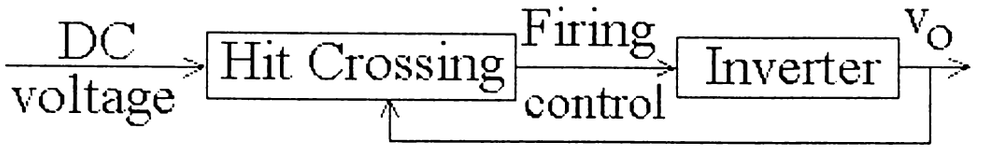

Figure 4-29 Feedback control loop for the inverter

The study is concerned with the effect of the variation of the DC control voltage level on the behavior of the feedback-controlled inverter. The analysis was performed by simulation in MATLAB environment, using the same accurate Simulink model of the inverter and the same parameters specified in Appendices F and G, respectively.

Again the bifurcation diagram is used for the presentation of the results. The peak values of the output voltage V_{om} were sampled (Fig. 4-14), stored and plotted as a function of the control parameter V_{DC}, where V_{DC} is the DC voltage which comparison with the inverter output voltage V_o determines the thyristors firing instants. The operation of the controlled system was started from the open loop inverter steady-state for each point of the bifurcation diagram in Fig. 4-30.

The results are basically similar to those obtained for open loop control. As in the previous study, the feedback-controlled inverter generates subharmonic as the DC voltage level is varied. The peak value V_{om} is changing between 320-480V. Taking approximately V_{om} = 400V, the subharmonic range $-15V < V_{DC} < 54V$ corresponds to a firing angle range $2.25^0 < \alpha < 8.1^0$. Comparing this firing angle range to the range $0^0 < \alpha < 12^0$ obtained on the basis of approximate analysis and plotted in Fig. 4-5, the deviation between the results originating from the approximate and accurate analysis is marginal. For the bifurcation diagram in Fig. 4-31 all states have been calculated from the previous neighboring state instead of starting the system from the open loop inverter steady-state and similar results were obtained.

CONTROL OF INVERTER BY TIME-DELAY AUTOSYNCHRONIZATION

It was already highlighted through the previous chapter that power electronic system controls should be designed for the required stable operation. In particular, for the high frequency time-sharing inverter introduced in this chapter, the use of a feedback control

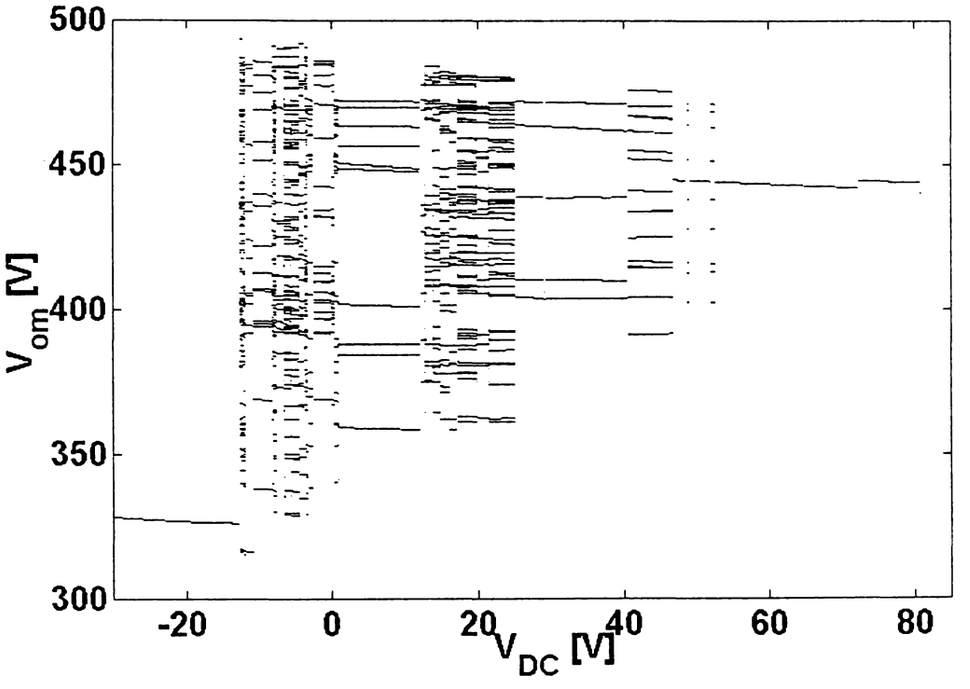

Figure 4-30 Bifurcation diagram of feedback control loop behavior (initial condition = steady-state of open loop inverter)

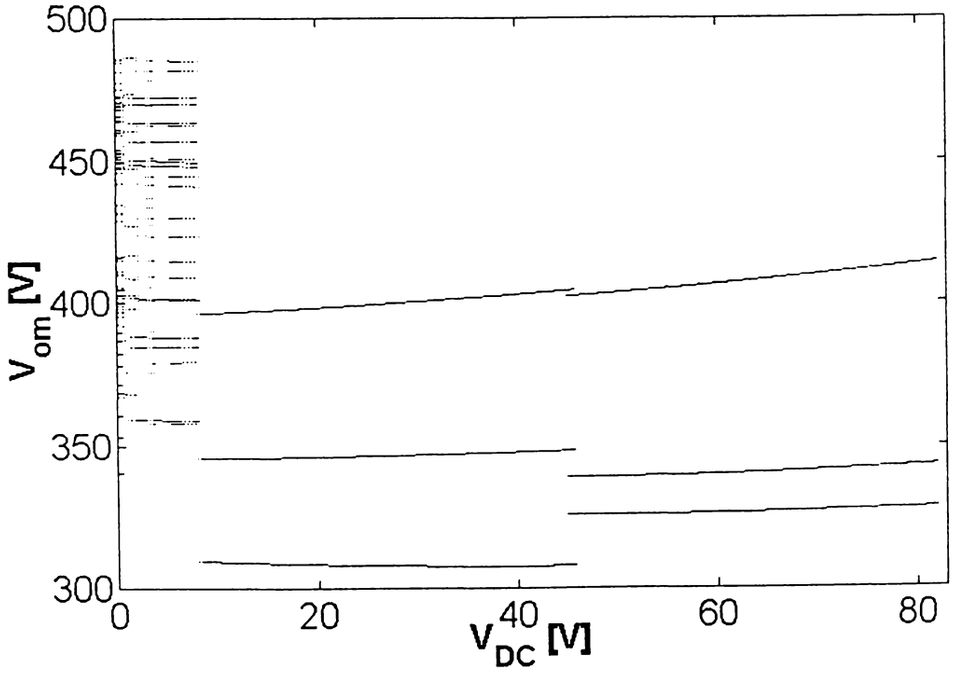

Figure 4-31 Bifurcation diagram of feedback control loop behavior (DC varied in both directions, with previous neighboring state as initial condition)

must guarantee stable period-1 operation and the subharmonic operation detected in the previous section is considered undesirable and should be avoided. Four distinct general control strategies were introduced in the previous chapter to this end. One of them, namely the *time-delay autosynchronization*, is used to remove the subharmonic regimes from the operation of the previously introduced feedback control loop (Fig. 4-29). The control by time-delay autosynchronization was defined and applied in section 3-5. Accordingly, the scheme of the proposed time-delay autosynchronization is drawn in Fig. 4-32. The control voltage whose crossings with the output voltage v_o of the inverter determines the firing of the thyristors, is obtained now by adding to the DC voltage a term proportional to the difference between the present output voltage $v_o(t)$ and its past value $v_o(t-T_o)$:

$$v_{TDAS}(t)=\eta\cdot[v_o(t)-v_o(t-T_o)] \tag{4-12}$$

where η is a dimensionless feedback gain and the resonant period of the oscillatory circuits T_o corresponds to the period of the desired stable period-1 operation.

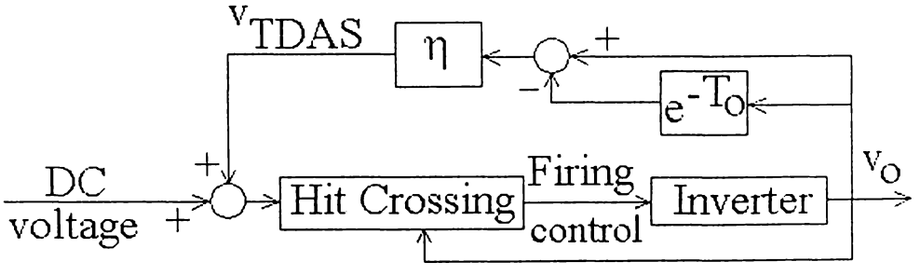

Figure 4-32 Block diagram of the feedback control loop with time-delay autosynchronization

Fig. 4-33 shows the result of a computer simulation for a DC voltage of 35 V, which corresponds to a period-5 behavior of the control loop without time-delay autosynchronization (Fig. 4-30) and for the time-delay autosynchronization turned on after 100 cycles of the output voltage (about 29msec), with gain η = -100. It can be clearly seen the collapse of the subharmonic state to the stabilized period-1 operation.

4-8 TEST RESULTS

The oscilloscope traces of the output voltage v_o, the series condenser voltages v_{c1}, v_{c3}, v_{c5} and the thyristor voltages v_{T1}, $-v_{T2}$ are shown in Fig. 4-34 and Fig. 4-35. The shapes of the time functions in Fig. 4-2 are in good agreement with the measurements and they verify the

relevant theoretical considerations. Due to the time sharing operation the turn-off time measured is a little bit longer than two half periods. The output frequency is 3.57kHz.

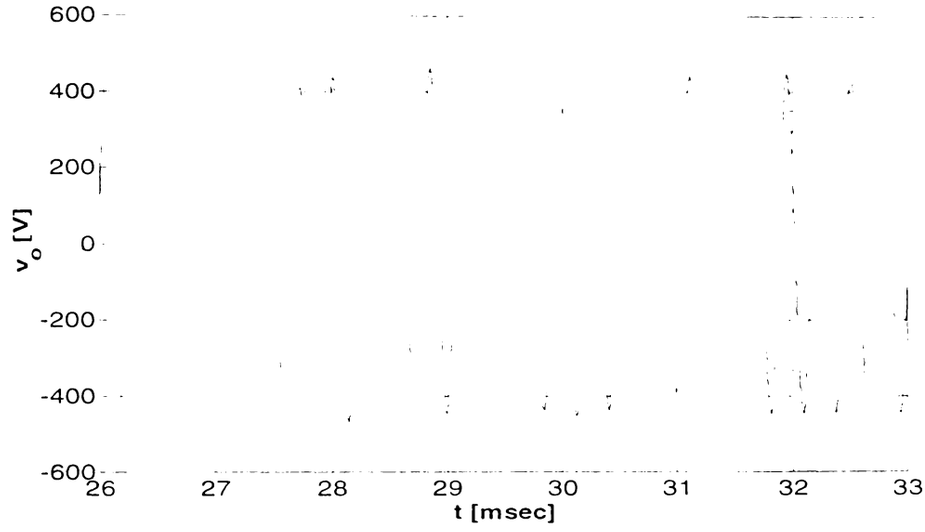

Figure 4-33 Inverter response with time-delay autosynchronization initiated after 100 cycles of the output voltage

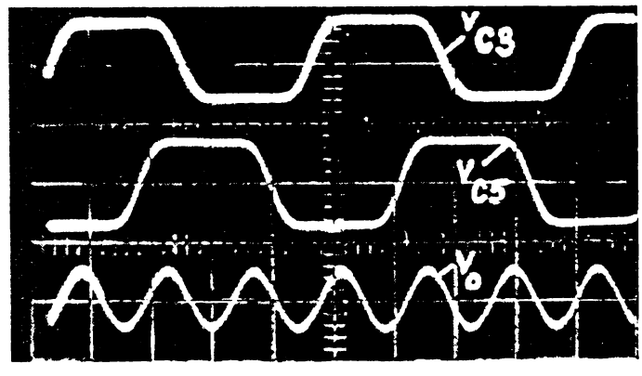

Figure 4-34 Oscilloscope traces of the output voltage v_o (V_{om}=200Vp.-p.) and the series condensers voltages v_{c3}, v_{c5} (V_{cm}=280Vp.-p.).
Time scale: 200μs/div, voltage scale: 200V/div.

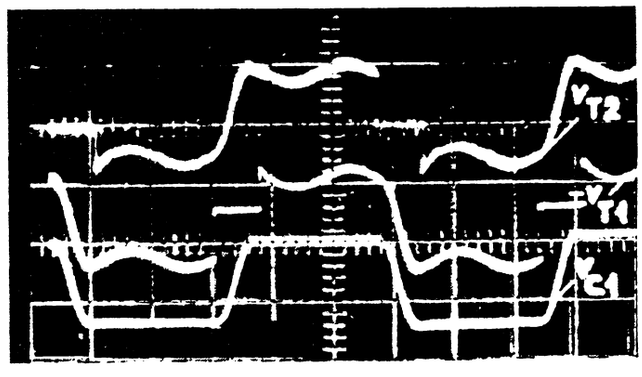

Figure 4-35 Oscilloscope traces of the series condenser voltage v_{c1} (V_{cm}=280Vp.-p.) and the thyristor voltages v_{T1}, $-v_{T2}$ (Turn-off time=440μs).
Time scale: 200μs/div, voltage scale: 200V/div.

CHAPTER 5

CONCLUSIONS AND ORIGINAL CONTRIBUTIONS

A summary and conclusions of the study reported in this Ph.D. dissertation are presented (section 5-1), followed by the enumeration of the original contributions (section 5-2) and further research topics (section 5-3).

5-1 GENERAL CONCLUSIONS

The main purpose of the present Ph.D. thesis was to offer a systemic approach for applying the investigation methods peculiar to the theory of nonlinear dynamics and chaos in the design and analysis of control systems for power electronics. The first introductory chapter justified the actuality of the research. Chaos begins where classical science ends since until recently chaos and order have been viewed as mutually exclusive. Because much of the study of dynamical systems is propelled by the necessity of predicting future states of systems, this predictable world of order was challenged by the unexpected discovery that simple deterministic systems can turn chaotic. Although certainly encountered by scientists many times in the last century and dismissed as physical noise, chaos was "discovered" as dynamics starting from very close initial conditions but diverging fast and leading to entirely different future states. This sensitive dependence on initial conditions in chaotic systems renders predictions impossible beyond a short-time frame since initial conditions cannot be measured or specified with infinite accuracy. Although admitted as being still young, "deterministic chaos" is now a very active field of research with many exciting results in almost every scientific discipline, mostly triggered by the studies of nonlinear systems using high-speed computers. In power electronics chaos has even been "rediscovered" after more than 50 years. All power electronic controls are nonlinear in the most general sense. Since control is implemented with switches and the switch action can occur at arbitrary times, the controls must take state, reference and input information and translate it into timing. Even though the underlying action is truly nonlinear, it is

conventional in many situations to use a linear framework for power electronics but it was shown that there are fundamental drawbacks to the use of averaging processes in predicting and investigating nonlinear effects such chaos, quasiperiodicity and subharmonics. A shift from linear systems thinking toward the unfamiliar realm of nonlinear dynamics is needed and was tried by power electronics engineers over the past twenty years.

The second chapter illustrates the application of the above-mentioned aspects by a feedback controlled resonant DC-DC converter. The investigated converter represents the buck member of a family of dual channel resonant DC-DC converters, with twelve distinct configurations. The common basic configuration contains two channels which transmit the power from input to output and are coupled by a resonating capacitor. The converters are recommended to be applied in the middle and higher power ranges. The study is restricted to the buck configuration in symmetrical operation, when the respective variables in the two channels vary symmetrically (without any energy exchange between channels). The converter has five energy storage components and its output voltage is controlled by a feedback loop. The controlled switches are turned on and off by a PWM pattern using a ramp function of constant frequency. The nonlinearity of the control system is due to the dependence of the turn-on time of the controlled switches on a system state variable. The feedback-controlled converter exhibits rather strange behavior, detected by simulations. Tools and concepts of the theory of nonlinear dynamics such as Poincaré maps and bifurcation diagrams are introduced and used to identify the interesting bifurcation phenomena developing in the course of changing the control gain. As a result of the switching train the controlled converter can be in periodic, quasiperiodic, subharmonic and chaotic state. The chaotic operation can be reached by quasiperiodicity, period-doubling and intermittency scenarios. Simulation results of this behavior with an emphasis on the main features of chaotic dynamics are presented in form of time functions, state-space trajectories, power spectra, Poincaré maps and bifurcation diagrams. Two methods are proposed for the confirmation of the bifurcation behavior by stability analysis. In the first method the characteristic multipliers of the Jacobian matrix of the Poincaré map function evaluated at the fixed point of the limit cycle located in the Poincaré hyperplane were determined. The stability is lost when one or more characteristic multipliers leave the interior of the unit circle. The second method for stability analysis employs the Rácz method and leads to the same results: the stability of the limit cycle describing the

operation of the converter is lost by increasing the control gain and a quasiperiodic state develops by Naimark-Sacker bifurcation.

In the third chapter several control strategies are proposed and analyzed in order to avoid the unstable regimes of the behavior of the converter (with an emphasis on chaotic dynamics) and to ensure the stable periodic state required by applications over the entire operating range. Four control methods are proposed to this end, as follows: linear compensation, fuzzy control, control of chaos using the *OGY* technique and time-delay autosynchronization. The first two strategies are inspired from the area of control engineering and achieve the control objectives by the insertion of feedback controllers into the configuration. The first method uses a series linear compensation whose parameters are tuned by using the stability analysis. The linear controller can be extended with nonlinear dynamics for improving the transient response. The second method employs a fuzzy controller extended with dynamic modules. The pseudo-fuzzy features of the correspondent conventional control are used to tune the parameters of the fuzzy inference system. The last two control strategies try to benefit from the feature that a chaotic attractor consists from an infinite number of unstable periodic trajectories. The Ott-Yorke-Grebogi algorithm is used by the third method to achieve a discrete-time control by time- and state-dependent small perturbations of an accessible system parameter. The algorithm exploits the fact that, during its wandering within the strange attractor, the system will eventually come near the target periodic trajectory on a given Poincaré section. When this happens, and only then, a small perturbation is applied to the parameter so as to make the next Poincaré intersection land on the stable manifold of the target saddle fixed point. The fourth control method applies the time-delay autosynchronization and involves a control signal formed with the difference between the current state of the system and the state of the system delayed by one period of the target periodic trajectory. The experimental setup including the power stage and the converter control implemented on a DSP board is presented and the test results confirmed those obtained by computer simulation.

The fourth chapter applies the already presented methods in investigating a special type of high frequency time-sharing inverter, used mostly in induction heating applications. The circuit uses the principle of time-sharing to enable the circuit turn-off time to be extended over two half-cycles of the output voltage. An approximate and after an accurate model with two and with eleven energy storage components were developed for the description of the strange behavior of the inverter, respectively. The approximate analysis applied simple mathematics and discovered an unstable operation region. The

accurate analysis of this region shown that the inverter generates a number of subharmonic states in the output variables within certain output power and output frequency range. First, reducing the output power, the subharmonic states disappear but a hysteresis loop develops with smaller and higher output voltages within the same output frequency range. Second, increasing the output power results smooth, periodic states in the entire frequency range and neither subharmonics nor hysteresis loop can be detected. Qualitatively both the approximate and the accurate model lead to the same results. The subharmonic frequencies of the subinverter variables are the third of those of the output variables in subharmonic states, i.e., the same frequency division occurs as in regular operation. Frequency spectra and limit cycle trajectories are also presented. The same subharmonic generation was found in the behavior of the inverter furnished by a feedback control loop. The control by time-delay autosynchronization is proposed and investigated in order to avoid the subharmonic generation and to conserve the stable period-1 operation demanded by applications. Laboratory test results support the theory.

5-2 ORIGINAL CONTRIBUTIONS

- Use of methods and ideas peculiar to the theory of nonlinear dynamics and chaos in analyzing two power electronic systems: a resonant DC-DC converter and a high frequency time-sharing inverter.
- Detection of chaotic, quasiperiodic and subharmonic states in the dynamics of the feedback-controlled converter.
- Detection of three routes to chaos in the bifurcation behavior of the feedback-controlled converter: quasiperiodicity, period-doubling and intermittency.
- Two distinct stability analysis methods (using the Poincaré map function and the Rácz method) to analytically confirm the bifurcation behavior.
- Four distinct control strategies for the suppression of the unstable operation, with an emphasis on the chaotic behavior: linear compensation, fuzzy control, control based on OGY technique, time-delay autosynchronization.
- Implementation of the various converter control strategies on a DSP board; test results verifying the theoretical conclusions.
- Two steady-state analysis approaches for the high frequency time-sharing inverter.
- Detection of subharmonic generation in the open loop controlled inverter.

- Detection of subharmonic generation in the feedback-controlled inverter.
- Control by time-delay autosynchronization for suppression of the unstable (subharmonic) operation of the inverter.

5-3 FURTHER RESEARCH TOPICS

- Extension of the study of nonlinear phenomena to the other members of the resonant DC-DC converter family.
- Extension of the stability analysis to the other bifurcations in the behavior of the buck converter.
- Development of new control strategies for stabilizing the chaotic dynamics of the converter.
- Further research regarding the implementation of converter control on the DSP board.
- Development of new control strategies for the high frequency time-sharing inverter.

APPENDICES

APPENDIX A

Parameter and Variable Values Used in Computer Simulations of the Resonant DC-DC Converter

CIRCUIT COMPONENTS	*VALUES*
Switched Capacitor C	25 nF
Inductance L	100 μH
Filter Capacitor $C_p = C_n$	100 μF
Load Resistance $R_p = R_n$	8 Ω
Input DC Voltages $v_{ip} = -v_{in}$	100 V
Reference Output Voltage v_{ref}	50 V
Upper and Lower Voltage Limits of the Sawtooth Waveform $V_U = -V_L$	50 V

APPENDIX B

Simulink Model of the Resonant DC-DC Converter

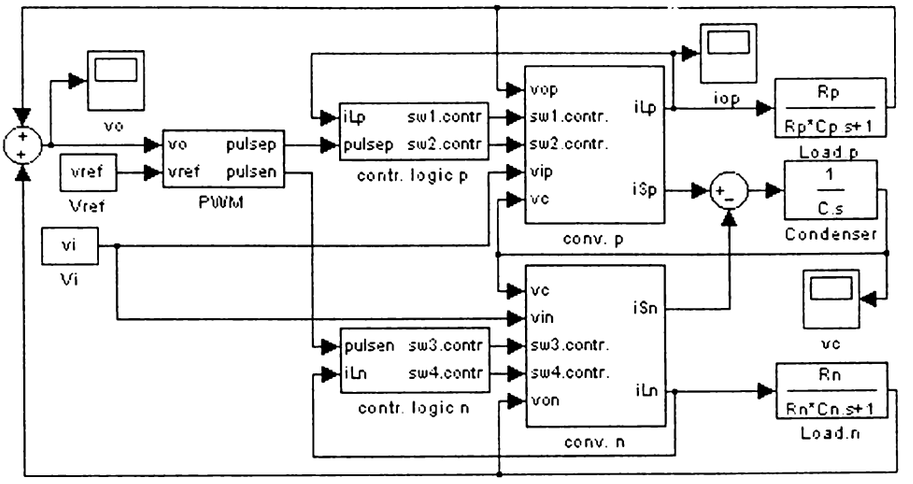

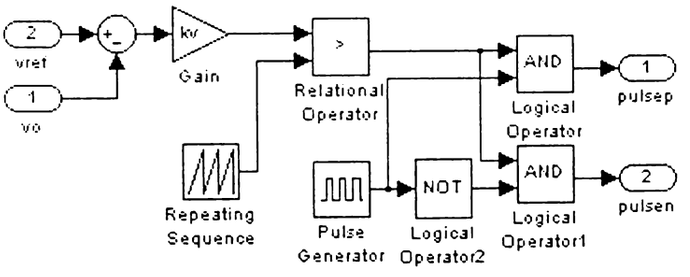

PWM

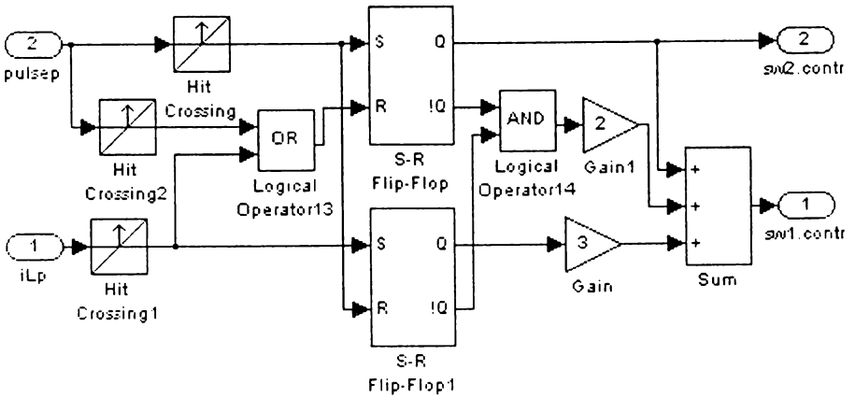

contr. logic p

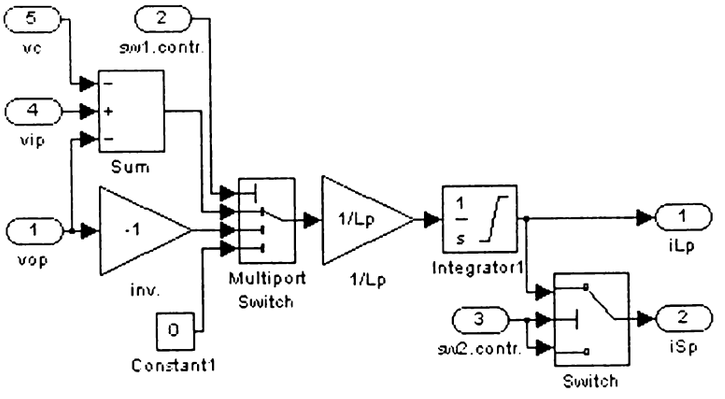

conv. p

APPENDIX C

MATLAB Program for the Stability Analysis of the Resonant DC-DC Converter

```
global vref VU VL vi kv R Co C L Ts A1 B1 xk K
U=[0 1  0 0 0
   1 0  0 0 0
   0 0 -1 0 0
   0 0  0 0 1
   0 0  0 1 0];
Tr=pi*sqrt(L*C);To=R*Co;Tc=R*C;Tl=L/R;a=Tr/To;b=Tr/Tc;c=Tr/Tl;
A1=[-a  0  0 a 0
     0 -a  0 0 a
     0  0  0 b 0
    -c  0 -c 0 0
     0 -c  0 0 0];
B1=[0 0 0 c 0]';
A2=[-a  0 0 a 0
     0 -a 0 0 a
     0  0 0 0 0
    -c  0 0 0 0
     0 -c 0 0 0];
K=[kv*vi kv*vi 0 0 0];
alfa=2*fzero('felalfa',[1e-6 pi/2]);
n=0;
newdr=alfa/pi;
olddr=0;
while abs(newdr-olddr)>1e-2,
   n=n+1;
   olddr=newdr;
   Phi1=expm(A1*olddr);
   Phi2=expm(A2*(1-olddr));
   xk=inv(U-Phi2*Phi1)*Phi2*(Phi1-eye(5))*inv(A1)*B1;
   newdr=fzero('kitoltes',[0 1]);
end
x1=Phi1*xk+(Phi1-eye(5))*inv(A1)*B1;
v1=A1*x1+B1;
v2=A2*x1;
M=eye(5)-(v1-v2)*K/(K*v1+VU-VL);
Z=U*Phi2*M*Phi1;
se=eig(Z);
plot(cos(0:pi/1000:2*pi),sin(0:pi/1000:2*pi),real(se),imag(se),'kx')
se'
abs(se')
```

APPENDIX D

MATLAB Function for the Fuzzy Logic Controller

```
function [y]=flc(x,a1,b1,c1)
er=[max(min(1,(-a1-x(1))/a1),0)
    max(min((x(1)+2*a1)/a1,-x(1)/a1),0)
    max(min((x(1)+a1)/a1,(a1-x(1))/a1),0)
    max(min(x(1)/a1,(2*a1-x(1))/a1),0)
    max(min((x(1)-a1)/a1,1),0)]';
der=[max(min(1,(-b1-x(2))/b1),0)
     max(min((x(2)+2*b1)/b1,-x(2)/b1),0)
     max(min((x(2)+b1)/b1,(b1-x(2))/b1),0)
     max(min(x(2)/b1,(2*b1-x(2))/b1),0)
     max(min((x(2)-b1)/b1,1),0)]';
com=[-2*c1 -c1 0 c1 2*c1];
sum1=0;
sum2=0;
   for j=find(der),
      for k=find(er),
         sum1=sum1+min([er(k) der(j)])*com(min(max(j+k-3,1),5));
         sum2=sum2+min([er(k) der(j)]);
      end
   end
y=sum1/sum2;
```

APPENDIX E

Parameter and Variable Values of the Experimental Converter Setup

CIRCUIT COMPONENTS	*VALUES*
Switched Capacitor C	100 nF
Inductance L	125 μH
Filter Capacitor $C_p = C_n$	100 μF
Load Resistance $R_p = R_n$	7 Ω
Input DC Voltages $v_{ip} = -v_{in}$	8 V
Reference Output Voltage v_{ref}	6 V
Upper and Lower Voltage Limits of the Sawtooth Waveform $V_U = -V_L$	6 V

APPENDIX F

Simulink Model of the High Frequency Time-Sharing Inverter

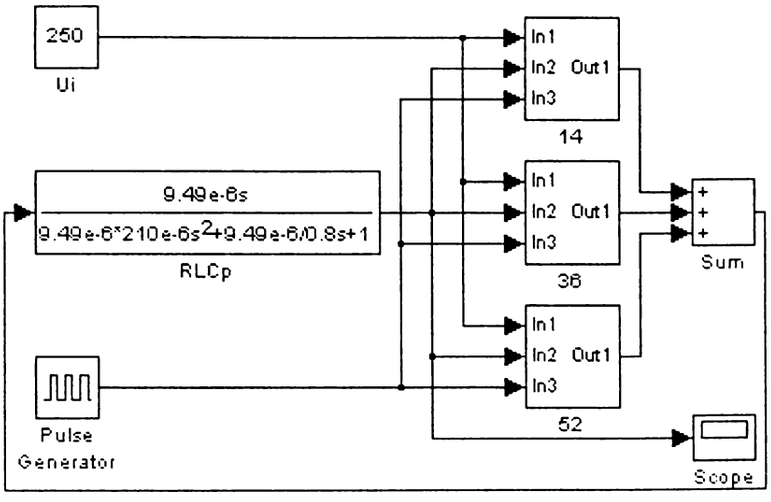

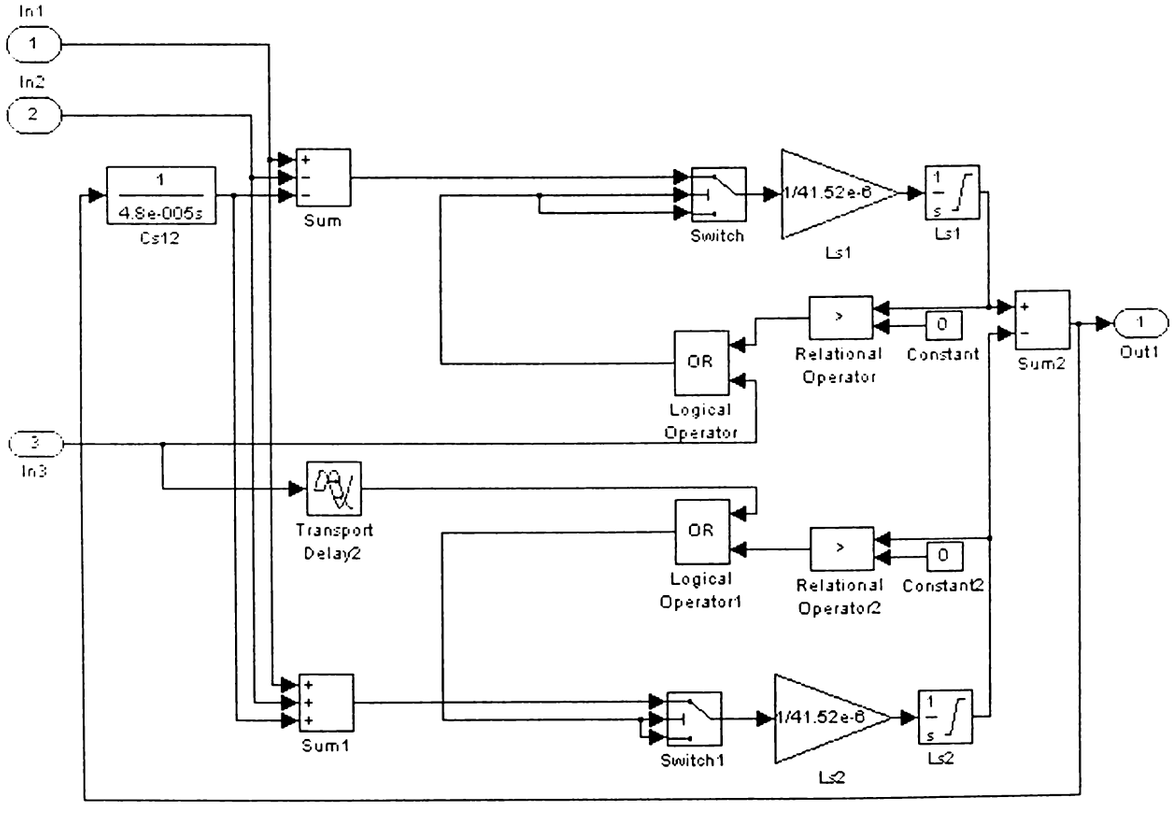

14

APPENDIX G

Parameter and Variable Values of the High Frequency Time-Sharing Inverter

CIRCUIT COMPONENTS	*VALUES*
Series Inductance L_s	41.52 μH
Series Capacitor C_s	48 μF
Load Resistance R_p	800 mΩ
Load Inductance L_p	9.49 μH
Load Capacitor C_p	210 μF
Input DC Voltage v_i	250 V

BIBLIOGRAPHY

[1] H. Poincaré, *Les Methodes Nouvelle de la Mecanique Celeste*, Paris: Gauthiers – Villars, 1899.

[2] E. N. Lorenz, "Deterministic nonperiodic flow", *J. Atmospheric Sciences,* vol. 20, no.2, pp. 130-141, 1963.

[3] T. Y. Li and J. A. Yorke, "Period three implies chaos", *American Mathematical Monthly,* vol. 82, pp. 985-992, 1975.

[4] R. M. May, "Simple mathematical models with very complicated dynamics", *Nature,* vol. 261, pp. 459-467, June 1976.

[5] M. J. Feigenbaum, "Universal behavior in nonlinear systems", in *Universality in Chaos* (Predrag Cvitanovic, ed.), Bristol, U.K., Adam Hilger Ltd., 1984.

[6] B. K. Bose, *Modern Power Electronics: Evolution, Technology and Applications.* New York: IEEE Press, 1992.

[7] R. E. Tarter, *Solid-State Power Conversion Handbook.* New York: Wiley-Interscience, 1993.

[8] N. Mohan, T. M. Undeland and W. P. Robbins, *Power Electronics: Converters, Applications and Design.* New York: Wiley, second ed., 1995.

[9] J. G. Kassakian, M. F. Schlecht, and G. C. Verghese, *Principles of Power Electronics*, Addison-Wesley, 1991.

[10] G. W. Wester and R. D. Middlebrook, "Low-frequency characterization of switched dc-to-dc converters", *IEEE Power Processing and Electronics Specialists' Conference* (Atlantic City), pp. 9-20, May 1972.

[11] R. D. Middlebrook and S. Čuk, "A general unified approach to modeling switching converter power stages", *IEEE Power Electronics Specialists' Conference* (Cleveland), pp. 18-34, 1976.

[12] S. Čuk and R. D. Middlebrook, "A general unified approach to modeling switching dc-to-dc converters in discontinuous conduction mode", *Power Electronics Specialists' Conference,* pp. 36-57, 1977.

[13] A. S. Kislovski, R. Redl and N.O. Sokal, *Dynamic Analysis of Switching-Mode DC/DC Converters.* New York: Van Nostrand Reinhold, 1991.

[14] V. Vorperian, "Simplified analysis of PWM converters using model of PWM switch -Part I: Continuous conduction mode", *IEEE Trans. on Aero and Elec. Systems*, vol. 26, pp. 490-496, May 1990.

[15] V. Vorperian, "Simplified analysis of PWM converters using model of pwm switch-Part II: Discontinuous conduction mode", *IEEE Trans. on Aero and Elec. Systems*, vol. 26, pp. 497-505, May 1990.

[16] J. H. B. Deane and D. C. Hamill, "Analysis, simulation and experimental study of chaos in the buck converter", *IEEE Power Electronics Specialists' Conference,* (San Antonio), pp. 491-498, 1990.

[17] D. C. Hamill and J. H. B. Deane, "Modeling of chaotic dc-dc converters by iterated nonlinear mappings", *IEEE Trans. on Power Electronics,* vol. 7, pp. 25-36, January 1992.

[18] E. Fossas and G. Olivar, "Study of chaos in the buck converter", *IEEE Trans. on Circuits and Systems-I,* vol. 43, no. 1, pp. 13-25, 1996.

[19] C. K. Tse, Y. M. Lai, and H. H. C. Iu, "Hopf bifurcation and chaos in a free-running autonomous Čuk converter", *IEEE Trans. on Circuits and Systems, Part I,* vol. 47, pp. 448-457, April 2000.

[20] B. van der Pol and J. van der Mark, "Frequency demultiplication", *Nature,* vol. 120, pp. 363-364, September 1927.

[21] M. P. Kennedy and L. O. Chua, "Van der Pol and chaos", *IEEE Trans. on Circuits and Systems*, vol. 33, pp. 974-980, October 1986.
[22] J. Baillieul, R. W. Brockett, and R. B. Washburn, "Chaotic motion in nonlinear feedback systems", *IEEE Trans. on Circuits and Systems*, vol. 27, pp. 990-997, November 1980.
[23] P. S. Linsay, "Period doubling and chaotic behavior in a driven anharmonic oscillator", *Physical Review Letters,* vol. 47, pp. 1349-1352, November 1981.
[24] L. O. Chua, "The genesis of Chua's circuit", *Archiv für Elektronik und Ubertragungstechnik,* vol. 46, no. 4, pp. 250-257, 1992.
[25] L. O. Chua, "Chua's circuit 10 years later", *Int. J. Circuit Theory and Appl.,* vol. 22, no. 4, pp. 279-305, 1994.
[26] R. W. Brockett and J. R. Wood, "Understanding power converter chaotic behavior in protective and abnormal modes", *in Powercon II*, 1984.
[27] D. C. Hamill and D. J. Jefferies, "Subharmonics and chaos in a controlled switched-mode power converter", *IEEE Trans. on Circuits and Systems*, vol. 35, no. 8, pp. 1059-1061, 1988.
[28] J. R. Wood, "Chaos: A real phenomenon in power electronics", *Applied Power Electronics Conference* (Baltimore), pp. 115-124, March 1989.
[29] J. H. B. Deane and D. C. Hamill, "Instability, subharmonics, and chaos in power electronics circuits", *IEEE Trans. on Power Electronics,* vol. 5, pp. 260-268, July 1990.
[30] J. H. B. Deane and D. C. Hamill, "Chaotic behaviour in current-mode controlled dc-dc converter", *Electronics Letters,* vol. 27, pp. 1172-1173, June 1991.
[31] J. H. B. Deane, "Chaos in a current-mode controlled boost dc-dc converter", *IEEE Trans. on Circuits and Systems-I*, vol. 39, pp. 680-683, August 1992.
[32] K. Chakrabarty, G. Podder and S. Banerjee, "Bifurcation behavior of buck converter", *IEEE Trans. on Power Electronics,* vol. 11, no. 3, pp. 439-447, 1996.
[33] S. Banerjee and K. Chakrabarty, "Nonlinear modeling and bifurcations in the boost converter", *IEEE Trans. on Power Electronics,* vol. 13, no. 2, pp. 252-260, 1998.
[34] W. C. Y. Chan and C. K. Tse, "Study of bifurcations in current programmed dc/dc boost converters: from quasiperiodicity to period doubling", *IEEE Trans. on Circuits and Systems - I*, vol. 44, no. 12, pp. 1129-1142, 1997.
[35] J. L. R. Marrero, J. M. Font and G. C. Verghese, "Analysis of the chaotic regime for dc-dc converters under current mode control", *IEEE Power Electronics Specialists' Conference,* pp. 1477-1483, 1996.
[36] M. di Bernardo, F. Garofalo, L. Glielmo and F. Vasca, "Quasi-periodic behaviors in dc/dc converters", *IEEE Power Electronics Specialists' Conference,* pp. 1376-1381, 1996.
[37] M. di Bernardo, C. Budd and A. Champneys, "Grazing, skipping and sliding: analysis of the non-smooth dynamics of the dc-dc buck converter", *Nonlinearity,* vol. 11, no. 4, pp. 858-890, 1998.
[38] M. di Bernardo, E. Fossas, G. Olivar and F. Vasca, "Secondary bifurcations and high-periodic orbits in voltage controlled buck converter", *Int. J. Bifurcation and Chaos*, vol. 7, no. 12, pp. 2755-2771, 1997.
[39] M. di Bernardo, F. Garofalo, L. Glielmo and F. Vasca, "Switchings, bifurcations and chaos in dc-dc converters", *IEEE Trans. on Circuits and Systems-I*, vol. 45, no. 2, pp. 133-141, 1998.
[40] S. Banerjee, "Coexisting attractors, chaotic saddles and fractal basins in a power electronic circuit", *IEEE Trans. on Circuits and Systems-I*, vol. 44, no. 9, pp. 847-849, 1997.

[41] S. Banerjee and K. Chakrabarty, "Nonlinear modeling and bifurcations in the boost converter", *IEEE Trans. on Power Electronics,* vol. 13, no. 2, pp. 252-260, 1998.
[42] S. Banerjee, E. Ott, J. A. Yorke and G. H. Yuan, "Anomalous bifurcations in dc-dc converters: Borderline collisions in piecewise smooth maps", *IEEE Power Electronics Specialists' Conference,* pp. 1337-1344, 1997.
[43] C. K. Tse, "Flip bifurcation and chaos in three-state boost switching regulators", *IEEE Trans. on Circuits and Systems-I,* vol. 41, pp. 16-23, January 1994.
[44] C. K. Tse and W. C. Y. Chan, "Instability and chaos in a current-mode controlled Čuk converter", *IEEE Power Electronics Specialists' Conference,* 1995.
[45] S. G. Jalali, I. Dobson and R. H. Lasseter, "Instabilities due to bifurcation of switching times in a thyristor controlled reactor", *IEEE Power Electronics Specialists' Conference*, (Toledo, Spain), pp. 546-552, May 28-31, 1992.
[46] R. Rajaraman, I. Dobson and S.G. Jalali, "Nonlinear dynamics and switching time bifurcations of a thyristor controlled reactor", *IEEE Int. Symposium on Circuits & Systems* (Chicago), pp. 2180-2183, May 1993.
[47] L. O. Chua, M. Hasler, J. Neirynck and P. Verburgh, "Dynamics of a piecewise-linear resonant circuit", *IEEE Trans. on Circuits and Systems,* vol. 29, pp. 535-547, August 1982.
[48] C. Kieny, "Application of the bifurcation theory in studying and understanding the global behavior of a ferroresonant electric power circuit", *IEEE Trans. on Power Delivery*, vol. 6, pp. 866-872, April 1991.
[49] A. E. A. Araujo. A. C. Soudack and J. R. Marti, "Ferroresonance in power systems", *IEE Proc., Part C*, vol. 140, pp. 237-240, May 1993.
[50] J. H. B. Deane, "Modeling of a chaotic circuit containing a saturating/hysteretic inductor", *Electronics Letters,* vol. 29, pp. 957-958, May 1993.
[51] J. H. B. Deane, "Modeling the dynamics of nonlinear inductor circuits", *IEEE Trans. on Magnetics,* vol. 30, pp. 2795-2801, September 1994.
[52] J. A. Mohamed, "Existence and stability analysis of ferroresonance using the generalized state-space averaging technique", PhD diss., EECS Depart., MIT, February 2000.
[53] Z. Sütő, I. Nagy and E. Masada, "Avoiding chaotic processes in current control of ac drive", *IEEE Power Electronics Specialists' Conference,* pp. 255-261, 1998.
[54] A. Magauer and S. Banerjee, "Bifurcations and chaos in the tolerance band PWM technique", *IEEE Trans. on Circuits and Systems-I*, vol. 47, pp. 254-259, February 2000.
[55] Y. Kuroe and S. Hayashi, "Analysis of bifurcation in power electronic induction motor drive systems", *IEEE Power Electronics Specialists' Conference,* pp. 923-930, 1989.
[56] M. Ohnishi and N. Inaba, "A singular bifurcation into instant chaos in a piecewise linear circuit", *IEEE Trans. on Circuits and Systems-I,* vol. 41, no. 6, pp. *433-442,* 1994.
[57] G. H. Yuan, S. Banerjee, E. Ott and J. A. Yorke, "Border collision bifurcations in the buck converter", *IEEE Trans. on Circuits and Systems-I,* vol. 45, no. 7, pp. 707-716, 1998.
[58] H. E. Nusse and J. A. Yorke, "Border-collision bifurcations including "period two to period three" for piecewise smooth maps", *Physica D,* vol. 57, pp. 39-57, 1992.
[59] H. E. Nusse and J. A. Yorke, "Border-collision bifurcations for piecewise smooth one dimensional maps", *Int. J. Bifurcation and Chaos*, vol. 5, no. 1, pp. 189-207, 1995.

[60] S. Banerjee, M. S. Karthik, G. H. Yuan and J. A. Yorke, "Bifurcations in one-dimensional piecewise smooth maps - theory and applications in switching circuits", *IEEE Trans. on Circuits and Systems-I,* vol. 47, no. 3, 2000.

[61] S. Banerjee, P. Ranjan and C. Grebogi, "Bifurcations in two-dimensional piecewise smooth maps - theory and applications in switching circuits", *IEEE Trans. on Circuits and Systems-I,* vol. 47, no. 5, 2000.

[62] M. di Bernardo, M. I. Feigin, S. J. Hogan and M. E. Homer, "Local analysis of *C*-bifurcations in *n*-dimensional piecewise smooth dynamical systems", *Chaos, Solitons & Fractals*, vol. 10, no. 11, pp. 1881-1908, 1999.

[63] H. H. C. Iu and C. K. Tse, "Instability and bifurcation in parallel-connected buck converters under a master-slave current sharing scheme", *IEEE Power Electronics Specialists' Conference* (Galway, Ireland), pp. 708-713, June 2000.

[64] H. H. C. Iu and C. K. Tse, "Bifurcation in parallel-connected boost dc/dc converters", *IEEE Int. Symp. on Circuits and Systems* (Geneva, Switzerland), pp. II-473-476, June 2000.

[65] C. K. Tse and W. C. Y. Chan, "Experimental verification of bifurcations in current-programmed dc/dc boost converters: from periodicity to period-doubling", *European Conf. On Circuit Theory and Design,* (Budapest), pp. 1274-1279, September 1997.

[66] E. Ott, C. Grebogi and J. A. Yorke, "Controlling chaos", *Physical Review Letters*, vol. 64. no. 11, pp. 1196-1199, 1990.

[67] G. Podder, K. Chakrabarty and S. Banerjee, "Experimental control of chaotic behavior of buck converter", *IEEE Trans. on Circuits and Systems-I,* vol. 42, no. 8, pp. 100-101, 1995.

[68] G. Podder, K. Chakrabarty and S. Banerjee, "Control of chaos in the boost converter", *Electronics Letters (IEE),* vol. 31, no. 11, p. 25, 1995.

[69] M. Di Bernardo, "An adaptive approach to the control and synchronization of continuous - time chaotic systems", *Int. J. Bifurcation and Chaos,* vol. 6, pp. 557-568, 1996.

[70] C. Batlle, E. Fossas and G. Olivar, "Time-delay stabilization of periodic orbits of the current mode controlled boost converter", *Linear Time Delay Systems* (L. D. J. Dion and M. Fliess, eds.), pp. 111-116, 1998.

[71] D. C. Hamill, "Power electronics: A field rich in nonlinear dynamics", *3rd Int. Specialists' Workshop on Nonlinear Dynamics of Electronic Systems* (University College, Dublin), pp 165-178. 1995.

[72] A. M. Stasnkovič, G. C. Verghese and D. J. Perreault, "Analysis and synthesis of randomized modulation schemes for power converters", *IEEE Trans. on Power Electronics,* vol. 10, no. 6, pp. 680-693, 1995.

[73] A. M. Stankovič, G. C. Verghese and D. J. Perrault, "Randomized modulation of power converters via Markov chains", *IEEE Trans. Control Systems Technology,* vol. 5, pp. 61-73, January 1997.

[74] J. H. B. Deane and D. C. Hamill, "Improvement of power supply EMC by chaos", *Electronic Letters*, vol. 32, p. 1045, June 1996.

[75] S. H. Isabelle, "A signal processing framework for the analysis and applications of chaotic systems", PhD diss., EECS Department, MIT, 1995.

[76] J. H. B. Deane, P. Ashwin, D. C. Hamill and D. J. Jefferies, "Calculation of the periodic spectral components in a chaotic dc-dc converter", *IEEE Trans. on Circuits and Systems - I*, vol. 46, no. 11, pp. 1313-1319, 1999.

[77] A. L. Baranovski, A. Mögel, W. Schwarz and O. Woywode, "Statistical analysis of a dc-dc converter", *Nonlinear Dynamics of Electronic Systems* (Ronne, Bornholm, Denmark), July 15-18, 1999.

[78] A. L. Baranovski, A. Mögel, W. Schwarz and O. Woywode, "Chaotic control of a dc-dc converter", *IEEE Int. Symp. on Circuits & Systems* (Geneva, Switzerland), May 28-31, 2000.
[79] R. S. Bueno and J. L. R. Marrero, "Control of a boost dc-dc converter in the chaotic regime", *IEEE Int. Conf. on Control Applications,* pp. 832-837, 1998.
[80] S. Banerjee, J. A. Yorke and C. Grebogi, "Robust chaos", *Physical Review Letters*, vol. 80, pp. 3049-3052, 1998.
[81] I. Nagy, "Resonant DC-DC configuration", *3rd European Conference on Power Electronics and Applications EPE'89*, (Aachen, Germany), pp. 1495-1500, 1989.
[82] I. Nagy, O. Dranga, „Bifurcation in a dual channel resonant DC-DC converter", *Proceedings of The 2000 IEEE International Symposium on Industrial Electronics ISIE'2000*, (Puebla, Mexico), December 4-8, pp. 495-500, 2000.
[83] O. Dranga, I. Nagy, "Stability analysis of a feedback controlled resonant DC-DC converter", *IEEE Transactions on Industrial Electronics*, under review.
[84] R. C. Hilborn, *Chaos and Nonlinear Dynamics: An Introduction for Scientists and Engineers*, Oxford University Press, 1994.
[85] M. P. Kennedy, *Basic Concepts of Nonlinear Dynamics and Chaos*, Lecture Notes, Budapest University of Technology and Economics, 2000.
[86] T. S. Parker, L. O. Chua, *Practical Numerical Algorithms for Chaotic Systems*, Springer-Verlag, 1989.
[87] O. Dranga, D. I. Curiac, F. Drăgan, "Nonlinear dynamics and chaotic behavior of a dual channel resonant dc-dc converter", *MicroCAD 2001 International Scientific Conference*, (Miskolc, Hungary), 1-2 March 2001.
[88] T. Kapitaniak, *Chaos for Engineers: Theory, Applications and Control*, Springer-Verlag, 1998.
[89] I. Nagy, *Változó strukturájú nemlineáris rendszerek*, Székfoglalók a Magyar Tudományos Akadémián, 2000.
[90] O. Dranga, I. Nagy, "Stability analysis of feedback controlled resonant DC-DC converter using Poincaré map function", *2001 IEEE International Symposium on Industrial Electronics*, (Pusan, Korea), June 12-16, 2001, accepted paper.
[91] B. J. Kuo, *Automatic Control Systems*, Fifth Edition, Prentice Hall, 1987.
[92] T. L. Dragomir, *Tehnici de optimizare,* Lecture Notes, "Politehnica" University of Timişoara, 1995.
[93] T. L. Dragomir, O. Dranga, S. Nanu, "About an electrohydraulic speed governor structure", *Proceedings of The International Symposium on Systems Theory,* (Craiova, Romania), June 6-7, pp. 87-95, 1996.
[94] T. L. Dragomir, O. Dranga, "About the behavior of an automatic control system of the speed of a hydrogenerator using a nonlinear speed governor", *Proceedings of the International Conference of Technical Informatics ConTI'96,* (Timişoara, Romania), vol. II., pp. 75-82, 1996.
[95] D. I. Curiac, I. Filip, O. Proştean, O. Dranga, "Self-tuning regulator based on reference compensation", *World Automation Congress WAC2000*, (Hawaii, USA), June 11-16, 2000.
[96] D. I. Curiac, C. Vaşar, I. Filip, O. Dranga, "About the automation of refuse water neutralization", *Proceedings of International Symposium on Civil Engineering*, (Timişoara, Romania), April 23-24, vol. I., pp. 203-210, 1998.
[97] D. I. Curiac, I. Filip, O. Proştean, O. Dranga, "About an on-line wind modeling strategy", *Proceedings of SyM'99 Simposio en Simulacíon y Modelística,* (Buenos Aires, Argentina), 10 de Septiembre, 1999.

[98] J. Hamar, O. Dranga, I. Nagy, "Nonlinear Behavior of a Twin Converter", *2000 IEEE International Conference on Industrial Electronics, Control and Instrumentation IECON-2000*, (Nagoya, Japan), October 22-28, pp. 1955-1960, 2000.
[99] R.-E. Precup, Şt. Preitl, *Sisteme de reglare avansată*, Lecture Notes, "Politehnica" University of Timişoara, 1995.
[100] R.-E. Precup, Şt. Preitl, *Fuzzy Controllers*, Editura Orizonturi Universitare, Timişoara, 1995.
[101] I. Filip, O. Dranga, "Comparative study above some types of fuzzy controllers", *Proceedings of the International Conference of Technical Informatics ConTI'96*, (Timişoara, Romania), vol. I., pp. 227-232, 1996.
[102] I Filip, O. Proştean, O. Dranga, C. Vaşar, "Fuzzy logic in installation control systems", *Proceedings of International Symposium on Civil Engineering*, (Timişoara, Romania), April 23-24, vol. II., pp. 203-210, 1998.
[103] I. Borza, I. Filip, D. I. Curiac, O. Dranga, "Fuzzy temperature control system for heat exchanger", *Proceedings of International Conference on Medical Engineering and Environment,* (Chişinău, Moldova), October 2-4, pp. 147-152, 1997.
[104] D. Szabó, O. Dranga, S. Kerekes, T. Gajdár, "A fuzzy sliding mode approach for the two-mass system", *Proceedings of the IEEE International Symposium on Industrial Electronics ISIE'99*, (Bled, Slovenia), 12-16 July, vol. I., pp. 348-352, 1999.
[105] O. Proştean, O. Dranga, I. Filip, D. I. Curiac, "Some new MATLAB functions for the design of fuzzy systems", *Proceedings of the International Conference on Microelectronics and Computer Science ICMCS-97*, (Chişinău, Moldova), vol. I., pp. 196-198, 1997.
[106] K. Pyragas, "Continuous control of chaos by self-controlling feedback", *Phys. Letters,* vol. A170, pp. 421-428, 1992.
[107] ***, *DS1102 User's Guide*, Document Version 3.0, dSPACE GmbH.
[108] ***, *Real-Time Workshop User's Guide*, Version 3, The MathWorks Inc.
[109] ***, *Real-Time Interface to Simulink RT1102 User's Guide*, Document Version 1.0, dSPACE GmbH.
[110] ***, *Simulink – Dynamic System Simulation for MATLAB*, Version 3, The MathWorks Inc.
[111] ***, *MATLAB – The Language of Technical Computing*, Version 5, The MathWorks Inc.
[112] ***, *COCKPIT Instrument Panel*, Document Version 3.2, dSPACE GmbH.
[113] I. Nagy, *Frekvenciaosztásos, középfrekvenciás inverter elmélete*, MTA Számítástechnikai és Automatizálási Kutató Intézet, Budapest, 1974.
[114] I. Nagy, "Nonlinear Dynamics in Power Electronics", *Proceedings of 11th EDPE Conference,* (Dubrovnik, Croatia), 9-11 October, pp. 1-15, 2000.
[115] I. Nagy, O. Dranga, E. Masada, "Bifurcations in a High Frequency Time-Sharing Inverter", *EPE-PEMC '2000 International Conference,* (Košice, Slovakia), 5-7 September, vol. 2, pp. 148-153, 2000.
[116] I. Nagy, O. Dranga, E. Masada, "Study of a Subharmonic Generation in a High Frequency Time-Sharing Inverter", *The Society Transactions of The IEE Japan*, 5-7 September, Vol. 120-D, No.4, April 2000, pp. 574-580, 2000.
[117] I. Nagy, O. Dranga, E. Masada, "Subharmonic Generation in a High Frequency Time-Sharing Inverter", *Proceedings of the 1999 Japan Industry Applications Society Conference JIASC'99,* (Nagaoka, Japan), pp. 137-142, 1999.